



HAL
open science

Contribution to the modelling of aircraft tyre-road interaction

Rimyalegdo Kiébré

► **To cite this version:**

Rimyalegdo Kiébré. Contribution to the modelling of aircraft tyre-road interaction. Other. Université de Haute Alsace - Mulhouse, 2010. English. NNT : 2010MULH4086 . tel-00601774

HAL Id: tel-00601774

<https://theses.hal.science/tel-00601774>

Submitted on 20 Jun 2011

HAL is a multi-disciplinary open access archive for the deposit and dissemination of scientific research documents, whether they are published or not. The documents may come from teaching and research institutions in France or abroad, or from public or private research centers.

L'archive ouverte pluridisciplinaire **HAL**, est destinée au dépôt et à la diffusion de documents scientifiques de niveau recherche, publiés ou non, émanant des établissements d'enseignement et de recherche français ou étrangers, des laboratoires publics ou privés.



UNIVERSITÉ DE HAUTE-ALSACE

Ph.D. T H E S I S

to obtain the title of

Ph.D. of Science

of Université de Haute-Alsace

Speciality : MECHANICS AND CONTROL THEORY

Defended by

Rimyalegdo KIÉBRÉ

**Contribution to the modelling of
aircraft tyre-road interaction**

Thesis Advisors : Floriane ANSTETT-COLLIN and Michel BASSET

Prepared at the MIPS Laboratory, MIAM Team

Defended on December 10th, 2010

Jury :

<i>Reviewers :</i>	Igo BESSELINK	Eindhoven - Tech. University (Netherlands)
	Thierry BASTOGNE	Nancy Université
<i>Examinator :</i>	Jean-Charles MARÉ	INSA Toulouse
<i>Advisors :</i>	Floriane ANSTETT-COLLIN	Université de Haute-Alsace
	Michel BASSET	Université de Haute-Alsace
<i>Invited :</i>	Olivier NOEL	Messier-Dowty
	Louis ZEFERINO	Messier-Dowty

To my sister Aminata.

To my parents who always support me.

Acknowledgements

Si la rivière abonde à son embouchure, c'est parce que son lit l'a bien drainée. [Rimyalegdo Kiébré]

La reconnaissance est la mémoire du cœur. [Hans Christian Andersen]

Les mots manquent aux émotions. [Victor Hugo]

Michel Basset

Pour entrer dans une maison, il faut qu'une porte s'ouvre. Merci pour la confiance témoignée, surtout pour avoir reporté de 6 mois le début de la thèse pour m'attendre.

Floriane Anstett-Collin

Si la façon de remercier doit être à la hauteur de ce que tu as donné pour ma thèse, je préfère renoncer car je n'y parviendrai pas. Grâce à toi, j'ai pris du plaisir à faire ma thèse.

Olivier Noël

Heureusement que tu donnes sans compter car tu t'en lasserai. En 6 mois avec toi, j'ai acquis une riche expérience professionnelle et humaine qui m'aurait requis plusieurs années ailleurs.

Louis Zéférino

Tu t'es fait discret quelques fois. Mais tes apparitions m'ont été d'une aide inestimable. A chaque fois que je prépare un exposé oral je pense à tes conseils.

L'Equipe MIAM

Il est évident que l'eau ruisselle plus facilement sur un sol humide que sur un sol aride. Gentillesse, disponibilité, solidarité, esprit d'équipe, service rendu, relation de confiance... ohh! comme il m'est difficile de trouver le mot magique qui saurait qualifier les membres de l'équipe! Jérôme Guillet, Jérémie Daniel, Benjamin Mourllion, Jean-Philippe Lauffenburger, Sacha Bernet, Christophe Lamy, Rodolfo Orjuela, Gaétan Pouly, Dmitry Grigoryev, Guillaume Girardin et Joël Lambert. Merci à vous tous pour ces merveilleux moments que je n'oublierai jamais.

To all those whose guidance, support, advise and criticism have been of great benefit to this research project.

Notations

The parameters presented below are used in this manuscript.

a	Half of contact patch length (unit: length)
b	Contact patch width (unit: length)
μ	Friction coefficient
k_x	Tread longitudinal stiffness (unit: force/length)
k_y	Tread lateral stiffness (unit: force/length)
C_S	Longitudinal slip stiffness (unit: force)
C_α	Lateral slip (or cornering) stiffness, (unit: force)
V	Tyre forward velocity (unit: length/time)
V_x	Longitudinal component of the forward velocity (unit: length/time)
V_y	Lateral component of the forward velocity (unit: length/time)
V_s	Slip velocity (unit: length/time)
V_{xs}	Longitudinal component of the slip velocity (unit: length/time)
V_{ys}	Lateral component of the slip velocity (unit: length/time)
w	Tyre angular velocity (unit: angle/time)
R_e	Effective rolling radius (unit: length)
S_L	Longitudinal slip ratio
α	Tyre side slip angle (unit: rad)
S_α	Lateral slip ratio
v_x	Longitudinal tyre tread displacement (unit: length)
v_y	Lateral tyre tread displacement (unit: length)
γ	Camber angle (unit: rad)
ψ	Yaw angle (unit: rad)
μ	Actual friction coefficient
μ_o	Tyre to road coefficient of static friction
F_x	Longitudinal tractive or braking tyre force (unit: force)
F_y	Lateral tyre force (unit: force)
F_z	Vertical tyre force (unit: force)

M_x	Tyre overturning moment (unit: force times length)
M_y	Tyre rolling resistance moment (unit: force times length)
M_z	Tyre self-aligning moment (unit: force times length)
B	Stiffness factor (Magic Formula)
C	Shape factor (Magic Formula)
D	Peak value (Magic Formula)
E	Curvature factor (Magic Formula)
S_H	Horizontal shift (Magic Formula)
S_V	Vertical shift (Magic Formula)
Y	Output variable F_x , F_y or M_z (Magic Formula)
X	Input variable S_α or S_L (Magic Formula)
BCD	Slope at the origin of the curve of $Y = f(X)$ (Magic Formula)

Le commencement de toutes les sciences, c'est l'étonnement de ce que les choses sont ce qu'elles sont.

Aristote

General introduction

The wheel is one of the oldest human inventions. It is more often assumed that the wheel appeared 3500 years before Jesus Christ in Mesopotamia. According to this hypothesis, it is after observing a pebble rolling that human realised the possible advantages that could offer this perfect circular shape. In the past, tree boles were used for moving heavy charges such as manufacturing materials. It is probably by understanding this principle eliminates a significant part of the friction force that the concept of wheel has borned. The evidence is that the invention of wheel is the origin of the revolution of human and goods transportation. Moreover, the wheel has been going through remarkable improvement with time. In fact, wheel was first made using stone, then wood, later with steel, aluminum and finally with composites. For example, the initial wood made wheel was circled (coated) with steel in order to increase its stiffness as well as its life time. Meanwhile, the notion of vehicle comfort has taken place and overcoming inconveniences due to the road unevenness has quickly become an important issue. The major wheel improvement has started with the use of rubber. Indeed, in 1869, Clément Ader, a french scientist and industrialist, decided to circle (coat) the wood-made (or steel-made) wheel with rubber. The main advantage is the damping property of the rubber. However, the wheel as described above designates a unique solid part. In England, Thomsom (1846) and John Boyd Dunlop (1889) produced what is commonly called hosepipe and bicycle 'gut': a rubber pipe vulcanised on a textile material frame and inflated with air. Edouard Michelin (1890), a former machine manufacturer, invented the steel rod tyre, which can be mounted and taken off from a circular support termed rim. It is the invention of the first tyre, which is relatively close to modern tyre in shape.

The tyre is the only contact point of ground vehicles with the road and therefore, the tyre properties play a fundamental role when determining the dynamic behaviour of these vehicles. Representative tyre model is then necessary for functional virtual simulation. However, the performances and the environment challenges have led to the use of more

and more complex composite materials in tyre manufacturing. As a consequence, it is difficult to physically represent the tyre real behaviour on the road. Indeed, it is required to consider either extensive and complex models or models with considerable simplification for representing the tyre full behaviour on the road. In this context, getting a suitable model for a given application becomes also a challenge for a simple model may not be realistic enough, and for a more complex one may be difficult to handle and perhaps, unnecessary for the given application.

In the aeronautical fields, contributing to better understanding the tyre dynamics as well as the improvement of the use of optimal and representative tyre models is one of the objectives of Messier-Dowty company, a landing gear manufacturer. This thesis is done in collaboration with Messier-Dowty and is founded by the french national project called MACAO (Modélisation Avancée de Composants Aéronautiques et Outils associés).

In the project MACAO, there are several industrial partners (Airbus-France, Messier-Dowty, Turbomeca, etc), research centres and universities (CEA, CS, ONERA, UHA, INSA-Toulouse, etc). This project has been launched in order to promote the use of numerical simulation by the different partners. In fact, the improvement of simulation performances has become necessary because of the new competitive challenges (productivity, time to market, reactivity) and technologies (environment, energy, etc). The objective is to take advantage of performances of the modern simulation tools by providing new models and developing tools which allow the simulation of systems and new physical phenomenon.

The industrial partner Messier-Dowty has the expertness in the landing gear domain. However, the landing gear is a part of a complex system, the aircraft, and is directly articulated to the fuselage and to the wheel. With respect to the load cases, the landing gear has to meet the JAR/FAR (airworthiness authority organisation) regulations in order to obtain an airworthiness certificate. These load cases include the influence of the aircraft fuselage as well as the one of the wheel (tyre). Messier-Dowty receives fuselage specifications from the aircraft manufacturer and tyre ones from the tyre manufacturer. If the JAR/FAR regulations to date aim to ensure robust landing gear, it does not require the analysis of the landing gear reaction under the various and complex behaviour of the wheel, specially its tyre. Therefore, the modelling of the tyre dynamics did not constitute a main issue for landing gear manufacturers for long time (specially in the civil aircraft fields). Nowadays, because of the competitive challenges, previously mentioned, the tendency started to change. Thus, the objective of Messier-Dowty is to develop models for

simulating the tyre-road interaction characteristics with respect to the aircraft run types. These run types include acceleration/braking during take off/landing, cornering and combined cornering-acceleration/braking during taxiing, at steady-state condition. This thesis is done in collaboration with Messier-Dowty company in order to contribute to answering this problematic.

The work performed can be described as follows. In one hand, the literature studies in the field of tyre-road interaction modelling are investigated and then, the motivations as well as the limitations of the models are highlighted. In fact, it is shown that each model is developed in a specific tyre run type condition, based on a given approach which involves a certain number of assumptions. With respect to the hypotheses adopted, the model derived may be more or less representative of the real tyre behaviour. In the other hand, based on the literature survey of tyre models, the study requirements and the measurements data constraints, an a priori choice of suitable tyre models is proposed for the tyre run types conditions proposed by Messier-Dowty. This a priori chosen models are investigated and the advantages as well as the limitations of each model are discussed. Extension of some models for improving their representativeness and a further development of tyre models are proposed in order to better capture the tyre physical behaviour with respect to the considered tyre run type.

Besides, it should be underlined that tyre models are mainly nonlinear and depend on parameters obtained from measurements data. These measurements data are often few or/and incomplete, especially in the aircraft domain, and involve high costs. Thus, some parameters are estimated with more or less precision. Among all the parameters, however, some only have a small or insignificant influence on the model response and therefore, do not need to be determined precisely. In the other hand, some parameters are determinant for the model response and thus influence its uncertainty significantly. These parameters may require additional measurement data in order to be estimated with relatively high accuracy. In order to prepare and plan the experiments, it is necessary to distinguish the parameters with an insignificant influence on the response uncertainty, so as to set them at their nominal value in their interval of variation. For this sake, a method for carrying out sensitivity analysis on a model is presented. This method helps to classify a model parameters into a hierarchy with respect to the importance of their influence on the model response.

The approach adopted for carrying out the objectives of the thesis is described within five chapters. In chapter 1, a survey of the literature steady-state tyre models are pre-

sented. The models are described according to the main categories commonly encountered in the literature, physical, semi-physical and empirical. Then, by taking into account the main factors which play an important role in tyre modelling, it is proposed a classification for the physical and the semi-empirical models, which are studied in the following chapters.

The physical category of models are investigated in chapter 2 in order to propose suitable tyre models for the applications in the context of the thesis. First, based on the literature survey of steady-state tyre models, the study requirements and the measurements data constraints, an a priori choice of suitable physical models is proposed. Then, the a priori chosen models are investigated and an extension of a model is also presented, which help to improve its representativeness. Then, it is shown that the physical models present some significant limitations or/and cannot be used in the context of the thesis. Therefore, the semi-empirical models are investigated in chapter 3. An a priori choice of a semi-empirical model is presented and the modelling results are discussed.

In chapter 4, a further study of the tyre forces and moment generation at the particular case of pure cornering in steady-state condition is shown. Based on a simple but comprehensive physical approach, the generation of the longitudinal component of the tyre force and the one of the self-aligning moment at pure cornering are exhaustively described.

Finally, in chapter 5, the necessity of performing sensitivity analysis is presented. Then, a methodology for carrying out sensitivity analysis on a model is proposed and applied on two examples of tyre models. All the parameters of each model are classified into a hierarchy with respect to the importance of their influence on the model response.

The work performed in the context of the thesis has led to the following publications.

Publications

International journals (2)

1. R. Kiébré, F. Anstett-Collin and M. Basset. *A physical model for induced longitudinal force on tyre during steady-state pure cornering*. **International Journal of Vehicle Systems Modelling and Testing**, Vol. 5, Nos. 2/3 (2010), pp: 161-175.
2. R. Kiébré, F. Anstett-Collin and M. Basset (2010). *Sensitivity analysis for studying influential parameters in tyre models*. **International Journal of Vehicle Systems**

Modelling and Testing. Accepted - To appear.

International journals under review (2)

3. R. Kiébré, F. Anstett-Collin and M. Basset (2010). *Better understanding the self-aligning moment generation at pure lateral slip.* **Vehicle System Dynamics.** Under review.
4. R. Kiébré, F. Anstett-Collin, M. Basset (2010). *Using the Magic Formula model for induced longitudinal force at pure lateral slip.* **International Journal of Vehicle Design.** Under review.

International Congress with selection panel and Proceedings

5. R. Kiébré, F. Anstett-Collin and M. Basset. *Analyse de sensibilité pour l'étude des paramètres influents dans les modèles d'interface pneu/sol.* **Proceedings of Sixième Conférence Internationale Francophone d'Automatique**, CIFA, Nancy, France, 02-03 June, 2010.
6. R. Kiébré, F. Anstett-Collin and M. Basset. *Sensitivity analysis for tyre/road interface model.* **Sixth International Conference on Sensitivity Analysis of Model Output**, SAMO - Milano, Italy, 19-22 July, 2010. *Procedia - Social and Behavioral Sciences*, Volume 2, Issue 6 (2010), pp: 7688-7689.
7. R. Kiébré, F. Anstett-Collin and M. Basset. *Real shear forces and moment generated by tyre during pure lateral slip.* **Proceedings of the 2010 ASME International Mechanical Engineering Congress & Exposition (IMECE)**, Vancouver, Canada 12-18 November, 2010.

Contents

General introduction	iii
1 Review of tyre models for steady-state responses	1
1.1 Introduction	1
1.2 Main types of tyres	3
1.3 Definitions of tyre characteristics	5
1.3.1 Coordinate systems and operating variables	5
1.3.2 Definitions	7
1.4 Physical models	8
1.4.1 Brush model	8
1.4.2 Fiala model	10
1.4.3 Elastic beam theory	11
1.4.4 HSRI - NBS models	12
1.4.5 Model of Sakai	14
1.4.6 Model of Ratti	15
1.4.7 Tread simulation model	15
1.4.8 Mathematical-physical 2D tyre model	15
1.4.9 Classification of the physical models	17
1.4.10 Comments on physical models	18
1.5 Semi-empirical models	19
1.5.1 Model of Smiley and Horne	20
1.5.2 Somieski model	20
1.5.3 Model of Shim and Margolis	20
1.5.4 Unified semi-empirical model	22
1.5.5 Model of Dugoff	22
1.5.6 Model of Kamm	23
1.5.7 Nicholas and Comstock model	23

1.5.8	Model of Rimondi and Gavardi	24
1.5.9	Model of Schieschke	24
1.5.10	Magic Formula	25
1.6	Empirical models	28
1.7	Conclusion	29
2	Choosing suitable physical models	31
2.1	Introduction	31
2.2	Available measurements data	32
2.3	A priori choice of suitable physical models	34
2.3.1	Sakai model	34
2.3.2	HSRI-NBS-III model	36
2.3.3	Fiala model	39
2.4	Comparison of Sakai, Fiala and HSRI-NBS-III models	41
2.4.1	General approach for estimating parameters	41
2.4.2	Modelling results	43
2.4.3	Discussion: a priori chosen models and measurements data	48
2.5	Limits of physical models: example of Fiala model	50
2.6	Enhancement of Fiala model	51
2.6.1	Modelling results	52
2.6.2	Expressing the Fiala model parameters as function of F_z	54
2.7	Conclusion	56
3	Choosing suitable semi-empirical models	57
3.1	Introduction	57
3.2	A priori choice of semi-empirical model	58
3.2.1	Magic Formula versions	59
3.2.2	Presentation of the parameters identification tool: MF-Tool	63
3.2.3	Magic Formula modelling results	64
3.3	Simulating Magic Formula as implemented in Msc Adams software	73
3.3.1	Tyre test rig model in Msc Adams	74
3.3.2	Steady-state pure cornering	75
3.3.3	Parking manœuvres	76
3.3.4	Lateral relaxation length σ_y	78
3.4	Conclusion	80

4	Real shear forces and moment at pure lateral slip	83
4.1	Introduction	83
4.2	Context and motivation of the study	85
4.2.1	Tyre deformation at pure lateral slip condition	85
4.2.2	Wheel structure and tyre-road contact representation	89
4.3	Longitudinal force model	91
4.4	Self-aligning moment model	97
4.5	Application	99
4.5.1	Longitudinal force modelling results	101
4.5.2	Self-aligning moment modelling results	102
4.6	Using the Magic Formula model for the induced longitudinal force	106
4.7	Modelling results	108
4.8	Conclusion	111
5	Sensitivity analysis for tyre models	113
5.1	Introduction	113
5.2	Sensitivity analysis	115
5.2.1	Description of the sensitivity analysis approach	116
5.2.2	Sensitivity indices	117
5.2.3	Estimating sensitivity indices	119
5.3	Application of sensitivity analysis on tyre models	121
5.3.1	Fiala tyre model	121
5.3.2	Magic Formula model	128
5.4	Conclusion	136
A	Coordinate systems	141
B	Equations	145
B.1	Physical Models	145
B.1.1	Brush Model (section 1.4.1)	145
B.1.2	Fiala model (section 1.4.2)	146
B.1.3	HSRI-NBS-I model (section 1.4.4)	147
B.1.4	HSRI-NBS-III Model (section 1.4.4)	148
B.1.5	Model of Sakai (section 1.4.5)	150
B.1.6	Model of Ratti (section 1.4.6)	151
B.1.7	Semi-Empirical models	152

C	How to enter data in MF-Tool? (TYDEX file format)	157
C.1	Introduction to the TYDEX file format	157
C.2	Example of TYDEX file for use in MF-Tool	162
D	Example of a tyre property file	165
	Bibliography	173
	References	178

Une bonne idée doit être simple sur le fond, ce qui ne l'empêche pas de prendre toutes les complexités imaginables dans la forme. Voyez la roue...

Bernard Tirtiaux

CHAPTER 1

Review of tyre models for steady-state responses

Carrying out a review of the current state of research regarding tyre-road interface modelling for steady-state responses is the first step towards choosing appropriate models for simulating the steady-state tyre responses with respect to the tyre run types under interest. To help comparing the different models, they are described according to the three categories commonly used in the literature, physical, semi-empirical and empirical. It is proposed a classification for the physical and the semi-empirical models, which are studied in the following chapters. This classification is based on the main factors playing an important role in tyre modelling. These factors include the distribution of the normal pressure over the contact patch, the definition of the friction coefficient at the tyre-road interface and the representation of the tyre carcass. The equations derived as well as the number of parameters involved are taken into account to assess the relative complexity of each model.

1.1 Introduction

The tyre properties play a crucial role when determining ground vehicle dynamic behaviour because the tyre-road interface is the only contact surface with the ground and the major part of the efforts applied to the vehicle passes through the tyre. Due to this fundamental role of tyres, a lot of studies have been focused on the derivation of tyre models. The description of the tyre behaviour on the road can be from simple expressions to more advanced ones, depending on the level of accuracy required for a specific purpose. Thus, several tyre models have been proposed in the literature. One can distinguish two main kinds of models describing the tyre behaviour, the steady-state and the transient dynamics

models. In the sense used in tyre dynamics work [1], the steady-state refers to the situation in which the phase relationships between all motions of the tyre structure are fixed and so, no longer vary with time. In this case, all the vehicle states, speed, yaw rate and path curvature, remain constant. This aspect is more devoted to pure tyre characteristics studies. In the other hand, in transient state, the phase relationship between the motions of the vehicle is varying with time. Thus, the transient investigations deal with forces and deformations at the tyre-road interface arising from road roughness, tyre-wheel assembly non-uniformities, the operating conditions, etc. An overview for transient response can be found in [2]. This chapter is focused exclusively on steady-state tyre models because it corresponds to the thesis requirement defined by Messier-Dowty company. Moreover, it is important to mention that the company has limited the objectives of the study to the tyre steady-state response because there are no measurements data of the tyre transient-dynamic behaviour. Thus, it would not be possible to validate any investigation on the tyre response under this condition.

Among the steady-state models, one can also distinguish the physical, the semi-empirical and the empirical models. The physical models are based on the theory of the tyre physical structure behaviour [3, 4, 5, 6]. Because of the tyre structure complexity, physical models which aim at describing the tyre in great details can become intractable. Thus, assumptions are often made so that they fail to be fully physical and can become semi-empirical or empirical models. The empirical models are mathematical models describing measured tyre characteristics through mathematical formulas and interpolation schemes [7, 8, 9]. These formulas have a given structure and involve parameters which are usually assessed with regression techniques to yield a best fit with measured data. The semi-empirical models are based on use of a number of tyre basic characteristics, typically obtained from measurements, and combined with the theory of the physical tyre structure behaviour [10, 11, 12, 13, 14, 15, 16].

The aim of this chapter is to provide a literature survey of the previous researches in tyre modelling for steady-state responses. Due to the important number of models encountered in the literature, there is a real need to list and classify these models in order to help choosing the appropriate models for the steady-state applications required in the present work. The different models are presented according to the three categories commonly used in the literature, physical, semi-empirical and empirical. The principle of development (assumptions or/and approximations) as well as the conditions of validity of each model are described. Then, based on the main factors playing an important role in tyre modelling, it is proposed a classification for the physical and the semi-empirical

1.2. Main types of tyres

models. These factors include the distribution of the normal pressure over the tyre-road contact patch, the definition of the friction coefficient at the tyre-road interface and the definition of the carcass. The equations derived, the number of parameters involved and the effort required for determining these parameters are taken into account to assess the relative complexity of each model.

The chapter is organized as follows. Section 1.2 presents the main types of tyres that are commonly encountered as well as their particularities. In section 1.3, the tyre orientation, characteristics and operating variables are defined. Then, in section 1.4, the current physical models are reviewed. The motivations and the limitations of these physical models are discussed and a classification is proposed. Section 1.5 is devoted to semi-empirical models and a classification is also provided. Empirical models are presented in section 1.6.

For the sake of clarity, the equations of physical models are voluntarily left out, in order to lighten the description of the models. However, the equations of some models are given in appendix B.

1.2 Main types of tyres

The aircraft tyre is a mechanical structure composed of a flexible carcass of high-tensile-strength cords fastened to steel-cable beads that firmly anchor the assembly to the rim. The behavioral characteristics of a tyre depend on the operating conditions and also on the tyre construction. Indeed, two basic types of tyre construction are broadly available, radial and bias-ply tyres.

Radial tyre

The radial tyre construction is characterized by parallel plies (rubberised fabrics reinforced by cords of nylon, rayon, polyester or fibreglass) running directly from one bead to the other at an angle of 90° to the circumference, figure 1.1A. These plies form the commonly termed tyre carcass. The advantages of this type of carcass construction are the extreme flexibility and the soft ride. The directional stability is ensured by the use of stiff belt fabric or steel wire 2 that runs around the circumference of the tyre between the carcass 5 and the tread 1. The cord angle helps to keep the tread flat during cornering despite the lateral deflection.

Bias tyre

In the bias tyre construction, the carcass is composed of two or more plies extending from bead to bead with the cords at angle of 35 to 40° to the circumference and alternating in direction from ply to ply, figure 1.1B. These cords angle results in soft tyres for ride comfort. Bias-ply carcass is laterally stiffer than a radial ply-carcass. Today, bias tyres are no longer widely used, however, they are still accepted for certain military aircrafts and for some ground vehicles (example of trucks).

Generally speaking, aircraft tyres and most ground vehicle tyres are relatively similar in structure and shape. However, there is a significant difference between their material characteristics and their operating conditions. Indeed, the tyres of most ground vehicle are designed either for high speed and relative low load, example of sport/racing cars (about 320Km/h), or for high load and low velocity, example of earth mover (top speed: 70Km/h, gross weight: 70Tonnes). In the other hand, an aircraft tyre is designed to combine both high load and high speed, example of Airbus A380 (maximum take off speed: 360Km/h, maximum weight: 560Tonnes).

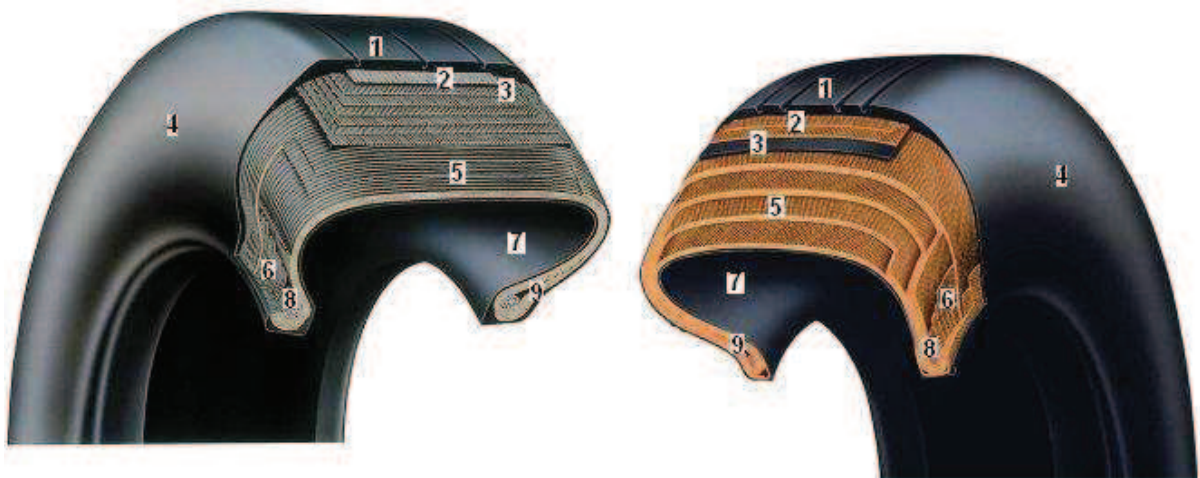


Figure 1.1: A. Radial tyre carcass - B. Belted - bias tyre carcass

- 1 Tread
- 2 Tread reinforcement ply (bias)/Protector ply (radial)
- 3 Undertread
- 4 Sidewall
- 5 Carcass plies

1.3. Definitions of tyre characteristics

- 6 Carcass plies turn-ups
- 7 Liner
- 8 Bead
- 9 Chafer strips (bias)/Flipper strip (radial)

To describe the tyre-road interaction characteristics, there is not a real need to make a distinction between bias and radial tyres. Therefore, such distinction is not made in this report.

1.3 Definitions of tyre characteristics

To describe and compare the literature tyre models, it is first necessary to define the operating variables (parameters), which describe the tyre orientation, motion and shear forces generation in the contact patch. The tyre models will be cast in the same coordinates system with the same operating variables, which are presented next.

1.3.1 Coordinate systems and operating variables

Several coordinate systems are used in tyre modelling and they differ mainly from the tyre orientation and from the sign conventions of the operating variables. Figures A.1 and A.2 in appendix A, describe the coordinate systems commonly used in the literature for tyre modelling. In the present study, ISO coordinate system is adopted (see also figure 1.2).

Besides, figure 1.2 represents a rolling tyre by a string with a given width. This tyre is inclined with respect to the vertical axis by an angle termed camber angle γ . The coordinate system originates at the centre of the contact patch, point C , and $x - y$ axes are in the road plane. The forward velocity V shows an angle, noted α , with respect to the wheel plane which is directed by the longitudinal axis x . This angle α is called side slip angle and results from tyre lateral deflection in the contact patch during cornering manoeuvre for example. Both angles α and γ are considered positive in their respective direction as shown in figure 1.2. V_x and V_y are the wheel velocity components. If a braking or driving torque is applied on the rolling wheel, the tyre material will begin to elongate in the contact patch. This displacement of the tyre material causes the rolling velocity, V_r , to exceed the longitudinal velocity V_x (driving torque) or to decrease relatively to it (braking torque). The difference between rolling velocity and longitudinal velocity represents the longitudinal slip velocity V_{sx} . A normalized parameter, termed longitudinal slip ratio S_L

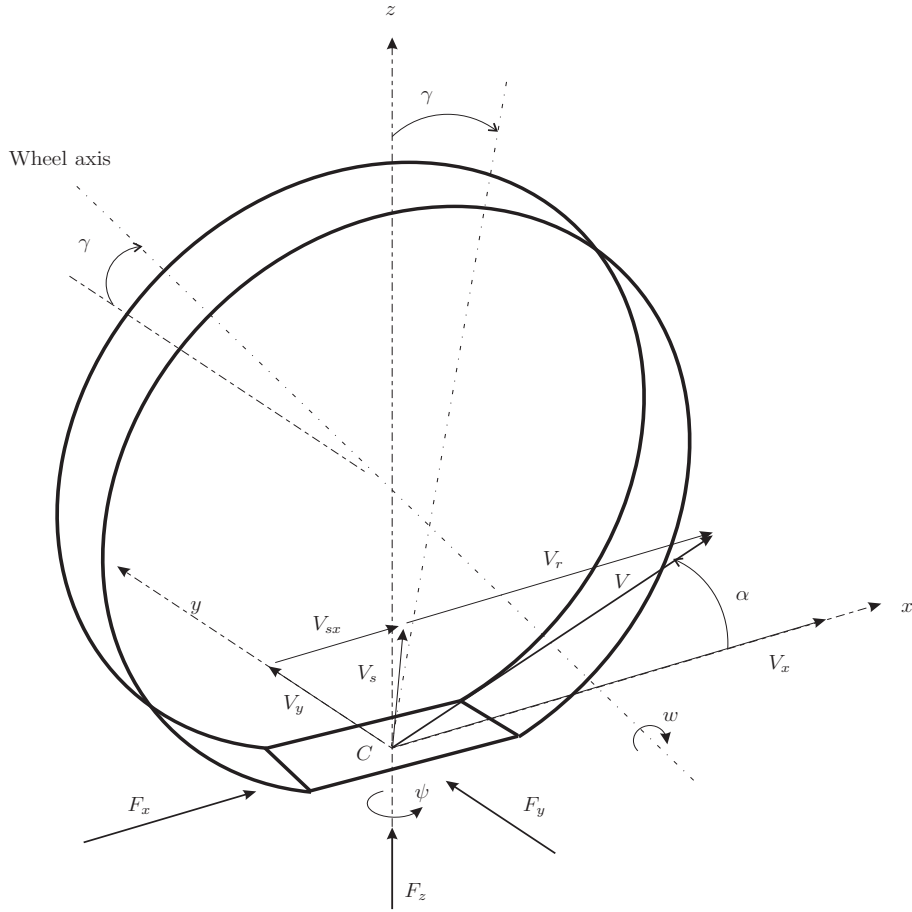


Figure 1.2: ISO tyre coordinate system

is then defined as follows:

$$S_L = -\frac{V_x - V_r}{V_x} = -\frac{V_x - R_e w}{V_x} \quad (\text{longitudinal slip ratio}) \quad (1.1)$$

where w is the wheel angular velocity and R_e , the effective rolling radius, which will be defined in the next paragraph. The following notation is often adopted: $V_{xs} = V_x - V_r$.

The lateral slip ratio, noted S_α , is defined as the ratio of the lateral velocity V_y and the longitudinal one V_x . It also corresponds to the tangent of the side slip angle α , figure 1.2.

$$S_\alpha = \frac{V_y}{V_x} = \tan \alpha \quad (\text{lateral or side slip ratio}) \quad (1.2)$$

The resultant slip velocity V_s and the resultant slip ratio S are defined as follow.

$$V_s = \sqrt{V_{sx}^2 + V_y^2} \quad (1.3)$$

$$S = \sqrt{S_L^2 + S_\alpha^2}$$

1.3. Definitions of tyre characteristics

When an inclined wheel (wheel with camber angle γ) is making a turn along a circular flat surface, it is appropriated to consider the turning motion in the description of the tyre shear forces and moments [17]. The turning motion is the resultant of the camber and the spin angular motion, noted γ and ψ respectively. The turn slip parameter φ is defined as follows:

$$\varphi = \frac{\dot{\psi}}{V_x} - \frac{\dot{V}_r}{V_x} \sin \gamma \quad (1.4)$$

where $\dot{\psi}$ represents the tyre spin angular speed and V_r the rolling velocity.

In steady-state motion condition of the wheel, the spin slip is simply equal to the road curvature: $\frac{\dot{\psi}}{V_x} = \frac{1}{\rho}$, where ρ is the radius of the circular path of the wheel.

1.3.2 Definitions

Free-rolling: it refers to a wheel in motion without driving/braking torque, side slip, camber, or turn slip. In this particular case, the longitudinal velocity V_x is equal to the rolling velocity V_r . The effective-rolling radius R_e is then defined as the ratio the longitudinal velocity V_x of the free-rolling wheel over its angular velocity w .

$$R_e = \frac{V_r}{w} = \frac{V_x}{w} \quad (\text{free-rolling}) \quad (1.5)$$

Pure longitudinal slip: it designates the situation where the wheel is submitted to driving or braking torque exclusively. The tyre deformation in the contact patch is then assumed to be exclusively in the longitudinal direction (x axis) and therefore, only longitudinal force F_x , also termed pure longitudinal force, is developed.

Pure lateral slip: it describes the condition in which the tyre is submitted to a cornering manoeuvre without driving/braking torque, camber and turn slip. The tyre is also said to be at pure side slip or pure cornering condition. The tyre deformation in the contact patch is then considered to be exclusively in the lateral direction (y axis), which induces a side slip angle noted α . This lateral deformation generates a lateral force F_y , also called pure lateral force.

Combined slip: it refers to a situation in which the wheel is submitted to braking or driving torque in combination with cornering manoeuvre.

Longitudinal slip stiffness C_L : it represents the slope at the origin of the curve $F_x = f(S_L)$.

$$C_S = \left. \frac{\partial F_x}{\partial S_L} \right|_{S_L=0, S_\alpha=0} \quad (1.6)$$

Cornering stiffness C_α : it is the slope at the origin of the curve $F_y = f(S_\alpha)$.

$$C_\alpha = \left. \frac{\partial F_y}{\partial S_\alpha} \right|_{S_\alpha=0, S_L=0} \quad (1.7)$$

1.4 Physical models

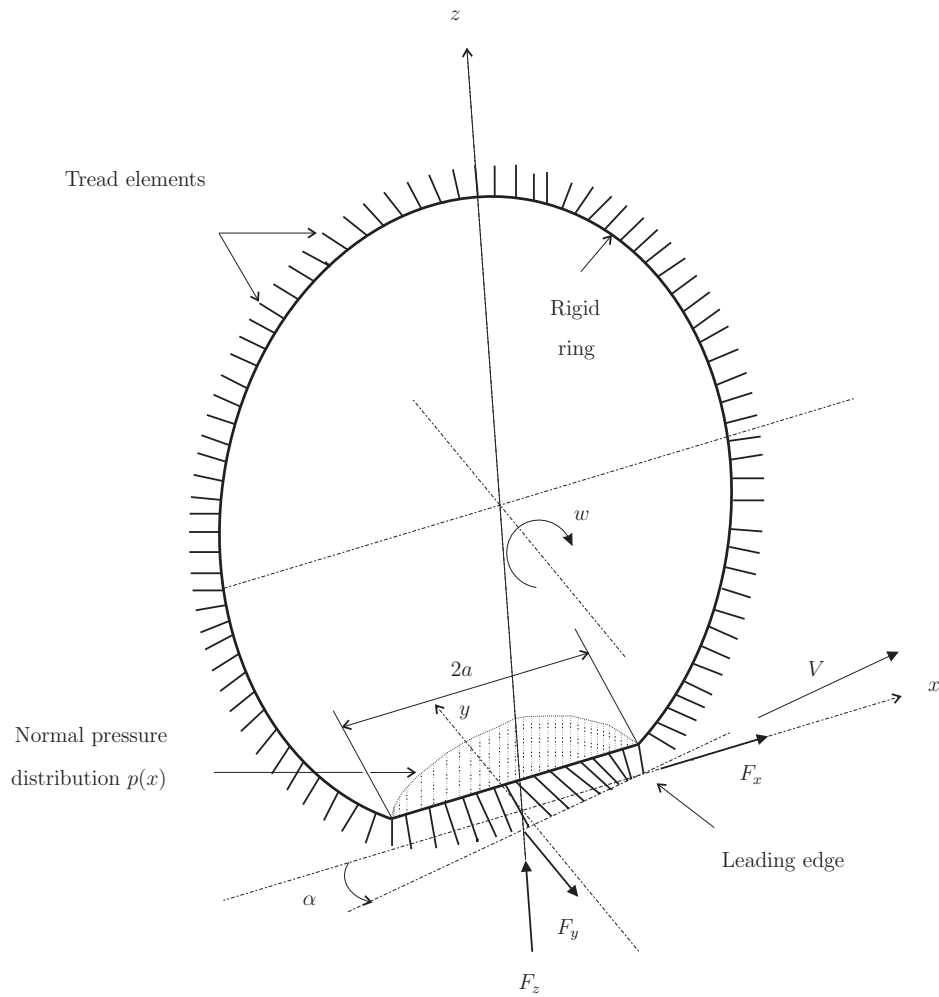
In physical models, the expressions of the tyre characteristics are developed based on tyre displacement in the contact patch, which depends on its physical properties. The main factors playing an important role in physical models development are the friction properties in the tyre-road interface, the distribution of the normal pressure, the compliances of the belt carcass and of the tread band.

Next, the literature survey of mathematical physical models are presented. The final equations of some models are provided in appendix B.1. References which contain description of the theoretical approach and the full equations of each model are also given.

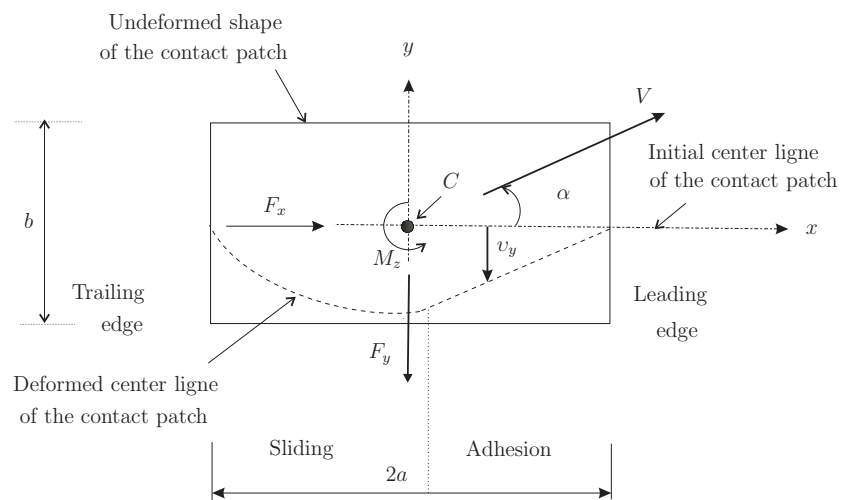
1.4.1 Brush model

The brush model [3, 5, 6, 18] is based on a relative simple representation of the tyre structure and it assumes the tyre to behave as an elastic material. In fact, the tyre tread are represented by an array of small elastic rectangular elements attached to a rigid ring, figure 1.3a.

1.4. Physical models



a) Tyre representation according to brush model



b) Contact patch representation (Top view)

The tread elements form the tread band surface which comes into contact with the road surface. The compliance of these elements is assumed to represent the elasticity of the combination of carcass, belt and actual tread elements of the real tyre. During free rolling of the tyre (that is without action of driving/braking torque, side slip, camber or turning), the wheel moves along a straight line parallel to the ground and in the direction of the wheel plane. In this particular case, the tread elements are deemed vertical and move from the leading edge to the trailing one without horizontal deflection and therefore, without fore/aft or side force. A possible presence of rolling resistance is disregarded and when tread element deflection occurs due to shear force, it is always supposed to be parallel to the road surface. The undeformed contact patch shape is assumed rectangular, figure 1.3b, where the letter a represents its half-length and b its width. A parabolic normal pressure distribution p , which vanishes at the contact entry and exit points, is considered in the contact patch. At small slips (longitudinal and/or lateral slip), the tread band is supposed to be in complete adhesion with the road surface. But, when slips parameters rise, a sliding zone appears from the trailing edge. This sliding zone increases with slips parameters up to full sliding. The tyre forces in the adhesion zone are assumed to be caused by the tyre elastic deformations. In the sliding zone, the tyre forces are caused by sliding friction. The model deals with pure and combined slips conditions.

Several models are derived from the brush model concept and they are presented in the following subsections.

1.4.2 Fiala model

In the Fiala model, the same approach as in the brush model is used to model the tyre structure and its deflection in the contact patch [19]. A parabolic normal pressure distribution over a rectangular contact patch is assumed. The static friction coefficient (friction at zero slip) is used in conjunction with the dynamic one (friction at full sliding) to define a linear friction vs slip velocity. The model equations are developed only for pure slip conditions (longitudinal or lateral slip). The pure lateral force, for example, is a parabolic curve for side slip angle values less than the critical one α^* , and is assumed to be constant (horizontal curve) after this critical value, figure 1.4. It should be noted that Fiala model is actually used by Messier-Dowty company and therefore, it will be further investigated in chapter 2.

1.4. Physical models

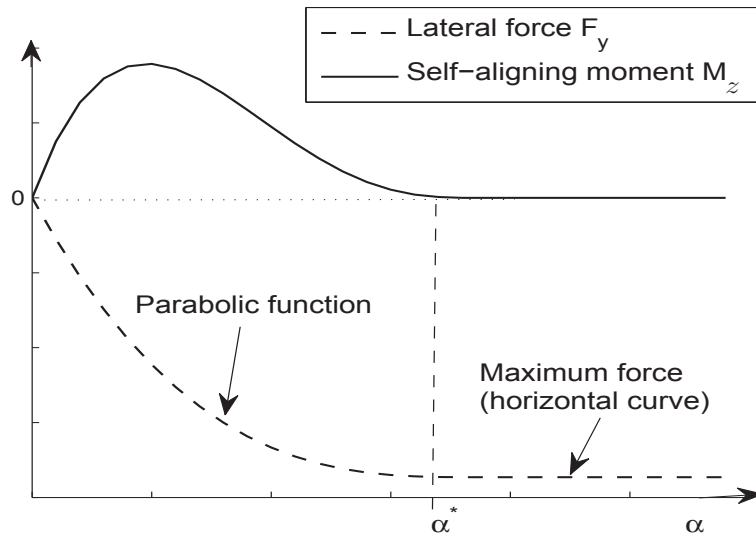


Figure 1.4: Lateral force and self-aligning moment curves shapes according to Fiala tyre model (same shape for brush model)

Next, the elastic beam model that handles differently the tread band modelling is presented.

1.4.3 Elastic beam theory

In the elastic beam theory, the tyre is treated as an elastic beam attached to a fixed base (wheel rim) [20]. In the contact patch, the tyre deflection is described using the classic elastic beam theory. The contact patch is assumed rectangular. If a parabolic normal pressure distribution is supposed, the shape of the tyre lateral displacement in the contact patch is quite similar to that obtained with the brush model as already illustrated in figure 1.3b. In fact, the lateral deflection of the tread band follows a linear shape in the adhesion region of the contact patch. In the sliding zone, the tyre deformation is caused by sliding friction and its shape is mainly governed by the normal pressure distribution. Besides, the model forces and moments equations are developed for pure and combined slips conditions.

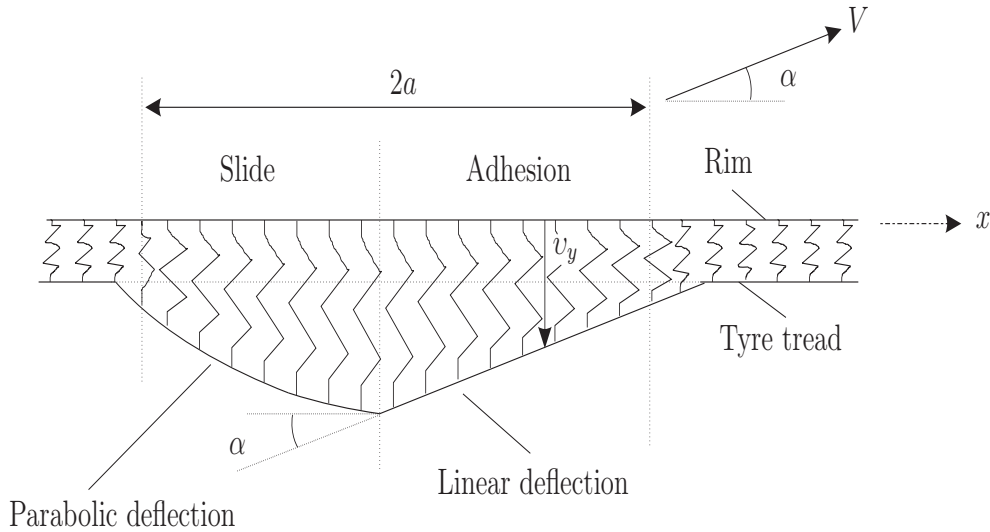


Figure 1.5: Top view of tyre lateral deflection - elastic beam theory

The previous presented models consider the tyre-road contact patch to be possibly divided into two zones, an adhesion zone and a sliding one, with respect to slips parameters. They do not assumed any transition between these two zones. The following models, termed HSRI - NBS, introduce a transition zone in their approach for describing the tyre deformation in the contact patch.

1.4.4 HSRI - NBS models

The United States Highway Safety Research Institute, HSRI, has developed a model termed HSRI-NBS [21]. Three versions are successively presented, each one being an extension of the previous model.

In the first version, HSRI-NBS-I model, the tyre tread are considered as an array of elastic rectangular blocks attached to an elastically supported ring, figure 1.6. The ring, which represents the tyre carcass, has a bending stiffness. It is separated from the rim by a spring foundation which allows to simulate the longitudinal and lateral carcass motion. Similar to the brush model concept, the tread elements form the tread band surface which comes into contact with the road surface and their shear deformations are supposed to be parallel to the road surface. The friction coefficient is supposed to be a linearly decreasing function of sliding speed. A rectangular contact patch, which may be divided into adhesion and sliding zones (relatively to the slips parameters) is also assumed. The normal pressure distribution is deemed uniform over the contact. However, it is found that the approximations made for this model do not allow a derivation of reasonable equations for

1.4. Physical models

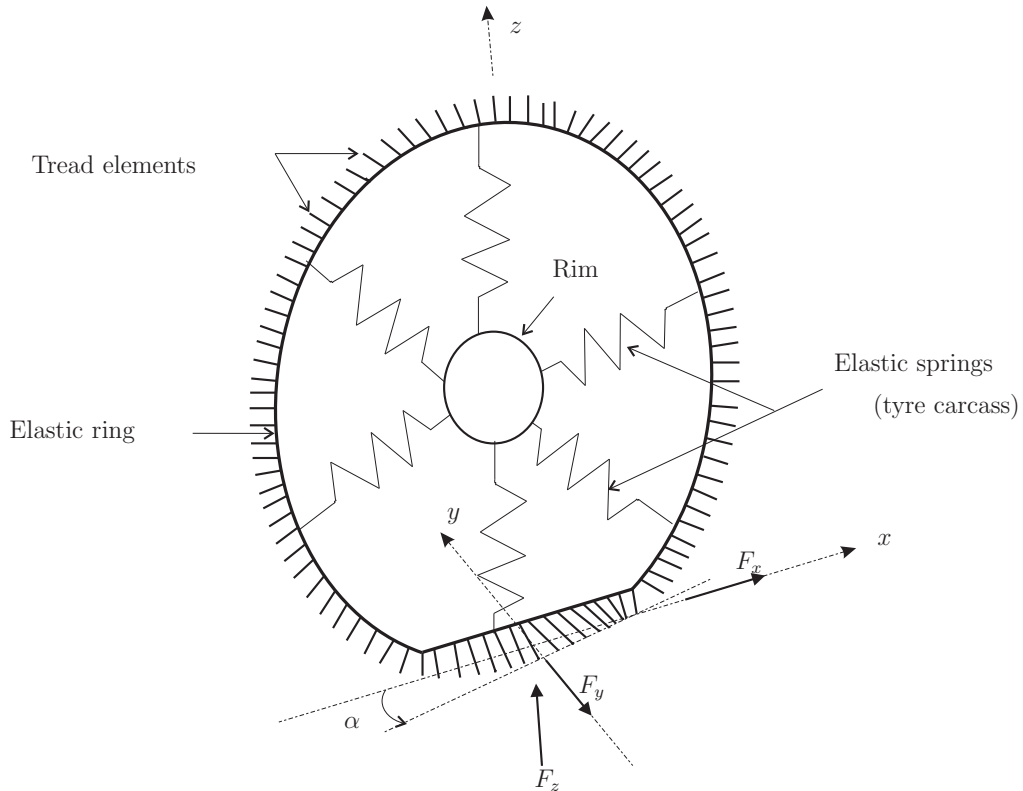


Figure 1.6: Tyre tread, belt and carcass representation - HSRI - NBS models

the tyre characteristics, especially for the self-aligning moment. Thus, a second version, HSRI - NBS- II model, is proposed.

In HSRI-NBS-II model [21], a transition region is introduced between the adhesion and the sliding regions to avoid an abrupt change from adhesion to sliding, figure 1.7. The definitions for the tyre carcass, the tread elements, the normal pressure and the friction coefficients remain the same as in the previous version. Nevertheless, the assumption of uniform normal pressure distribution in the HSRI - NBS-II model is found not to be realistic enough and a third version, HSRI-NBS-III model, is proposed. In this third version, a parabolic normal pressure distribution is assumed and the simulation results were found better when compared to those of the previous versions. The model forces and moments equations are developed for pure and combined slips conditions, see appendix B.1.3.

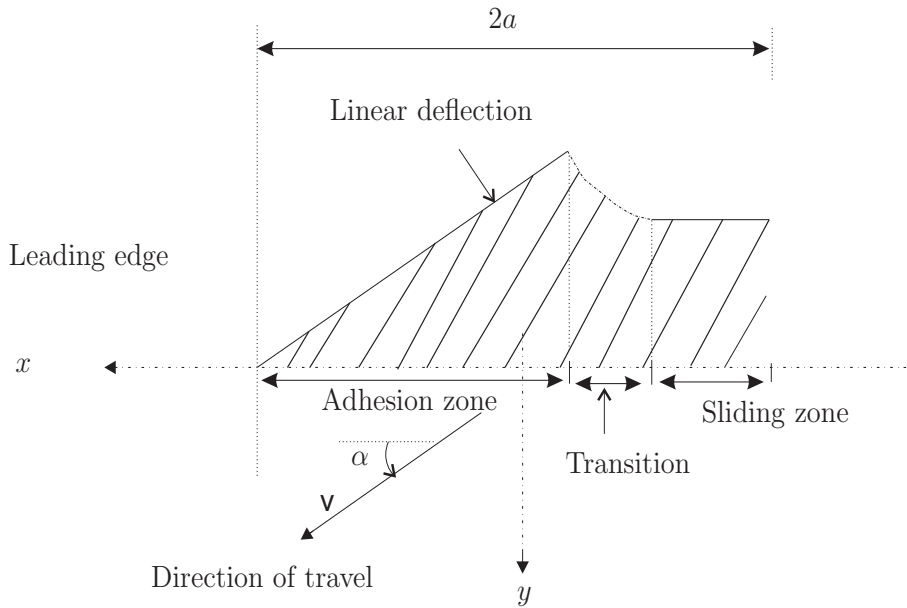


Figure 1.7: Tread deflection in the contact patch - HSRI - NBS model

Sakai model, presented next, uses the brush model concept in combination with the elastic beam theory to defined the tyre structure and its contact with the road.

1.4.5 Model of Sakai

In the model of Sakai [21, 22], the contact patch is represented using the brush model concept, which assumes tread elements to form a rectangular contact with the road surface. The tread elements are considered to be attached to the tyre carcass. The tyre carcass is supposed to behave as an elastic beam. A parabolic normal pressure distribution, which vanishes at the contact entry and exit points, is considered. Besides, a static friction coefficient is assumed in the adhesion zone and an anisotropic sliding friction coefficient in the sliding zone. In combined slip conditions, the lateral force is expressed as function of both longitudinal and lateral slip parameters S_L and S_α , respectively. This expression is presumed to take into account the influence of the braking and driving tractive force (longitudinal force) on lateral force generation. In [21], it is shown that Sakai model provides reasonable modelling results for the traction and cornering forces when compared with measurements data. The models forces and moments equations are developed for pure and combined slips conditions, see appendix B.1.5.

Ratti model, presented below, is also based on brush model concept.

1.4. Physical models

1.4.6 Model of Ratti

In the model of Ratti [23], the tyre structure representation is similar to that of the brush model, except the ring which is supposed flexible with a given stiffness instead of a rigid ring. It is proposed a model, which describes the contact patch dimensions as function of the vertical load and of the tyre vertical stiffness. As in the Sakai model, the lateral force is expressed as function of both longitudinal and lateral slips parameters S_L and S_α , respectively, which is also assumed to take into consideration the influence of the driving/braking tractive force on lateral force generation. The models forces and moments equations are developed for pure and combined slip conditions, see appendix B.1.6.

The tread simulation model, presented next, is a further extension of the brush model which enables to enlarge its application range with finer and more accurate description of the tyre features.

1.4.7 Tread simulation model

In the tread simulation model [10], the contact patch is divided into a number of zones of equal length, in each of which a tread element is followed. In this way, the forces and moments acting on the tread elements are determined while moving through the zones. Then, the total forces and moments are obtained by integration over the entire zones. The belt distortion caused by these forces can be also calculated. The tread simulation model enables to investigate the effects of an arbitrary pressure distribution, the velocity and the pressure dependent friction coefficient, the anisotropic stiffness properties of the tyre, the combined lateral, longitudinal and camber or turn slip and the lateral bending of the tyre carcass. The tread simulation model is actually one of the most advanced mathematical physical models that provide simulation results close to the reality [10].

The next model proposes a new approach for modelling the tyre and the contact patch.

1.4.8 Mathematical-physical 2D tyre model

The mathematical-physical 2D model describes the tyre behaviour using two main elements [24], as illustrated in figure 1.8. In one hand, the tyre structure is modelled by two rigid bodies, a disc and a ring, linked to each other with elastic springs and viscous linear dampers (for dynamic studies). In the other hand, the contact patch is modelled by a number of parallel brush elements which are linked to a flexible truss. The truss is

Chapter 1. Review of tyre models for steady-state responses

supported by a rigid plate which is joined to the ring by residual stiffnesses and damping elements. An arbitrary distributed normal pressure is assumed. The model forces and moments expressions are developed under pure and combined slips conditions, and also take into account the influence of camber, yaw and turn slip.

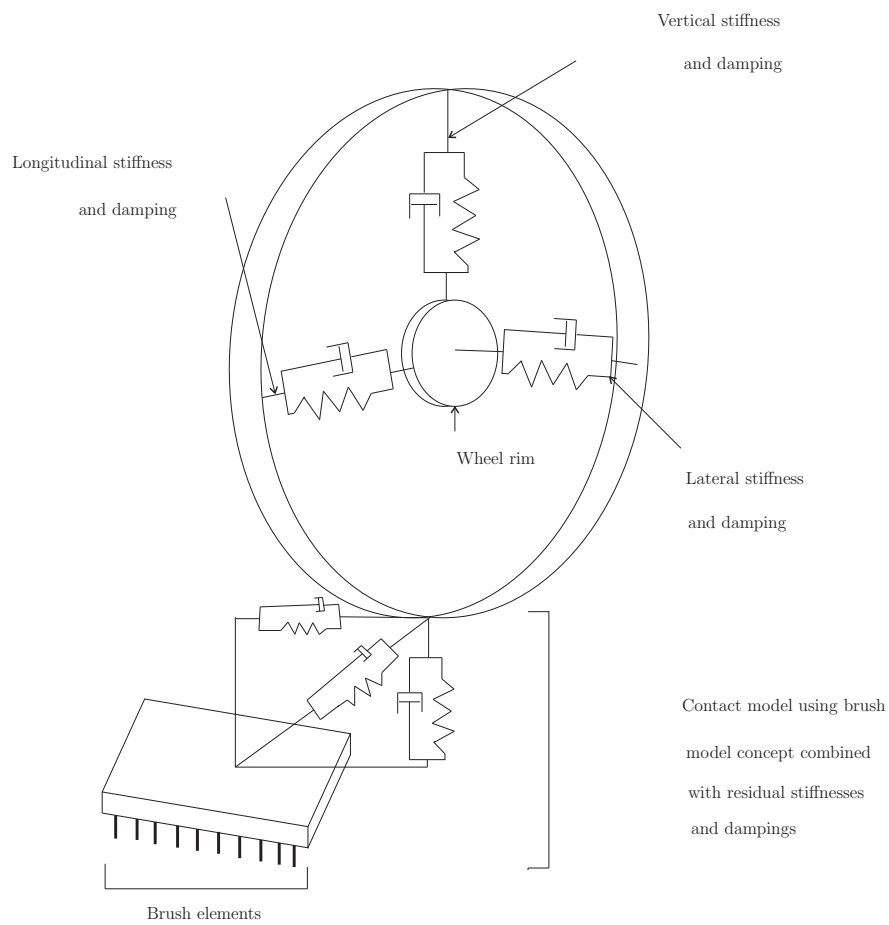







Figure 1.8: Tyre and tyre-road contact representation - Mathematical-physical 2D tyre model

1.4. Physical models

1.4.9 Classification of the physical models

Table 1.1 attempts to provide a classification of the different physical models presented previously. The criteria considered for this classification are the following:

- Definition of the friction coefficient: isotropic or not.
Isotropic friction coefficient would assume same value for friction coefficient in the two directions of the contact patch plane, $\mu = \mu_x = \mu_y$.
- Distribution of the normal pressure: uniform, parabolic or arbitrary.
- Definition of the tyre belt and carcass: flexible or rigid.
- Consideration of the influence of camber γ and yaw ψ angles.
- Complexity: the complexity includes the level of approximation made on the tyre structure, the contact patch modelling and the number of parameters involved in the model equations. It is worth emphasizing that the notion of complexity is very relative because the effort for obtaining required measurements data and the computation time of each model should also be considered as well as the above mentioned criteria. These last two criteria cannot be checked in the case of this study due to a lack of required measurements data. Therefore, they are not considered in the classification. In Table 1.1, the complexity is represented by different bar chart, as explained below:

-  : low complexity model
-  : relative simple model
-  : middle complexity model
-  : high complexity model
-  : very high complexity model









Models	Friction coefficient	Normal pressure	Carcass definition	γ, ψ considered	Complexity
Tread simulation	Anisotropic	Parabolic Arbitrary	Flexible	Yes	
Mathematical physical 2D	Anisotropic	Arbitrary	Flexible	Yes	
HSRI-NBS-III	Isotropic	Parabolic	Flexible	No	
Ratti	Anisotropic	Parabolic Arbitrary	Flexible	Yes	
Sakai	Anisotropic	Parabolic	Flexible	No	
Brush model	Isotropic	Parabolic	Rigid	Yes	
Fiala	Isotropic	Parabolic	Rigid	No	
Beam theory	Isotropic	Parabolic	Rigid	No	

Table 1.1: Classification of physical models

1.4.10 Comments on physical models

Based on the above description of each model, relative realistic approximations of tyre structure would include at least a flexible carcass in addition to the flexibility of the tread band. An assumption of parabolic distribution for the normal pressure would be relatively reasonable while arbitrary or distribution based on interpolation of experiments data might be more realistic. In general, the influence of the carcass definition in the modelling results of physical models is remarkable when computing lateral force and self aligning moment [4, 21]. In fact, it is shown that the modelling results of traction/braking force (longitudinal force) do not show significant difference between both rigid and flexible carcass assumptions. The normal pressure distribution model is a major factor which determines the status of the contact patch: adhesion or/and sliding. Consequently, the normal pressure distribution has a direct influence on physical model capability since their forces and moments development are based on tyre deformations in the contact patch. Besides, in practice, the friction coefficient is more often considered isotropic for most tyre models.

Table 1.1 can be summarized as follows. First, the tread simulation model is stated to be more complex because, in addition to the criteria mentioned in table 1.1, it assumes a friction model which is considered to depend on both sliding speed and normal pressure

1.5. Semi-empirical models

distribution in the contact patch. To achieve the technique which consists in dividing the contact into a number of small zones followed by tread elements, it is required a good knowledge of the tyre features such as the tread band dimensions and properties (compliances), the bending and yaw compliances of the carcass. The computation time will be certainly higher.

In addition to the separated description of the tyre belt and the contact patch in the Mathematical physical 2D model, it is required an important set of specific tyre measurements data (or comparison with results provided by 3D finite element model) for determining the contact properties as well as the main and the residual stiffnesses [24]. It is then classified with a middle complexity.

In the other hand, Fiala model is similar to the brush model. The models of Sakai and Ratti are extensions of the brush model in which the main additional feature is the assumption of a flexible carcass. HSRI-NBS-III model mainly differs from Ratti model by its definition of a transition zone between adhesion and sliding zones. However, when considering a given condition of the tyre modelling, the effort for computing Fiala, Sakai, Ratti, HSRI-NBS-III and brush models may be considered to be the same, even though they would not give exactly the same modelling results. They are classified with low complexity.

In the literature, the development of some models is achieved by combining the physical approaches with tendency of observed data. These models are termed semi-empirical models and are presented in the next section.

1.5 Semi-empirical models

The semi-empirical models are an alternative to the physical models. Indeed, they are based on observed data and also contain structures that find their origin in physical models. The main objective of this category of models is to provide a relative accurate description of the tyre behaviour based on observed data and by using parameters that are physically related to the tyre and the tyre-road interface properties. Each model forces and moments are expressed using some of the physical parameters defined in section 1.3 in combination with empirical parameters, which can be considered as fitting parameters without physical meanings. In the next subsections, the semi-empirical functions proposed in the literature for modelling the tyre shear forces and moments are shown.

1.5.1 Model of Smiley and Horne

In [25], Smiley and Horne propose empirical expressions for the nonrolling and rolling tyre characteristics. Efforts are made to express the tyre static and dynamic responses as function of the tyre. However, these expressions derived from interpolation of bias aircraft tyres around 1960. Nevertheless, a general expression is derived for the lateral force at pure lateral slip condition [4]:

$$F_y = -C_\alpha \alpha \left(1 - \frac{\alpha^2}{3(\alpha^*)^2}\right) \quad \text{if } \alpha \leq \alpha^*,$$

$$F_y = -\mu F_z \operatorname{sgn}(\alpha) \quad \text{else}$$
(1.8)

where $\alpha^* = \frac{3\mu F_z}{2C_\alpha}$ is the critical side slip angle.

The expressions of Somieski model presented below are also based on the definition of critical slip angle.

1.5.2 Somieski model

The nonlinear mathematical model of Somieski [15] proposes the following expressions for the lateral force F_y and the self aligning moment M_z at pure lateral slip condition:

$$F_y = -C_\alpha \alpha F_z \quad \text{for } \alpha \leq \alpha^*$$

$$F_y = -C_\alpha \alpha^* F_z \operatorname{sgn}(\alpha) \quad \text{for } \alpha \geq \alpha^*$$

$$\frac{M_z}{F_z} = C_{M\alpha} \frac{\alpha_g}{180} \sin\left(\frac{180\alpha}{\alpha_g}\right) \quad \text{for } \alpha \leq \alpha_g$$

$$M_z = 0 \quad \text{else}$$
(1.9)
(1.10)

where α_g is the critical slip angle for the self-aligning moment, α^* the critical slip angle for lateral force, C_α the cornering stiffness and $C_{M\alpha}$, the self-aligning moment derivative parameter.

Next, the model of Shim and Margolis is presented.

1.5.3 Model of Shim and Margolis

The analytical model proposed by Shim and Margolis [14] describes the pure driving/braking, pure cornering and combined slip tyre shear longitudinal and lateral forces. The model is

1.5. Semi-empirical models

described belows:

- At pure longitudinal or lateral slip condition the shear forces are expressed as follows:

$$F_{xo} = \mu_{pm} F_{zo} \frac{F_z \mu_p S_L}{F_{zo} \mu_{pm} S_{Lo}} \quad (1.11)$$

$$F_{yo} = -C_\alpha \alpha_o F_{zo} \frac{F_z \mu_p \alpha}{F_{zo} \mu_{pm} \alpha_o \operatorname{sgn}(\alpha)_o}$$

where F_{xo} and F_{yo} designate the pure longitudinal and the pure lateral force respectively.

- For a tyre rolling at pure slip condition with a camber angle γ , the shear forces become:

$$F_x = F_{xo} \cos \gamma \quad (1.12)$$

$$F_y = F_{yo} \sin \gamma$$

- In combined slip conditions, normalized expressions are proposed for the longitudinal and lateral forces F_x and F_y , respectively, as follows:

$$\bar{F}_x = \bar{S}_L \bar{\mu}_p \bar{F}_z \left[\frac{n^2(1 - \bar{\alpha}^2)}{n^2 - \bar{\alpha}^4} \right]^{\frac{1}{2}} \quad (1.13)$$

$$\bar{F}_y = \bar{\alpha} \bar{\mu}_p \bar{F}_z \left[\frac{n^2 - \bar{\alpha}^4(1 - \bar{S}_L^2) - \bar{\alpha}^2 \bar{S}_L^2}{n^2 - \bar{\alpha}^4} \right]^{\frac{1}{2}}$$

where:

- n the shape factor,
- μ_{pm} the maximum friction coefficient, about 1.05 for a dry road,
- μ_p the maximum friction coefficient under current road conditions,
- F_{zo} the nominal vertical load,
- F_z the actual vertical load,
- S_{Lo} the longitudinal slip ratio at which the pure traction force is maximum,
- α_o the lateral slip angle at which the pure lateral force is maximum,
- C_α the cornering stiffness.

$$\bar{F}_y = \frac{F_y}{C_\alpha \alpha_o}; \quad \bar{S}_L = \frac{S_L}{S_{Lo}}; \quad \bar{\alpha} = \frac{\alpha}{\alpha_o}; \quad \bar{F}_z = \frac{F_z}{F_{zo}}; \quad \bar{\mu}_p = \frac{\mu_p}{\mu_{pm}}; \quad \bar{F}_x = \frac{F_x}{\mu_{pm} F_{zo}}$$

The unified semi-empirical model, presented next, is also based on the used of normalized slip parameters.

1.5.4 Unified semi-empirical model

The unified semi-empirical model proposes expressions for the tyre shear forces where the slip parameters are normalized with the vertical load [13]. The longitudinal and lateral forces, F_x and F_y respectively, are proposed in both pure and combined slip conditions as follows:

$$\begin{aligned}\bar{F}_x &= 1 - \exp(-\phi_x - E_1\phi_x^2 - (E_1^2 + \frac{1}{12})\phi_x^3) \\ \bar{F}_y &= 1 - \exp(-\phi_y - E_1\phi_y^2 - (E_1^2 + \frac{1}{12})\phi_y^3)\end{aligned}\tag{1.14}$$

The normalized resultant force in combined slip condition is then derived:

$$\bar{F} = 1 - \exp(-\phi - E_1\phi^2 - (E_1^2 + \frac{1}{12})\phi^3)$$

where:

$$\phi_x = \frac{C_S S_L}{\mu_x F_z} \quad \text{the normalized longitudinal slip ratio,}$$

$$\phi_y = \frac{C_\alpha S_\alpha}{\mu_y F_z} \quad \text{the normalized lateral slip,}$$

$$\phi = \sqrt{\phi_x^2 + \phi_y^2} \quad \text{the normalized resultant slip.}$$

The parameter E_1 is given by $E_1 = \frac{0.5}{1 + \exp(-(F_z - a_1)/a_2)}$, where $a_{1,2}$ are constant.

Remark: The same approach based on normalizing the shear forces and moments expressions is also presented by Milliken in [26].

Next, the model of Dugoff is presented.

1.5.5 Model of Dugoff

In the model of Dugoff [3], the longitudinal and lateral forces F_x and F_y , respectively, in combined slip condition are expressed as follows:

$$\begin{aligned}F_x &= C_S \frac{S_L}{1 + S_L} f(\lambda) \\ F_y &= -C_\alpha \frac{\tan(\alpha)}{1 + S_L} f(\lambda)\end{aligned}\tag{1.15}$$

1.5. Semi-empirical models

where

$$\lambda = \frac{\mu F_z (1 + S_L)}{2 [(C_S S_L)^2 + (C_\alpha \tan(\alpha))^2]^{\frac{1}{2}}}$$

and

$$\begin{aligned} f(\lambda) &= (2 - \lambda)\lambda & \text{if } \lambda < 1 \\ f(\lambda) &= 1 & \text{if } \lambda \geq 1 \end{aligned} \tag{1.16}$$

$f(\lambda)$ is somewhat a weighting function, which adjusts the friction coefficient with respect to the vertical load F_z and the tyre slip parameters.

The model of Kamm is presented next.

1.5.6 Model of Kamm

The model of Kamm [4] is based on the slip-circle concept. In the slip-circle concept, the curve of the lateral force plotted against the longitudinal force (or inversely) is assumed to be inside a portion of a circle. The slip-circle concept is also termed the friction circle concept. The model proposes the resultant force F in combined slip condition as function of the longitudinal force (or the lateral force) and the slip parameters.

$$\begin{aligned} \text{Longitudinal force: } & F_x = F(S) \frac{S_L}{S} \\ \text{Lateral force: } & F_y = k_s F(S) \frac{S_\alpha}{S} \end{aligned} \tag{1.17}$$

where F is the resultant force, $S = \sqrt{S_L^2 + S_\alpha^2}$ and k_s a correlative factor.

In the model presented next, the tyre shear forces in combined slip condition are proposed as function of those at pure slip condition.

1.5.7 Nicholas and Comstock model

In the model of Nicholas and Comstock [4], it is assumed that a relationship exists between shear forces at pure and in combined slip conditions. Moreover, in combined slip conditions, the model considers the longitudinal slip has an influence on the lateral force

generation and inversely. The longitudinal and lateral shear forces in combined slip condition are then proposed as follows:

$$\begin{aligned}
 \text{Longitudinal force: } F_x(S_L, S_\alpha) &= \frac{F_x(S_L) F_y(S_\alpha) S_L}{\sqrt{S_L^2 F_y^2(S_\alpha) + \tan^2(\alpha) F_x^2(S_L)}} \\
 \text{Lateral force: } F_y(S_L, S_\alpha) &= \frac{F_x(S_L) F_y(S_\alpha) \tan(\alpha)}{\sqrt{S_L^2 F_y^2(S_\alpha) + \tan^2(\alpha) F_x^2(S_L)}}
 \end{aligned} \tag{1.18}$$

where $F_x(S_L)$ and $F_y(S_\alpha)$ designate respectively the pure longitudinal and the pure lateral forces. $F_x(S_L, S_\alpha)$ and $F_y(S_L, S_\alpha)$ represent respectively the longitudinal and the lateral forces at combined slip condition.

Next, the model of Rimondi and Gavardi is presented.

1.5.8 Model of Rimondi and Gavardi

In the model of Rimondi and Gavardi [9], the longitudinal force F_x and the lateral force F_y are expressed using exponential function.

$$\begin{aligned}
 F_y &= \mu F_\mu \left[1 - \exp \left\{ -\frac{C_{\alpha\alpha}}{\mu F_z} \left(1 + A \frac{C_{\alpha\alpha}}{\mu F_z} \right) \right\} \right] \\
 F_x &= C_S \exp(-A\sqrt{\kappa}) + \mu F_z \left(1 - \exp\left(\frac{C_{S\kappa}}{\mu F_z}\right) \right) \left(1 - \exp(-A\sqrt{\kappa}) \right)
 \end{aligned} \tag{1.19}$$

where A is a shape factor that is supposed to depend on the vertical load F_z and $\kappa = -S_L$.

The model Schieschke is presented below.

1.5.9 Model of Schieschke

In the model of Schieschke [7], the lateral force is expressed by using 2-order polynomial functions, which are defined with respect to a critical slip angle $\alpha^o = -\frac{a_1}{2a_2}$.

$$\begin{aligned}
 F_y &= a_1\alpha + a_2\alpha^2 \quad \text{for } \alpha \leq \alpha^o \\
 F_y &= a_1\alpha_1 + a_2\alpha_1^2 \quad \text{for } \alpha > \alpha^o \\
 \alpha_1 &= \alpha_s - (\alpha_s - \alpha^o) \exp[-(\alpha - \alpha^o)/(\alpha_s - \alpha^o)]
 \end{aligned}$$

1.5. Semi-empirical models

where $a_1 = C_\alpha$ (cornering stiffness) and $a_2 = \frac{-1}{4C_\alpha^2 F_y^*}$. α_s is the side slip angle at which F_y reaches its asymptotic value F_y^* .

A common used model, termed Magic Formula, is presented next.

1.5.10 Magic Formula

The Magic Formula is a widely used tyre model which permits to calculate the tyre forces and the moments in various conditions [27]. It was first an empirical model based on a $\sin(\text{atan})$ function and was used for pure longitudinal or lateral slip condition. The original function is presented below:

$$y(x) = D \sin[C \arctan(Bx - E(Bx - \arctan(Bx)))]$$

$$Y(X) = y(x) + S_v \tag{1.20}$$

$$x = X + S_h$$

where

- B the stiffness factor,
- C the shape factor,
- D the peak value,
- E the curvature factor,
- S_h the horizontal shift,
- S_v the vertical shift,
- Y the model output F_x , F_y or M_z ,
- X the input variable S_α or S_L .
- BCD the slope at the origin ($x = 0, y = 0$)

Figure 1.9 illustrates an example of a shear force representation by Magic Formula, where y_s is the asymptotic value at large slip values, $y_s = D \sin(\pi C/2)$ and x_m the input variable at which the shear force reaches its peak value D .

Then, several versions of Magic Formula in which its use is extended to combined longitudinal and lateral slip, camber or turn slip situation are proposed from a physical view point [10, 11, 27, 28]. The equations derived include then a set of an important number of fitting micro-coefficients which have to be determined from experiments data. Nevertheless, it provides simulation results that better fit measurements data. The equations of the shear forces and moment at both pure longitudinal and lateral slip conditions of the

2002 version of Magic Formula model [10] are presented in appendix B.1.7.

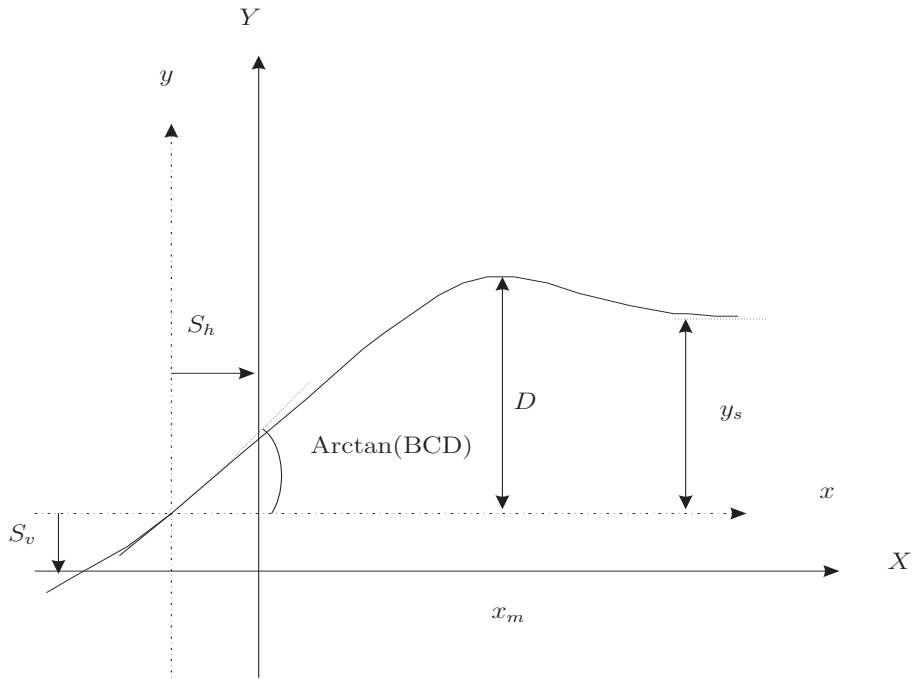


Figure 1.9: Example a shear force representation by Magic Formula

Remark:

Some other models propose new approaches for modelling the tyre shear forces and moments. For instance, the similarity method [7, 29] is based on the observation that the pure slip curves remain approximately similar in shape when the tyre runs at conditions different from the reference one. The reference condition refers to the tyre running at its nominal load, at zero camber angle, at either free rolling or at zero side slip angle and on a given flat road surface. The equations of the forces and moments, in the current slip situation, are then proposed as functions of those in the reference condition. The Dihua model, proposed in [16], uses the tread simulation model concept (Section 1.4.7) which consists in dividing the contact length into a number of equal elements. Then, functions are proposed for each shear force and moment developed in each element. The total force and moment are obtained by summing the contribution of each element. In tyre model TMeasy [30], the shear force characteristic (curve) is divided into mainly four parts. The limits of each part are defined such that an interpolation function (parabolic function or rational function) would fit the corresponding portion of curve. At pure slip condition, the self-aligning moment is proposed as the product of the lateral force and a pneumatic trail. For they are similar to at least one of the already presented models and therefore

1.5. Semi-empirical models

do not provide new relevant features, and also for clarity reason, a full description of the models mentioned in this paragraph are not presented.

Besides, providing modelling results of semi-empirical models would be the best way to compare them. Due to the lack of required measurements data, it is just chosen to list semi-empirical models in table 1.2 in which information about each model complexity is given by the same bar chart as already described in section 1.4.9. It is also mentioned whether the model takes into account the influence of camber and turn slip.











Models	Camber γ	Complexity
Magic Formula	Yes	
TMeasy	Yes	
Rimondi and Gavardi	No	
Unified semi-empirical	No	
Nicholas and Comstock	Yes	
Kamm	No	
Dugoff	No	
Shim and Margolis	Yes	
Smiley and Horne	Yes	
Somieski	No	

Table 1.2: Semi-empirical models

Based on the classification criteria, table 1.2 can be summed up as follows.

Firstly, the Magic Formula has been classified with high complexity. Indeed, a significant effort is required to estimate the model set of fitting parameters as well as their variation limits. Due to the important number of these parameters (see late version of Magic Formula in [10]), the required effort is clearly greater than the one required for the other models presented in table 1.2. In the other hand, when considering the expressions of the remaining semi-empirical models, it can be underlined that they are represented by relative simple functions and therefore, they can be associated with the same complexity bar chart.

The next section presents models that describe the tyre properties based exclusively on interpolation of experiments data. These models are known as empirical models.

1.6 Empirical models

The empirical models are based on mathematical functions that describe the tyre characteristics by interpolation schemes. Indeed, these functions have a given structure (polynomial, exponential, ...) and possess parameters which are assessed by regression techniques to yield a best fit to the measured data [7, 8, 9]. An important number of experiments data are often required to establish the model range of application and validity. As in the semi-empirical models, the development of the different equations are based on the tendency of tyre characteristics curves. The parameters involved in empirical models do not necessary have any physical meaning and do not describe any features of the contact patch or of the tyre structure. The empirical models proposed in the literature are listed in table 1.3. The literature does not show relevant references with application of the listed empirical models and therefore, they cannot be reasonably compared to each other as well as it is hard to state on their level of complexity. Thus, it is chosen to only list these models.

1.7. Conclusion

Models	Equations
<p>Model of Chiesa [4] In combined slip condition, the lateral force F_y is proposed as a n-order polynomial function of the slip angle α. F_x is supposed known.</p>	$F_y = \sqrt{1 - \left(\frac{F_x}{2\mu F_z}\right)^n} F_z ((a_1 + a_2 F_z)\alpha + (a_3 + a_4 F_z)\alpha^2 + \dots)$ <p>where $a_{1,2,3,\dots}$ are constant (coefficients), F_z is the normal force and μ the friction coefficient.</p>
<p>Model of Holmes [4] At pure lateral slip condition, the lateral force F_y is given as a polynomial function of the side slip angle α and the longitudinal velocity V_x.</p>	$F_y = a_0 + a_1 V_x + a_2 V_x^2 + a_3 a_4 \alpha^2 + a_5 \alpha^3 + a_6 Q + a_7 P$ <p>where P is the tyre-pattern constant, Q a tyre-tread constant. The coefficients $a_{1,\dots,7}$ are constant.</p>
<p>Model of Burckhardt [4] In combined slip condition, the resultant force F is supposed to be an exponential function of the resultant slip S and the tread elements lateral deflection v_y.</p>	$F = (a_1(1 - e^{a_2 S}) - a_3 S)e^{-c_4 S v_y}(1 - c_5 F_z^2)$ <p>where $a_{1,2,3}$ and $c_{4,5}$ are constant.</p>
<p>Model of Szostak [8] In combined slip condition, the resultant force F is expressed as a rational function. This expression can also be extended to the longitudinal and lateral tyre forces, F_x and F_y respectively, by replacing the combined slip parameter σ with σ_x or σ_y.</p>	$F = \mu F_z \frac{a_1 \sigma^3 + a_2 \sigma^2 + C \sigma / \mu F_z}{a_1 \sigma^3 + a_3 \sigma^2 + a_4 \sigma + 1}$ <p>a_1, a_2, a_3, a_4 are constant, C is the slope at the origin of F curve as function of σ. $\sigma_x = \frac{S_L}{1 - S_L}$; $\sigma_y = -\tan \alpha$; $\sigma = \sqrt{\sigma_x^2 + \sigma_y^2}$</p>

Table 1.3: The empirical models and their equations

1.7 Conclusion

From the present study, it can be underlined that the organisation of the models into the three categories, physical, semi-empirical and empirical, helps to compare them to each other but, it does not provide enough information for choosing a model for a given application. In fact, due to the complexity of the tyre structure and its behaviour, each model from the same category shows more or less significant particularity. Indeed, each

physical model proposes a different approach in the tyre structure description, and each semi-empirical or empirical model uses a different form of function for representing the tyre-road interface shear forces and moments. The classification provided in tables 1.1 and 1.2 attempts to underline these particularities by appreciating each model according to its specific approach. Based on these classifications in combination with the literature description of each model, it can be underlined that more a model is accurate, more it involves advanced and complex approach and consequently, complex equations are derived. It is then clear that choosing a tyre model requires the following considerations. If the time and the measurements data constraints do not constitute a drawback and if a precise description of the tyre physical parameters (example of material stiffnesses) is required, then, advanced physical models are suitable. However, a too comprehensive physical model can sometime lead to an inefficient use of computation time and resources. In this case, a suitable semi-empirical model may lead to more appropriate compromise. If the purpose is only a rough description of the tyre physical behaviour, a simple physical or semi-empirical model may be considered. Finally, if physical interpretation of the results and parameters used is not required, then empirical models may be studied.

In the context of this thesis, Messier-Dowty company is interested in physical oriented tyre models. The possibility to physically interpret the majority of a model parameters will be considered and thus, the suitable model(s) would either be physical or semi-empirical.

In the next chapter, based on the above description of the steady-state tyre models and the objectives of the present work, some physical models are a priori chosen and investigated.

CHAPTER 2

Choosing suitable physical models

In chapter 1, the current steady-state tyre models are reviewed and a classification is proposed. The present chapter aims at taking this classification into account in combination with the needs of the study in order to choose suitable model(s) for modelling the tyre characteristics in the required conditions. For this purpose, the physical category of models are first investigated and an a priori choice of models is given. They are Sakai and HSRI-NBS-III. The model of Fiala, actually used by Messier-Dowty, is also investigated. The modelling results of the three models are compared to measurements data. Then, their limitations are underlined. Propositions for improving and extending them are also carried out and discussed. The different modelling results presented in this chapter mainly concern pure cornering because the available measurements data, which can be used for the validation, are limited to this condition (pure cornering).

2.1 Introduction

The review of existing steady-state tyre models presented in chapter 1 has clearly underlined the large spectrum of these models and their conditions of validity. It is shown that for the same application, several models based on different approaches are available. These approaches can be distinguished in the following manner. In one hand, there are simple models which rely on considerable simplification of the tyre structure representation and the development of the equations. In the other hand, there are extensive and complex models with relative high accuracy and prediction capability. It is shown that choosing a tyre model requires first the consideration of a certain number of practical constraints, such as measurements data, time, physical meaning of parameters involved and the level of accuracy required for the model responses. Since the ability to physically interpret the model(s) parameters is required in the scope of this thesis (defined by Messier-Dowty

company), models based on physical approaches will be first preferred. Then, the measurements data constraint has to be considered for the available data are limited. The accuracy of the desired model will be determined by the possibility of estimating its parameters.

The aim of this chapter is first to make an a priori choice of physical oriented tyre models capable of representing the steady-state forces and moments of an aircraft tyre during its manoeuvres conditions such as pure driving/braking, pure cornering, combined slip and parking. Then, the modelling results of the a priori chosen models will be compared to measurements data in order to validate this choice. A more appropriate compromise between modelling results agreement with measurements data and the above mentioned practical constraints will be considered.

Since the choice of an a priori model should take into account the possibility to validate it, the different types of measurements data available in the context of this study and which could be used for validating a model are first presented, section 2.2. Then, physical category models are investigated in section 2.3. The modelling results of a priori chosen physical models are discussed in section 2.4 and their limitations are underlined in section 2.5. Finally, in section 2.6, an extension of the Fiala model is proposed in order to improve its representativeness.

2.2 Available measurements data

The available measurements data are presented below according to the type of manoeuvre performed on the wheel.

◇ *Pure cornering*

Pure cornering has been performed on a civil aircraft wheel (tyre) mounted on a test bench (flat-track type). Three different inflation pressures, 11.3 bars, 14 bars and 16 bars, are considered. The nominal inflation pressure of the tyre is 16 bars. At each inflation pressure, the longitudinal force F_x , the lateral force F_y and the self-aligning moment M_z data are recorded vs the side slip angle α , $0 \leq \alpha \leq 20^\circ$, in steady-state conditions. The experiment is repeated for five different vertical loads, $24.4kN$, $68.3kN$, $112.2kN$, $156kN$ and $200kN$. During each test, the vertical load is kept constant as well as the forward velocity, $V = 8m/s$. No driving/braking torque, camber or turn slip is applied on the wheel.

◇ *Static longitudinal loading*

The static longitudinal loading has consisted in mounting the tyre on a test bench

2.2. Available measurements data

and loading it at the desired vertical load F_z . The rotational movement is blocked, $w = 0$. The part of the test bench that represents the road is gradually displaced in the longitudinal direction while recording the longitudinal force vs the longitudinal displacement. The test is repeated for the same inflation pressures and vertical loads already mentioned at the pure cornering condition. The tyre longitudinal carcass stiffness k_x is derived as the slope at the origin of the curve representing the longitudinal static force F_x vs the longitudinal displacement v_x .

◇ *Static lateral loading*

The static lateral loading test procedure is the same as in the case of static longitudinal loading except that the test bench displacement is performed in the lateral direction. The lateral force is then recorded vs the lateral displacement. The experiment is repeated for inflation pressures 14 bars and 16 bars, and for vertical loads already mentioned at the pure cornering condition. The tyre lateral stiffness k_y is derived as the slope at the origin of the curve representing the static lateral force F_y vs the lateral displacement v_y .

◇ *Torsion torque*

After setting the tyre at the desired inflation pressure and vertical load, a torsion torque is applied relatively to the vertical axis of the unrolling wheel. The torsion torque is then recorded vs the torsion angle. The tyre torsional stiffness k_ψ is derived as the slope at the origin of the curve representing the torsion torque vs the torsion angle. Inflation pressures 14 bars and 16 bars are used. The vertical loads are the same as those used at the pure cornering condition.

It can be underlined that the measurements data presented above concern only pure cornering and static loading conditions. When considering the tyre run types which should be studied in this thesis, it is remarked that measurements data are not available for the pure driving/braking, the combined slip and parking conditions. Therefore, it will not be possible to validate any model representativeness of tyre in the mentioned conditions.

Next, the above measurements data are taken into account to choose a priori suitable physical models.

2.3 A priori choice of suitable physical models

The main criteria for choosing appropriate models are the tyre run types conditions, the models structural requirement (physical based models in the present case) and the measurements data constraints. The structural criterion can be answered by considering the physical category of models enumerated in table 1.1 from chapter 1, section 1.4.9. All the models presented in this table allow the simulation of the pure cornering, the pure driving/braking. Except Fiala model, all of them also deal with the combined slip. Based on the literature description of the physical models, a first a priori choice of model would be Tread simulation model because it is found to be the more advanced physical model which provides modelling results close to the reality [10]. However, the measurements data required for estimating this model parameters cannot be satisfied in the context of this study, especially the tyre structure properties (carcass and tread stiffnesses) and the contact patch properties (anisotropic friction coefficients, precise normal pressure distribution over the contact, etc). In the same manner, when considering the Mathematical physical 2D model, the available measurements data do not allow the determination of the main and residual stiffnesses as well as the tyre tread stiffnesses.

Sakai and HSRI-NBS-III models are studied and compared in [21] for passenger car tyres, and they can be considered to present relative acceptable compromise between tyre structure representation and measurements data requirement. Ratti and HSRI-NBS-III models are similar, except the definition of a transition region between adhesion and sliding zones of the contact patch in HSRI-NBS-III model. Therefore, HSRI-NBS-III model may be expected to provide either similar or better modelling results relative to Ratti model. Moreover, the measurements data required for estimating Sakai, HSRI-NBS-III and Ratti models can satisfied in the context of the study. The a priori choice would then be Sakai and HSRI-NBS-III models. Fiala model is actually used by Messier-Dowty company and will be used in addition to Sakai and HSRI-NBS-III models for comparison.

In the next section, the complete forces and moments expressions of each a priori chosen model are first presented.

2.3.1 Sakai model

The final expressions for the longitudinal force F_x , the lateral force F_y and the self aligning moment M_z are reminded below.

2.3. A priori choice of suitable physical models

- Tyre forces and moment before full sliding ($0 < \xi_a \leq 2a$)

$$F_x = C_S \frac{S_L}{1 - S_L} \left(\frac{\xi_a}{2a}\right)^2 - \mu_x F_z \frac{S_L}{\sqrt{S_L^2 + S_\alpha^2}} \left[1 - 3\left(\frac{\xi_a}{2a}\right)^2 + 2\left(\frac{\xi_a}{2a}\right)^3\right]$$

$$F_y = -(C_\alpha + C_S S_L) \frac{S_\alpha}{1 - S_L} \left(\frac{\xi_a}{2a}\right)^2 - \mu_y F_z \frac{S_\alpha}{\sqrt{S_L^2 + S_\alpha^2}} \left[1 - 3\left(\frac{\xi_a}{2a}\right)^2 + 2\left(\frac{\xi_a}{2a}\right)^3\right] \quad (2.1)$$

$$M_z = \frac{a}{3} \left[3(C_\alpha + C_S S_L) - 2C_\alpha \frac{\xi_a}{a}\right] \left(\frac{\xi_a}{2a}\right)^2 \frac{S_\alpha}{1 - S_L} - a \left[\mu_x S_L \left(1 + 3\frac{\xi_a}{2a}\right) - 3\mu_y \frac{\xi_a}{2a}\right] F_z \frac{S_\alpha}{\sqrt{S_L^2 + S_\alpha^2}} \left(1 - \frac{\xi_a}{2a}\right)^2 \frac{\xi_a}{2a} - \frac{F_x F_y}{k_y} \quad (2.2)$$

- Full sliding case ($\xi_a = 0$)

$$F_x = \mu_x F_z \frac{S_L}{\sqrt{S_L^2 + S_\alpha^2}} \quad (2.3)$$

$$F_y = -\mu_y F_z \frac{S_\alpha}{\sqrt{S_L^2 + S_\alpha^2}}$$

$$M_z = \frac{\mu_x \mu_y F_z^2 S_L S_\alpha}{k_y (S_L^2 + S_\alpha^2)} \quad (2.4)$$

where ξ_a is the length of the adhesion zone in the contact patch and is expressed as follows:

$$\frac{\xi_a}{2a} = 1 - \frac{\sqrt{(S_L C_S)^2 + (S_\alpha C_\alpha)^2}}{3\mu_0 F_z (1 - S_L)} \quad (2.5)$$

Sakai model parameters are listed in table 2.1.

a	half length of the contact patch
k_y	carcass (ring) lateral stiffness
C_S	longitudinal slip stiffness
C_α	cornering stiffness
μ_0	static friction coefficient
μ_x	longitudinal friction coefficient
μ_y	lateral friction coefficient

Table 2.1: Sakai model parameters

Next, HSRI-NBS - III model final equations are presented.

2.3.2 HSRI-NBS-III model

The main particularity of HSRI-NBS-III model is its definition of a transition zone between the adhesion and the sliding zones in the contact patch. For instance, the lateral tyre force F_y is developed distinctly from each zone and its total expression is the sum of the contribution of the three zones. The final expressions for the longitudinal force F_x , the lateral force F_y and the self-aligning moment M_z are reminded below.

- Forces expressions in the adhesion zone: $0 \leq \xi_a \leq 2a$.

$$F_{xa} = C_S \frac{S_L}{1 - S_L} \left(\frac{\xi_a}{2a} \right)^2 \tag{2.6}$$

$$F_{ya} = -C_\alpha \frac{S_\alpha}{1 - S_L} \left(\frac{\xi_a}{2a} \right)^2$$

- Forces expressions in the transition zone: $0 \leq \xi_a \leq \xi_s \leq 2a$.

$$F_{xt} = \left[\frac{1}{3} C_S \frac{S_L}{1 - S_L} \left(3 - \frac{\xi_a}{a} - \frac{\xi_s}{2a} \right) \frac{\xi_a}{2a} / \left(1 - \frac{\xi_a}{2a} \right) + \mu F_z \frac{S_L}{\sqrt{S_L^2 + S_\alpha^2}} \left(3 - \frac{\xi_s}{a} - \frac{\xi_a}{2a} \right) \frac{\xi_s}{2a} \right] \left(\frac{\xi_s}{2a} - \frac{\xi_a}{2a} \right)$$

$$F_{yt} = - \left[\frac{1}{3} C_\alpha \frac{S_\alpha}{1 - S_L} \left(3 - \frac{\xi_a}{a} - \frac{\xi_s}{2a} \right) \frac{\xi_a}{2a} / \left(1 - \frac{\xi_a}{2a} \right) + \mu F_z \frac{S_\alpha}{\sqrt{S_L^2 + S_\alpha^2}} \left(3 - \frac{\xi_s}{a} - \frac{\xi_a}{2a} \right) \frac{\xi_s}{2a} \right] \left(\frac{\xi_s}{2a} - \frac{\xi_a}{2a} \right) \tag{2.7}$$

2.3. A priori choice of suitable physical models

- Forces expressions in the sliding zone.

$$\begin{aligned}
 F_{xs} &= \mu F_z \frac{S_L}{\sqrt{S_L^2 + S_\alpha^2}} \left[1 - 3\left(\frac{\xi_s}{2a}\right)^2 + 2\left(\frac{\xi_s}{2a}\right)^3 \right] \\
 F_{ys} &= -\mu F_z \frac{S_\alpha}{\sqrt{S_L^2 + S_\alpha^2}} \left[1 - 3\left(\frac{\xi_s}{2a}\right)^2 + 2\left(\frac{\xi_s}{2a}\right)^3 \right]
 \end{aligned} \tag{2.8}$$

- Self-aligning moment expression in the adhesion zone: $0 \leq \xi_a \leq 2a$.

$$M_{za} = \frac{2a}{3} \left[2(C_S - C_\alpha) \frac{S_L}{1 - S_L} \frac{\xi_a}{2a} - \frac{1}{2} C_\alpha \left(2\frac{\xi_a}{a} - 3 \right) \right] \frac{S_\alpha}{1 - S_L} \left(\frac{\xi_a}{2a} \right)^2 \tag{2.9}$$

- Self-aligning moment expression in the sliding zone.

$$\begin{aligned}
 M_{zs} &= 2aS_\alpha \left\{ \left(\frac{1}{C_\alpha} - \frac{1}{C_S} \right) \frac{S_L \mu^2 F_z^2}{(S_L^2 + S_\alpha^2)^{5/2}} \left[1 + 3\frac{\xi_s}{2a} + 6\left(\frac{\xi_s}{2a}\right)^2 \right] \left(1 - \frac{\xi_s}{2a} \right)^2 \right. \\
 &\quad \left. - \frac{\mu F_z}{\sqrt{S_L^2 + S_\alpha^2}} \left[1 + \frac{\xi_s}{2a} + \left(\frac{\xi_s}{2a}\right)^2 \right] \right\} \left(1 - \frac{\xi_s}{2a} \right)
 \end{aligned} \tag{2.10}$$

- Self-aligning moment expression in the transition zone: $0 \leq \xi_a \leq \xi_s \leq 2a$.

$$\begin{aligned}
 M_{zt} = & 2aS_\alpha \left[(C_S - C_\alpha) \left\{ \frac{S_L}{(1 - S_L)^2} \left(\frac{\xi_a}{2a}\right)^2 \frac{1}{15} \left[6\left(\frac{\xi_a}{2a}\right)^2 + 3\frac{\xi_a \xi_s}{4a^2} \right. \right. \right. \\
 & + \left. \left. \left(\frac{\xi_s}{2a}\right)^2 - 15\frac{\xi_s}{2a} - 5\frac{\xi_s}{2a} + 10 \right] / \left(1 - \frac{\xi_a}{2a}\right)^2 \right. \right. \\
 & + \frac{S_L \mu F_z}{(1 - S_L) \sqrt{S_L^2 + S_\alpha^2}} \left(\frac{1}{C_S} + \frac{1}{C_\alpha} \right) \frac{\xi_a \xi_s}{40a^2} \left[3\left(\frac{\xi_s}{2a}\right)^2 \right. \\
 & + \left. 3\left(\frac{\xi_a}{2a}\right)^2 + \frac{\xi_a \xi_s}{a^2} - 5\left(\frac{\xi_a}{a} + \frac{\xi_s}{a}\right) + 10 \right] / \left(1 - \frac{\xi_a}{2a}\right) \\
 & + \frac{S_L \mu^2 F_z^2}{(S_L^2 + S_\alpha^2) C_S C_\alpha} \frac{3}{10} \left[6\left(\frac{\xi_s}{2a}\right)^2 + \frac{3\xi_a \xi_s}{4a^2} + \left(\frac{\xi_a}{2a}\right)^2 \right. \\
 & \left. \left. - 15\frac{\xi_s}{2a} - 5\frac{\xi_a}{2a} + 10 \right] \right\} \\
 & + \frac{C_\alpha}{1 - S_L} \frac{\xi_a}{12a} \left[3 - 3\frac{\xi_a}{2a} \left(2 - \frac{\xi_a}{2a}\right) - \frac{\xi_s}{2a} \left(3 - \frac{\xi_s}{2a}\right) + \frac{\xi_a \xi_s}{2a^2} \right] / \left(1 - \frac{\xi_a}{2a}\right) \\
 & + \frac{\mu F_z}{\sqrt{S_L^2 + S_\alpha^2}} \frac{\xi_s}{4a} \left[3 - 3\frac{\xi_s}{2a} \left(2 - \frac{\xi_a}{2a}\right) - \frac{\xi_a}{2a} \left(3 - \frac{\xi_a}{2a}\right) \right. \\
 & \left. + \frac{\xi_a \xi_s}{2a^2} \right] \left(\frac{\xi_s}{2a} - \frac{\xi_a}{2a} \right)
 \end{aligned} \tag{2.11}$$

- Final expressions for the longitudinal and lateral forces

$$\begin{aligned}
 F_x &= F_{xa} + F_{xt} + F_{xs} \\
 F_y &= F_{ya} + F_{yt} + F_{ys}
 \end{aligned}$$

- Final expression for the self-aligning moment

$$M_z = M_{za} + M_{zt} + M_{zs}$$

Remarks:

F_{xa}, F_{ya}, M_{za} are the contributions of the adhesion zone.

2.3. A priori choice of suitable physical models

F_{xt}, F_{yt}, M_{zt} are the contributions of the transition zone.

F_{xs}, F_{ys}, M_{zs} are the contributions of the sliding zone.

The length of the adhesion zone ξ_a and that of the transition zone ξ_s are given by the following expressions:

$$\frac{\xi_a}{2a} = 1 - \frac{\sqrt{(S_L C_S)^2 + (S_\alpha C_\alpha)^2}}{3\mu_0 F_z (1 - S_L)} \quad (2.12)$$

$$\frac{\xi_s}{2a} = 1 - \left(\frac{C_S C_\alpha}{C_S + C_\alpha} \right) \frac{\sqrt{S_L^2 + S_\alpha^2}}{3\mu F_z (1 - S_L)}$$

The friction coefficient is proposed as follows: $\mu = \mu_o(1 - A_s V_s)$, where μ is the actual friction coefficient and A_s , the sensitivity parameter of the static friction coefficient μ_o relative to the resultant sliding speed V_s .

HSRI-NBS-III model parameters are presented in table 2.2.

a	half length of the contact patch
C_S	longitudinal slip stiffness
C_α	cornering stiffness
μ_0	static friction coefficient
A_s	sensitivity parameter of μ_o relatively to the sliding speed V_s
μ	actual friction coefficient

Table 2.2: HSRI-NBS-III model parameters

Fiala model final equations are presented next.

2.3.3 Fiala model

Fiala model is developed exclusively for pure slip conditions. The final expressions of the forces and the moments are reminded below.

- Expression of the pure longitudinal force F_x

$$F_x = C_S S_L \quad \text{if } |S_L| \leq S_L^*$$

$$F_x = \text{sgn}(S_L) \left\{ \mu F_z - \frac{(\mu F_z)^2}{4|S_L|C_S} \right\} \quad \text{if } |S_L| > S_L^* \quad (2.13)$$

- Expression of the pure lateral force F_y

$$\begin{aligned}
 F_y &= -\mu F_z (1 - H^3) \text{sgn}(\alpha) \quad \text{if } |\alpha| \leq \alpha^* \\
 F_y &= -\mu F_z \text{sgn}(\alpha) \quad \text{if } |\alpha| > \alpha^*
 \end{aligned}
 \tag{2.14}$$

- Expression of the self-aligning moment M_z

$$\begin{aligned}
 M_z &= 2\mu F_z R_2 (1 - H) H^3 \text{sgn}(\alpha) \quad \text{if } |\alpha| \leq \alpha^* \\
 M_z &= 0 \quad \text{if } |\alpha| > \alpha^*
 \end{aligned}
 \tag{2.15}$$

where R_2 is the tyre carcass radius also equivalent to the tyre half-width. The term $\text{sgn}(\alpha)$ designates the sign of the side slip angle α .

- Expression of the rolling resistance moment M_y

$$\begin{aligned}
 M_y &= -C_r F_z \quad \text{tyre in forward motion} \\
 M_y &= C_r F_z \quad \text{tyre in backward motion}
 \end{aligned}
 \tag{2.16}$$

The parameter H is given by:

$$H = 1 - \frac{C_\alpha |\tan \alpha|}{3\mu F_z}
 \tag{2.17}$$

The critical limit of the longitudinal slip parameter is expressed as follows:

$$S_L^* = \frac{\mu F_z}{2C_s}
 \tag{2.18}$$

The critical limit of the side slip angle is given by:

$$\alpha^* = \arctan\left(\frac{3\mu F_z}{C_\alpha}\right)
 \tag{2.19}$$

The friction coefficient μ is proposed as function of the resultant slip parameter, which is termed comprehensive slip ratio and noted $S_{L\alpha}$.

$$\mu = \mu_0 - S_{L\alpha}(\mu_0 - \mu_s)$$

where μ_0 is the static friction coefficient, μ_s the full sliding friction coefficient and $S_{L\alpha} = \sqrt{S_L^2 + S_\alpha^2}$.

2.4. Comparison of Sakai, Fiala and HSRI-NBS-III models

Fiala model parameters are summarized in table 2.3.

R_2	tire carcass radius
C_S	longitudinal slip stiffness
C_α	cornering stiffness
C_r	rolling resistance stiffness
μ_o	static friction coefficient
μ_s	full sliding friction coefficient
μ	actual friction coefficient

Table 2.3: Fiala model parameters

Next, the modelling results of these three models are compared to measurements data.

2.4 Comparison of Sakai, Fiala and HSRI-NBS-III models

This section focuses on simulating the three models which equations have been reminded above. First, an approach for measuring or estimating (identifying) the parameters values is presented. Then, for each a priori chosen model, the lateral force F_y and the self-aligning moment M_z parameters are estimated using the measurements data described in section 2.2. Finally, the modelling results are compared with the corresponding measurements data.

2.4.1 General approach for estimating parameters

Two groups of parameters can be distinguished for the considered models, static and dynamic parameters. Static parameters refer to parameters which are measured from non rolling tyre and dynamic parameters designate those measured (or estimated) from rolling tyre.

Static parameters

- ◇ Contact patch dimensions

The contact patch dimensions can be directly measured on the mark of the loaded tyre footprint.

- ◇ Longitudinal stiffness k_x

The value of the tyre longitudinal carcass stiffness k_x is obtained by estimating the slope at the origin of the curve representing the longitudinal static force $F_{xstatic}$ vs

the longitudinal displacement v_x .

$$k_x = \left. \frac{\partial F_{xstatic}}{\partial v_x} \right|_{v_x=0}$$

- ◇ Lateral stiffness k_y

The value of the tyre lateral stiffness k_y is estimated as the slope at the origin of the curve representing the static lateral force $F_{ystatic}$ vs the lateral displacement v_y .

$$k_y = \left. \frac{\partial F_{ystatic}}{\partial v_y} \right|_{v_y=0}$$

Dynamic parameters

- ◇ Longitudinal slip stiffness C_S

The longitudinal slip stiffness C_S is determined as the slope at the origin of the curve representing the longitudinal force F_x of the rolling tyre vs the longitudinal slip S_L (see chapter 1, section 1.3).

$$C_S = \left. \frac{\partial F_x}{\partial S_L} \right|_{S_L=0, S_\alpha=0}$$

- ◇ Cornering stiffness C_α

The cornering stiffness C_α is assumed to be the slope at the origin of the curve representing the rolling tyre lateral force F_y vs the side slip angle S_α . (see chapter 1, section 1.3).

$$C_\alpha = \left. \frac{\partial F_y}{\partial S_\alpha} \right|_{S_\alpha=0, S_L=0}$$

- ◇ Tyre/road interface friction parameters μ_o , μ_x , μ_y and A_s

There are two approaches for estimating the values of these parameters, direct and indirect methods.

Direct methods

Direct methods are based on mathematical formulas which allow to determine the friction coefficients from measurements data such as tyre forces, slip stiffnesses, velocity... For instance, a common used method consists in evaluating the friction coefficient as the ratio of the maximum longitudinal or lateral force over the vertical

2.4. Comparison of Sakai, Fiala and HSRI-NBS-III models

$$\text{force, } \mu_{x,y} = \frac{F_{x,y\max}}{F_z}.$$

Indirect methods

More often, indirect methods consist in recording the noise produced in the tyre-road interface using noise sensor or in recording the road properties with an optical sensor. Then, these measurements data are correlated with the friction coefficients. One main inconvenient of the method which uses noise sensor is the fact that it is not possible to completely distinguish the environment noise from that of the tyre-road interface.

Remark:

The friction coefficient will be assumed uniform and constant all over the contact patch for the three a priori chosen models. Moreover, since the modelling takes an interest exclusively in the lateral tyre behavior (pure cornering), only μ_y is concerned and it will be simply noted μ .

Next, the lateral force F_y and the self-aligning moment M_z parameters values are determined for each model.

2.4.2 Modelling results

Table 2.4 presents the lateral force F_y and the self-aligning moment M_z parameters values for Sakai, HSRI NBS III and Fiala models. Parameter C_α is estimated as described in the above section 2.4.1. The value of μ is determined (approximatively) as the ratio of the maximum lateral force over the vertical load F_z , $\mu \sim \frac{F_{y\max}}{F_z}$. The value of parameter R_2 (Fiala model) is supposed to be the half-length of the tyre width, $R_2 = 0.2275m$. However, it is important to mention that this value for parameter R_2 assumes a theoretical tyre with full surface (without grooves). Values for parameter a (half-length of the contact patch) are obtained by extrapolating measurements data, which give values of a vs vertical loads F_z . The formula shown in equation (2.20) is used for calculating the error.

$$Error_F = 100 \sqrt{\frac{\sum_{i=1}^n (F_{Measure,i} - F_{Model,i})^2}{\sum_{i=1}^n (F_{Measure,i})^2}} \quad (2.20)$$

where $F_{Measure,i}$ and $F_{Model,i}$ are each measurement point and the model evaluation, respectively.

Chapter 2. Choosing suitable physical models

Inflation pressure $p = 11.3$ bars		
$F_z = 112.2kN$	$F_z = 156kN$	$F_z = 200kN$
$C_\alpha = 6.4175 \times 10^5 N/rad$	$C_\alpha = 6.6910 \times 10^5 N/rad$	$C_\alpha = 6.5882 \times 10^5 N/rad$
$a = 0.228m$	$a = 0.245m$	$a = 0.263m$
$R_2 = 0.2275m$	$R_2 = 0.2275m$	$R_2 = 0.2275m$
$\mu = 0.526$	$\mu = 0.482$	$\mu = 0.4419$
$F_{ymax} = 59.05kN$	$F_{ymax} = 75.25kN$	$F_{ymax} = 88.38kN$
Inflation pressure $p = 16$ bars		
$F_z = 112.2kN$	$F_z = 156kN$	$F_z = 200kN$
$C_\alpha = 6.4663 \times 10^5 N/rad$	$C_\alpha = 7.5717 \times 10^5 N/rad$	$C_\alpha = 8.0217 \times 10^5 N/rad$
$a = 0.203m$	$a = 0.225m$	$a = 0.234mm$
$R_2 = 0.2275m$	$R_2 = 0.2275m$	$R_2 = 0.2275m$
$\mu = 0.513$	$\mu = 0.4872$	$\mu = 0.451$
$F_{ymax} = 57.55kN$	$F_{ymax} = 76.25kN$	$F_{ymax} = 90.2kN$

Table 2.4: Models parameters values

Remark

It is only chosen to presents the modelling results for inflation pressures 11.3 bars and 16 bars for clarity reason. Indeed, the tendency of each model representativeness is similar for inflation pressure 14 bars and therefore, presenting its modeling results would not necessary provide additional information for the models analysis.

The parameters values presented in table 2.4 are used to simulate each model lateral force F_y and self-aligning moment M_z according to their corresponding expressions presented previously. In one hand, figures 2.1 and 2.2 show that all three models present approximatively the same agreement for the lateral force. Their corresponding curves coincide and present relative good agreement with measurements data. The maximum error is about 1.1%. In the other hand, it is observed that Sakai and HSRI-NBS-III models show similar modelling results for M_z , which are in general lower than measurements data, figures 2.3 and 2.4. The maximum error is about 45%. In the case of Fiala model, figures 2.5 and 2.6, significant deviations are also observed between measurements data and modelling results. The maximum error is about 30%.

It can be concluded all three models may be adopted for representing the pure lateral

2.4. Comparison of Sakai, Fiala and HSRI-NBS-III models

force F_y in steady-state conditions but, they cannot be used in their original version for representing the self-aligning moment M_z . Thus, it might be necessary to thoroughly investigate each model M_z expression in order to determine the limitations.

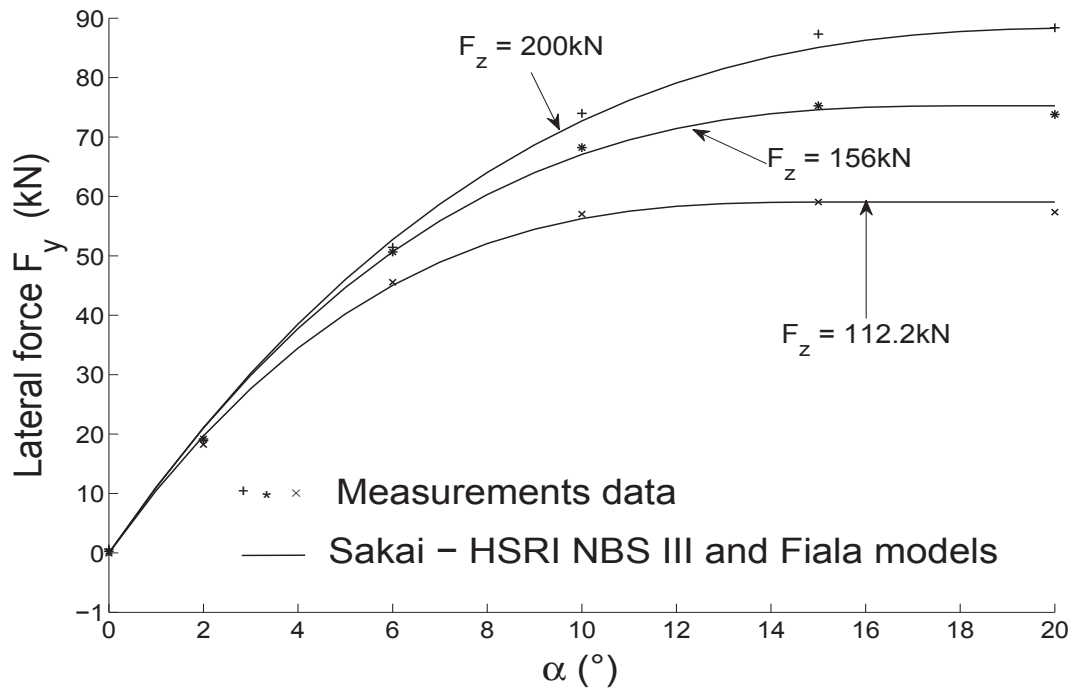


Figure 2.1: Pure lateral force F_y - Inflation pressure $p= 11.3$ bars

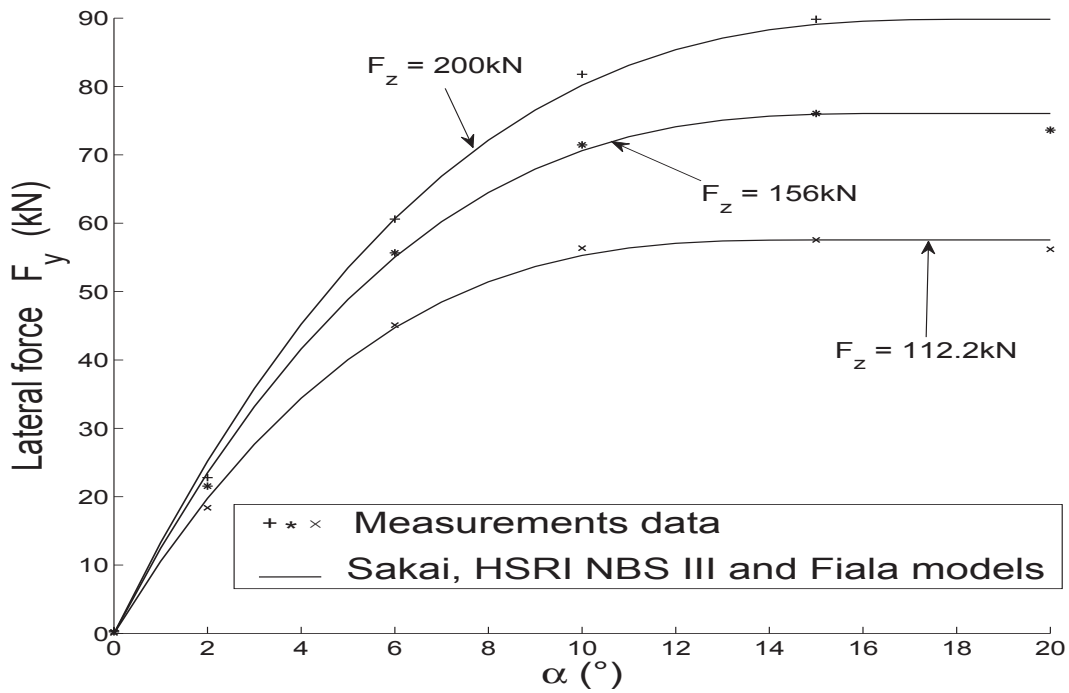


Figure 2.2: Pure lateral force F_y - Inflation pressure $p = 16$ bars

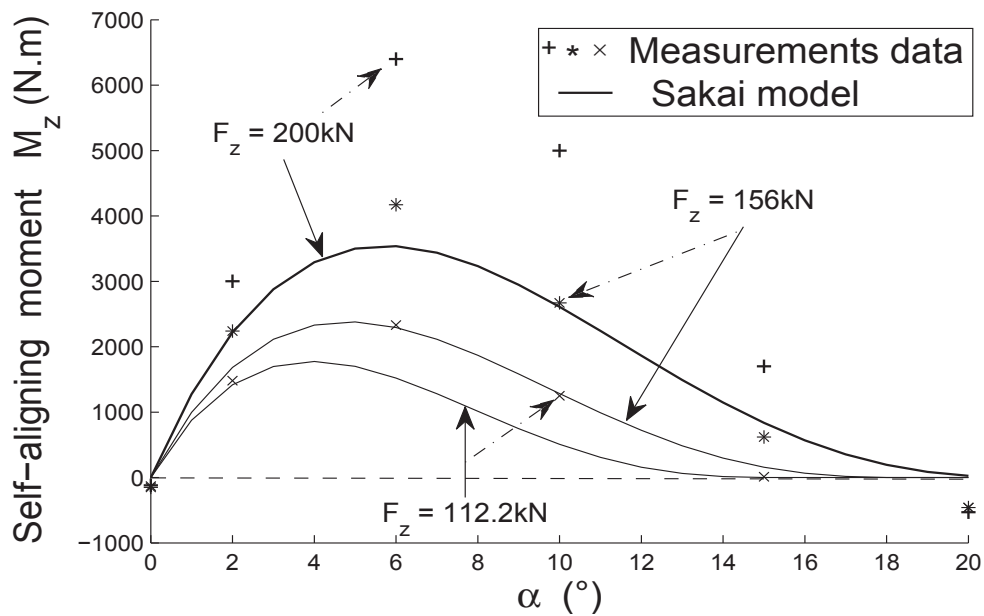


Figure 2.3: Sakai models: pure cornering self-aligning moment M_z - Inflation pressure $p = 11.3$ bars

2.4. Comparison of Sakai, Fiala and HSRI-NBS-III models

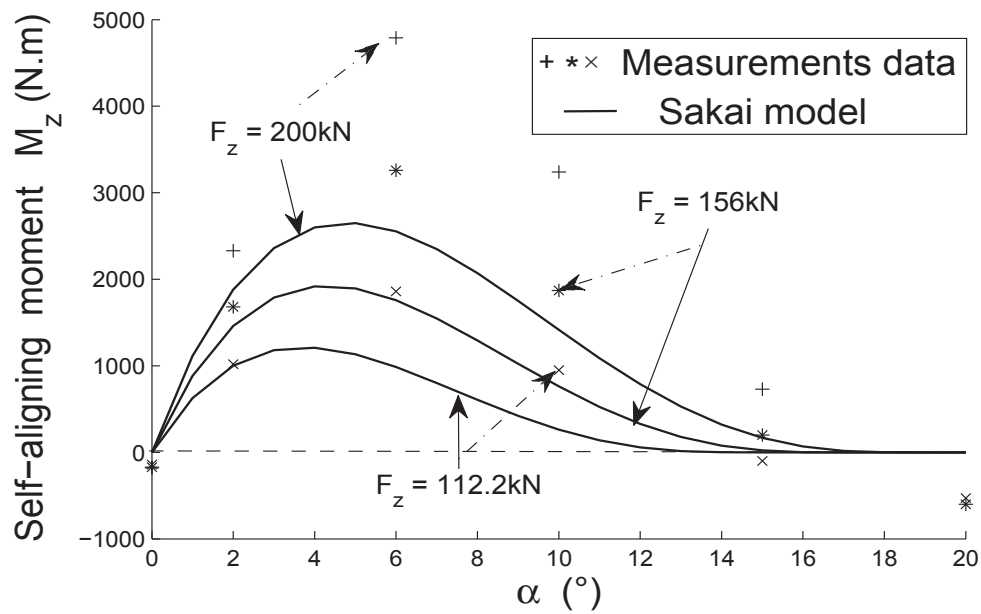


Figure 2.4: Sakai models: pure cornering self-aligning moment M_z - Inflation pressure $p = 16$ bars

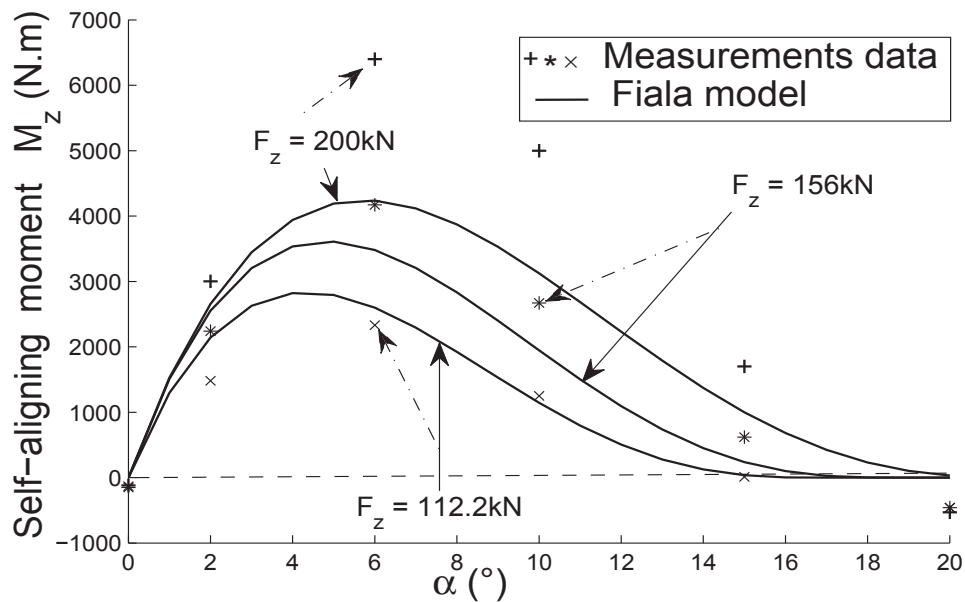


Figure 2.5: Fiala model: pure cornering self-aligning moment M_z - Inflation pressure $p = 11.3$ bars. (Similar curves are obtained for HSRI-NBS-III model non presented)

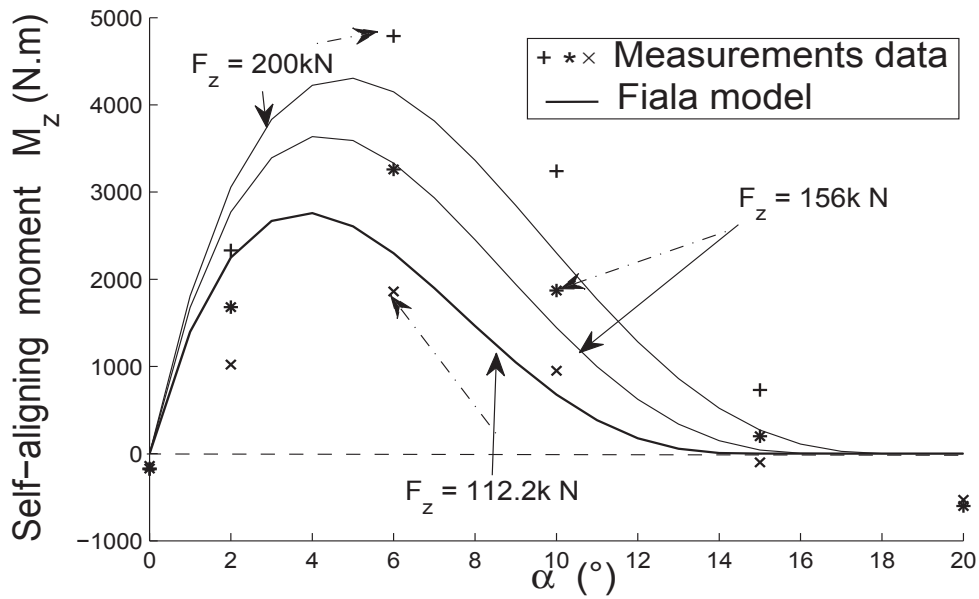


Figure 2.6: Fiala model: pure cornering self-aligning moment M_z - Inflation pressure $p = 16$ bars. (Similar curves are obtained for HSRI-NBS-III model non presented)

2.4.3 Discussion: a priori chosen models and measurements data

To understand the theoretical concept of Sakai, HSRI NBS III and Fiala tyre models, a schematic representation of the lateral force F_y and the self aligning moment M_z is shown in figure 2.7. In this figure, α_{max} corresponds to the value of the side slip where the self-aligning moment reaches its maximum value M_{zmax} . Parameter α^* is the critical side slip at which the lateral force reaches its maximum F_{ymax} value and remains constant. Moreover, at α^* , the self-aligning moment becomes zero et remains constant too. In the Sakai and HSRI NBS III models, the critical side slip α^* is determined when the parameter $\xi_a = 0$ (full sliding).

2.4. Comparison of Sakai, Fiala and HSRI-NBS-III models

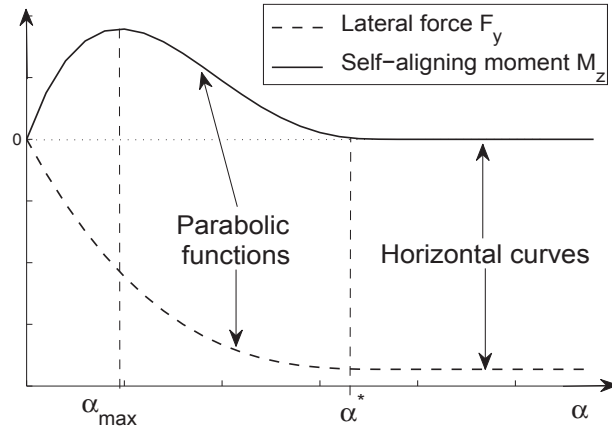


Figure 2.7: Fiala tyre model: theoretical concept of F_y and M_z

The measurements data show that when the self-aligning moment reaches zero, it does not stay constant but rebuilds in the negative part of the graph (see figure 2.4 for example). Besides, the value of the side slip at which the self-aligning moment reaches zero does not necessary correspond to the point where the lateral force reaches its maximum value F_{ymax} . For example, for $F_z = 156kN$ and at $p = 16$ bars, the self-aligning moment reaches zero at $\alpha \sim 16$ degrees (figure 2.4) while the lateral force reaches its maximum value at $\alpha \sim 14.5^\circ$ (figure 2.2). Moreover, the lateral force does not stay constant after reaching this maximum value but, slightly decreases. The remark is valid for all the measurements data used in the context of this study.

In figures 2.1 and 2.2, the values of α , at which the different modelling results of the lateral force reach the maximum value F_{ymax} , do not correspond to full sliding condition. In the other hand, the values of α at which the different modelling results of the self-aligning moment reach zero in figures 2.3, 2.4, 2.5 and 2.6 do not correspond to full sliding condition too. The real full sliding (real values of α^*) will occur after these points. The tests results used in the context of this study did not reach full sliding point.

Conclusion

The values of the critical side slip α^* in the application of section 2.4.2 are underestimated. It is reminded that the friction coefficient μ , used for estimating the critical slip limit α^* , is assumed constant and equal to the ratio of F_{ymax} over the vertical load F_z . This assumption may not be realistic enough and would contribute to the incorrect value of α^* . Besides, the models studied are based on a simple approach (brush model ap-

proach), which assumes the tyre to behave as an elastic material. Due to the complexity of the tyre behaviour, this assumption certainly presents important deviation at relative high side slip angle and may also contribute to the uncertainty on the value of α^* . However, since the modelling results of the lateral force are considered acceptable for the study, it is decided to investigate the models of the self-aligning moment and possibly overcome the limitations.

In the next section, the Fiala tyre model M_z expression is analysed and its limitations are underlined. Extension of its equation is proposed in order to better fit the measurements data. Notice that only Fiala model M_z expression is investigated, but the same approach can be used for both Sakai and HSRI-NBS-III models. The choice of the Fiala model is due to the fact that it shows relative smaller deviation when it is compared to the two other models.

2.5 Limits of physical models: example of Fiala model

Consider the self-aligning moment function, equation (2.15) and note H_{max} , the value of H at which the self-aligning moment reaches its maximum value M_{zmax} . The derivative of equation (2.15) relatively to parameter H , $(\frac{dM_z}{dH})$, allows to determined H_{max} as follows:

$$H_{max} = \frac{3}{4} \quad (2.21)$$

From equation (2.17), the following expression is also deduced for H_{max} :

$$H_{max} = 1 - \frac{C_\alpha |\tan(\alpha_{max})|}{3\mu F_z}$$

then

$$|\tan(\alpha_{max})| = \frac{3\mu F_z}{4C_\alpha} \quad (2.22)$$

α_{max} corresponds to the value of the side slip angle α at which the self-aligning moment reaches its maximum value. α_{max} also represents the inflection point of the parabolic function which repasses by zero at α^* (saturation point for the Fiala model). If the above expression of $\tan(\alpha_{max})$ is compared with equation (2.19), the following relation can be derived:

$$\tan(\alpha^*) = 4\tan(\alpha_{max}) \quad (2.23)$$

The equation (2.23) presents a constraint (relation) between α^* and α_{max} which may not be always verified in practice. Besides, in equation (2.15), parameter R_2 represents the

2.6. Enhancement of Fiala model

maximum value of the pneumatic trail, often noted t . This pneumatic trail t allows a definition of an equivalent expression for the self-aligning moment M_z : $M(\alpha) = t(\alpha)F_y(\alpha)$, with $t_{max} = R_2$. However, the tyre surface contains grooves and the contact is not perfect. Therefore, this assumption, $t_{max} = R_2$, is not necessary verified.

In the following section, an attempt to enhance the Fiala self-aligning moment expression to better fit the measurements data is proposed.

2.6 Enhancement of Fiala model

The objective of this section is to propose a modified version of Fiala model self-aligning moment expression, equation (2.15), to better fit the measurements data and eventually make Fiala model full applicable at steady-state pure cornering condition.

The main limitations in the Fiala tyre model are the constraint between α^* and α_{max} (equation (2.23)), the fact of considering a constant friction coefficient μ which is based on the Coulomb static friction law (and may not be realistic enough for a rolling tyre) and the use of the tyre half-width R_2 as maximum of the pneumatic trail.

In order to adjust the pneumatic trail (to make it more realistic), a weighting factor, noted λ_R , is adopted. Then, $\lambda_R R_2$ is used in stead of R_2 in the Fiala M_z equation (2.15), where $0 < \lambda_R \leq 1$.

To adjust the value of α^* (hence α_{max}), measurements data up to full sliding are necessary. Moreover, a new expression has to be proposed for M_z between the point where it reaches zero for the first time and the point of full sliding. Due to the lack of data up to full sliding, it is decided to estimate a value of the side slip angle, noted α_0 , which corresponds to the point where M_z passes by zero for the first time. Then, the validity of the Fiala self-aligning moment model will be extended up to α_0 . Parameter α_0 is estimated by adjusting the friction coefficient in equation (2.19). In fact, a weighting factor λ_μ is used and μ is adjusted within its range of variation, $0 \leq \mu \leq 1$. $\lambda_\mu \mu$ is then used in stead of μ in equation (2.15).

The expression of the self-aligning moment M_z , equation (2.15), becomes then:

$$M_z = 2\lambda_\mu \mu F_z \lambda_R R_2 (1 - H) H^3 \text{sgn}(\alpha) \quad \text{if } |\alpha| \leq \alpha_0 \quad (2.24)$$

For $|\alpha| > \alpha_0$, the self-aligning moment would be 0, which is not realistic according to the measurements data. This part will be studied later in chapter 4. We also prefer the notation α_0 in stead of α^* , because α^* is assumed to be the point where full sliding starts.

When analysing the modified version of the self-aligning moment, equation (2.24), the weighting factors λ_R and λ_μ are finally used in a product form and they seem to represent one weighting factor which would be $\lambda = \lambda_R \lambda_\mu$. However, one weighting factor cannot be used because λ_R is used for adjusting the magnitude of the self-aligning moment and λ_μ is independently used for estimating α_0 in equation (2.19).

Next the new expression of M_z , equation (2.24) is used and the modelling results are compared to the measurements data.

2.6.1 Modelling results

The Fiala model M_z new expression, equation (2.24), is simulated using the same parameters values from table 2.4. The values of the weighting factors λ_R and λ_μ are determined by using the optimisation function *fminsearch* from Matlab software. The different values for λ_μ and λ_R are shown in table 2.5.

Inflation pressure p = 11.3 bars		
$F_z = 112.2kN$	$F_z = 156kN$	$F_z = 200kN$
$\lambda_R = 0.81m$	$\lambda_R = 0.9m$	$\lambda_R = 0.96m$
$\lambda_\mu = 1.349$	$\lambda_\mu = 1.433$	$\lambda_\mu = 1.527$
Inflation pressure p = 16 bars		
$F_z = 112.2kN$	$F_z = 156kN$	$F_z = 200kN$
$\lambda_R = 0.66m$	$\lambda_R = 0.78m$	$\lambda_R = 0.88m$
$\lambda_\mu = 1.364$	$\lambda_\mu = 1.408$	$\lambda_\mu = 1.49$

Table 2.5: Weighting factors for the modified version of the Fiala model

Figures 2.8 and 2.9 show the comparison of the modelling results with the measurements data. The expression ‘Fiala - M’ means modified version of the Fiala model. The new expression of the self-aligning moment gives better modelling results when compared to the original M_z model. The maximum error observed is about 15% when the side slip angle varies up to α_0 (between 16° and 20° depending on the vertical load). Besides, in practice, the landing gear is rarely steered up to these values estimated for α_0 . Thus, the new version of the Fiala model may be used for simulating the steady-state pure cornering with relative satisfactory, figures 2.8 and 2.9.

2.6. Enhancement of Fiala model

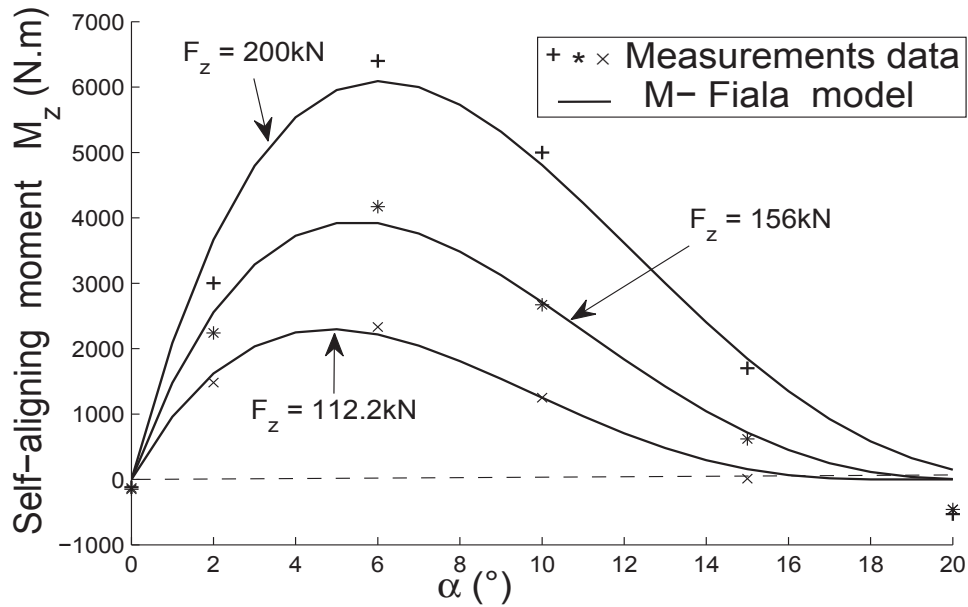


Figure 2.8: Modified version of Fiala model: M_z at pure cornering - $p = 11.3$ bars

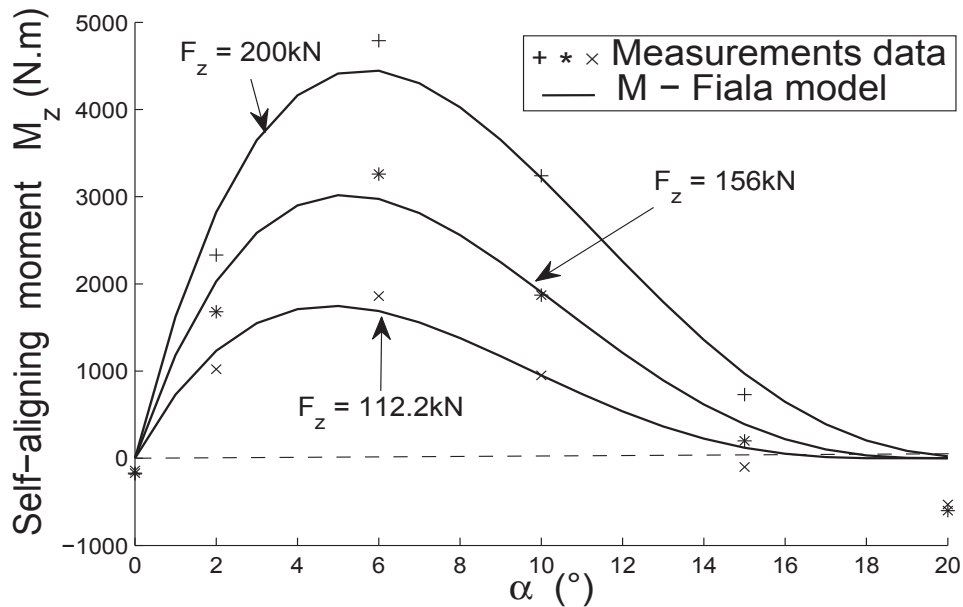


Figure 2.9: Modified version of Fiala model: M_z at pure cornering - $p = 16$ bars

Nevertheless, a major inconvenient remains when using Fiala physical type of models, even the above new version, because their parameters are only valid for a given vertical

load F_z and a given inflation pressure. If one of these two conditions is changed, new parameters have to be identified or measured. Some interpolation functions are proposed in the literature in order to overcome this constraint, see for example [10, 31]. In the next section, an extension of Fiala model is proposed by expressing its parameters as function of the vertical load F_z .

2.6.2 Expressing the Fiala model parameters as function of F_z

The parameters of Fiala model are determined for a given vertical load F_z and a given inflation pressure. Now, the objective is to propose an extension of Fiala model in which its parameters are expressed as a function of the vertical load F_z .

From the description of Fiala model in section 2.3.3, it is deduced that the parameters to express as a function of F_z are the cornering stiffness C_α and the friction coefficient μ . In [10], Pacejka proposes an empirical function for C_α and μ . The same functions are adopted in the present study. The corresponding expressions are presented in the following equation:

$$\begin{aligned} C_\alpha &= a_\alpha \sin \left[2 \arctan \left(\frac{F_z}{b_\alpha} \right) \right] \\ \mu_c &= (a_\mu + b_\mu F_z) \end{aligned} \quad (2.25)$$

where μ_c represents the corrected value of the friction coefficient: $\mu_c = \lambda_\mu \mu$. Quantities a_α , b_α , a_μ and b_μ are empirical parameters to be identified from sets of C_α and μ_c data. In equations (2.24), parameters C_α and $\lambda_\mu \mu = \mu_c$ are replaced by their corresponding expressions from equation (2.25). The values of parameters a_α , b_α , a_μ and b_μ are estimated by using the optimisation function *fminsearch* from Matlab software. The data of C_α are taken from table 2.4 and those for μ_c are obtained by multiplying each value of μ in table 2.4 by the corresponding weighting factor λ_μ shown in table 2.5.

For inflation pressure $p = 11, 3$ bars, C_α and μ_c read:

$$\begin{aligned} C_\alpha &= 6.7714 \times 10^5 \sin \left[2 \arctan \left(\frac{F_z}{1.5686 \times 10^5} \right) \right] \\ \mu_c &= -3.9 \times 10^{-7} \times F_z + 0.75 \end{aligned} \quad (2.26)$$

and for inflation pressure $p = 16$ bars, C_α and μ_c read:

2.6. Enhancement of Fiala model

$$C_\alpha = 8.0722 \times 10^5 \sin \left[2 \arctan \left(\frac{F_z}{2.2394 \times 10^5} \right) \right] \quad (2.27)$$

$$\mu_c = -3.4 \times 10^{-7} \times F_z + 0.74$$

Figure 2.10 and 2.11 show the modelling results obtained for C_α and μ_c as function of F_z using equation (2.25). The model of C_α shows good agreement with measurements data. In fact the least squares fitting shows correlation coefficients more than 0.99. The linear model proposed for the friction coefficient μ_c also presents relative good agreement with measurements data but, since reference values for this parameter are not available, a conclusion cannot be made on its tendency.

Remark

The extensions proposed to enhance the validity of Fiala model have included empirical parameters which must be estimated from measurements data. In order to properly identify these parameters, it is necessary to determine the reference values as well as the variation limits of each parameter. Therefore, several tests have to be performed on tyres in various conditions, such as forward speed, longitudinal and lateral slips, vertical loads, etc. However, such investigation is not possible in the case of this study. Secondly, because empirical parameters are involved into the new equations, the model fails to be fully physical and becomes semi-empirical.

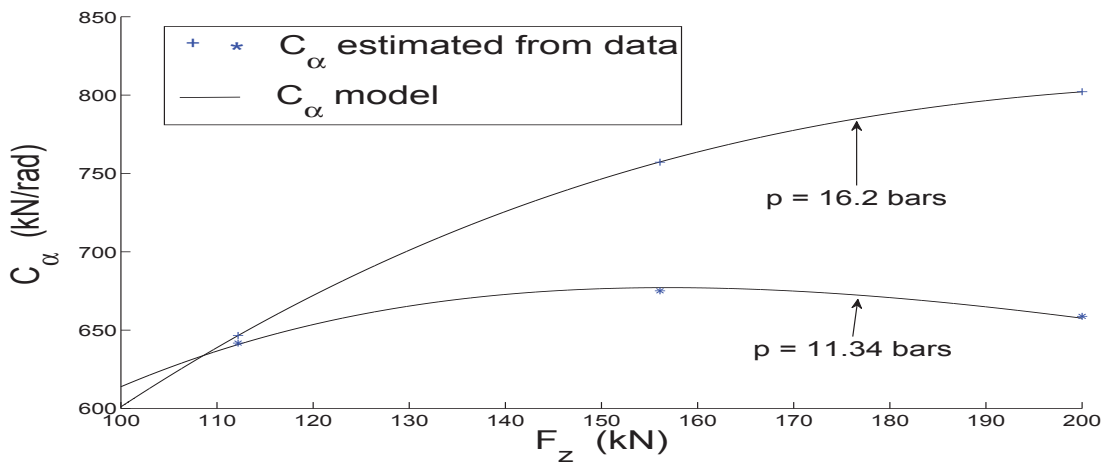


Figure 2.10: Fiala model parameters extension - Evolution of C_α vs F_z

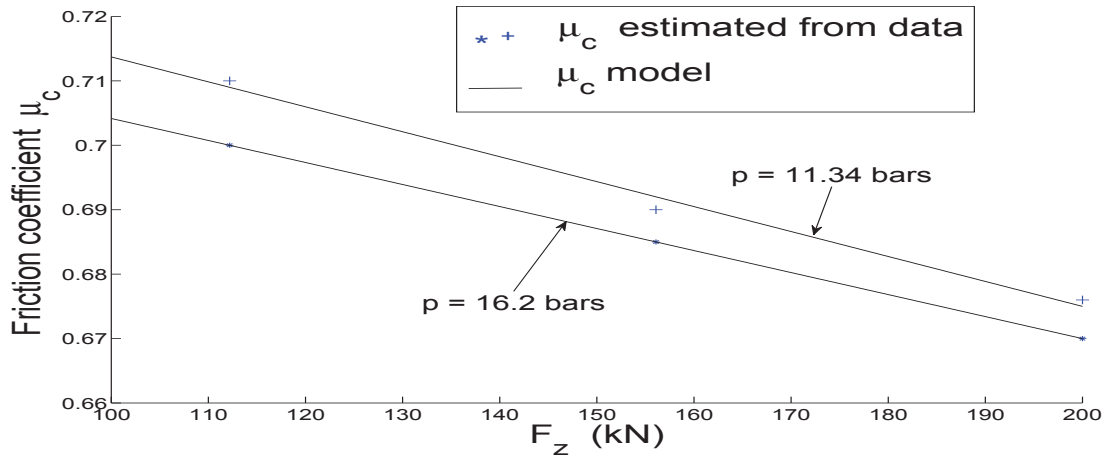


Figure 2.11: Fiala model parameters extension - Evolution of μ_c vs F_z

2.7 Conclusion

The present study requirements are taken into account with the practical constraints to choose a priori suitable physical models, Sakai, HSRI-NBS-III. The Fiala model, which is actually used by Messier-Dowty company, is also studied. The modelling results have shown that the lateral force is relatively better represented by all three models in the range of the side slip angle used. However, the self-aligning moment modelling results present significant deviation when compared to measurements data. An attempt to enhance the self-aligning moment equation of the Fiala model is proposed in order to better fit measurements data. Moreover, the parameters are expressed as function of the vertical load, that allows prediction capability of the Fiala model with respect to the vertical load. However, it is shown that this enhancement of the Fiala model still presents some limitations (unrealistic saturation point) and includes empirical parameters. The model becomes semi-physical in stead of physical. Besides, the included empirical parameters require some sets of measurements data in order to determine their reference values as well as their limits of variation. Since such investigation is not possible in the context of the present study, it is found worth investigating existing semi-empirical models which have already been used in the literature.

CHAPTER 3

Choosing suitable semi-empirical models

In this chapter, the semi-empirical models presented in chapter 1 are first analysed. Then, Magic Formula model is a priori chosen for studying the steady-state tyre forces and moments. At pure cornering condition, the modelling results of this model show better agreement with measurements data when they are compared to those obtained with the physical models in chapter 2. Moreover, a tyre test rig is built in the simulation environment, Msc Adams software, and Magic Formula model is used to characterise the tyre-road interaction. It is also shown that the pure cornering modelling results from the test rig are quite similar to those obtained with the direct use of the model equations. Besides, Magic Formula proposes expressions for modelling the tyre characteristics in the entire steady-state conditions required for the present study and therefore, it is adopted as adequate model.

3.1 Introduction

The physical models investigated in chapter 2 have shown significant limitations for use in the context of this thesis. Moreover, advanced physical models could not be considered since the data required for their use are not available. An attempt to adapt a model has been presented. However, it is shown that this extension has included empirical parameters and the model becomes semi-physical in stead of physical. Therefore, it is found worth investigating existing semi-empirical models.

The objective of this chapter is first to make an a priori choice of semi-empirical tyre model(s) capable of representing the steady-state forces and moments of an aircraft tyre during its manœuvres conditions such as pure driving/braking, pure cornering, combined slip and parking. Then, the modelling results of the a priori chosen model(s) will

be compared to measurements data in order to validate this choice. The possibility to physically interpret the majority of the model(s) parameters will be considered as well as their representativeness with respect to the limited available measurements data. The measurements data are the same as those presented in chapter 2.

This chapter is organised as follows. The semi-empirical category models are investigated in section 3.2. Then, the modelling results of an a priori chosen model, Magic Formula, are discussed. A tyre test rig is modelled in section 3.3 in order to simulate the pure cornering using the Magic Formula model as it is implemented in the software Msc Adams. It is reminded that this software is the one actually used by Messier-Dowty company.

3.2 A priori choice of semi-empirical model

Among the literature steady-state semi-empirical models presented in chapter 1, one of the common used models is Magic Formula (MF), also termed Pacejka model. It is a predictive model which parameters take into account the dependency of camber, yaw or turn slip, vertical load and inflation pressure. Because of its set of important number of parameters and the effort required for estimating them, Magic Formula is found to be the more complex model when it is compared to the other semi-empirical models presented in chapter 1. But, it is also the model for which the literature provides sufficient references of application studies, [7, 10, 11, 32]. Moreover, a parameter identification tool, termed MF-Tool, is available and allows the estimation of the parameters used in the model. In addition, Magic Formula is a part of a complete model, termed MF-Swift (Magic Formula - Short Wavelength Intermediate Frequency Tyre), which is commercially available as a software. The complete model MF-Swift is composed of two main parts, MF (Magic Formula) that handles the steady-state tyre behaviour, and Swift that handles the transient dynamics part. The transient-dynamic part, Swift, is not treated in this thesis because of the lack of required measurements data but it may be an interest for Messier-Dowty company. Even though the model is based on an empirical interpolation function, several of its parameters are associated with the physical properties of the tyre and the tyre-road interface, such as the cornering stiffness, the friction coefficient, the vertical stiffness, etc. The model is then termed semi-empirical. Magic Formula is then the a priori chosen semi-empirical model.

Next, a list of the common used versions of MF are reminded as well as their particu-

3.2. A priori choice of semi-empirical model

larities. For the sake of clarity, only the pure cornering lateral force and the self-aligning moment expressions of the 2002 version of Magic Formula are reminded. A brief description of the parameters identification tool, termed MF-Tool, is also presented in section 3.2.2. Then, by using the 2002 version of Magic Formula, the pure cornering modelling results by direct use of the model equations are presented in section 3.2.3 as well as those obtained by using the same model in the simulation environment Msc Adams software.

3.2.1 Magic Formula versions

Several versions of Magic Formula have been developed, see for example [10, 11, 27, 33]. Among the different versions of Magic Formula model, one may mention PAC89/94, MF-Tyre5.1/5.2 MC-Tyre1.0/1.1, MF-Swift 6.0 and MF-Swift 6.1. Figure 3.1 illustrates the particularities of each version.

The main differences between them are the simulation conditions (steady-state or dynamics, pure or/and combined slip) and the number of parameters involved. For example, PAC94 is the extended version of PAC89, which takes into account the combined slip condition. Versions MF-Tyre5.1 and MF-Tyre5.2 represent the same tyre conditions but version MF-Tyre5.2 includes additional fitting parameters for reducing interpolation error. In the same manner, version MF-Swift6.1 is the extended version of MF-Swift6.0, which proposes an expression for the rolling resistance and includes inflation pressure dependency in the model parameters expressions. The 2002 version of Magic Formula, which is equivalent to the steady-state part (MF part) of MF-Swift6.0, is adopted in this part for the investigation. Notice that the steady-state part of the version MF-Swift6.1 would be the complete and suitable version (latest version) to use. However, the inflation pressure dependency in the expressions of its parameters is its main difference from the 2002 version, and it is not possible to model and validate this aspect (the inflation pressure dependency) with the available measurements data. The 2002 version is then preferred. Moreover, the 2002 version is a default version implemented in the software Msc Adams.

		Run type						
		PAC89	PAC94	MF-Tyre 5.1/5.2	MC-Tyre 1.0/1.1	MF-Swift 6.0	MF-Swift 6.1	
Steady-state analysis	Pure longitudinal force F_x	●	●	●	●	●	●	
	Pure lateral force F_y	●	●	●	●	●	●	
	Pure overturning moment M_x			●	●	●	●	
	Pure self-aligning moment M_z	●	●	●	●	●	●	
	Combined slip forces F_x and F_y		●	●	●	●	●	
	Combined slip aligning moment M_z		●	●	●	●	●	
Tyre basic parameters	Loaded radius & rolling radius					●	●	
	Contact patch length and width					●	●	
	Longitudinal stiffness			●		●	●	
	Lateral stiffness			●		●	●	
	Rolling resistance						●	
Dynamic analysis	Enveloping behaviour					●	●	
	2D cleat experiments					●	●	
	3D cleat experiments					●	●	

Figure 3.1: Examples of Magic Formula and MF-Swift versions

Remark on figure 3.1:

- ◇ *Enveloping*: it consists in recording the longitudinal force F_x and the vertical force F_z while the tyre running over a specified cleat at a fixed axle height and relative low velocity. Expressions are proposed for describing the profile of these two forces.

3.2. A priori choice of semi-empirical model

- ◇ *Cleat experiments*: it consists in recording the tyre forces and moments during enveloping test but at relative high speed. These tests allow to estimate tyre undamped natural frequencies, tyre belt mass, tyre moments of inertia, and load and speed influences. The specific shapes and dimensions of the cleats are described in MF-Swift software manual.

The pure cornering lateral force and self-aligning moment expressions of the 2002 version of Magic Formula are reminded below.

The lateral shear force F_y is given by:

$$F_y = D_y \sin \left[C_y \arctan B_y \alpha_y - E_y (B_y \alpha_y - \arctan(B_y \alpha_y)) \right] + S_{Vy} \quad (3.1)$$

where :

$$\alpha_y = \alpha + S_H \quad (3.2)$$

$$\gamma_y = \gamma \cdot \lambda_{\gamma y} \quad (\text{corrected camber angle}) \quad (3.3)$$

$$C_y = p_{Cy1} \cdot \lambda_{Cy} \quad (3.4)$$

$$D_y = \mu_y F_z \xi_2 \quad (3.5)$$

μ_y is the lateral friction coefficient and reads:

$$\mu_y = (p_{Dy1} + p_{Dy2} \cdot df_z) (1 + p_{Dy3} \cdot \gamma_y^2) \lambda_{\mu y} \quad (3.6)$$

$$E_y = (p_{Ey1} + p_{Ey2} \cdot df_z) [1 - (p_{Ey3} + p_{Ey4} \cdot \gamma_y) \text{sgn}(\alpha_y)] \gamma_{Ey} \quad \text{where } E_y \leq 1 \quad (3.7)$$

The cornering stiffness is derived as shown below:

$$C_\alpha = K_y = \left. \frac{\partial F_y}{\partial s_\alpha} \right|_{S_\alpha=0}$$

$$C_{\alpha 0} = K_{y0} = p_{Ky1} \cdot F_{z0} \sin \left[2 \arctan \left(\frac{F_z}{p_{Ky2} F_{z0} \lambda_{Fz0}} \right) \right] \lambda_{Fz0} \cdot \lambda_{Ky} \quad (3.8)$$

$$C_\alpha = K_y = K_{y0} (1 - p_{Ky3} |\gamma_y|) \xi_3 \quad (3.9)$$

$$B_y = \frac{C_\alpha}{C_y D_y} \quad (3.10)$$

$$S_{Hy} = (p_{Hy1} + p_{Hy2} \cdot df_z) \lambda_{Hy} + p_{Hy3} \cdot \gamma_y \cdot \xi_0 + \xi_4 - 1 \quad (3.11)$$

$$S_{Vy} = F_z \{ (p_{Vy1} + p_{Vy2} \cdot df_z) \lambda_{Vy} + (p_{Vy3} + p_{Vy4} \cdot df_z) \gamma_y \} \lambda_{\mu y} \cdot \xi_4 \quad (3.12)$$

The self-aligning moment M_z at pure lateral slip condition is proposed as follows :

$$M_z = -t F_y + M_{zr} \quad (3.13)$$

where t represents the pneumatic trail and is expressed as shown below:

$$t = D_t \cos[C_t \arctan\{B_t \alpha_t - E_t(B_t \alpha_t - \arctan(B_t \alpha_t))\}] \cos(\alpha) \quad (3.14)$$

$$\alpha_t = \alpha + S_{Ht}$$

The residual self-aligning moment M_{zr} is given by:

$$M_{zr} = D_r \cos[C_r \arctan(B_r \alpha_r)] \cos(\alpha) \quad (3.15)$$

$$\alpha_r = \alpha + S_{Hf} \quad (3.16)$$

$$S_{Hf} = S_{Hy} + S_{Vy}/K_y \quad (3.17)$$

$$\gamma_z = \gamma \cdot \lambda_{\gamma z} \quad (3.18)$$

$$B_t = (q_{Bz1} + q_{Bz2} \cdot df_z + q_{Bz3} \cdot df_z^2) (1 + q_{Bz4} \cdot \gamma_z + q_{Bz5} |\gamma_z|) \lambda_{Ky} / \lambda_{\mu y} \quad (3.19)$$

$$C_t = q_{Cz1} \quad (3.20)$$

$$D_t = F_z (q_{Dz1} + q_{Dz2} \cdot df_z) (1 + q_{Dz3} \cdot \gamma_z + q_{Dz4} \cdot \gamma_z^2) \frac{R_0}{F_{z0}} \lambda_t \xi_5 \quad (3.21)$$

3.2. A priori choice of semi-empirical model

$$E_t = (q_{Ez1} + q_{Ez2} \cdot df_z + q_{Ez3} \cdot df_z^2) \left\{ 1 + (q_{Ez1} + q_{Ez2} \cdot \gamma_z) \left(\frac{2}{\pi} \arctan(B_t C_t \alpha_t) \right) \right\} \quad \text{with } E_t \leq 1 \quad (3.22)$$

$$S_{Ht} = q_{Hz1} + q_{Hz2} \cdot df_z + (q_{Hz3} + q_{Hz4} \cdot df_z) \gamma_z \quad (3.23)$$

$$D_r = F_z [q_{Dz6} + q_{Dz7} \cdot df_z] \gamma_r + (q_{Dz8} + q_{Dz9} \cdot df_z) \gamma_z R_0 \lambda_{\mu\gamma} + \xi_8 - 1 \quad (3.24)$$

$$df_z = \frac{F_z - F_{z0}}{F_{z0}}$$

F_{z0} is the nominal tyre vertical load and F_z the actual tyre vertical load.

R_0 is the tyre unloaded radius.

Next, a programme, termed MF-Tool, that is used for estimating Magic Formula parameters is presented.

3.2.2 Presentation of the parameters identification tool: MF-Tool

MF-Tool is a programme which allows the estimation of parameters values for MF and MF-Swift versions presented previously in figure 3.1. It uses Levenberg-Marquardt algorithm [34], which is based on an iterative technique locating the minimum of a multivariate function that is expressed as the sum of squares of non-linear real-valued functions. To identify a given version of MF or MF-Swift parameters with MF-Tool, it is required to provide inputs (tyre forces, moments, stiffnesses, etc) in some recommended conditions which are described in MF-Tool users manual. These conditions are mainly the slip conditions (pure or combined slips), the vertical load F_z , the inflation pressure and the wheel speed. Indeed, according to the chosen version of model and the measurements data provided, MF-Tool determines the values of the corresponding parameters that permit better fitting of these measurements data.

Figure 3.2 presents the different steps before using a given version of MF or MF-Swift. Between these steps, the parameters estimation one can be mentioned, which can be achieved with MF-Tool. The measurements data should be saved in a standard file format, TYDEX Files (TF) [35], which is the formal file format recognised by MF-Tool (see an example of TYDEX file in appendix C). After the fitting process, a tyre property file, with extension '.tir', is exported from MF-Tool and contains all the parameters that have been estimated as well as the tyre specific parameters (example: the nominal load, the nominal inflation

pressure, the unloaded radius, the tyre width, tyre vertical stiffness, etc). This property file is used in the simulation environment (simulation software). An example of a tyre property file is presented in appendix D.

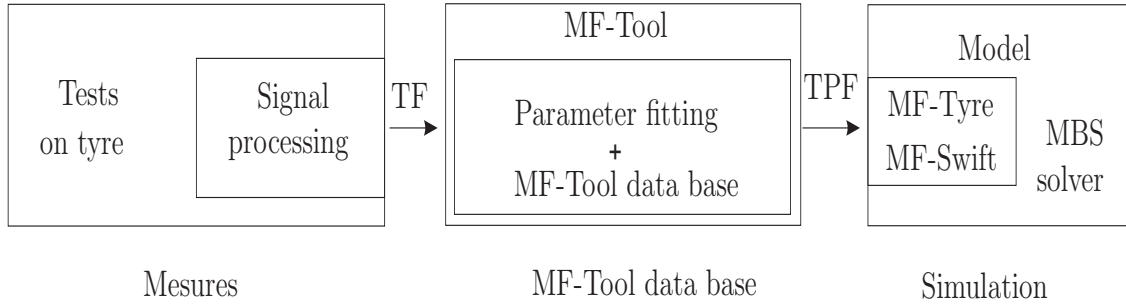


Figure 3.2: The different steps before using MF or MF-Swift. TF: TYDEX File - TPF: Tyre Property File - MBS: Multi Body System

3.2.3 Magic Formula modelling results

In this section, the interpolation capability of the 2002 version of Magic Formula is checked by interpolating the measurements data of the lateral force F_y and the self-aligning moment M_z at pure cornering condition. Then, its prediction capability is also checked by carrying out cross-validation. The cross-validation consists first in determining the parameters values of F_y and M_z models at some given vertical loads F_z and secondly, in using these values for estimating (predicting) the same characteristics (F_y and M_z) at vertical loads different from those used for the interpolation. Then, the estimated results are compared to the measurements data.

MF-Tool is used to determine the values of the model parameters. MF-Tool manual recommends to use measurements data at three different vertical loads corresponding to 40%, 80% and 120% of the nominal load. The nominal load for the considered tyre is $F_{z0} = 243.8kN$. The three recommended vertical loads would then read, $97.52kN$, $195.04kN$ and $292.56kN$ respectively. It can be remarked that the available measurements data do not match this requirement. However, a judicious choice of three vertical loads data between those available can lead to relative good interpolation results in MF-Tool. Several combinations of data for the interpolation have been tried but the one corresponding to loads $68.3kN$, $112.2kN$ and $156kN$ gives the smallest error for the cross-validation. Thus, the lateral force and the self-aligning moment results for these three vertical loads are used for the interpolation in MF-Tool. Next, the parameters determined from this

3.2. A priori choice of semi-empirical model

interpolation are used for estimating the lateral force and the self-aligning moment for vertical loads: $24.4kN$ and $200kN$.

To take into account the dependency of parameters with respect to the inflation pressure, it is recommended to use measurements data at p_0 and $p_0 \pm 0.5$ for the interpolation (fitting) process, where p_0 represents the nominal inflation pressure and is equal to 16 bars. In contrary to the case of the vertical loads, no option was found for determining reasonable parameters with inflation pressures, 11.3 bars, 14 bars and 16 bars. It is then chosen to not consider its influence.

Figures 3.3, 3.4, 3.5 and 3.6 show the modelling results obtained for the lateral force F_y and the self-aligning moment M_z at pure cornering at inflation pressure 11.3 bars and 16 bars. In these figures, the expression 'MF - Fitted data' means that the corresponding measurements data have been used in the fitting (interpolation) process with MF-Tool. The corresponding curves represent then the interpolation results of MF. It is the case of data at vertical loads $68.3kN$, $112.2kN$ and $200kN$. The second expression, 'MF - Estimated data', means that the designated measurements data have not been used in the fitting process with MF-Tool, and therefore, the proposed curves are estimated (predicted) by the model. It is the case of data at vertical loads $24.38kN$ and $156kN$. For each vertical load, the interpolated or estimated results are compared with the measurements data. The maximum of the standard deviation between measurements data and simulation (interpolated or predicted) is 1.9% for F_y and 8.8% for M_z . Therefore, the model better represents the lateral force than the self-aligning moment. Nevertheless, deviations observed for both lateral force and self-aligning moment can be considered to be within acceptable range.

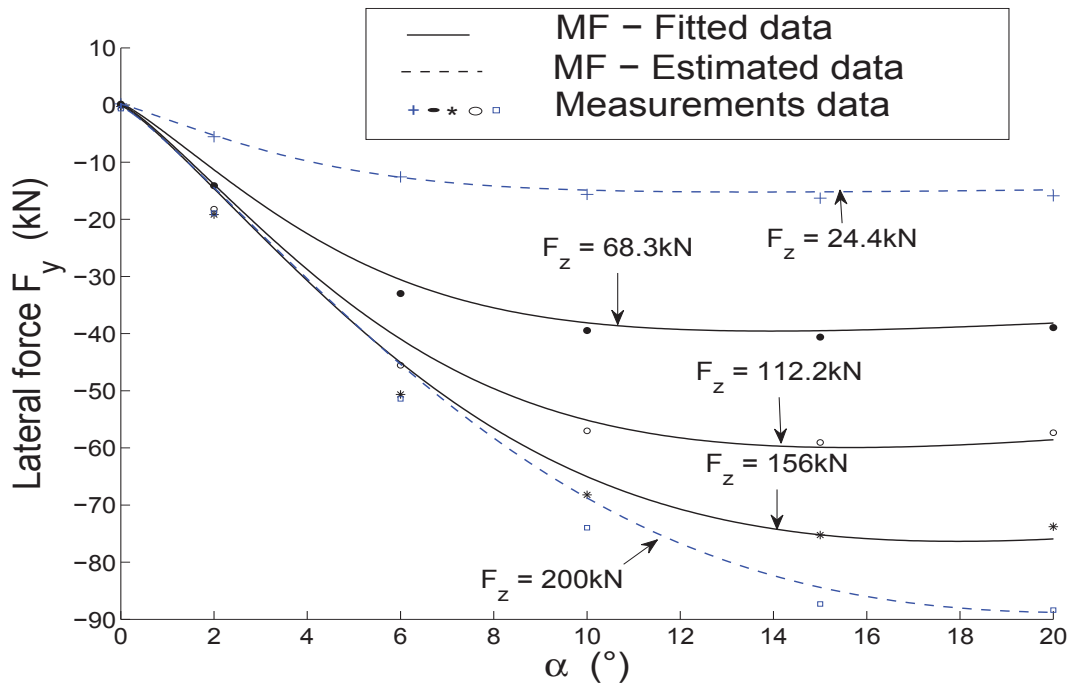


Figure 3.3: Magic Formula - pure lateral force F_y - inflation pressure $p = 11.3$ bars

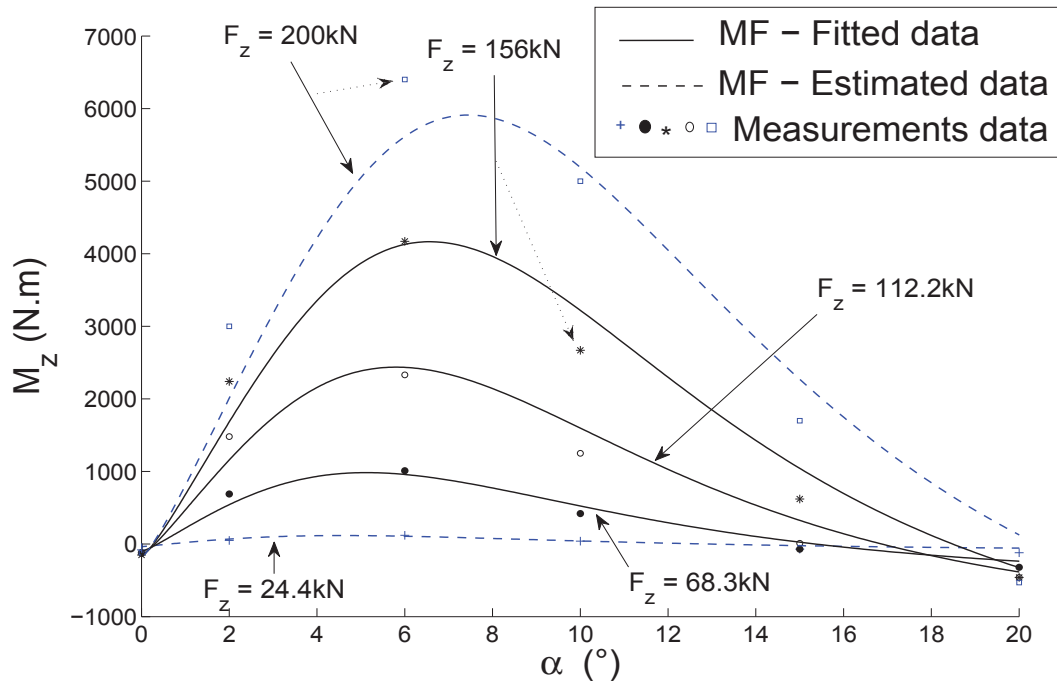


Figure 3.4: Magic Formula - pure lateral slip self-aligning moment M_z - inflation pressure $p = 11.3$ bars:

3.2. A priori choice of semi-empirical model

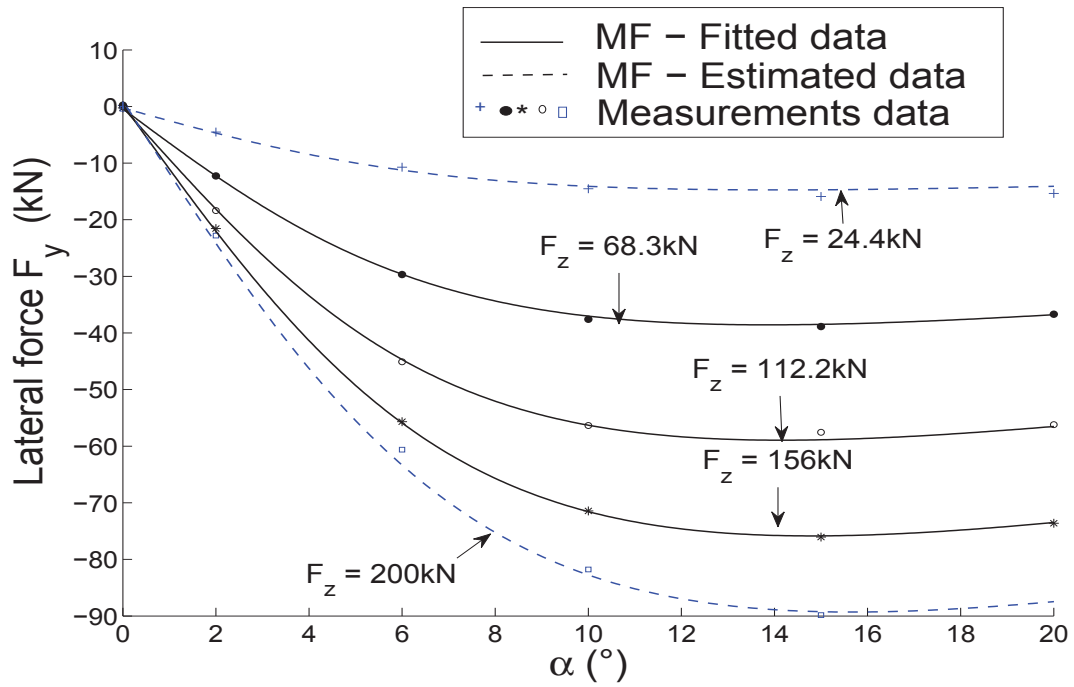


Figure 3.5: Magic Formula - pure lateral force F_y - inflation pressure $p = 16$ bars

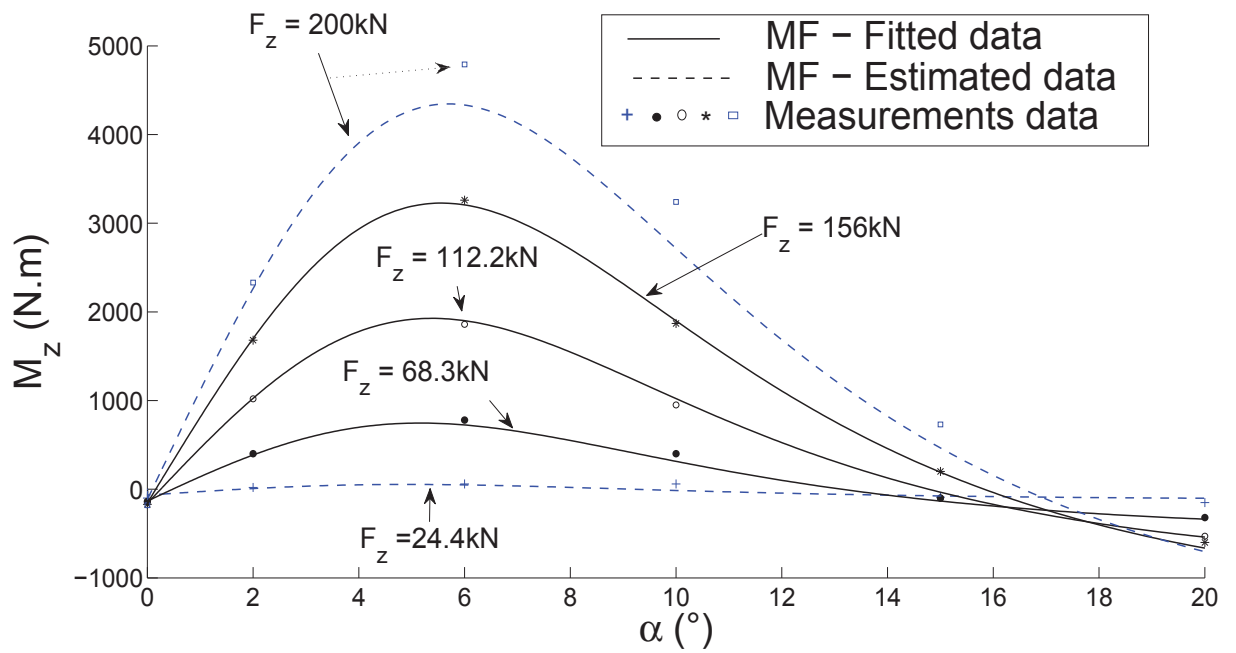


Figure 3.6: Magic Formula - pure lateral slip self-aligning moment M_z - inflation pressure $p = 16$ bars

The influence of the inflation pressure on the pure cornering force and moment cannot be modelled because the inflation pressures used for the measurements are too different from each other and cannot be handled by MF-Tool. Nevertheless, in the next paragraphs, the measurements data are commented and compared to the literature studies, example [33].

3.2.3.1 Effect of inflation pressure on F_y

Consider the cornering stiffness C_α , which is the gradient of the curve $F_y = f(\alpha)$, measured at zero side slip angle at a given vertical load. In [33], it is observed for passenger car tyres that an increase of inflation pressure at low vertical load leads to low cornering stiffness C_α . However, at relative high vertical load, an increase of inflation pressure leads to a rise of cornering stiffness. The same phenomenon seems to appear on aircraft tyres as shown in figures 3.7, 3.8, 3.9 and 3.10. For example, in figure 3.7, which corresponds to the vertical load of $24.4kN$ (10% of nominal load), the slope C_α tends to slightly decrease when inflation pressure is increased. C_α takes the values $165.3kN/rad$, $148.4kN/rad$ and $134kN/rad$ for inflation pressures 11.3 bars, 14 bars and 16 bars respectively. In the other hand, figure 3.10 shows that for the vertical load of $200kN$ (82% of nominal load), the slope C_α slightly increases when the inflation pressure rises. C_α takes the values $658.8kN/rad$, $712.5kN/rad$ and $802.2kN/rad$ for inflation pressures 11.3 bars, 14 bars and 16 bars respectively. However, since, the measurements data do not cover sufficient range of the tyre vertical load, it is not possible to conclude on the general tendency of the lateral force with regard to the inflation pressure. Equation (3.25) shows the current Magic Formula expression for the cornering stiffness as a function of the inflation pressure [33].

$$C_\alpha = K_y = p_{Ky1}(1 + p_{py1}dp^2)F_{z0} \sin\left[2 \arctan\left(\frac{F_z}{p_{Ky2}(1 + p_{py2}dp^2)F_{z0}\lambda_{F_{z0}}}\right)\right] \quad (3.25)$$

where $dp = \frac{p - p_0}{p_0}$, p the current inflation pressure, p_0 the nominal inflation pressure and F_z the current vertical load. p_{Ky1} , p_{py1} and p_{Ky2} , p_{py2} are constants.

The influence of inflation pressure on the peak of the lateral force is taken into account in the expression of the lateral friction coefficient μ_y :

$$\mu_y = (p_{Dy1} + p_{Dy2}df_z)(1 + p_{Dy3}dp + p_{Dy4}dp^2) \quad (3.26)$$

where $df_z = \frac{F_z - F_{z0}}{F_{z0}}$ and F_{z0} the nominal vertical load. p_{Dy1} , p_{Dy2} , p_{Dy3} , p_{Dy4} are constants.

3.2. A priori choice of semi-empirical model

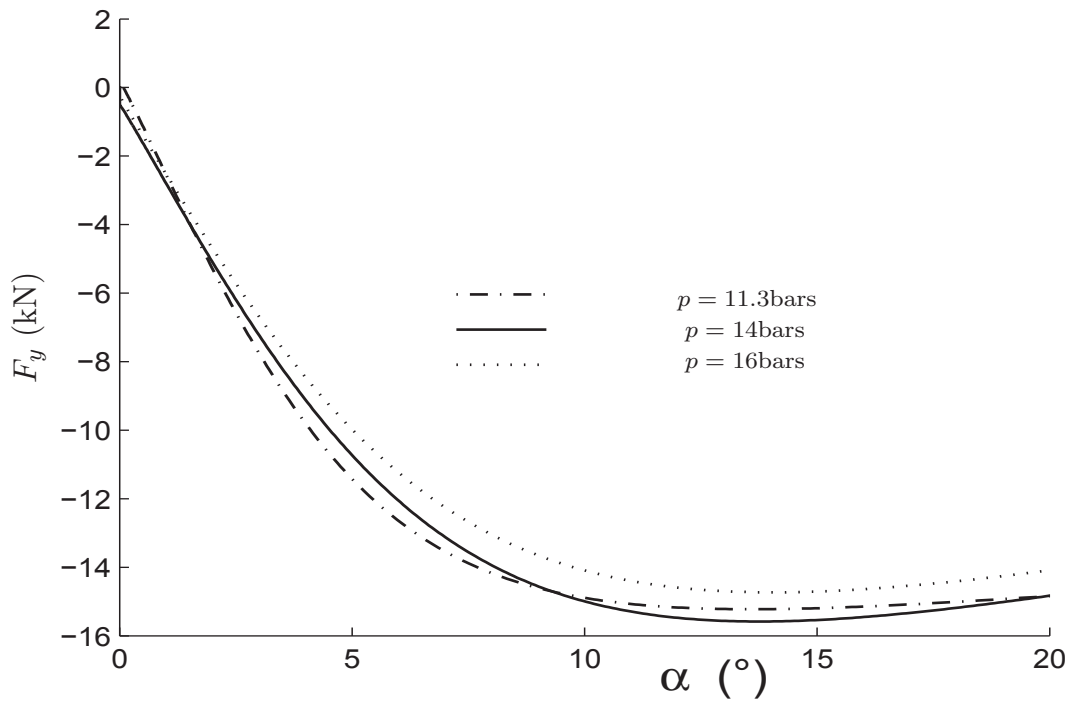


Figure 3.7: Influence of inflation pressure on F_y $F_z = 24.4kN$

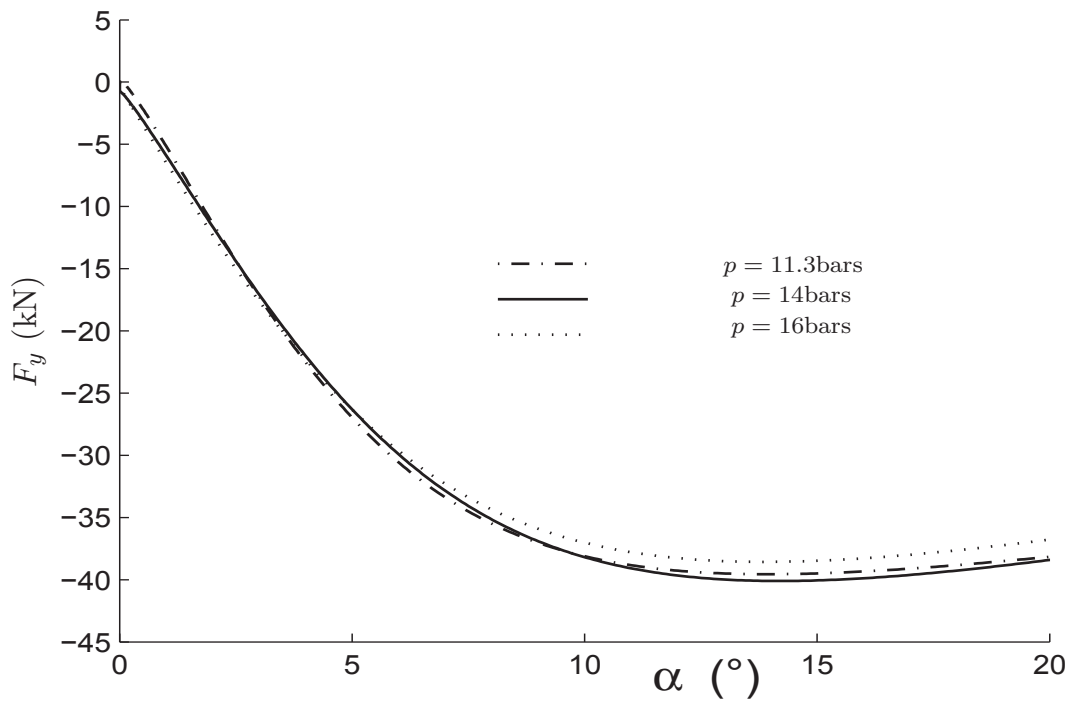


Figure 3.8: Influence of inflation pressure on F_y $F_z = 68.3kN$

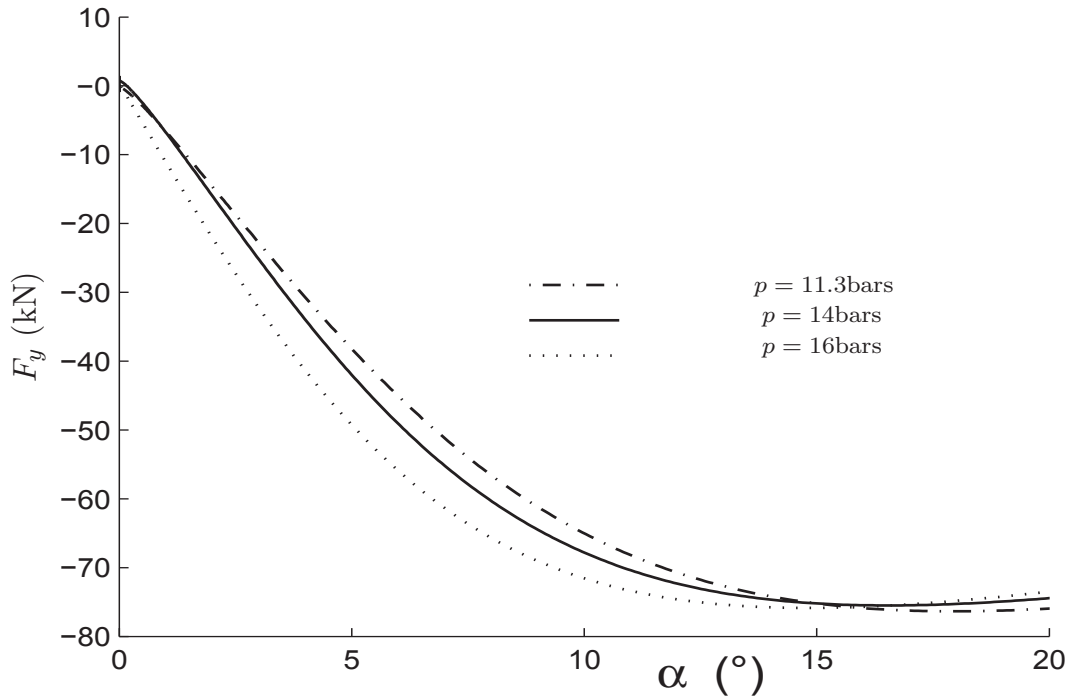


Figure 3.9: Influence of inflation pressure on $F_y - F_z = 156kN$

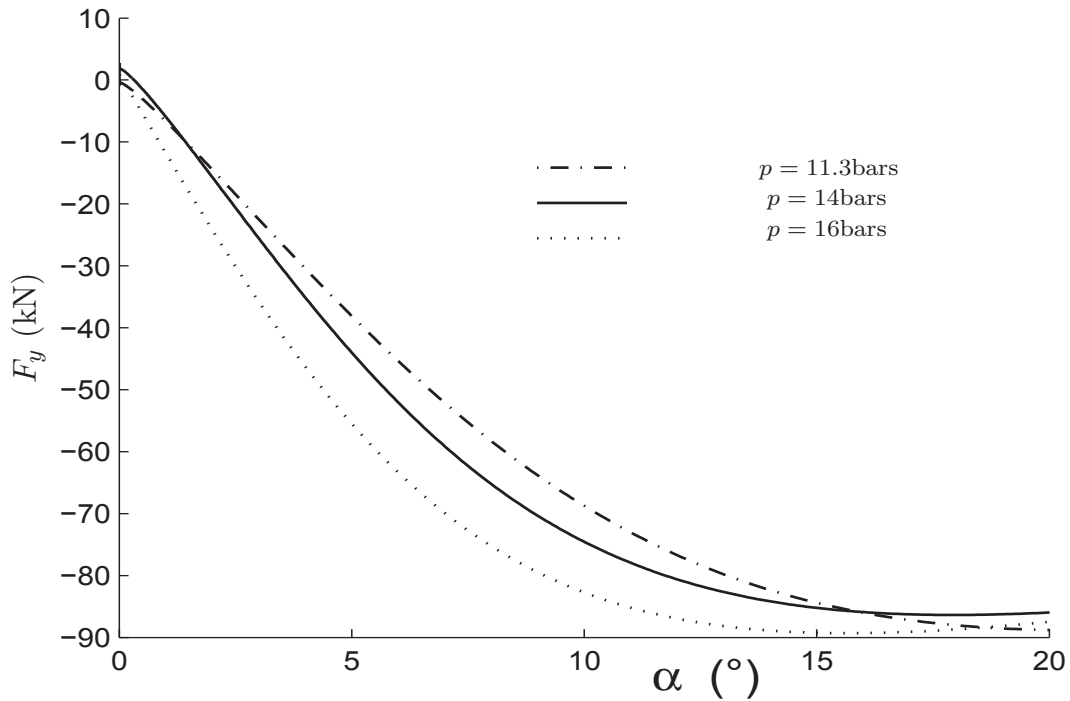


Figure 3.10: Influence of inflation pressure on $F_y - F_z = 200kN$

3.2. A priori choice of semi-empirical model

3.2.3.2 Effect of inflation pressure on M_z

In figures 3.11, 3.12, 3.13 and 3.14, the inflation pressure also shows an influence on the self-aligning moment M_z . When the inflation pressure is increased, the peak of M_z tends to decrease for all the considered vertical loads. In addition, the slope at the origin of the curve $M_z = f(\alpha)$ tends to slightly decrease with the inflation pressure at relative low vertical loads, see curves for vertical load $24.4kN$ in figure 3.11. In fact, the slope takes the values $3725Nm/rad$, $3440Nm/rad$ and $3250Nm/rad$ for the inflation pressures 11.3 bars, 14 bars and 16 bars respectively. But, at relative high vertical loads, example of $200kN$ in figure 3.14, the influence of the inflation pressure on the slope becomes less significant and unpredictable while its influence on the peak value of M_z remains important.

In general, an increase of the inflation pressure results in a higher vertical stiffness, and therefore in a shorter contact length and a smaller pneumatic trail. The pneumatic trail is the relation of the self-aligning moment and the lateral force. In addition, the change in contact length is relatively larger than the change of lateral force, which causes the self-aligning moment to decrease with the inflation pressure [33].

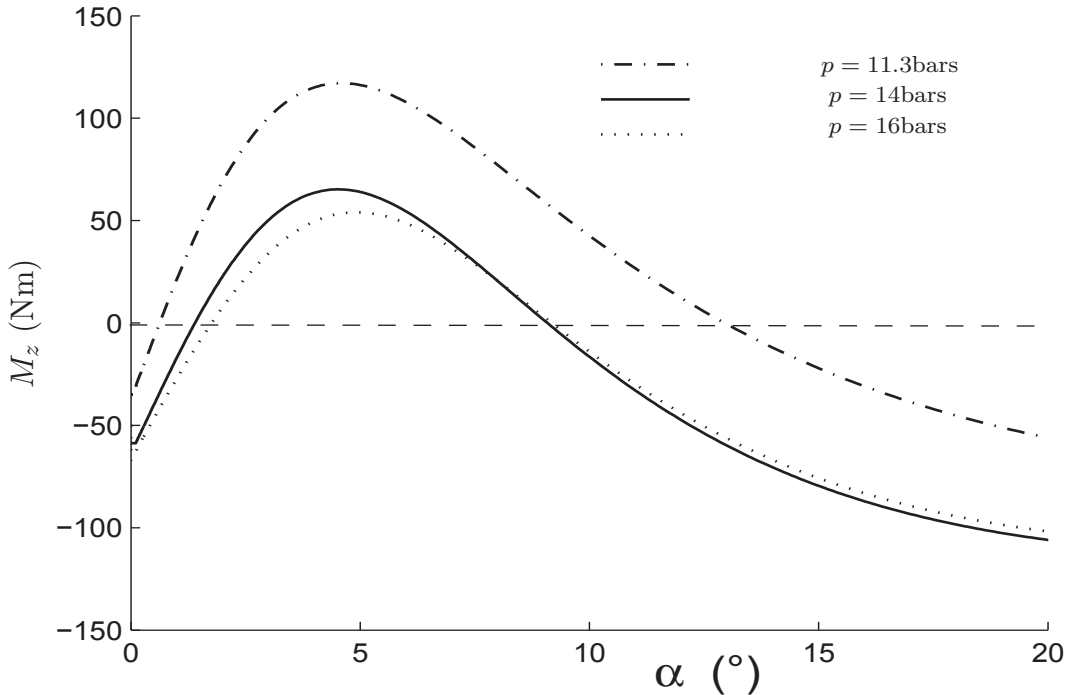


Figure 3.11: Influence of inflation pressure on $M_z - F_z = 24.4kN$

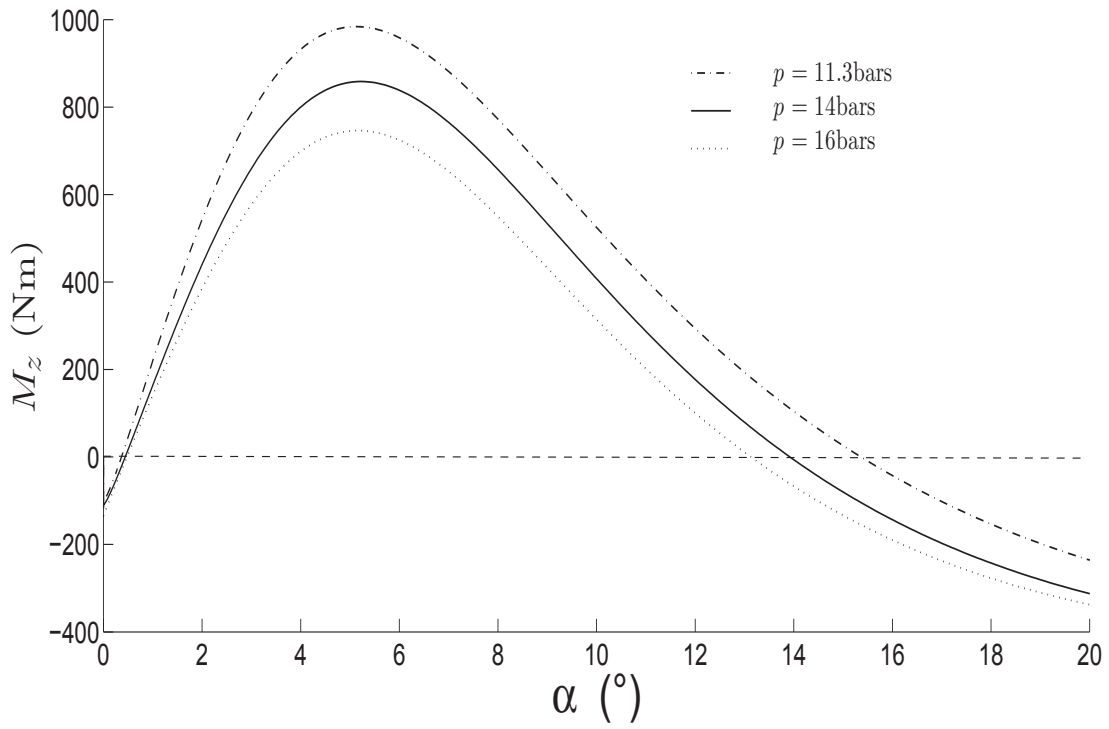


Figure 3.12: Influence of inflation pressure on M_z - (b) $F_z = 68.3kN$

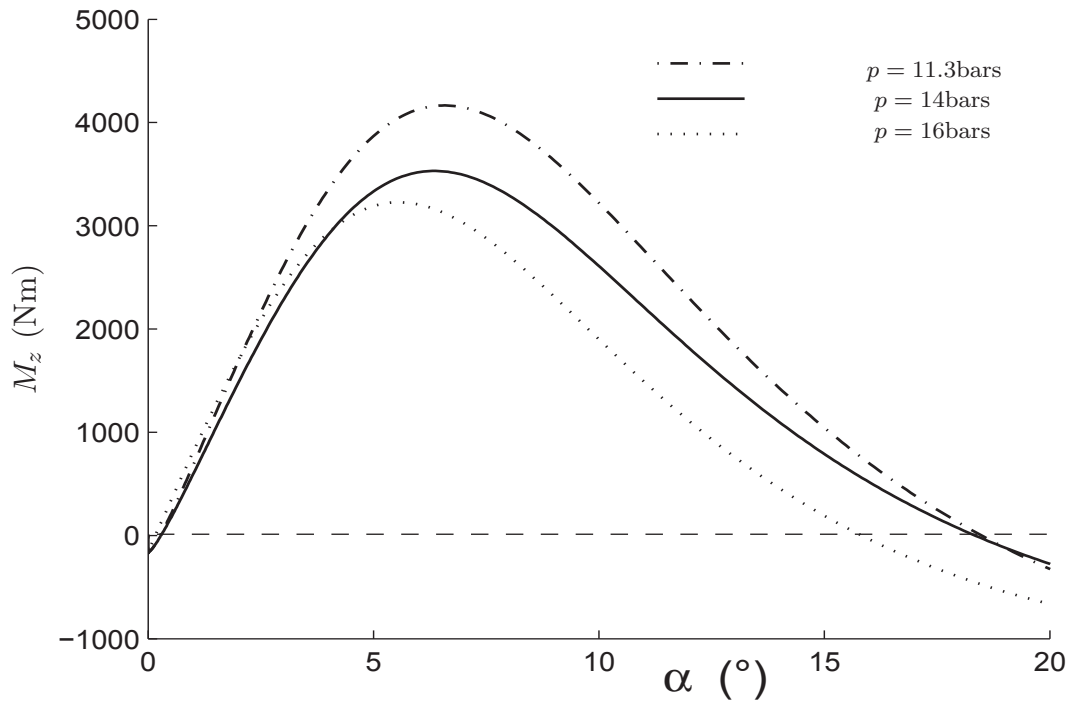


Figure 3.13: Influence of inflation pressure on M_z - $F_z = 156kN$

3.3. Simulating Magic Formula as implemented in Msc Adams software

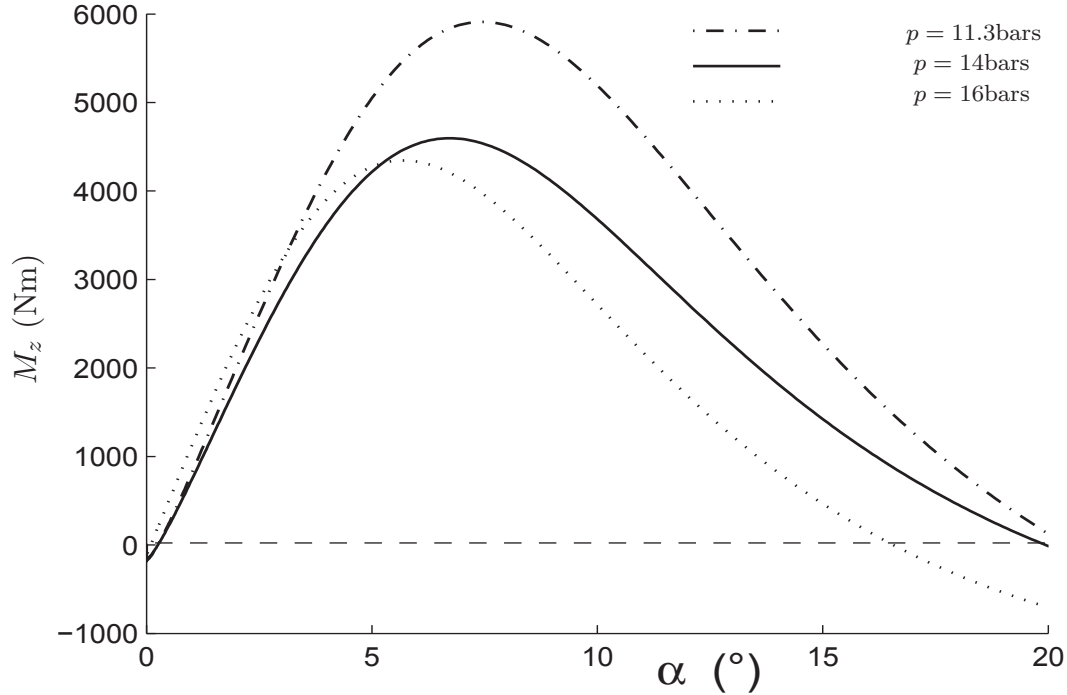


Figure 3.14: Influence of inflation pressure on M_z $F_z = 200kN$

Equation (3.27) describes the current Magic Formula expression of the pneumatic trail as a function of the inflation pressure.

$$D_t = F_z(q_{Dz1} + q_{Dz2}df_z)(1 - q_{pz1}dp)\frac{R_0}{F_{z0}} \quad (3.27)$$

where q_{Dz1} , q_{Dz2} and q_{pz1} are constants. R_0 is the unloaded tyre radius. F_{z0} , F_z and df_z are same as already defined in equation (3.26).

3.3 Simulating Magic Formula as implemented in Msc Adams software

The objective is to integrate Magic Formula in a multi-body system that represents a tyre test machine and to model pure cornering in the same conditions used for the previous mentioned measurements data. The simulation environment used is Msc Adams software. It will help to validate the choice of Magic Formula model for studying the steady-state tyre-road interaction forces and moments and also to check the ability of the model to be integrated in the simulation environment.

Up to year 2009, PAC89/94, PAC-Time and PAC2002 are default versions of MF imple-

mented in Msc Adams software. In the application presented next, PAC2002 version as implemented in Msc Adams is considered. The simulation is carried out by developing a tyre test rig that can reproduce the functional model of a real test machine. Measurements data are used to validate the tyre model results from the test rig.

3.3.1 Tyre test rig model in Msc Adams

Figure 3.15 presents a schematic representation of the test rig model that illustrates the principle of operation. The tyre test rig contains a tyre-part that rolls forward and interacts on a flat uniform road surface. The tyre-part is connected to a frame-part by a revolute joint aligned with the spin axis of the wheel. The frame-part is connected to the sideslide-part by a cylindrical joint that is aligned in the vertical direction. The cylindrical joint allows in one hand, a rotational motion that is used to set or vary the side slip angle of the tyre during simulation. In the other hand, the cylindrical joint allows a vertical translation motion that can be used to control the vertical position of the wheel center relative to the runway. This translation motion can be deleted, and a vertical wheel load can be defined that allows the tyre to locate on the runway as a function of the tyre vertical stiffness and damping. The definition of the wheel load introduces then another degree of freedom in the model.

The model is set to ignore gravitational force, so that the applied wheel load can be varied and set equal to the desired vertical load during simulation. The sideslide-part is connected to the carrier-part by a translation joint aligned in the lateral direction. This motion is used to set the lateral position of the tyre. Then, the tyre can be dragged in a sideways direction relative to the runway. The carrier-part is connected to the ground (road-part) by a translation joint aligned with the direction of travel of the wheel. The forward velocity of the tyre during simulation is controlled by applying a motion on this translation joint. The model has therefore two rigid body degrees of freedom. The first degree of freedom is associated with the spin motion of the tyre which depends on the longitudinal force: traction, braking or rolling resistance. The second degree of freedom is the vertical position of the wheel center that is defined by the wheel load, the vertical stiffness and damping of the tyre. In the present work, a vertical load is defined and the vertical translation motion of the cylindrical joint is canceled. Only pure cornering is considered and therefore, it is considered that no traction or braking force is generated. All parts are supposed rigid relative to the tyre stiffnesses.

Remark: The camber angle motion is not modelled in the test rig because it is not taken into account in this study.

3.3. Simulating Magic Formula as implemented in Msc Adams software

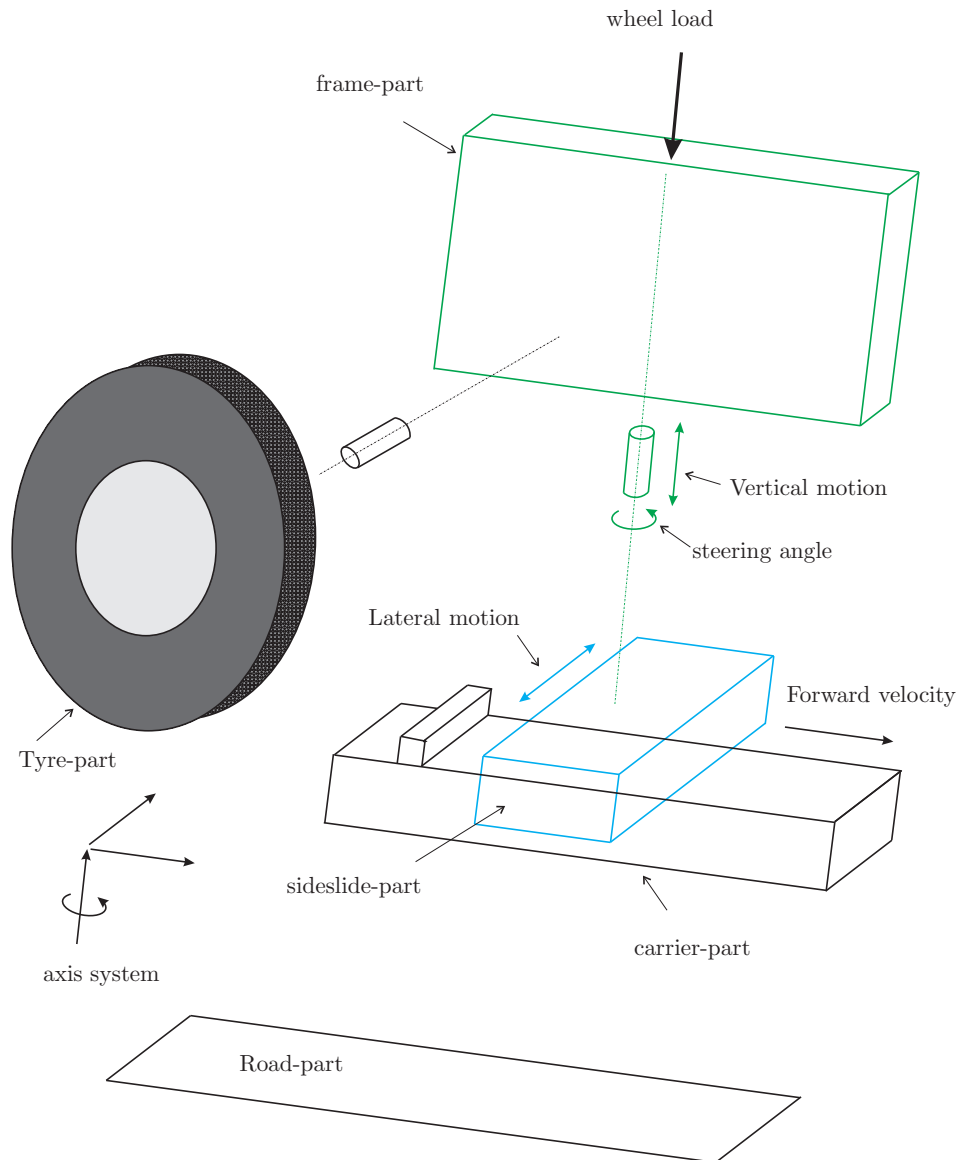


Figure 3.15: Adams tyre test rig model used in Adams - Principle of operation

3.3.2 Steady-state pure cornering

For each inflation pressure, a tyre property file (with extension '.tir') is exported from MF-Tool and contains all the parameters that have been estimated for the model. On the test rig, the steering rate is set at $2^\circ/s$ and the slip angle α is swept from 0 to 20° . The forward velocity is set constant at 8 m/s . Msc Adams uses the property file with the test rig to determine the lateral force F_y and the self-aligning moment M_z at each step of the simulation. The simulation is repeated for the following vertical loads: 24.4 kN , 68.3 kN ,

112.2kN, 156kN and 200kN.

Simulation results

The lateral force and the self-aligning moment simulation results obtained from Msc Adams tyre test rig are compared to measurements data. It is found that the simulation results are quite similar to those obtained from the direct use of the model equations already presented in section 3.2.3. Thus, it is chosen to not repeat the same curves in this section.

3.3.3 Parking manœuvres

When the wheel is being steered at low or zero speed, the manœuvre is often termed parking. Experiments have shown that the torque acting on the tyre at such conditions often becomes very large [10].

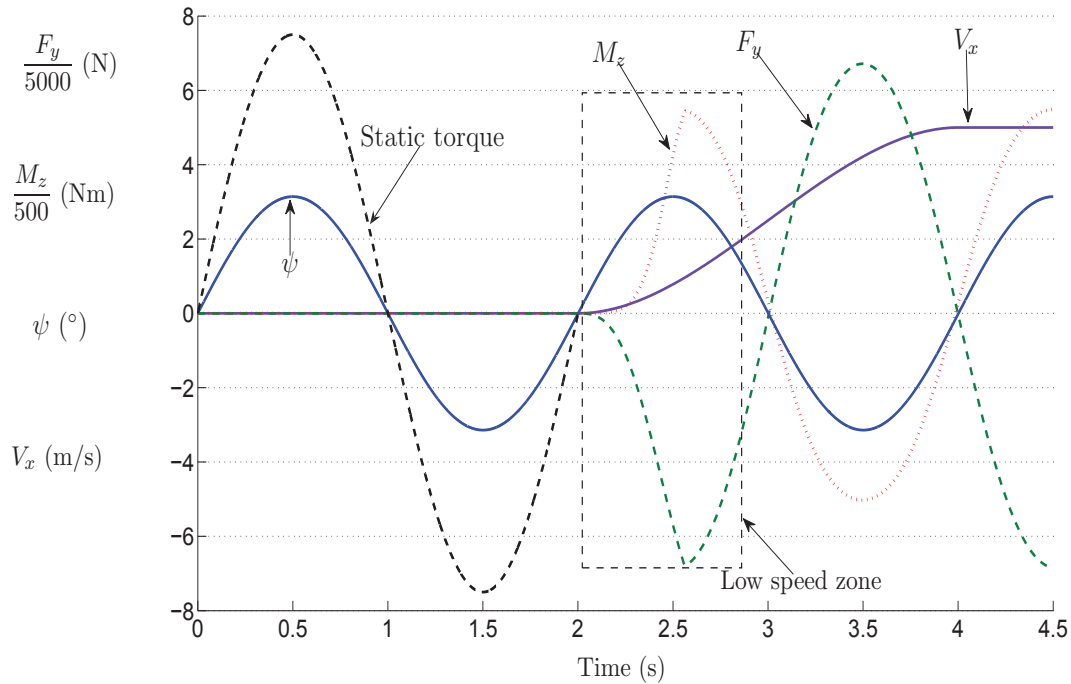


Figure 3.16: F_y and M_z evolution from static torsion to dynamic cornering

Figure 3.16 presents simulation results of a tyre submitted to static torsion and to dynamic pure cornering successively. The test rig described previously is used and the tyre is first loaded at the vertical load of $F_z = 150kN$ with the inflation pressure of 16 bars. Then a sinusoidal steer angle variation ψ is imposed on the cylindrical joint, that links the frame-

3.3. Simulating Magic Formula as implemented in Msc Adams software

part to the sideslip-part, at time $t = 0$. The longitudinal velocity V_x is kept zero from time $t = 0$ to time $t = 2s$, after which it is progressively increased up to 5m/s at time $t = 4s$. Since Magic Formula describes the tyre-road interaction for a rolling wheel. It can be remarked that the lateral force (its absolute value $|F_y|$) as well as the self-aligning moment M_z start building up at time $t = 2s$ where the longitudinal speed V_x is different from zero. Before this time, $V_x = 0$ and the tyre responds to the steer angle by developing a torsion torque exclusively.

The Magic Formula equation used previously for representing the self-aligning moment is only valid for a rolling wheel in which the lateral motion generates lateral tyre tread displacement (lateral slip) and thus a lateral force. The self-aligning moment is then supposed to be the product of this lateral force and the pneumatic trail, which represents the shift of the lateral force line of action from the contact patch center. However, at very low or zero speed, the torsional deformation of the tyre is quantitatively more dominant and the tyre lateral slip definition ($S_\alpha = \frac{V_y}{V_x}$) tends to be infinite and does not make sense. Then, the Magic Formula equations cannot be used in their original form. Based on the work of Van der Jagt [36], Pacejka [10] proposes the following empirical expressions for modelling the tyre torque at low and zero speed.

$$M_z = M_{z\varphi1} + M_{z\varphi2} \quad (3.28)$$

where

$$\begin{aligned} M_{z\varphi1} &= w_{Vlow} \cdot D_{Dr\varphi} C_{Dr\varphi} B_{Dr\varphi} R_0 \varphi' \\ M_{z\varphi2} &= (1 - w_{Vlow}) \cdot D_{Dr\varphi} \sin \left[C_{Dr\varphi} \arctan(B_{Dr\varphi} R_0 \varphi') \right] \end{aligned} \quad (3.29)$$

w_{Vlow} is an empirical parameter defined as follow:

$$\begin{aligned} w_{Vlow} &= \frac{1}{2} \left[1 + \cos \left(\pi \frac{V_x}{V_{low}} \right) \right] \quad \text{if } |V_x| \leq V_{low} \\ w_{Vlow} &= 0 \quad \text{else} \end{aligned} \quad (3.30)$$

V_{low} represents the critical limit of the longitudinal velocity below which the self-aligning moment is significantly influenced by the tyre velocity. Consequently, the previous Magic Formula equation for M_z is no longer valid below this critical speed and equation (3.28) should be considered. R_0 is the free unloaded tyre radius. $D_{Dr\varphi}$, $C_{Dr\varphi}$ and $B_{Dr\varphi}$ are empirical parameters and φ' is the transient turn slip angle.

From equation (3.29), it can be remarked that the first component $M_{z\varphi1}$ decreases in

magnitude with increasing speed until it vanishes at $V_x = V_{low}$ while the second component $M_{z\varphi 2}$ increases from zero to its maximum value at $V_x = V_{low}$.

In figure 3.16, the static torsion torque for $0 \leq t \leq 2s$, is simply a hand calculation obtained as the product of the tyre torsional stiffness ($\sim 86kN/rad$) and the torsion angle ψ . However, for $2 < t \leq 4.5s$, the curves corresponding to the self-aligning torque M_z and the lateral force F_y are estimated by Msc Adams using Magic Formula pure cornering equations. Since the critical speed V_{low} as well as the empirical parameters are not available (not provided in the tyre property file), the transition phase (low speed zone), which describes the influence of the tyre speed on M_z from zero to V_{low} , is not taken into account. However, it is found worth presenting figure 3.16 because it helps to emphasise the difference between the static torque and the torque of the dynamic tyre. For the considered tyre, it can be remarked that for the same steering angle, the static torque is twice greater than the dynamic one.

3.3.4 Lateral relaxation length σ_y

In general, experimental determination of the lateral relaxation length is performed by first applying a steering angle to the wheel, then loading it at the desired vertical load and finally, starting rolling the wheel at a relative low velocity (e.g. $0.5m/s$). A lateral force builds up progressively in the tyre-ground interface. Then, the lateral relaxation length corresponds to the distance rolled by the tyre before the lateral force F_y reaches 63% of its maximum value F_{ymax} . In the literature, the lateral relaxation length σ_y is often defined as the ratio of the cornering stiffness C_α over the tyre lateral stiffness k_y .

$$\sigma_y = \frac{C_\alpha}{k_y} \quad (3.31)$$

In the latest version of Magic Formula implemented in Msc Adams, for a given inflation pressure, the lateral stiffness k_y is assumed constant independently of the vertical load [33]. In fact, only the average stiffness for all vertical load conditions used in the measurement process is considered:

$$k_y = \frac{1}{N} \sum_{i=1}^N k_{yi} \quad (3.32)$$

where k_y is the average value of lateral stiffness, k_{yi} the stiffness value at the vertical load F_{zi} , and N the number of vertical load conditions.

In the tyre test rig, the vertical load is set at $F_z = 200kN$, the side slip angle α at 1° and the forward velocity V_x at $0.5m/s$. Then, the relaxation length is determined as shown in figure 3.17. The relaxation length is found to be $\sigma_y = 0.65m$ that corresponds to the

3.3. Simulating Magic Formula as implemented in Msc Adams software

lateral force $|F_y| \sim 7.8kN$.

Finally, the vertical load is varied from $130kN$ to $300kN$ and the corresponding relaxation lengths are modelled. The results at both inflation pressures 14 bars and 16 bars are plotted in figure 3.18 (the lateral stiffness values are only available for these two inflation pressures). Since Pacejka model PAC2002 considers that the lateral stiffness k_y does not depend on the vertical load at each inflation pressure, equation (3.31), the lateral relaxation length σ_y is therefore governed by the cornering stiffness C_α . At low vertical loads, when the inflation pressure is increased, the cornering stiffness decreases, which leads to low relaxation length, figure 3.18. However, at relative high vertical loads, the cornering stiffness increases with inflation pressure, which leads to high relaxation length.

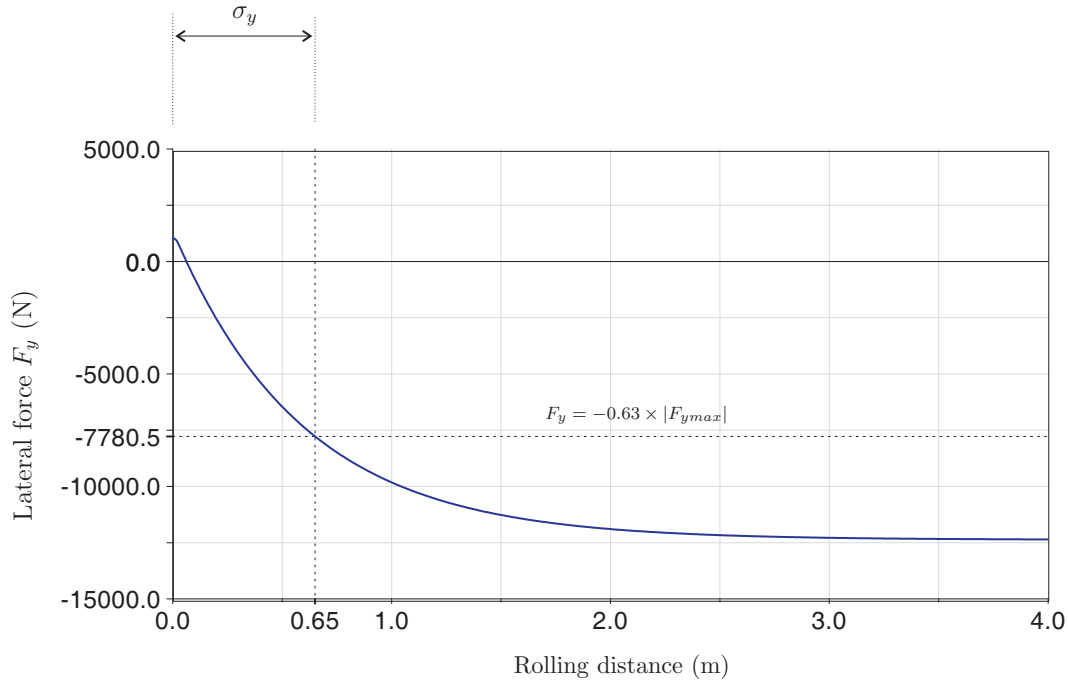


Figure 3.17: Determination of lateral relaxation length σ_y (Msc Adams)

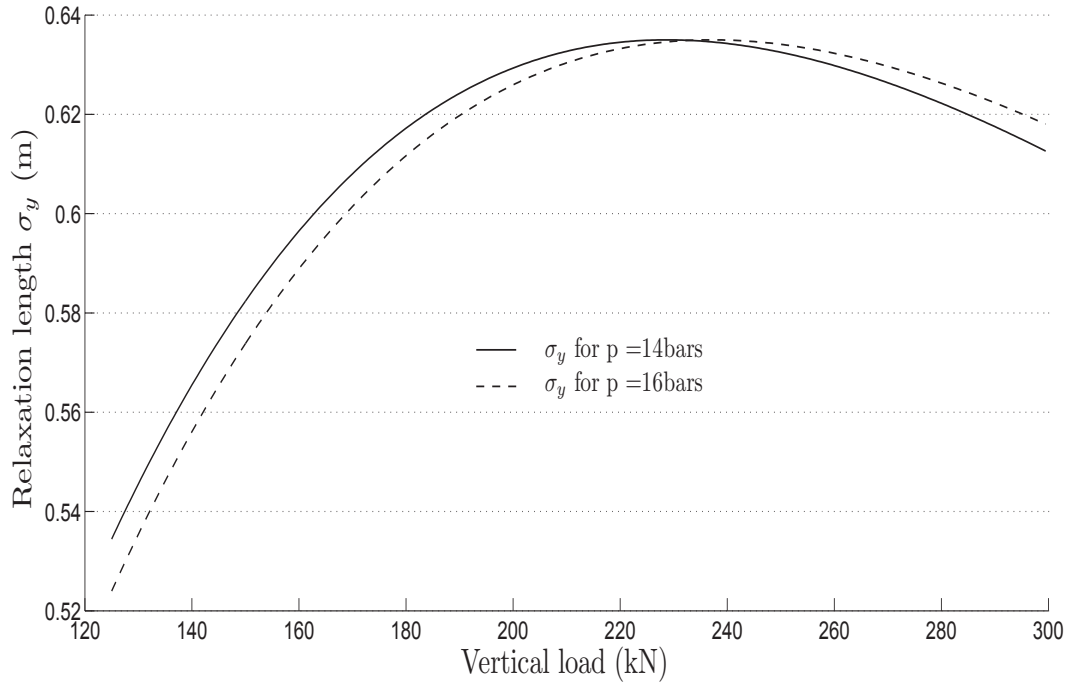


Figure 3.18: Estimated relaxation length σ_y

Remark

From the study of physical and semi-empirical models, chapters 2 and 3 respectively, it can be underlined that the lack of measurements data in the required manoeuvre conditions makes it difficult to provide a definitive choice of suitable model(s). In fact, the estimation of a chosen or/and a developed model parameters as well as the validation of the modelling results require measurements data. Magic Formula model is adopted as suitable model for the investigation but its validity is only checked at pure cornering condition. Validation of this model in the remaining tyre manoeuvre conditions such as pure longitudinal slip (driving/braking), combined slip and parking are then necessary in order to make a definitive choice.

3.4 Conclusion

The interpolation and the prediction capability of Magic Formula model (2002 version) have been tested at pure cornering condition. Indeed, in one hand, some measurements data (of the lateral force and of the self-aligning moment) are used for estimating Magic Formula parameters with MF-Tool (interpolation step). In the other hand, the determined parameters are used to estimate the lateral force and the self-aligning moment at verti-

3.4. Conclusion

cal loads different from those used for the interpolation with MF-Tool (prediction step). The maximum of the standard deviation between measurements data and modelling results (interpolated or predicted) is 1.9% for the lateral force and 8.8% for the self-aligning moment. These deviations can be considered to be within acceptable range. Because of lack of measurements data, pure driving/braking, combined slip, parking and influence of inflation pressure could not be studied.

A tyre test rig model has been developed in Msc Adams software for simulating pure cornering using the version PAC2002 (in steady-state conditions, PAC2002 is equivalent to the 2002 version of MF). In the case of pure cornering, it is found that the modelling results are quite similar to those obtained from the direct use of the model equations.

Moreover, it is underlined that Magic Formula current versions (example of the 2002 version) propose expressions for modelling the tyre characteristics in the entire steady-state conditions required for the present study. With respect to the satisfactory agreement obtained at pure cornering, it may be expected that the model will provide similar modelling results for the tyre characteristics at pure driving/braking, combined slip and parking conditions.

Besides, it can be remarked that Magic Formula as well as the other literature tyre models studied do not consider a longitudinal force F_x during pure cornering and therefore, the models do not propose any expression for it. However, the measurements data described in chapter 2 mentioned that a longitudinal force has been recorded at pure cornering. Moreover, this longitudinal force increases with the side slip angle and also with relative significant magnitude when compared to the lateral force one. It is then obvious that the side slip angle has significant influence on the tyre drag force (longitudinal force), and this phenomenon is neither modelled by Magic Formula nor by the models presented in chapter 1. Thus, the next chapter will focus on studying the generation of this longitudinal force at pure cornering.

CHAPTER 4

Real shear forces and moment at pure lateral slip

From the tyre models investigation performed in chapters 2 and 3, it is underlined that longitudinal force has been neglected in general at pure cornering condition. Therefore, in the contact patch, the total force is assumed to be equal to its lateral component. However, in the context of this study, a longitudinal force has been recorded at pure cornering performed on an aircraft tyre. It is shown that this force increases with the side slip angle and also with relative significant magnitude when compared to the lateral force one. In this chapter, the Poisson ratio, which describes the contraction of an incompressible material when it is stretched in one direction, is taken into account in a comprehensive physical approach to describe the generation of this longitudinal force. This force is also referred as induced longitudinal force. Moreover, an exhaustive description of the self-aligning moment generation at pure lateral slip is proposed by decomposing it into contributions of the induced longitudinal force and the lateral force. Relative simple model is proposed for the induced longitudinal force as well as for the self-aligning moment and finally, both models results are compared to measurements data [37, 38, 39].

4.1 Introduction

The behaviour of the tyre is complex and it is required to consider either extensive and complex models or models with considerable simplification for its full solution. Indeed, the major part of the steady-state tyre mathematical models that exist in the literature are all developed according to two hypotheses. The first hypothesis is pure longitudinal or pure lateral tyre slip condition and the second is combined tyre slip condition. Pure

lateral slip describes the transversal velocity of the tyre during cornering manoeuvre without braking/driving torque, camber and turn slip. The tyre is also said to be at pure cornering condition. At pure lateral slip condition, it has been also deemed that the tread band displacement in the contact patch is exclusively in the transversal (lateral) direction and therefore, only transversal (lateral) force is developed.

It is worth mentioning that in reality, longitudinal force is always generated by the tyre during pure cornering. But, for some types of tyres (example of passenger cars tyres), this longitudinal force is often negligible when compared to the lateral force during pure cornering. However, with respect to the considered tyre properties and its loading conditions (example of aircraft tyres), this assumption of zero longitudinal force at pure cornering may lead to a misinterpretation of the tyre real behaviour. In fact, the non uniform lateral tread stretching in the contact patch generates a longitudinal tread contraction (displacement) and as a result, a longitudinal force is developed [37, 38, 39].

The aim of the present chapter is to physically describe the generation of this longitudinal force at pure cornering. For this purpose, a simple but comprehensive physical approach is first used to describe the tyre tread displacement in the longitudinal direction at pure cornering and a model is proposed for the corresponding longitudinal force. This force is referred as induced longitudinal force. Then, the same approach is used to provide an exhaustive description of the self-aligning moment generation. The relative simplicity of the approach used in this chapter is achieved by the means of some assumptions on the tyre structure modelling. These assumptions are similar to those adopted in the basic brush model development as they are presented in [3, 10] for example. Due to this basic representation of the tyre structure, the scope of this chapter is mainly to provide a comprehensive description of the longitudinal force and the self-aligning moment generation at pure lateral slip rather than deriving models that better fit with measurements data. Finally, the Magic Formula model is proposed for representing this longitudinal force at pure lateral slip.

This chapter is organised as follows. In section 4.2, the context and the motivation of this study are presented. Then, section 4.3 describes the tyre deformation in the contact patch and also presents the development of the induced longitudinal force model. In section 4.4, the self-aligning moment model is presented. The developed models are validated using measurements data in section 4.5. Finally, in section 4.6, a Magic Formula based model is proposed for representing the induced longitudinal force.

4.2 Context and motivation of the study

4.2.1 Tyre deformation at pure lateral slip condition

The approach of pure lateral slip is widely used in tyre-road interface modelling. In fact, several models for the tyre-road interface characteristics have been developed under the assumptions that defines pure lateral slip, which will be briefly described in this section.

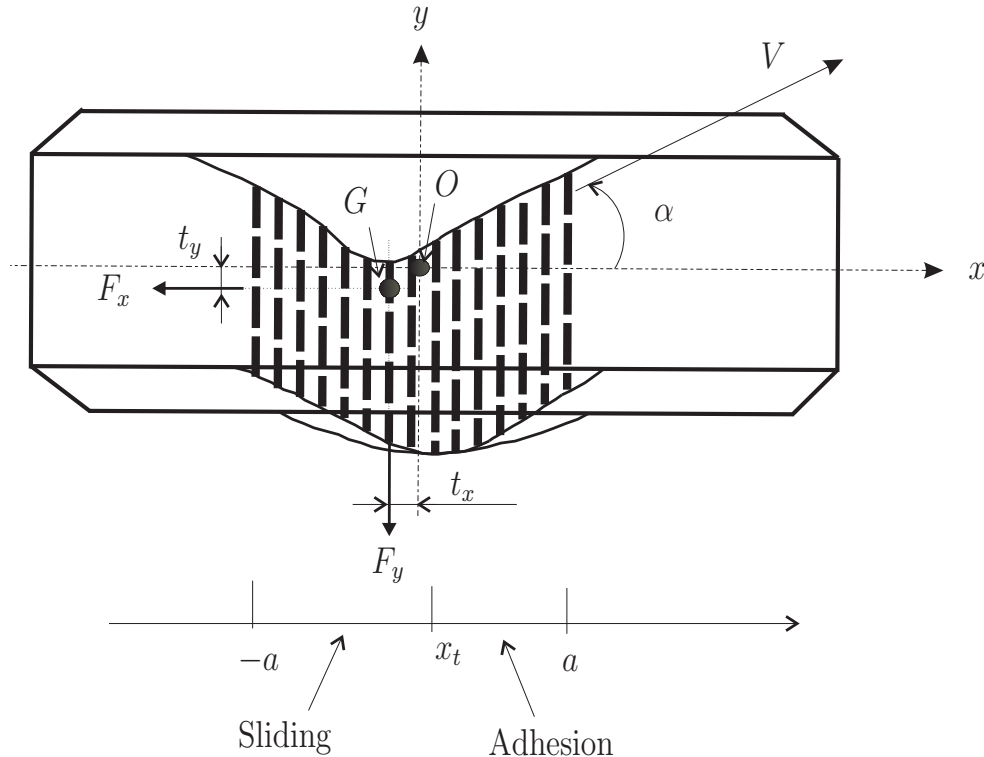


Figure 4.1: Pure cornering - General view of the tyre deformation in the contact patch

Consider a rolling tyre without camber and turn slip. When a cornering manoeuvre is performed on the wheel, the wheel speed vector V shows an angle with respect to the wheel plane. This angle is commonly designated as the side slip angle α , figure 4.1. If neither braking nor driving torque is applied in addition to the side slip, the tyre is said to be at pure lateral slip (or pure cornering) condition. The tread band deflection is considered to be exclusively in the lateral direction and therefore, only a lateral force F_y is generated. The longitudinal force F_x is then assumed zero. The line of action of this force F_y is shifted from the centre O of the contact patch with distance of t_x , in (O, \vec{x}, \vec{y}) axis system of the contact patch plane. Thus, a moment designated as the self-aligning moment M_z is generated and can be expressed as follows:

$$|M_z| = t_x |F_y| \quad (4.1)$$

where t_x is termed the pneumatic trail.

For relative small side slip angle α , the tyre tread band surface is considered to be in full adherence with the road surface. But, as α rises, sliding occurs progressively from the trailing edge of the contact patch where the friction limit is reached first. The contact patch is then divided into two zones: adhesion and sliding zones. At the same time, the deformation shape of the contact patch becomes more symmetric and, as a result, the pneumatic trail t_x gets smaller. If the side slip angle α is increased enough, the tyre will completely lose adherence with the road surface and will start sliding. The tyre is said to be at full sliding condition and the line of action of F_y coincides with the contact patch y axis. It results in a zero self-aligning moment M_z independently of angle α .

However, with some type of tyres, the longitudinal force F_x at pure cornering may not be negligible. As it is underlined in [37], the non symmetric lateral deformation of the tyre in the contact induces tread deformation in the longitudinal direction (along the x axis). Consequently, a longitudinal force F_x is generated and acts as a braking force. The line of action of F_x is shifted from the centre O of the contact patch with distance of t_y . Suppose that point G represents the point of action of both forces F_x and F_y , figure 4.1. Its coordinates read $G(X_G, Y_G)$, where

$$\begin{aligned} t_x &= |X_G| \\ t_y &= |Y_G| \end{aligned} \quad (4.2)$$

The self-aligning moment M_z is now the sum of two moments, one caused by F_x and the other by F_y :

$$M_z = X_G F_y - Y_G F_x \quad (4.3)$$

If $\alpha \neq 0$, it can be remarked from equation (4.3) that a zero value of M_z does not necessarily imply the tyre is in full sliding condition with respect to the road surface and the point of action G of the forces coincides with the centre O of the contact patch. Indeed, the condition of zero M_z may be also satisfied if $X_G F_y = Y_G F_x$.

Consider figures 4.2, 4.3, 4.4 and 4.5 which present measurements data obtained in real situation of pure cornering performed on a civil aircraft tyre. This tyre is mounted on a

4.2. Context and motivation of the study

test bench and pure cornering is performed. The longitudinal force F_x , the lateral force F_y and the self-aligning moment M_z data are recorded vs the side slip angle α . During each test, the vertical load is kept constant as well as the forward velocity V , ($V = 8m/s$). No driving/braking torque, camber or turn slip is applied on the wheel. In one hand, it is observed that a longitudinal force F_x , which acts like a braking force and increases with side slip angle α , is generated in addition to the lateral force F_y , figures 4.2 and 4.4. In the other hand, it is remarked that the evolution of the self-aligning moment M_z can be decomposed into three phases. In the first phase, M_z increases with the side slip angle α up to its maximum value. In the second phase, M_z decreases with the side slip angle α until it reaches zero. The third phase corresponds to the range of α for which M_z restarts building up but, with an opposite sign (in the opposite sign part of the graph).

The measurements data described above are in good agreement with the previous remark on the real shear forces developed in the contact patch during pure lateral slip. In fact, the data show the longitudinal force F_x may not be neglected and therefore, the self-aligning moment would obey to the theoretical representation of equation (4.3).

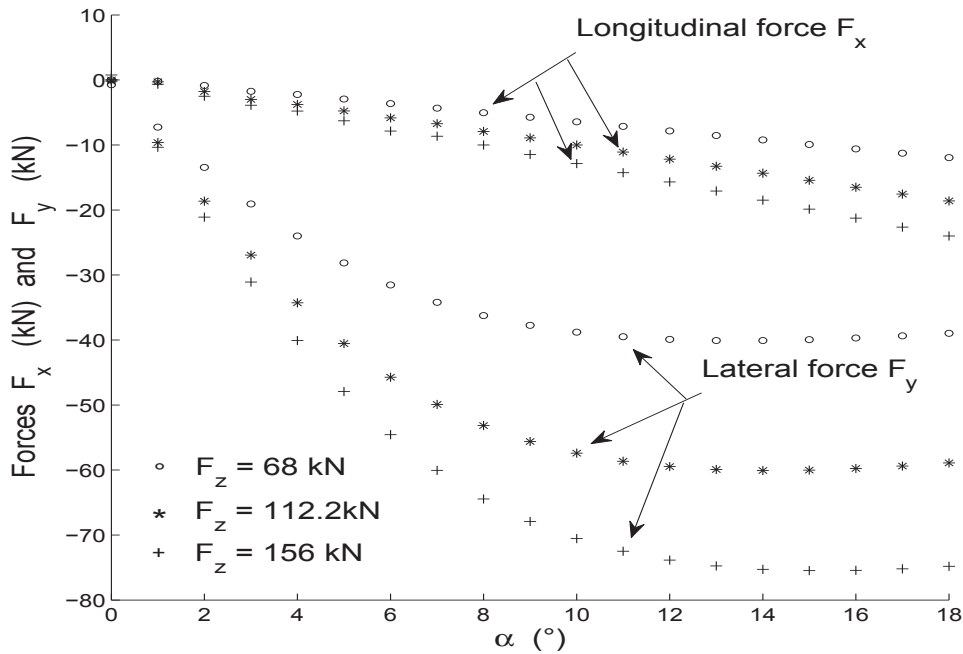


Figure 4.2: Pure cornering - lateral force F_y and induced longitudinal force F_x - $p = 14$ bars

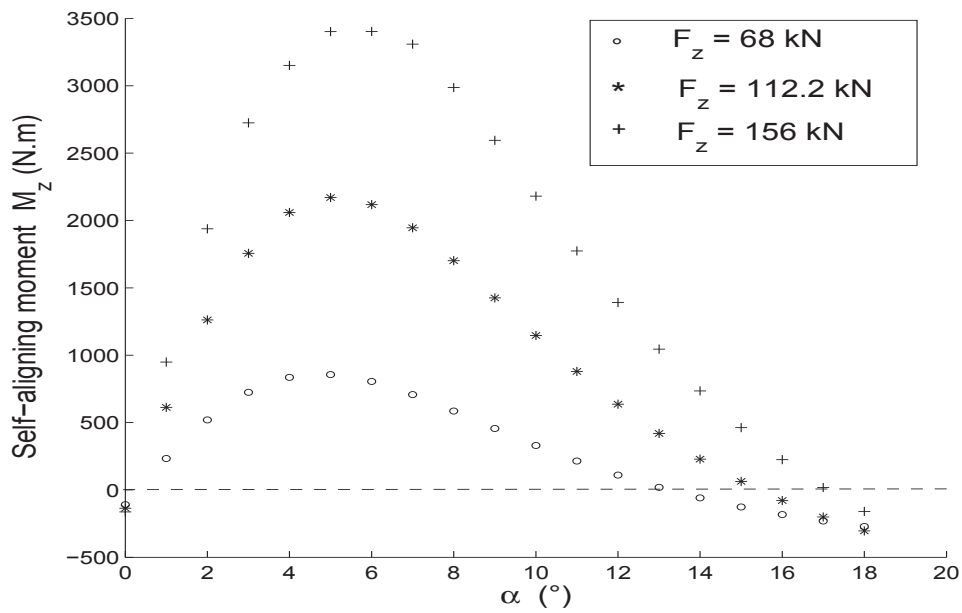


Figure 4.3: Pure cornering - self-aligning moment M_z - $p = 14$ bars

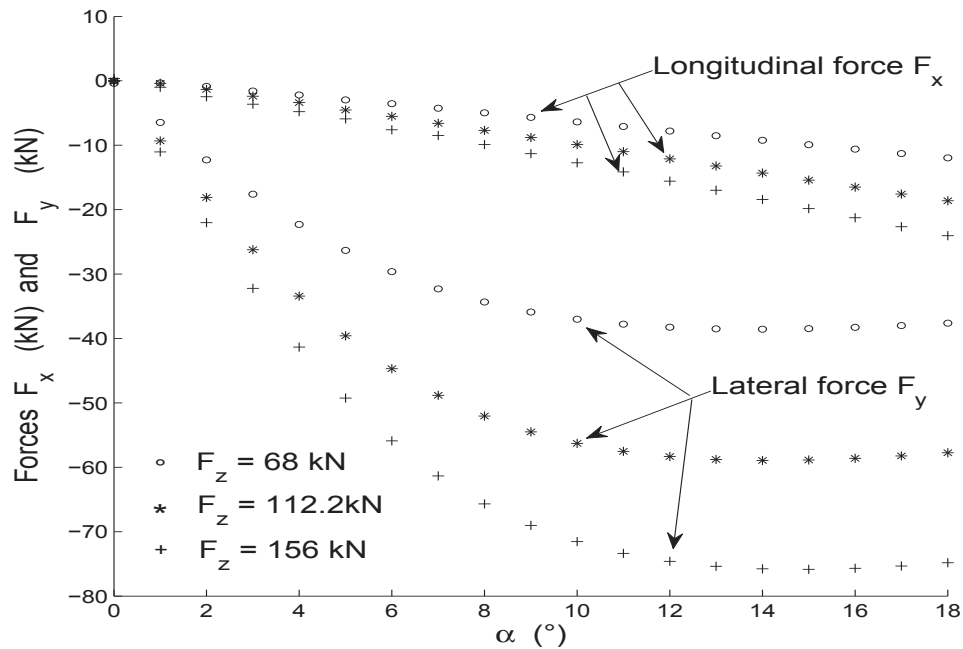


Figure 4.4: Pure cornering - lateral force F_y and induced longitudinal force F_x - $p = 16$ bars

4.2. Context and motivation of the study

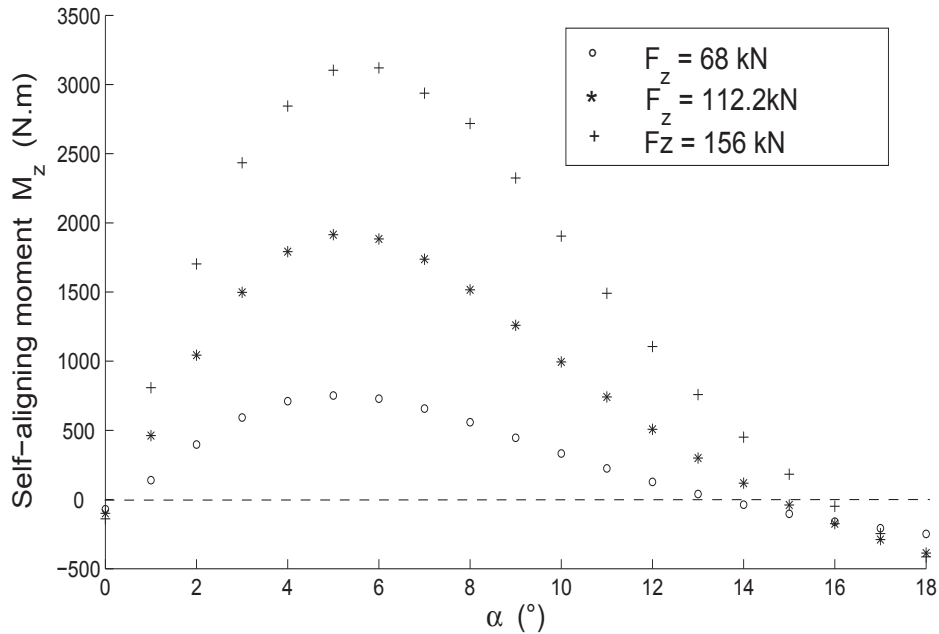


Figure 4.5: Pure cornering - self-aligning moment M_z - $p = 16$ bars

Next, the objective is to physically describe the generation of this longitudinal force. Then, the self-aligning moment model, equation (4.3), is derived by determining the coordinates (X_G, Y_G) of the action point G of both forces F_x and F_y .

The approach used in the present document for modelling the wheel structure and the contact between the tyre and the road is first described below.

4.2.2 Wheel structure and tyre-road contact representation

In the model derived in this study, the tyre tread are represented by an array of small elastic rectangular elements attached to a rigid ring, figure 4.6. The tread elements form the tread band surface which comes into contact with the road surface. The compliance of these elements is assumed to represent the elasticity of the combination of carcass, belt and actual tread elements of the real tyre. During free rolling of the tyre (that is without action of driving/braking torque, side slip, camber or turning), the wheel moves along a straight line parallel to the ground and in the direction of the wheel plane. In this particular case, the tread elements are deemed vertical and move from the leading edge to the trailing one without horizontal deflection and therefore, without fore/aft or side force. A possible presence of rolling resistance is disregarded and when tread element deflection occurs due to shear force, it is always supposed to be parallel to the road surface. The

Chapter 4. Real shear forces and moment at pure lateral slip

undeformed contact patch shape is assumed rectangular, figure 4.7, where the letter a represents its half-length and b its width. A parabolic normal pressure distribution p , which vanishes at the contact entry and exit points, is considered in the contact patch. Equation (4.4) describes the normal pressure distribution.

$$p(x) = p_0 \left(1 - \frac{x^2}{a^2}\right) \quad (4.4)$$

The parameter p_0 is a constant and is deduced from the condition that this pressure distribution equilibrates the vertical force F_z . Thus, $p_0 = \frac{3F_z}{4ab}$ and equation (4.4) becomes:

$$p(x) = \frac{3F_z}{4ab} \left(1 - \frac{x^2}{a^2}\right) \quad (4.5)$$

The two zones that may exist in the contact patch are shown in figure 4.7. The lateral tread deflection in the adhesion zone is assumed linear up to the transition abscissa x_t . In the sliding zone, the shape of the lateral deflection is mainly determined by the shape of the normal pressure distribution p . In the present case, it has a parabolic shape. The point of action of both forces F_x and F_y is represented by $G(X_G, Y_G)$.

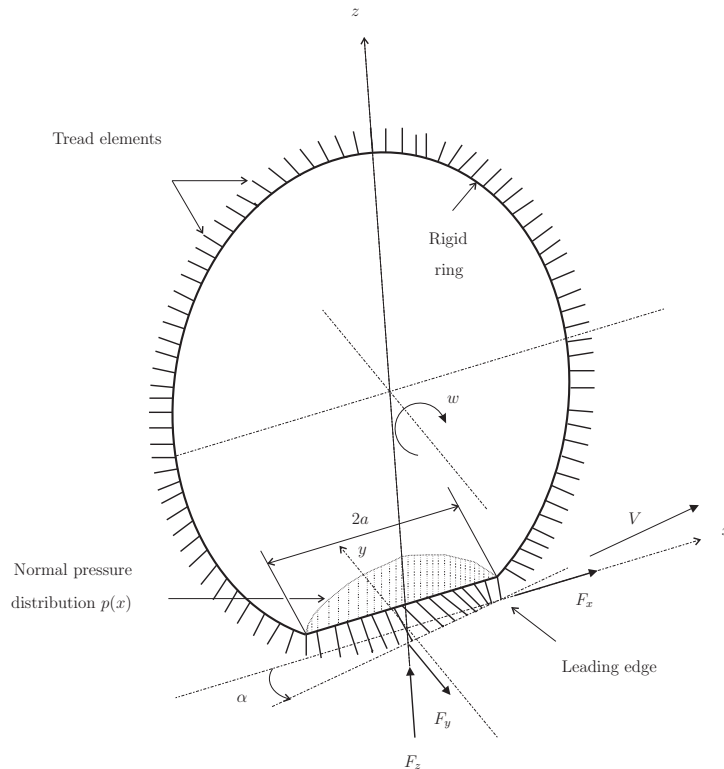


Figure 4.6: Tyre representation (Brush model)

4.3. Longitudinal force model

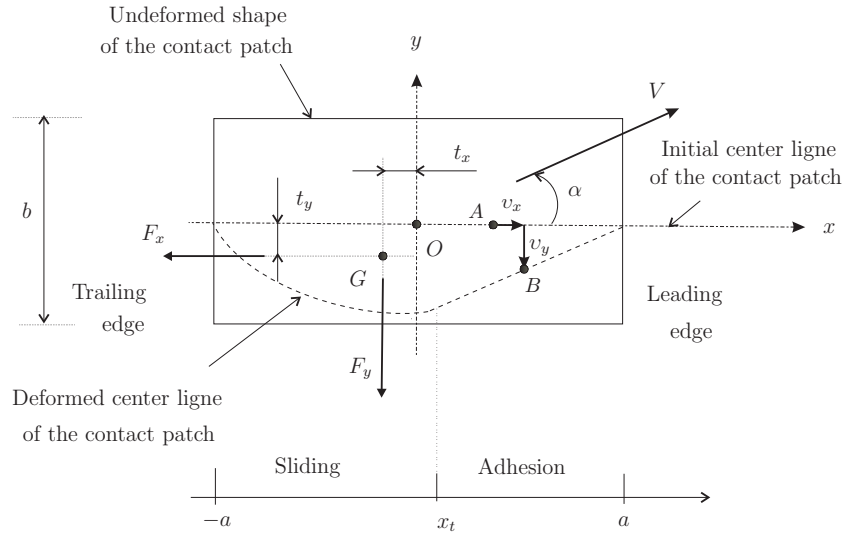


Figure 4.7: Contact patch presentation (Top view)

In the next section, based on the contact patch approach described above, expressions for the lateral displacement v_y and for the longitudinal contraction v_x are derived. Then, the induced longitudinal force model is proposed.

4.3 Longitudinal force model

Consider the tyre contact patch as presented in figure 4.7. During cornering, the direction of the forward velocity V shows an angle, denoted side slip angle α , with respect to the wheel plane. The tread band is then displaced in the lateral direction. In the contact patch, two zones may occur depending on the magnitude of the side slip angle α , the adhesion and the sliding zones. In the adhesion zone, the lateral tread band displacement, v_y , is assumed to be a linear function of x while in the sliding zone its shape is governed by the normal pressure distribution (parabolic shape in this case).

In the case of relative small side slip angles, the tread band surface can be considered to be in full adhesion with the road surface in the entire contact patch. Thus, the tread band lateral displacement, v_y , is assumed exclusively linear along the contact patch. Its magnitude depends on the side slip angle α as shown in the following expression:

$$v_y = -(a - x) \tan \alpha \quad (4.6)$$

By assuming the tyre tread band as an elastic material, the lateral force per unit contact length $\frac{dF_y}{dx}$ is proportional to the displacement v_y of the tread band.

$$\frac{dF_y}{dx} = k_y v_y = -k_y(a - x) \tan \alpha \quad (4.7)$$

where k_y represents the lateral compliance (stiffness) of the elastic tread band. The total lateral force is obtained by integrating the elementary force, equation (4.7), over the entire contact patch.

$$F_y = \int_{-a}^a dF_y = -2a^2 k_y \tan \alpha \quad (4.8)$$

In the literature ([3, 10] for example), it is assumed that $C_\alpha = 2a^2 k_y$ is the cornering stiffness (unit: force) and represents the slope at the origin of the curve $F_y = f(\alpha)$.

$$C_\alpha = \left. \frac{\partial F_y}{\partial \alpha} \right|_{\alpha=0} \quad (4.9)$$

In the same manner, it is assumed that $C_S = 2a^2 k_x$, where k_x represents the longitudinal (tangential) stiffness of the elastic tyre tread band, and C_S is the longitudinal slip stiffness (unit: force). C_S also represents the slope at the origin of the longitudinal force F_x vs the longitudinal slip.

Next, the following expressions for k_x and k_y will be used:

$$k_x = \frac{C_S}{2a^2}, \quad k_y = \frac{C_\alpha}{2a^2} \quad (4.10)$$

Besides, the lateral deformation of the tyre tread band ε_y reads:

$$\varepsilon_y = \frac{|v_y|}{b} \quad (4.11)$$

As it is shown in [37], the nonuniform tyre lateral stretching, v_y , in the contact patch induces a non compensated longitudinal contraction $\vec{v}_x = v_x \vec{x}$, which is oriented towards the leading edge. For example, a point will move from its initial and undeformed position A to its deformed one B due to the side slip angle as shown in figure 4.7. The displacement of the point from A to B has two components: a displacement v_x along the x axis and a displacement v_y along the y axis. v_x is responsible for the induced longitudinal force F_x , and v_y for the lateral force F_y .

The Poisson coefficient ν can be defined as the ratio of the longitudinal deformation ε_x over the lateral deformation ε_y .

4.3. Longitudinal force model

$$\varepsilon_x = \frac{|v_x|}{a-x} \quad (\text{longitudinal deformation}), \quad x \neq a \quad (4.12)$$

$$\nu = \frac{\varepsilon_x}{\varepsilon_y} \quad (\text{Poisson ratio})$$

By using equations (4.6), (4.11) and (4.12), the expression for the longitudinal displacement (contraction), v_x is derived as follows:

$$v_x = \frac{\nu(a-x)^2}{b} |\tan \alpha| \quad (4.13)$$

By assuming the tyre tread band as an elastic material, the longitudinal force per unit contact length $\frac{dF_x}{dx}$ is proportional to the displacement v_x of the tread band.

$$\frac{dF_x}{dx} = -k_x v_x = -\frac{\nu(a-x)^2}{2ba^2} C_S |\tan \alpha| \quad (4.14)$$

where k_x is replaced by its corresponding expression from equation (4.10). The minus sign in equation (4.14) illustrates the reaction force of the ground on the tyre in the longitudinal direction.

For relative small side slip angle, the total longitudinal force is obtained by integrating the elementary force, equation (4.14), over the entire contact patch.

$$F_x = \int_{-a}^a dF_x$$

$$F_x = -\frac{\nu C_S |\tan \alpha|}{2ba^2} \int_{-a}^a (a-x)^2 dx \quad (4.15)$$

$$F_x = -\frac{4a\nu C_S}{3b} |\tan \alpha|$$

The expression of F_x obtained in equation (4.15) is only valid for relative small side slip angle for which it is assumed a full adhesion in the contact patch. However, when the slip angle α reaches a certain limit, the maximum friction force will be attained in some areas of the contact patch and the tread will start sliding. The sliding area occurs first at the trailing edge and increases with slip angle α . Therefore, when considering the general case (no assumption of small side slip), the contact patch must be divided into two zones: adhesion and sliding zones, figure 4.7. Quantity x_t represents the transition abscissa between adhesion and sliding zones. The elementary longitudinal force is developed distinctly in each zone and the total longitudinal force F_x is the sum of two forces

generated in each zone. The tread band lateral displacement v_y is considered linear in the adhesion zone and the corresponding longitudinal force per unit contact length, $\frac{dF_{xa}}{dx}$, has the same expression as already presented in equation (4.14).

$$F_{xa} = \int_{x_t}^a dF_{xa} \quad (4.16)$$

$$F_{xa} = -\frac{\nu C_S}{6ba^2}(a^3 - 3a^2x_t + 3ax_t^2 - x_t^3)|\tan \alpha|$$

where F_{xa} represents the longitudinal force induced in the adhesion zone.

The longitudinal and lateral forces in the sliding zone are noted F_{xs} and F_{ys} respectively. By considering the Coulomb friction law, the lateral force per unit contact length in the sliding zone reads:

$$\frac{dF_{ys}}{dx} = -\mu \frac{dF_z(x)}{dx} \text{sgn}(\alpha) \quad (\text{Coulomb friction law}) \quad (4.17)$$

where $F_z(x)$ is the vertical load distribution along the x axis and $\text{sgn}(\alpha)$ denotes the sign of the slip angle α in the ISO coordinate system. The friction coefficient μ is generally comprised between 0 and 1, and is function of road and tyre surfaces state. The maximum adherence between tyre and road is obtained when $\mu = 1$. Values of μ close to 0 represent poor adherence condition as for instance the cases of contact with wearied tyre, wet, snow or ice road. More often, μ is interpreted as the ratio of the maximum lateral or longitudinal force (F_{ymax} , F_{xmax} respectively) over the total vertical load F_z .

From the normal pressure distribution given in equation (4.5), the vertical load distribution $F_z(x)$ reads:

$$\frac{dF_z(x)}{dx} = bp(x) = \frac{3F_z}{4a} \left(1 - \frac{x^2}{a^2}\right) \quad (4.18)$$

Since the tyre tread band is assumed elastic and associated with a compliance of k_y , the lateral displacement v_{ys} in the sliding zone is derived as follows:

$$v_{ys} = \frac{1}{k_y} \frac{dF_{ys}}{dx} \quad (4.19)$$

By using equations (4.17) and (4.18), the lateral displacement v_{ys} from equation (4.19) becomes:

$$v_{ys} = -\frac{3\mu F_z}{2aC_\alpha} (a^2 - x^2) \text{sgn}(\alpha) \quad (4.20)$$

where k_y has been replaced by its expression from equation (4.10).

From equations (4.12) and (4.20), the longitudinal contraction induced by the tread lateral displacement in the sliding region is deduced:

4.3. Longitudinal force model

$$v_{xs} = \frac{\nu}{b}(a-x)|v_{ys}| \quad (4.21)$$

$$v_{xs} = \frac{3\mu\nu F_z}{2baC_\alpha}(a^2-x^2)(a-x)$$

The longitudinal force per unit contact length in the sliding zone is derived as follows: $\frac{dF_{xs}}{dx} = -k_x v_{xs}$. Then, k_x and v_{xs} are replaced by their corresponding expression from equations (4.10) and (4.21), respectively. Finally, the contribution of the sliding zone to the total longitudinal force is obtained by integrating dF_{xs} over the sliding zone.

$$F_{xs} = \int_{-a}^{x_t} dF_{xs} \quad (4.22)$$

$$F_{xs} = -\frac{\mu\nu F_z C_S}{16ba^3 C_\alpha}(12a^3 x_t - 6a^2 x_t^2 - 4ax_t^3 + 3x_t^4 + 11a^4)$$

At the transition point x_t , a continuity of the lateral displacement is supposed: $v_{ya}(x_t) = v_{ys}(x_t)$. In the same manner, both longitudinal displacements v_{xa} and v_{xs} from the adhesion and the sliding zones, respectively, are equal at the transition point x_t .

$$v_{xa}(x_t) = v_{xs}(x_t) \quad (4.23)$$

If v_{xa} ($v_{xa} = v_x$ from equation (4.13)) and v_{xs} (equation (4.21)) are replaced by their corresponding expressions, equation (4.23) becomes:

$$\frac{\nu(a-x_t)^2}{b} |\tan \alpha| = \frac{3\mu\nu F_z}{2baC_\alpha}(a^2-x_t^2)(a-x_t) \quad (4.24)$$

$$|\tan \alpha| = \frac{3\mu F_z}{2aC_\alpha}(a+x_t)$$

By noting $K = \frac{x_t}{a}$ and from equation (4.24):

$$K = \frac{2C_\alpha |\tan \alpha|}{3\mu F_z} - 1 \quad (4.25)$$

Then, the longitudinal force from the adhesion zone and from the sliding zone, equation (4.16) and (4.22) respectively, become:

$$F_{xa} = -\frac{\nu a C_s}{6b}(1-3K+3K^2-K^3)|\tan \alpha| \quad (4.26)$$

$$F_{xs} = -\frac{\mu\nu a F_z C_S}{16bC_\alpha}(12K-6K^2-4K^3+3K^4+11)$$

The total longitudinal force is then the sum of the contributions of the adhesion and the sliding zones.

$$\begin{aligned}
 F_x &= F_{xa} + F_{xs} \\
 F_x &= -\frac{\nu a C_s}{6b} (1 - 3K + 3K^2 - K^3) |\tan \alpha| \\
 &\quad - \frac{\mu \nu a F_z C_S}{16b C_\alpha} (12K - 6K^2 - 4K^3 + 3K^4 + 11)
 \end{aligned} \tag{4.27}$$

Remark:

From equation (4.25), it can be verified that the transition point will never coincide with the trailing edge unless the side slip angle α is zero ($x_t > -a$ always if $\alpha \neq 0$). Therefore, there will always be sliding in the contact patch if a parabolic normal pressure distribution is assumed. This will not be the case if a uniform normal pressure distribution was supposed, but it provides less accurate modelling results when compared to parabolic normal pressure assumption [21].

If the side slip angle α is increased enough, full sliding may occur. In the particular case of full sliding, the transition abscissa x_t will coincide with the leading edge, $x_t = a$. Consider α_{fs} as the value of the side slip angle at which the tyre reaches full sliding. The expression of α_{fs} may be determined by taking $x_t = a$ in equation (4.25).

$$\alpha_{fs} = \arctan\left(\frac{3\mu F_z}{C_\alpha}\right) \tag{4.28}$$

After the critical value α_{fs} of the side slip angle, the lateral tread displacement is uniform along the x axis. The lateral force is supposed to reach its maximum value and its point of application is deemed to coincide with the center of the contact patch. The entry and exit points (leading and trailing edges) of the contact patch are free to contract uniformly too. Therefore, the induced longitudinal forces (which are considered proportional to the longitudinal tread displacement) from both leading and trailing edges equilibrate each other.

4.4. Self-aligning moment model

Finally, the induced longitudinal force can be summarized as follows:

if $\alpha < \alpha_{fs}$ (full adhesion or adhesion + sliding)

$$F_x = -\frac{\nu a C_s}{6b}(1 - 3K + 3K^2 - K^3)|\tan \alpha| - \frac{\mu \nu a F_z C_S}{16b C_\alpha}(12K - 6K^2 - 4K^3 + 3K^4 + 11) \quad (4.29)$$

if $\alpha \geq \alpha_{fs}$ (full sliding)

$$F_x = 0$$

with K and α_{fs} being given in equations (4.25) and (4.28) respectively.

Comment on the critical side slip

The expression of α_{fs} in equation (4.28) is exactly the same as the one given for the critical side slip limit α^* of the Fiala model (see equation (2.19) in chapter 2). This equivalence is due to the fact that the brush model approach is used in the development of both models. As it is already underlined in section 2.4.3 of chapter 2, the brush model approach presents some limitations at relative high side slip angle and need to be improved in order to derive a more realistic expression for the critical side slip angle α_{fs} (or α^* for the Fiala model). Tyre data which would help to use an improved approach are not available in the context of this study.

In the next section, based on the contact patch approach described above, expressions for the coordinates (X_G, Y_G) are derived and a model for the self-aligning moment M_z is proposed based on equation (4.3).

4.4 Self-aligning moment model

Consider the contact patch as presented in figure 4.7. It can be remarked that the position (coordinates X_G and Y_G) of the action point G depends on the lateral displacement v_y of the tyre in the contact patch.

Chapter 4. Real shear forces and moment at pure lateral slip

When considering the general case (no assumption of small side slip angle), this lateral displacement can be summarized as follows:

$$\begin{aligned} &\text{if } -a \leq x_t \leq x \leq a \quad (\text{adhesion zone}) \\ &v_y = v_{ya} = -(a - x) \tan \alpha \\ &\text{if } -a \leq x < x_t \leq a \quad (\text{sliding zone}) \end{aligned} \tag{4.30}$$

$$v_y = v_{ys} = -\frac{3\mu F_z}{2aC_\alpha}(a^2 - x^2)\text{sgn}(\alpha)$$

where v_{ya} and v_{ys} represent the tyre lateral displacement in the adhesion zone and in the sliding zone respectively. Equation (4.30) also describes the shape of the deformed centre line of the contact as shown in figure 4.7. The barycentre G of the surface generated by the centre line deformation is also the point of action of both forces F_x and F_y . It is assumed that the displacement of the contact patch in the longitudinal direction is negligible when compared to its initial length $L = 2a$. Therefore, the contact patch length is deemed unchanged and equal to $2a$.

Now, we focus on determining the coordinates (X_G, Y_G) of the barycenter G . Consider that S is the total surface generated by the centre line deformation. The derivative of S vs the variable x is: $dS = v_y dx$. S is then given by the following equation:

$$\begin{aligned} S &= \int_{-a}^{x_t} |v_{ys}| dx + \int_{x_t}^a |v_{ya}| dx \\ S &= \frac{\mu F_z}{2aC_\alpha}(2a^3 + 3a^2 x_t - x_t^3) + \frac{\tan(\alpha)}{2}(a^2 - 2ax_t + x_t^2) \end{aligned} \tag{4.31}$$

From the definition of the barycenter of a flat surface, the value of the coordinates X_G and Y_G read:

$$X_G = \frac{1}{S} \int \int x dS, \quad Y_G = \frac{1}{S} \int \int y dS \tag{4.32}$$

where y is the lateral tread displacement designated by v_y . Equation (4.32) can then be rewritten as shown below:

$$\begin{aligned} X_G &= \int_{-a}^{x_t} x v_{ys} dx + \int_{x_t}^a x v_{ya} dx \\ Y_G &= \int_{-a}^{x_t} v_{ys}^2 dx + \int_{x_t}^a v_{ya}^2 dx \end{aligned} \tag{4.33}$$

4.5. Application

By solving equation (4.33), with v_{ya} and v_{ys} given by equation (4.30), the following expressions are obtained for the coordinates X_G and Y_G .

$$\begin{aligned}
 X_G &= \frac{1}{S} \left[\frac{3\mu F_z}{8aC_\alpha} (-a^4 + 2a^2x_t^2 - x_t^4) + \frac{\tan \alpha}{6} (a^3 - 3ax_t^2 + 2x_t^3) \right] \\
 Y_G &= \frac{1}{S} \left[\left(\frac{3\mu F_z}{2\sqrt{15}aC_\alpha} \right)^2 (8a^5 + 15a^4x_t - 10a^2x_t^3 + 3x_t^5) \right. \\
 &\quad \left. + \frac{(\tan \alpha)^2}{3} (a^3 - 3a^2x_t + 3ax_t^2 - x_t^3) \right]
 \end{aligned} \tag{4.34}$$

When using the notation $K = \frac{x_t}{a}$, where K has the same expression as presented in equation (4.25), the expressions for X_G and Y_G shown in equations (4.34) become:

$$\begin{aligned}
 X_G &= \frac{a^3}{S} \left[\frac{3\mu F_z}{8C_\alpha} (-1 + 2K^2 - K^4) + \frac{\tan \alpha}{6} (1 - 3K^2 + 2K^3) \right] \\
 Y_G &= \frac{a^3}{S} \left[\left(\frac{3\mu F_z}{2\sqrt{15}C_\alpha} \right)^2 (8 + 15K - 10K^3 + 3K^5) \right. \\
 &\quad \left. + \frac{(\tan \alpha)^2}{3} (1 - 3K + 3K^2 - K^3) \right]
 \end{aligned} \tag{4.35}$$

where X_G and Y_G determine the position of the action point G of both forces F_x and F_y .

Finally, the self-aligning moment M_z model is obtained by replacing X_G and Y_G in equation (4.3) by their corresponding expression in equation (4.35).

Next, the modelling results of both longitudinal force and self-aligning moment models are compared to measurements data.

4.5 Application

The aim of this section is to compare modelling results of the longitudinal force F_x and the self-aligning moment M_z models derived from the contact patch investigation, equations (4.29) and (4.3) respectively, with measurements data presented in section 4.2.

To compute the developed models, it is assumed that the tyre tread stiffnesses are isotropic.

Chapter 4. Real shear forces and moment at pure lateral slip

Thus, the longitudinal and lateral tread stiffnesses, k_x and k_y respectively, are assumed equal: $k_x = k_y = k$. Therefore, $C_S = C_\alpha = 2a^2k$. In this application, the value of k is determined through static load deflection curves. In fact, k is the slope at the origin of the curve that gives the static longitudinal or lateral load vs tyre longitudinal or lateral displacement. k slightly varies with the vertical load F_z . The mean value of k is therefore considered for this application. The values of the contact patch length $2a$ are determined through an interpolation of static vertical loading data which give contact patch length $2a$ vs vertical load F_z . The values of X_G and Y_G are determined by using their corresponding expression from equation (4.35).

In order to determine the friction coefficient, a reference value at each inflation pressure and at each vertical load is necessary. Indeed, as already mentioned in chapter 2, the fact of considering a constant friction coefficient, which equal to the ratio of the maximum lateral (or longitudinal) force over the vertical load, is based on the Coulomb friction law (in static) and is not accurate enough for a dynamic study. However, reference data of the friction coefficient are not available in the context of this study.

Average values of 0.87 and 0.9 are adopted for μ at inflation pressure 14 bars and 16 bars, respectively. The value of μ at inflation pressure 16 bars is chosen relatively higher because the average value of the ratio of the longitudinal force (or of the lateral force) over the vertical load at inflation pressure 16 bars was found relatively higher in the same order. Finally, the Poisson ratio is assumed equal to 0.35 at room temperature. This value is an estimation but common at room temperature for many polymers used in tyres, see for example [40]. The values of the different parameters are given in table 4.1.

Inflation pressure $p = 14$ bars; $\nu = 0.35$; $k = 3350kN/m$		
$F_z = 68kN$	$F_z = 112.2kN$	$F_z = 156kN$
$a = 0.175m$	$a = 0.22m$	$a = 0.235m$
$b = 0.22m$	$b = 0.24m$	$b = 0.27m$
$\mu = 0.87$	$\mu = 0.87$	$\mu = 0.87$
Inflation pressure $p = 16$ bars; $\nu = 0.35$; $k = 3350kN/m$		
$F_z = 68kN$	$F_z = 112.2kN$	$F_z = 156kN$
$a = 0.16m$	$a = 0.203m$	$a = 0.225m$
$b = 0.19m$	$b = 0.221m$	$b = 0.25m$
$\mu = 0.9$	$\mu = 0.9$	$\mu = 0.9$

Table 4.1: Values of the models parameters

4.5. Application

4.5.1 Longitudinal force modelling results

The longitudinal force model presented in equation (4.29) is simulated using the parameters values shown in table 4.1. Since the induced longitudinal displacement v_x (or v_{xs}) is a function of the side slip angle α , we chose to plot the longitudinal force against the side slip angle, as presented in figures 4.8 and 4.9. These figures show the modelling results which are compared with the experimental data. It can be remarked that the dispersion between data and modelling results increases with the side slip angle, which is certainly due to the fact that the approach used presents some limitations at relative high side slip. For both inflation pressures, 14 bars and 16 bars, the maximum error is approximately 9.5%, which may be considered reasonable. Therefore, at relative small side slip, it may be said the physical approach used in the development of the model allows a relative good representation of the real longitudinal behaviour of the tyre during pure cornering.

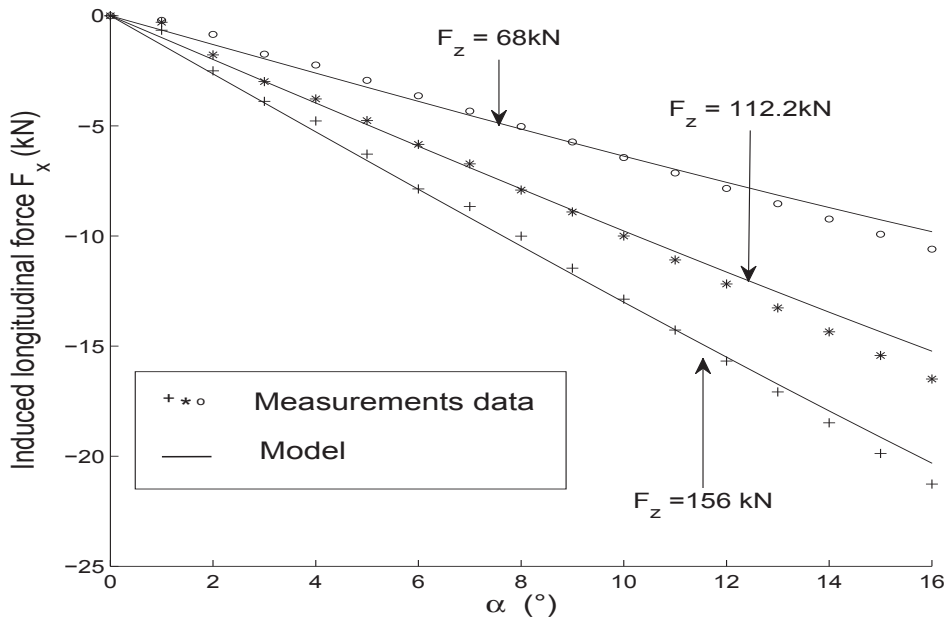


Figure 4.8: Pure cornering - Induced longitudinal force F_x - inflation pressure $p = 14$ bars
- maximum error: $Error_{F_y} \sim 8\%$

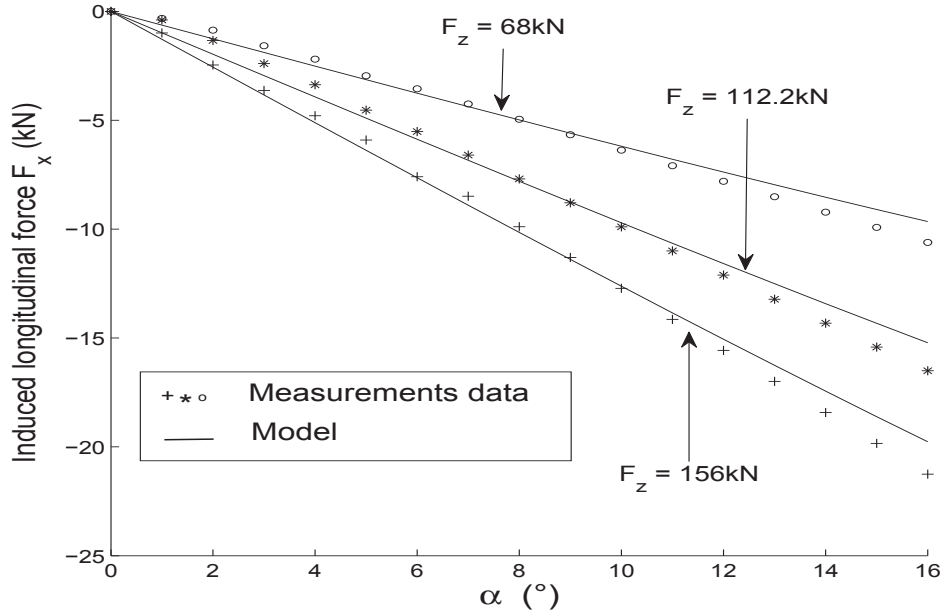


Figure 4.9: Pure cornering - Induced longitudinal force F_x - inflation pressure $p = 16$ bars - maximum error: $Error_{F_y} \sim 9.5\%$

4.5.2 Self-aligning moment modelling results

Figures 4.10a and 4.10b illustrate the modelling results of the individual contribution of F_x and F_y to the self-aligning moment for inflation pressure 14 bars and 16 bars, respectively. It can be underlined that the longitudinal force F_x plays a crucial role in the evolution of the tyre self-aligning moment M_z . Consider α_{max} as the value of the side slip angle α at which M_z attains its maximum value M_{zmax} . It can be remarked that M_z is mainly due to the contribution of the lateral force F_y for side slip angle $0 \leq \alpha < \alpha_{max}$. Beyond this limit of α , the contribution of F_x becomes progressively significant vs α while the contribution of F_y decreases. Since the part of M_z due to F_x is opposite in sign to the one due to F_y , the sum of both contributions will be equal to zero at a certain value of the side slip angle that we may designate by α_{mz0} , $M_z(\alpha_{mz0}) = 0$. However, because the contribution of each force is not zero at α_{mz0} , the point of their action G does not coincide with the centre O of the contact patch and therefore, the tyre is not in full sliding condition (adhesion still exists in the contact patch). Beyond α_{mz0} , the contribution of F_x to M_z continues increasing while the one of F_y decreases. M_z becomes then mainly due to F_x and that explains why its curve passes in the negative side of the graph.

4.5. Application

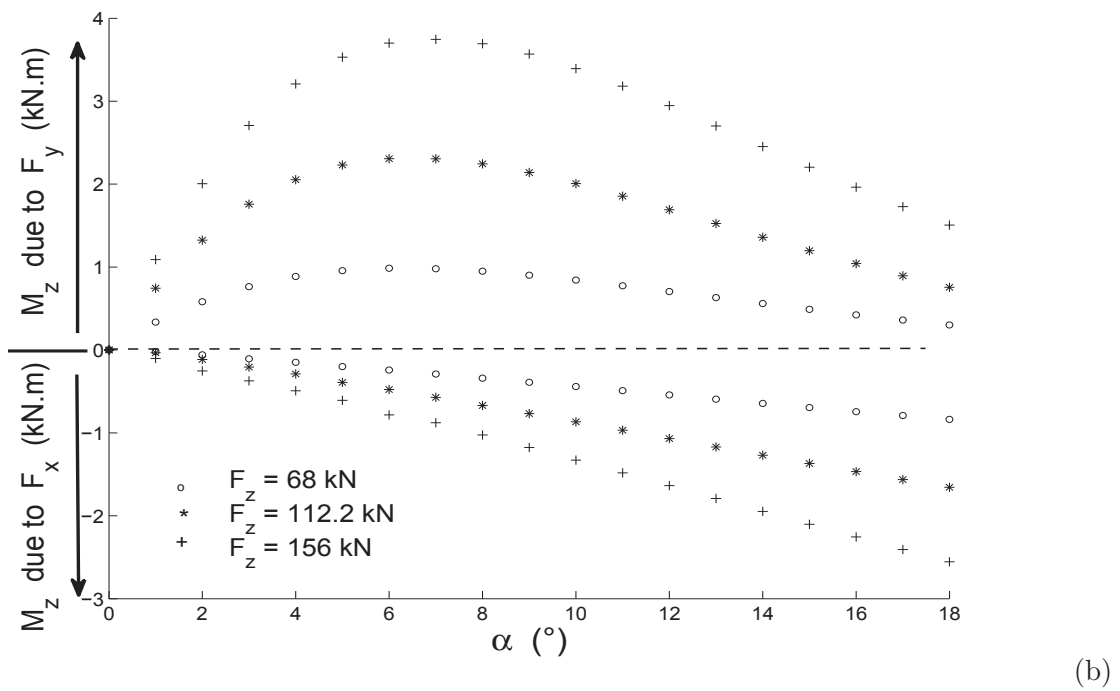
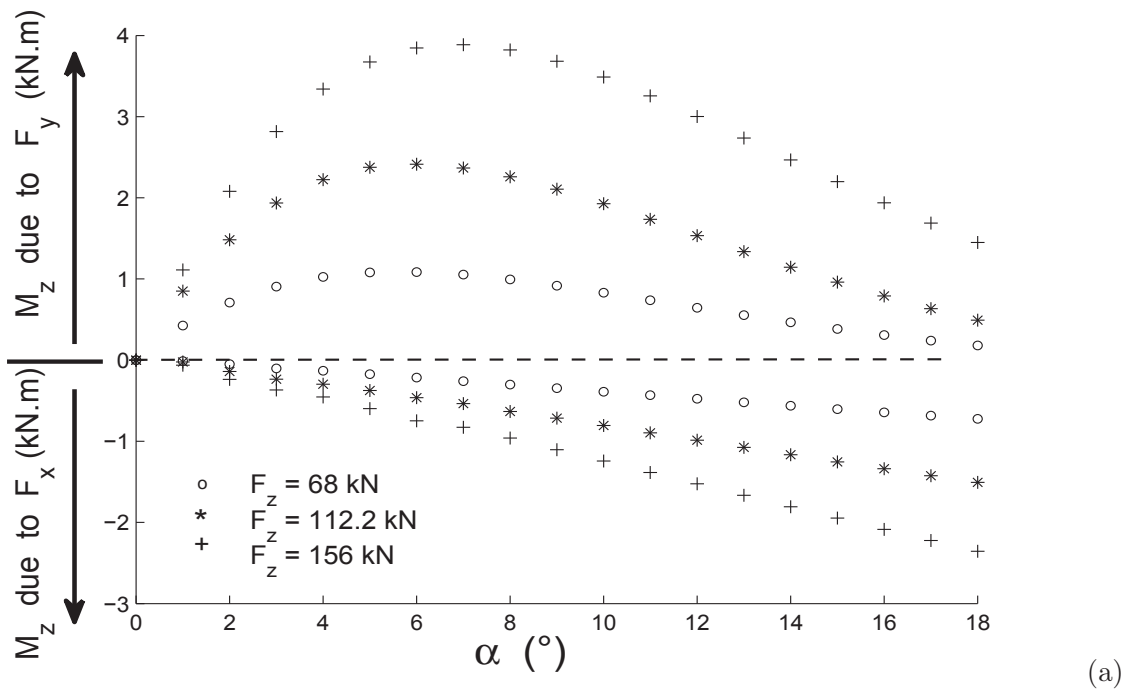


Figure 4.10: Decomposition of M_z into contribution of F_x and F_y - (a) $p = 14$ bars - (b) $p = 16$ bars

Figures 4.11 and 4.12 show the modelling results of M_z model which are compared with the experiments data. For both inflation pressures, 14 bars and 16 bars, the dispersion

between modelling results and measurements data becomes significant when α gets relatively higher, and specially after M_z repasses by zero. This is due to the limitations of the approach used in the development the current model. The maximum error is about 20%. For each curve, the dispersion may be considered acceptable up to the point where M_z reaches zero (maximum error less than 15%). Moreover, the tendency of the modelling results helps to understand the reason why the self-aligning moment does not stay constant after reaching zero. It may be concluded that, the physical approach adopted allows a relative good description of the self-aligning moment generation during pure cornering.

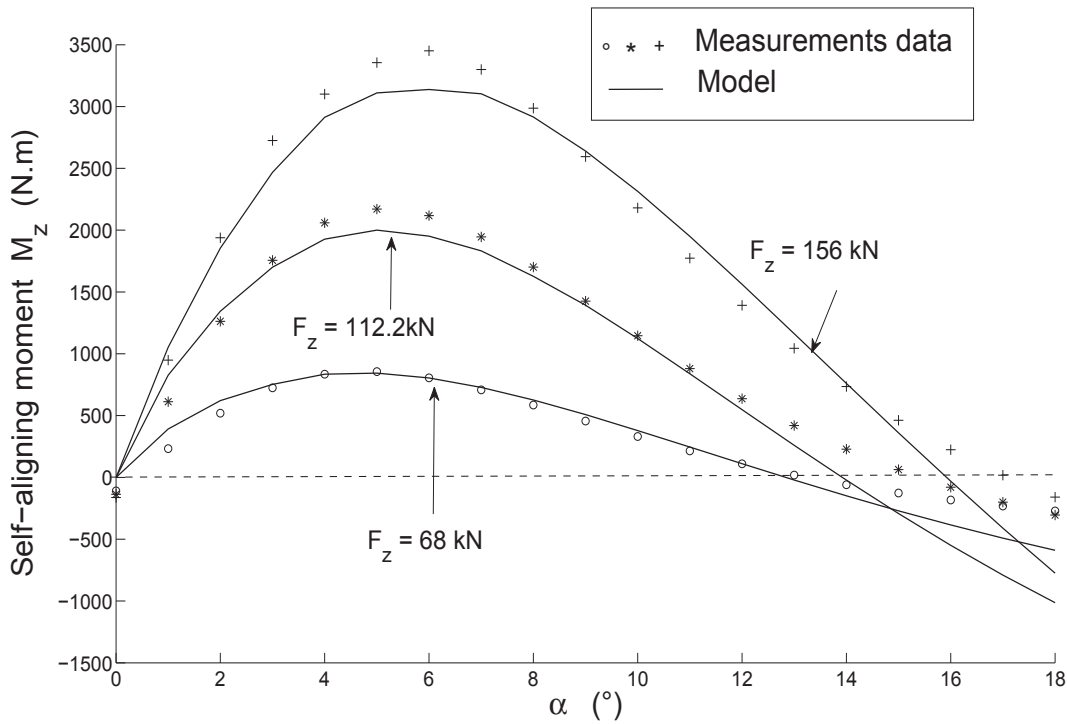


Figure 4.11: M_z at pure cornering - $p = 14$ bars - maximum error: $Error_{M_z} \sim 20\%$

4.5. Application

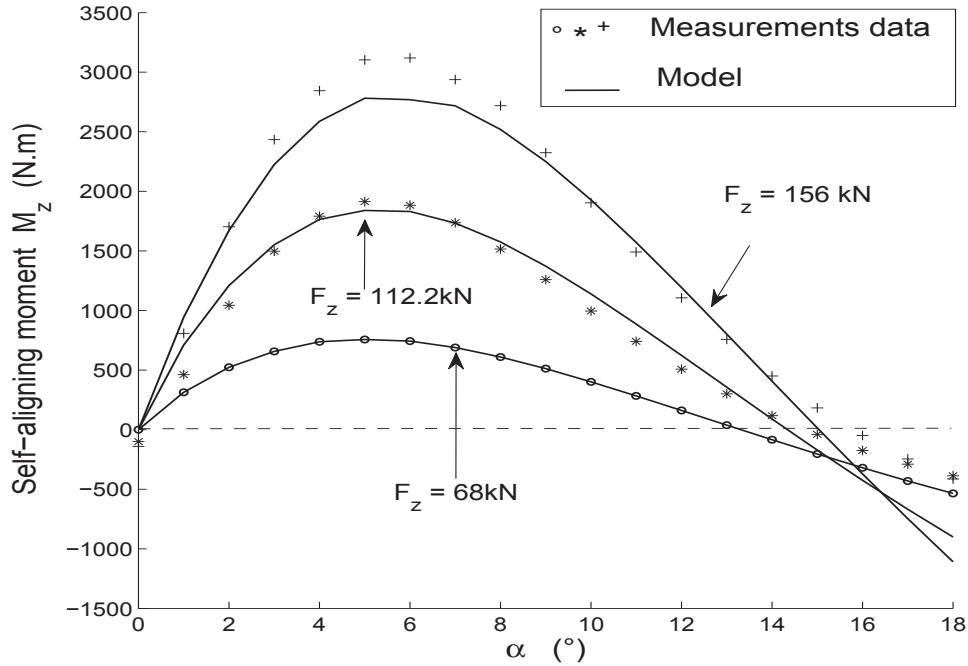


Figure 4.12: M_z at pure cornering - $p = 16$ bars - maximum error: $Error_{M_z} \sim 18.5\%$

Remarks

By neglecting the longitudinal force F_x in their approach for tyre-road interface modelling during pure cornering, the majority of the physical mathematical models in the literature can only approximate the self-aligning moment up to the side slip angle at which $M_z = 0$. Beyond this limit, the models equations are unable to provide a possible evolution of M_z and consider the tyre to be in full sliding conditions. Thus, $M_z = 0$ independently of α . Some models (Magic Formula [10], TMeasy [30] for example) provide interpolation functions for M_z all over its range of variation. But a comprehensive description of M_z is not provided.

Besides, it is worth mentioning that some parameters used for this application, such as the contact patch dimensions, the tyre lateral stiffness, are determined from static loading tests. In reality, when the tyre rolls, these parameters may change more or less significantly. Moreover, the normal pressure distribution over the contact patch is most likely arbitrary than parabolic and, the tread band displacement does not vanish exactly at the entry and exit points (or sides) of the contact patch. When the side slip angle gets relatively higher, the behaviour of the tyre becomes complexer than an elastic material. Thus, one can believe that the model agreement can be improved by taking into consideration the

remarks on these features. In addition, the investigation is focused on steady-state pure cornering. Further investigation could extend the study to the tyre transient dynamics behaviour.

4.6 Using the Magic Formula model for the induced longitudinal force

As already mentioned in the introduction, Magic Formula as well as the majority of the tyre models that exist in the literature, see chapter 1, are developed according to two hypotheses. The first hypothesis is pure longitudinal or pure lateral tyre slip conditions and the second is combined tyre slip conditions. In the first hypothesis, the term pure is used to mean that the tyre tread band displacement (deflection) in the contact patch is exclusively in the mentioned direction. At pure lateral slip for example, it has been also deemed that the tread band displacement in the contact patch is exclusively in the transversal (lateral) direction and therefore, only transversal (lateral) force is developed. Therefore, Magic Formula model only proposes expression for modelling the tyre lateral force. However, in the previous section, the mechanism of generation of the longitudinal force during pure lateral slip has been described. Moreover, it is shown that this force may not be negligible for some aircraft tyres, specially when the side slip gets relatively higher. The previous approach has mainly provided a comprehensive description of the longitudinal force generation at pure lateral slip rather than deriving models that better fit with measurements data. In this section, a method for using the Magic Formula to model the induced longitudinal force is proposed. In fact, by using the induced longitudinal displacement derived previously, a Magic Formula based expression is proposed for representing the induced longitudinal force [41].

Consider the equation (4.36) which reminds the longitudinal tread contraction in the adhesion and the sliding zones, respectively.

$$\begin{aligned}
 &\text{if } -a \leq x_t \leq x \leq a \quad (\text{adhesion zone}) \\
 &v_{xa} = \frac{\nu(a-x)^2}{b} |\tan \alpha| \\
 &\text{if } -a \leq x < x_t \leq a \quad (\text{sliding zone}) \\
 &v_{xs} = \frac{3\mu\nu F_z}{2baC_\alpha} (a^2 - x^2)(a - x)
 \end{aligned} \tag{4.36}$$

4.6. Using the Magic Formula model for the induced longitudinal force

The total tread contraction v_{xtot} is obtained by integrating equation (4.36) over the entire contact patch length.

$$v_{xtot} = \int_{-a}^{x_t} v_{xa} dx + \int_{x_t}^a v_{xs} dx$$

$$v_{xtot} = -\frac{\nu a^3}{3b}(1 - 3K + 3K^2 - K^3)|\tan \alpha| - \frac{\mu \nu a^3 F_z}{8bC_\alpha}(12K - 6K^2 - 4K^3 + 3K^4 + 11) \quad (4.37)$$

The induced longitudinal slip, noted S_{Lind} , can be defined as the ratio of total tread contraction v_{xtot} over the length of the contact patch.

$$S_{Lind} = \frac{v_{xtot}}{2a} \quad (4.38)$$

Consider the general form of Magic Formula for a given value of vertical load and camber angle as presented in [10]:

$$Y(X) = D \sin \left[\text{Carctan} \left(B(X + S_h) - E \left(B(X + S_h) - \arctan B(X + S_h) \right) \right) \right] + S_v \quad (4.39)$$

where:

B	stiffness factor,
C	shape factor,
D	peak value,
E	curvature factor,
BCD	slope at the origin ($X = 0, Y = 0$),
S_h	horizontal shift,
S_v	vertical shift,
Y	output variables F_x, F_y or M_z ,
X	input variables S_L (for F_x) or S_α (for F_y and M_z),

Remark

In the late versions of Magic Formula, parameters B, C, D, E, S_h, S_v are expressed as function of vertical load, camber or turn slip (example of [10]), and of inflation pressure (example of [33]). But in the present study, we limit the model to its original expression presented above.

To use equation (4.39) for representing the induced longitudinal force F_x , it is necessary to define the input variable S_L , which represents the longitudinal slip. Generally speaking, S_{Lind} from equation (4.38) is equivalent to S_L . Next, the notation S_{Lind} is used in stead of S_L . The equation (4.38) is used for estimating S_{Lind} . The induced longitudinal force model is then represented by equation (4.39) in which the term X is replaced by S_{Lind} .

4.7 Modelling results

The induced longitudinal slip S_{Lind} is calculated using equation (4.37) and the results are plotted in figures 4.13 and 4.14. Then, the model parameters B, C, D, E, S_h, S_v are estimated using measurements data of the induced longitudinal force and the optimization function *fminsearch* from Matlab software. Quantity S_{Lind} represents the input variable of the model. The model parameters values are presented in table 4.2 for both inflation pressures 14 bars and 16 bars. It is underlined that at zero side slip angle α , the induced longitudinal slip is assumed zero (condition of free rolling) and the possible longitudinal force is attributed to rolling resistance. Therefore, parameters S_h and S_v are assumed to be equal to zero.

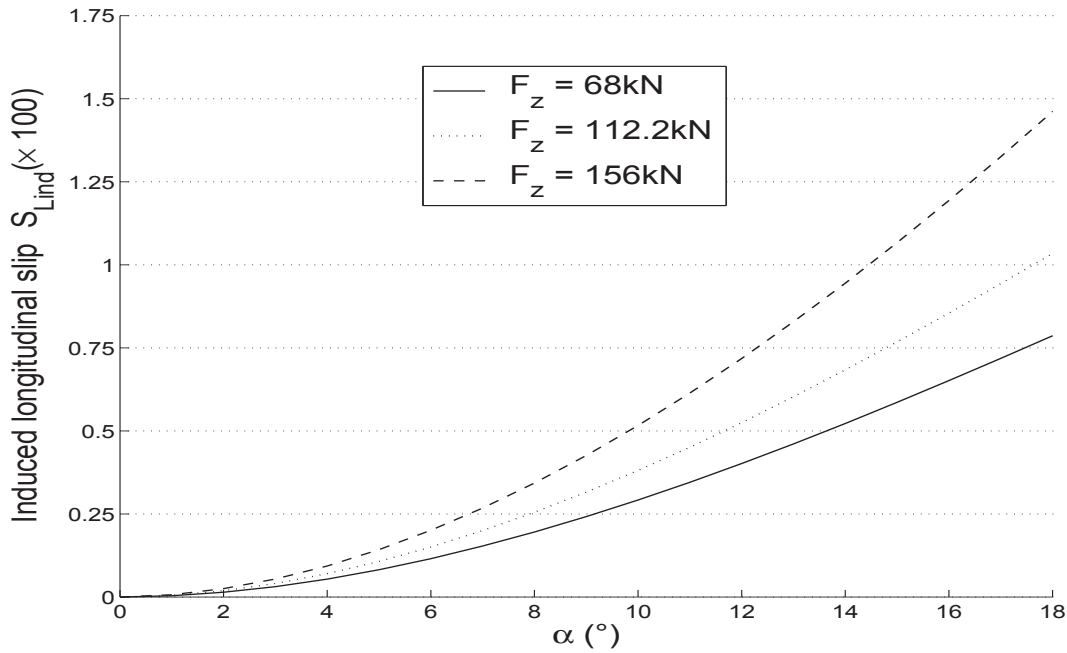


Figure 4.13: Induced longitudinal slip S_{Lind} - inflation pressure $p = 14$ bars

4.7. Modelling results

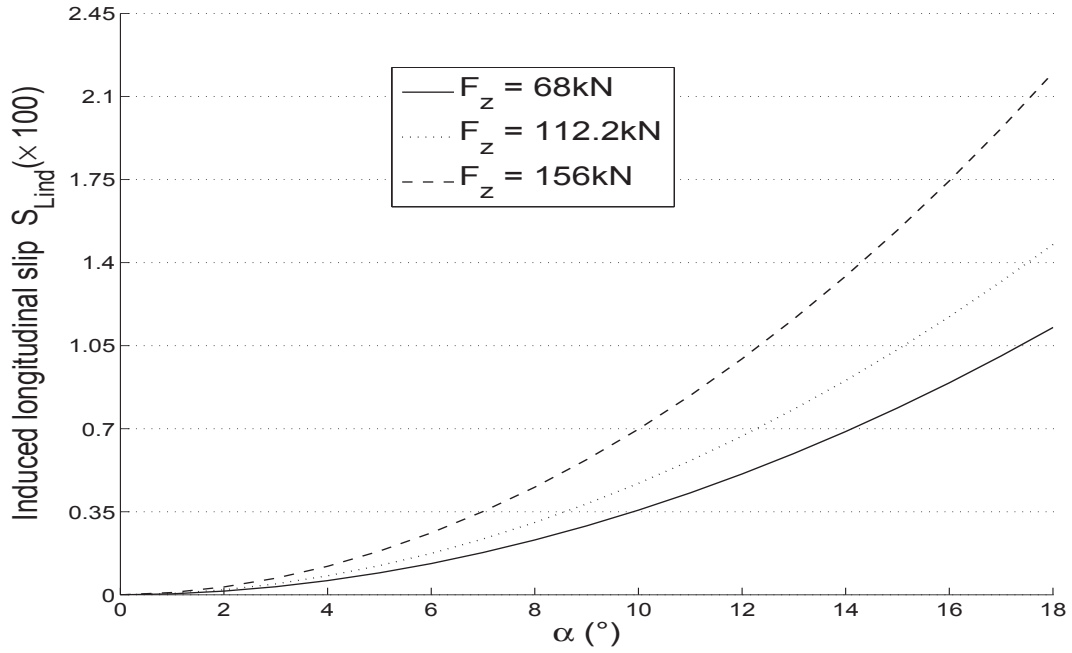


Figure 4.14: Induced longitudinal slip S_{Lind} - $p = 16$ bars

Inflation pressure $p = 14$ bars		
$F_z = 68kN$	$F_z = 112.2kN$	$F_z = 156kN$
$B = 4$	$B = 3.996$	$B = 3.32$
$C = 1.482$	$C = 1.315$	$C = 1.605$
$E = -7.197$	$E = -5.097$	$E = 0$
$Sh = 0$	$Sh = 0$	$Sh = -0.0001$
$Sv = 0$	$Sv = 0$	$Sv = 0$
$D = 16292N$	$D = 29700N$	$D = 38110N$
Inflation pressure $p = 16$ bars		
$F_z = 68kN$	$F_z = 112.2kN$	$F_z = 156kN$
$B = 4$	$B = 3.96$	$B = 3.775$
$C = 1.468$	$C = 1.439$	$C = 1.364$
$E = -8.162$	$E = -8.448$	$E = -6.118$
$S_h = 0$	$S_h = 0$	$S_h = 0$
$S_v = 0$	$S_v = 0$	$S_v = 0$
$D = 16048N$	$D = 25301N$	$D = 38188N$

Table 4.2: Values of the model parameters

Figures 4.15 and 4.16 presents the modelling results obtained using the proposed Magic Formula model. The results are compared with the measurements data as well as the results obtained by using the physical brush model based expression presented in equation (4.29). It can be remarked that the Magic Formula model better fits measurements data than the brush model based expression.

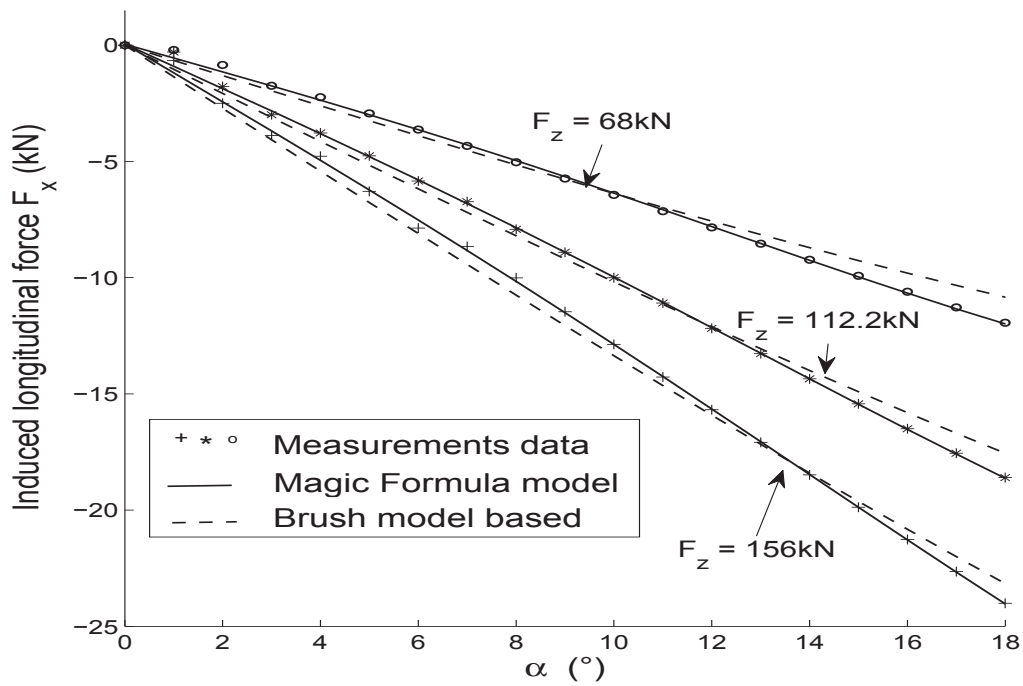


Figure 4.15: Magic Formula model - induced longitudinal force at pure cornering - $p = 14$ bars

4.8. Conclusion

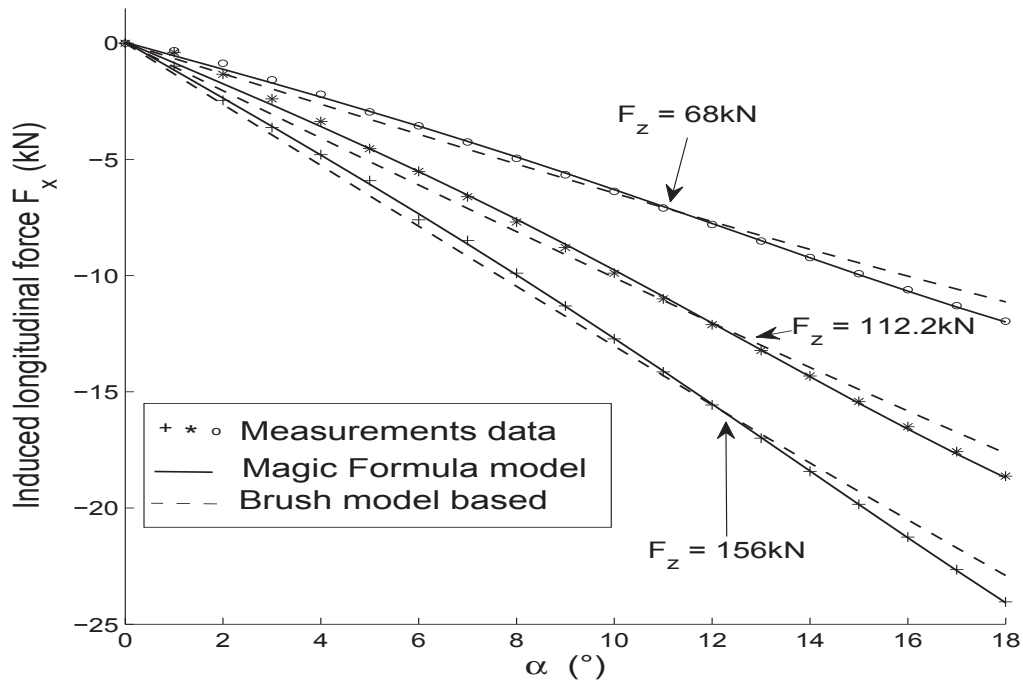


Figure 4.16: Magic Formula model - induced longitudinal force at pure cornering - $p = 16$ bars

4.8 Conclusion

In this chapter, the brush model concept is taken into account in a comprehensive physical approach to describe the tyre deformation in the contact patch at pure cornering.

In one hand, it is shown that the non uniform tyre lateral tread displacement in the contact patch may generate longitudinal tread contraction. This longitudinal contraction is similar to the longitudinal tread displacement when a braking action is applied on the wheel. Therefore, a longitudinal force is developed and acts as a braking force. With respect to the tyre properties and loading conditions, this force may be more or less significant. A relative simple and physical model is proposed for this force, which is referred as induced longitudinal force. In the other hand, the self-aligning moment at pure cornering condition is decomposed into contributions of the induced longitudinal force and the lateral force. This decomposition has allowed an exhaustive description of the self-aligning moment generation. It is shown that the induced longitudinal force may be determinant

in the generation of the self-aligning moment. Indeed, by taking this force into consideration, it has been possible to explain why the self-aligning moment may become zero before the tyre reaches its full sliding condition. Moreover, the fact that the sign of the self-aligning moment can change during its evolution, relative to the side slip angle, has been physically explained. A model for the self-aligning moment is derived as function of both induced longitudinal force and lateral force. Finally, an extension of Magic Formula model for induced longitudinal force, at pure cornering, is proposed.

Besides, since the major part of a given model parameters have to be estimated from measurements data, it may be possible to wonder how close is an estimated value to the real one? What is the importance of a specific parameter on the model response? Is it necessary to precisely estimate its value? The aim of the next chapter is to provide means that help to respond to these questions.

CHAPTER 5

Sensitivity analysis for tyre models

Through the tyre models investigations presented in chapters 2, 3 and 4, it can be underlined that tyre models are mainly nonlinear and depend on parameters which have to be estimated from measurements data. One of the problems of great importance related to this issue is to efficiently prepare and plan the experiments. Indeed, it may be necessary to determine the parameters that have more influence on the model output and thus, are responsible for the output uncertainty which has to be reduced. For this sake, a methodology for carrying out sensitivity analysis on a model is presented. Then, the variance-based global sensitivity analysis is described. This type of sensitivity analysis consists in studying and quantifying the contribution of each parameter in the total variance of the model response. Application is presented for two tyre models, Fiala and Magic Formula (the basic Magic Formula version) models. Then, each model parameters are classified into a hierarchy with respect to the importance of their influence on the model response [42, 43, 44]. Thus, to improve the accuracy of these models responses, it is necessary to pay particular attention to measurements data which help to better estimate the values of their more influential parameters.

5.1 Introduction

In general, the tyre models available in the literature are nonlinear and complex. They depend on a certain number of parameters obtained from experimental data. These measurement data are often few or/and uncomplete, especially in the aircraft domain, and involve high costs. A number of parameters are estimated with more or less precision, which may lead to unacceptable uncertainty on the model output. Among all the parameters, however, some only have a small or insignificant influence on the model response and therefore, do not need to be determined precisely. In the other hand, some parameters

are determinant for the model response and thus influence its uncertainty significantly. These parameters may require additional measurement data in order to be estimated with relatively high accuracy. In order to prepare and plan the experiments, it is necessary to distinguish the parameters with an insignificant influence on the response uncertainty, so as to set them at their nominal value in their interval of variation, thanks to the sensitivity analysis.

Different approaches have been proposed in the literature, for sensitivity analyses of non-linear models [45, 46, 47, 48, 49, 50, 51, 52]. There are qualitative [48] and quantitative approaches [47]. The qualitative approaches help to classify the parameters into a hierarchy with respect to the importance of their influence on the model response. The quantitative approaches are constructive in the sense that they not only allow the classification of the parameters into a hierarchy but also provide the means for the quantification of each parameter influence, contrary to the qualitative approaches. The present study focuses exclusively on the quantitative approaches. There are two types of quantitative approaches: local and global. Local approaches help to determine the impact of a small parameter variation around a nominal value. This impact is determined by calculating the partial derivative of the output function vs the corresponding parameter at the nominal value [53]. The global approaches also allow the determination of the same impact but by varying the parameter in its entire range of variation. These methods are based on the analysis of the output variance [46, 47, 51]. They consist in calculating the contribution of the individual parameter to the total variance of the model output. Each parameter has two types of contribution to the total output variance. In one hand, there is the main contribution of the parameter, which corresponds to the contribution of the parameter alone. In the other hand, there is the collective contribution of the parameter, which represents the influence of its interactions with the other parameters. The total contribution of the parameter is the sum of its main and collective contributions.

The aim of this chapter is first to provide a methodology for sensitivity analysis [42, 43, 44]. Then, variance-based global sensitivity analysis is performed on two tyre models, the Fiala model [19] and the Pacejka model, which is a basic function of the Magic Formula [10]. The study focuses on these two models because they are already studied and used for modelling the tyre forces and moments in chapters 2 and 3. Moreover, only the analysis of the lateral force and the self-aligning moment models is presented but the same approach can be used for studying the remaining tyre characteristics expressions.

This chapter is organised as follows. Section 5.2 presents the main objectives of the sensitivity analysis and the proposed approach, followed by the definition of the sensitivity

5.2. Sensitivity analysis

indices and a method for their estimation. Then, the tyre models are studied in section 5.3 and a variance-based sensitivity analysis is carried out. For each model, the influence of the parameters is quantified and the most influential parameters are highlighted.

5.2 Sensitivity analysis

The main objectives of sensitivity analysis can be summarized as follows.

- To attest the reliability of or the confidence in the model prediction. For example, if the sensitivity analysis shows a high influence of an input parameter which in reality is known to have little (or no) influence, then the model is not reliable and should be modified.
- To determine the parameters which have the greatest influence on the total output variance. These parameters are responsible for the uncertainty of the output. So, the quality of the output can be increased by reducing the error in the most influential parameters.
- To identify the parameters which have little or no influence on the total variance of the model output. These parameters can be set at their nominal values, which will reduce the number of parameters (and also reduce the model complexity) with no significant effect on its accuracy.
- To determine which parameters interact with the others. In fact, a parameter on its own may not be influential, while its interactions with the others have a greater importance in the model response.

Consider a mathematical model in its general form:

$$M : y = f(x_1, \dots, x_n) \quad (5.1)$$

where $y \in \mathbb{R}$ represents the model output and $x_i \in \mathbb{R}$, $i = 1, \dots, n$ the n unknown parameters, which are considered as random and independent variables. The function f is nonlinear with respect to x_i . Performing a sensitivity analysis on model M allows the identification of the parameters x_i which have the greatest influence on its response y .

The approach describing the steps necessary to carry out a sensitivity analysis is presented below.

5.2.1 Description of the sensitivity analysis approach

Performing a sensitivity analysis requires the following steps.

a) *Definition of the model*

This first step consists in clearly determining the output y of the model M as a function of the predefined parameters x_i .

b) *Assignment of the variation limits and the probability density function*

Each parameter x_i is considered as a random variable. It is then necessary to determine the variation limits of each parameter x_i and to estimate the most probable value of the parameter within these limits in order to choose the most appropriate probability density function. The variation limits as well as the probability density function may depend on various issues such as physical, technical and economical possibilities or/and limitations. The probability density functions most often considered are normal, lognormal and uniform distributions.

c) *Generation of input vectors*

This step consists in choosing an appropriate sampling method for generating the possible values for each parameter x_i within its limits of variation and according to its distribution function during simulation. Among the sampling procedures, one can distinguish random sampling, quasi-random sampling and Latin hypercube sampling [54, 55, 56]. As mentioned in [56], Latin hypercube sampling may be an appropriate method for computationally demanding models. When it is not the case, random sampling may be considered.

d) *Determination of the model response distribution*

For each sample value of the parameters x_i , the output y is calculated. It is then possible to have an overview on the model uncertainty by plotting (for example) the histogram of frequencies as well as the cumulative frequencies for y .

e) *Calculation of the sensitivity indices*

The final step consists in evaluating quantitatively the influence of the parameters x_i on the output y , by calculating the sensitivity indices.

The next subsection presents the definition of the sensitivity indices based on the analysis of the output variance.

5.2. Sensitivity analysis

5.2.2 Sensitivity indices

Consider the model M described by equation (5.1). In order to appreciate the contribution of the parameter x_i to the total variance of the output y , it is necessary to calculate the conditional variance of y while setting $x_i = x_i^*$, denoted $V(y|x_i)$. Since the true value x_i^* of x_i is not known, the expectation of $V(y|x_i)$ for all possible values in the interval of variation of x_i is considered instead. This expectation is denoted $E(V(y|x_i))$. The greater the contribution of parameter x_i to the total variance of y is, the lower quantity $E(V(y|x_i))$ will be. The total variance of y , denoted $V(y)$, can be expressed as a function of the expectation $E(V(y|x_i))$. $V(y)$ then becomes:

$$V(y) = V(E(y|x_i)) + E(V(y|x_i)) \quad (5.2)$$

where the term $V(E(y|x_i))$ is the variance of the conditional expectation of y when x_i is set (x_i supposed known). This term is also an indicator of the influence of x_i on the total variance of y . Indeed, the more parameter x_i contributes to the total variance of y , the greater quantity $V(E(y|x_i))$ will be. In order to use a normalized indicator, the sensitivity index of parameter x_i , denoted S_i [57, 58], is defined as follows:

$$S_i = \frac{V(E(y|x_i))}{V(y)} \quad (5.3)$$

The value of the sensitivity index S_i lies between 0 and 1. The closer to 1 its value is, the more parameter x_i contributes to the total variance of y .

The sum of the sensitivity indices S_i , $i = 1, \dots, n$, associated to each parameter x_i verifies the following relation:

$$\sum_{i=1}^n S_i \leq 1 \quad (5.4)$$

Remark: If the model M is additive, it can be re-expressed as follows:

$$M : \quad y = a_0 + \sum_{i=1}^n f_i(x_i) \quad (5.5)$$

where a_0 is a constant, the functions f_i , $i = 1, \dots, n$, are possibly nonlinear with respect to x_i . In the case of an additive model, the following expression holds:

$$\sum_{i=1}^n S_i = 1 \quad (5.6)$$

If model M is nonlinear and non additive, the interactions between the different parameters will also influence the total variance of y . In this case, the sensitivity index S_i is no longer

the most appropriate indicator and the total sensitivity index, denoted S_{T_i} [57, 58], is preferred. The total sensitivity index is defined as:

$$S_{T_i} = 1 - \frac{V(E(y|x_{\sim i}))}{V(y)} \quad (5.7)$$

where the term $V(E(y|x_{\sim i}))$ represents the variance of the conditional expectation of y when all parameters are supposed known except parameter x_i . The total sensitivity index S_{T_i} includes the contribution due to parameter x_i alone, which also corresponds to index S_i , and the contribution due to the interactions of x_i with the other parameters. In [46], it is demonstrated that the total variance of y can be decomposed as:

$$V(y) = \sum_{i=1}^n V_i + \sum_{i=1}^n \sum_{j=i+1}^n V_{ij} + \dots + V_{12\dots n} \quad (5.8)$$

where :

$$\begin{aligned} V_i &= V(E(y|x_i)) \\ V_{ij} &= V(E(y|x_i, x_j)) - V_i - V_j \\ &\vdots \end{aligned} \quad (5.9)$$

If equation (5.8) is divided by $V(y)$, the following relation is obtained:

$$1 = \sum_{i=1}^n S_i + \sum_{i=1}^n \sum_{j=i+1}^n S_{ij} + \dots + S_{12\dots n} \quad (5.10)$$

where S_i represents the sensitivity index of parameter x_i (contribution of x_i alone to the total variance $V(y)$) and is often called first order sensitivity index. The terms S_{ij} , ..., $S_{12\dots n}$ are given by:

$$\begin{aligned} S_{ij} &= \frac{V_{ij}}{V(y)} \\ &\vdots \\ S_{12\dots n} &= \frac{V_{12\dots n}}{V(y)} \end{aligned} \quad (5.11)$$

The term S_{ij} represents the contribution due to the interaction of parameter x_i with parameter x_j and is called second order sensitivity index. In the same manner, the term $S_{12\dots n}$ represents the contribution due to the interaction of parameter x_i with the remaining parameters and is called n order sensitivity index. Thus, the total sensitivity index S_{T_i} of parameter x_i is expressed as:

$$S_{T_i} = S_i + \sum_{\substack{j=1 \\ j \neq i}}^n S_{ij} + \sum_{\substack{j=1 \\ j \neq i}}^n \sum_{\substack{k=j+1 \\ k \neq i \\ j \neq i}}^n S_{ijk} + \dots + S_{ijk\dots n} \quad (5.12)$$

5.2. Sensitivity analysis

The sensitivity indices presented previously are often calculated analytically when the function f of model M is known and relatively simple. However, some models may be complex with a high number of parameters so that analytical calculations of the sensitivity indices become time consuming or even sometimes impossible. It is therefore necessary to estimate them.

The following subsection presents a method of estimating the sensitivity indices, often referred to as the Monte Carlo method.

5.2.3 Estimating sensitivity indices

Several methods of estimating the sensitivity indices are available in the literature [45, 46, 52, 59, 60]. The approach used in this study is based on the Monte Carlo method [46]. Consider a random sample of size N for each parameter of model M and suppose that x_i^k denotes the k th value of parameter x_i in its random sample. The estimated value of the expectation of y , denoted $\hat{E}(y)$, is given by:

$$\hat{E}(y) = \frac{1}{N} \sum_{k=1}^N f(x_1^k, \dots, x_n^k) \quad (5.13)$$

In the same manner, the estimated value of the variance of y , denoted $\hat{V}(y)$, is the following:

$$\hat{V}(y) = \frac{1}{N} \sum_{k=1}^N f^2(x_1^k, \dots, x_n^k) - (\hat{E}(y))^2 \quad (5.14)$$

In [46], a technique for the estimation of the conditional variance of y with respect to x_i is proposed. It is based on the estimation of the expectation of y and requires two samples of the same size N for each parameter x_i . Suppose that x_i^{k1} denotes the k th value of the parameter x_i from sample 1 and x_i^{k2} , the k th value of parameter x_i from sample 2. The estimated value of the conditional variance of y with respect to x_i , denoted \hat{V}_i , is the following [46]:

$$\hat{V}_i = \hat{U}_i - (\hat{E}(y))^2 \quad (5.15)$$

where \hat{U}_i is given by the expression below:

$$\begin{aligned} \hat{U}_i = \frac{1}{N} \sum_{k=1}^N & f(x_1^{k1}, \dots, x_{i-1}^{k1}, x_i^{k1}, x_{i+1}^{k1}, \dots, x_n^{k1}) \\ & \times f(x_1^{k2}, \dots, x_{i-1}^{k2}, x_i^{k1}, x_{i+1}^{k2}, \dots, x_n^{k2}) \end{aligned} \quad (5.16)$$

The estimated value of the first order sensitivity index, denoted \hat{S}_i , is then obtained:

$$\hat{S}_i = \frac{\hat{V}_i}{\hat{V}(y)} \quad (5.17)$$

Moreover, the estimated value of the second order sensitivity index, \hat{S}_{ij} , is:

$$\hat{S}_{ij} = \frac{\hat{V}_{ij}}{\hat{V}(y)} \quad (5.18)$$

where \hat{V}_{ij} is given by:

$$\hat{V}_{ij} = \hat{U}_{ij} - (\hat{E}(y))^2 - \hat{V}_i - \hat{V}_j \quad (5.19)$$

The term \hat{U}_{ij} is the estimated value of the mean square of y and is obtained by varying all its parameters except x_i and x_j :

$$\begin{aligned} \hat{U}_{ij} = \frac{1}{N} \sum_{k=1}^N f(x_1^{k1}, \dots, x_{i-1}^{k1}, x_i^{k1}, x_{i+1}^{k1}, \dots, x_{j-1}^{k1}, x_j^{k1}, x_{j+1}^{k1}, \dots, x_n^{k1}) \\ \times f(x_1^{k2}, \dots, x_{i-1}^{k2}, x_i^{k1}, x_{i+1}^{k2}, \dots, x_{j-1}^{k2}, x_j^{k1}, x_{j+1}^{k2}, \dots, x_n^{k2}) \end{aligned} \quad (5.20)$$

The same method is used to estimate the sensitivity indices of a higher order. Finally, the total sensitivity index of x_i is expressed as:

$$\hat{S}_{Ti} = 1 - \frac{\hat{V}_{\sim i}}{\hat{V}(y)} \quad (5.21)$$

where $\hat{V}_{\sim i}$ is the estimated conditional variance of y with respect to all parameters except x_i . It also means that $\hat{V}_{\sim i}$ is estimated by varying only x_i while keeping all the other parameters constant. $\hat{V}_{\sim i}$ is given by:

$$\begin{aligned} \hat{V}_{\sim i} = \hat{U}_{\sim i} - (\hat{E}(y))^2 \\ \hat{U}_{\sim i} = \frac{1}{N} \sum_{k=1}^N f(x_1^{k1}, \dots, x_{i-1}^{k1}, x_i^{k1}, x_{i+1}^{k1}, \dots, x_n^{k1}) \\ \times f(x_1^{k1}, \dots, x_{i-1}^{k1}, x_i^{k2}, x_{i+1}^{k1}, \dots, x_n^{k1}) \end{aligned} \quad (5.22)$$

In the next section, these sensitivity indices are determined for two tyre models in order to determine their most influential parameters.

5.3 Application of sensitivity analysis on tyre models

For the two models considered in this chapter, the study will focus exclusively on each model expression for the lateral force and for the self-aligning moment at steady-state pure lateral slip. The measurements data used here are taken from those presented in chapter 2. Besides, the parameters of each considered model are assumed independent.

5.3.1 Fiala tyre model

5.3.1.1 Lateral force model F_y

For the Fiala model, the steady-state lateral force F_y at pure lateral slip is expressed as follows:

$$F_y = -\mu_y F_z \left(1 - \left(1 - \frac{C_{\alpha y} |\tan \alpha_y|}{3\mu_y F_z} \right)^3 \right) \text{sgn}(\alpha_y) \quad (5.23)$$

where $C_{\alpha y}$ is the cornering stiffness, F_z the vertical load ($F_z > 0$) and μ_y the lateral friction coefficient. Parameter α_y is the side slip angle. The term $\text{sgn}(\alpha_y)$ represents the sign of the side slip angle α_y . A sensitivity analysis is performed on the Fiala lateral force model F_y . The approach presented in section 5.2.1 is applied to complete this study.

a) *Definition of the model*

The lateral force F_y represents the model output. The vertical load F_z is measured and thus considered as known. It will be fixed at $F_z = 90\text{kN}$. However, it is remarked that the tendency of the sensitivity analysis results is similar if a different value (within the variation range used for the measurements data presented in chapter 2) is used for F_z . Parameters $C_{\alpha y}$, μ_y and α_y are unknown and their values are determined from measurements data. Therefore, they are the parameters whose influence should be studied.

b) *Assignment of the variation limits and probability density function*

The variation limits of $C_{\alpha y}$ are estimated using a database, which considers an interpolation function similar to that presented in [10] and which gives $C_{\alpha y}$ as a $\sin(\text{atan})$ function of the vertical load F_z . The variation interval of $C_{\alpha y}$ is estimated to be [179.02kN/rad; 1165kN/rad]. The value of $C_{\alpha y}$ strongly depends on the tyre lateral stiffness. In fact, it may be considered that the stiffer the tyre carcass is, the greater $C_{\alpha y}$ will be independently of the friction state in the tyre-road interface.

Then, the maximum value F_{ymax} which the lateral force can reach, depends on the tyre-road contact state and is most often assumed to be proportional to the maximum value of the friction coefficient, $F_{ymax} = \mu_{ymax}F_z$. The value of μ_{ymax} corresponds to the upper limit of the friction coefficient interval. In the present case, it is supposed that $\mu_{ymax} = 1$, which is simply based on the Coulomb's friction law and means that the maximum value which the lateral force can reach is 90kN. μ_y is assumed to vary in the interval [0.4; 1]. However, for some specific tyres, μ_{ymax} can be greater than 1 and as a result, the importance of μ_y in the output may be significantly different [42].

Finally, parameter α_y is supposed to vary in the interval [0; 20°] ([0; 0.35rad]). It can be mentioned that, for the measurements data used in this thesis, the maximum lateral force is observed for side slip angle beyond 14° and it may reach up to 20° with respect to the road and vertical load conditions for most civil aircraft tyres. Parameters $C_{\alpha y}$, μ_y and α_y are assumed independent. They are deemed to follow a uniform distribution law in their corresponding interval.

Remark

Simulations with a normal distribution law for each parameter within its range of variation, not presented here, were also performed. The simulation results show the same trend in the distribution of the output and the sensitivity indices are not significantly different from those obtained under assumption of a uniform distribution law. It seems that the variation limits of the parameter are more influential than the distribution itself.

c) *Generation of the parameters*

The model presented in equation (5.23) is not computationally demanding and so, random sampling has been adopted (function `rand` from Matlab software). A sample size of $N = 100000$ is considered for each parameter.

d) *Determination of the output distribution*

The output F_y is generated according to equation (5.23) and using the previous samples for μ_y , $C_{\alpha y}$ and α_y .

Figure 5.1 presents the histogram of frequencies for the lateral force F_y with respect to its classes. Figure 5.2 presents the cumulative frequencies for F_y , which has been normalized. The mean value of F_y is -52.85 kN and its 95% confidence interval is [-120.95kN;-8.64kN], revealing an uncertainty of 112.3 kN which represents 212% of

5.3. Application of sensitivity analysis on tyre models

the mean value of F_y . The objective is to estimate the contribution of α_y , μ_y and $C_{\alpha y}$ to this uncertainty.

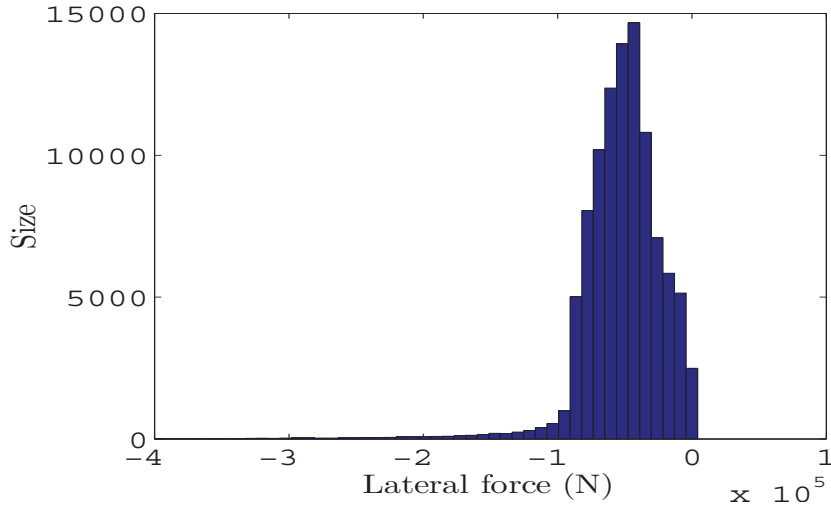


Figure 5.1: Fiala lateral force model: Histogram of frequencies

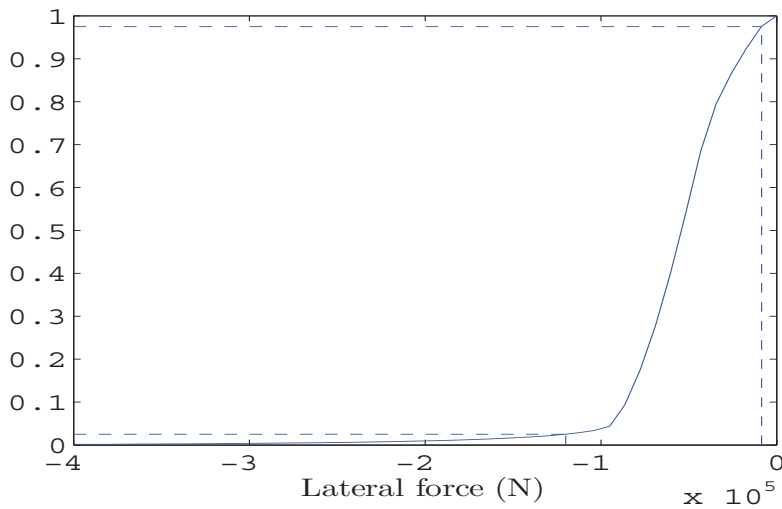


Figure 5.2: Fiala lateral force model: Cumulative frequencies

e) *Calculation of the sensitivity indices*

Consider the lateral force F_y given by equation (5.23). To estimate the sensitivity indices, two samples of the same size $N = 100000$ are assumed for each parameter. Equations (5.13) and (5.14) are used to estimate the mean value of model F_y , $\hat{E}(F_y) = -52.85\text{kN}$, and its variance, $\hat{V}(F_y) = 1.40 \times 10^8$, respectively. Then,

the first order sensitivity indices, S_{μ_y} , $S_{C_{\alpha_y}}$ and S_{α_y} , are estimated using equation (5.17).

The different indices are plotted in figure 5.3 and their corresponding values are given in table 5.1.

First order indices	Total indices
$S_{\alpha_y} = 0.348$	$S_{T\alpha_y} = 0.758$
$S_{C_{\alpha_y}} = 0.1665$	$S_{TC_{\alpha_y}} = 0.5574$
$S_{\mu_y} = 0.0166$	$S_{T\mu_y} = 0.3417$

Table 5.1: Sensitivity indices for the Fiala lateral force model F_y

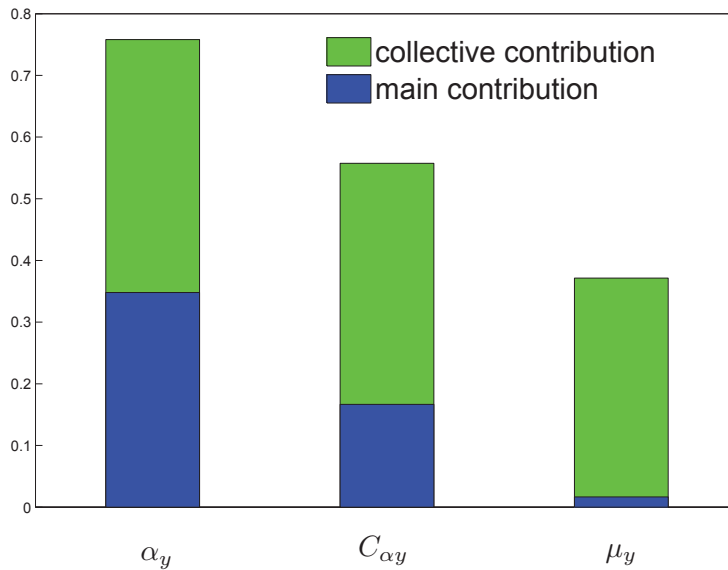


Figure 5.3: Sensitivity indices for the Fiala lateral force model F_y

The first order index of the parameter α_y is the most important ($S_{\alpha_y} = 0.348$). So, the slip angle is the most influential parameter in the lateral force model. Parameter C_{α_y} follows ($S_{C_{\alpha_y}} = 0.1665$). Finally, the sensitivity index of μ_y is low ($S_{\mu_y} = 0.0166$). As a result, it can be underlined that when considering the influence of each parameter alone, only the side slip angle α_y and the cornering stiffness C_{α_y} have significant influence on the Fiala lateral force model response. However, for each

5.3. Application of sensitivity analysis on tyre models

parameter, the value of the total sensitivity index is higher than the one of the first order. This is due to important influence of the interactions between the parameters. Indeed, the sum of the first order indices is about 0.53 ($S_{\mu_y} + S_{C_{\alpha_y}} + S_{\alpha_y} = 0.5311$), which means that the contribution due to the interactions of the parameters is as important as their individual contribution.

In fact, the parameter μ_y determines the maximum value which the lateral force F_y can reach. However, this maximum value of F_y is also determined by a given value of the side slip angle α_y . This explains the influence of the interaction between parameters μ_y and α_y . In the other hand, parameter C_{α_y} determines the lateral deflection of the tyre. The influence of the parameter C_{α_y} on its own and of its interaction with the other parameters is not negligible as the lateral force is related to this tyre lateral deflection. In a word, for the Fiala lateral force model, the improved accuracy in the slip angle α_y , in the cornering stiffness C_{α_y} and in the friction coefficient μ_y is necessary in order to reduce the uncertainty in the lateral force.

Remark on the sample size

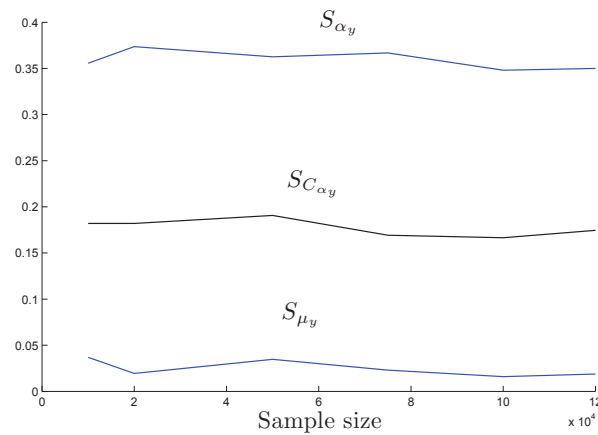


Figure 5.4: Fiala lateral force model F_y : sensitivity indices for different sample sizes

Tests with smaller and higher sample sizes have also been considered in the investigation of the Fiala lateral force model. It has been noted that the values of the sensitivity indices do not vary significantly with the sample size. For example, figure 5.4 shows the values obtained for the different indices of the Fiala lateral force model with respect to the sample

size. The sensitivity indices seem to be mainly sensitive to parameters limits of variation rather than to the sample size. However, further investigations could help to determine the sample size(s) which lead(s) to a better compromise between precision and computation time.

The same remark can be done for the self-aligning moment and for the Magic Formula model presented in the next sections.

5.3.1.2 Self-aligning moment model M_z

The equation (5.24) presents the self-aligning moment expression of the Fiala model at pure lateral slip in steady-state condition.

$$M_z = 2\mu_z R_2 F_z (1 - H) H^3 \text{sign}(\alpha_z) \quad (5.24)$$

where $H = 1 - \frac{C_{\alpha_z} |\tan(\alpha_z)|}{(3\mu_z F_z)}$.

Quantity R_2 represents the tyre half width. The parameters C_{α_z} , μ_z and α_z have the same meaning and the same variation limits as parameters C_{α_y} , μ_y and α_y already presented in the case of the pure lateral force F_y , equation (5.23). The subscript z is only used to distinguish the self-aligning moment parameters from those of the lateral force F_y designated with subscript y . A sensitivity analysis is performed on the self-aligning moment model M_z using the previous approach as presented below.

a) *Definition of the model*

The self-aligning moment M_z represents the model output. As in the case of the Fiala lateral force model, the vertical load, F_z , is supposed known and it is fixed at $90kN$. The tyre half width, R_2 , is also supposed known and its value is $0.2275m$. Parameters C_{α_z} , μ_z and α_z are unknown and their values are determined from measurements data. Thus, they are the parameters whose influence should be studied.

b) *Assignment of the variation limits and probability density function*

The parameters C_{α_z} , μ_z and α_z have the same meaning and the same variation limits as the parameters C_{α_y} , μ_y and α_y already presented in the case of the pure lateral force F_y , equation (5.23). Thus, the following intervals [$179.02kN/rad$; $1165kN/rad$], $[0.4; 1]$, $[0; 0.35rad]$ are considered for the parameters C_{α_z} , μ_z and α_z , respectively. Moreover, parameters C_{α_z} , μ_z and α_z are assumed independent. They are deemed to follow a uniform distribution law in their corresponding interval.

5.3. Application of sensitivity analysis on tyre models

c) *Generation of the parameters*

The model presented in equation (5.24) is not computationally demanding and so, random sampling has been adopted (function `rand` from Matlab software). A sample size of $N = 100000$ is considered for each parameter.

d) *Determination of the output distribution*

The output M_z is generated according to equation (5.24) and using the previous samples for μ_z , $C_{\alpha z}$ and α_z . The mean value of M_z is 1.721kNm and its 95% confidence interval is [0.5kNm; 3.81kNm]. This interval indicates an uncertainty of 3.31kNm which is equivalent to 192% of the mean value of M_z . The objective is to estimate the contribution of μ_z , $C_{\alpha z}$ and α_z to this uncertainty.

e) *Calculation of the sensitivity indices*

Consider the self-aligning moment M_z model given in equation (5.24). Two samples of the same size $N = 100000$ are assumed for each parameter. Equations (5.13) and (5.14) are used to estimate the mean value of model M_z , $\hat{E}(M_z) = 1.721\text{kNm}$, and its variance, $\hat{V}(M_z) = 6.87 \times 10^6$, respectively. Then, the first order sensitivity indices, S_{μ_z} , $S_{C_{\alpha z}}$ and S_{α_z} , are estimated using equation (5.17).

The different indices are plotted in figure 5.5 and their corresponding values are given in table 5.2.

First order indices	Total indices
$S_{\alpha_z} = 0.368$	$S_{T\alpha_z} = 0.768$
$S_{C_{\alpha z}} = 0.092$	$S_{TC_{\alpha z}} = 0.63$
$S_{\mu_z} = 0.071$	$S_{T\mu_z} = 0.522$

Table 5.2: Sensitivity indices for the Fiala self-aligning moment model M_z

Parameter α_z has the highest first order sensitivity index ($S_{\alpha_z} = 0.368$). The first order sensitivity indices of parameters $C_{\alpha z}$ ($S_{C_{\alpha z}} = 0.092$) and μ_z ($S_{\mu_z} = 0.071$) are low and close to each other. Nevertheless, the total sensitivity indices of parameters $C_{\alpha z}$ ($S_{TC_{\alpha z}} = 0.63$) and μ_z ($S_{T\mu_z} = 0.522$) cannot be neglected. The sum of the first order indices is 0.531 ($S_{\mu_z} + S_{C_{\alpha z}} + S_{\alpha} = 0.531$), which implies that the contribution due to the interactions of the parameters is relatively as important as their individual contribution. As in the case of the lateral force, the improved accuracy in the slip

angle α_z , in the cornering stiffness $C_{\alpha z}$ and in the friction coefficient μ_z are necessary in order to reduce the uncertainty in the self-aligning moment.

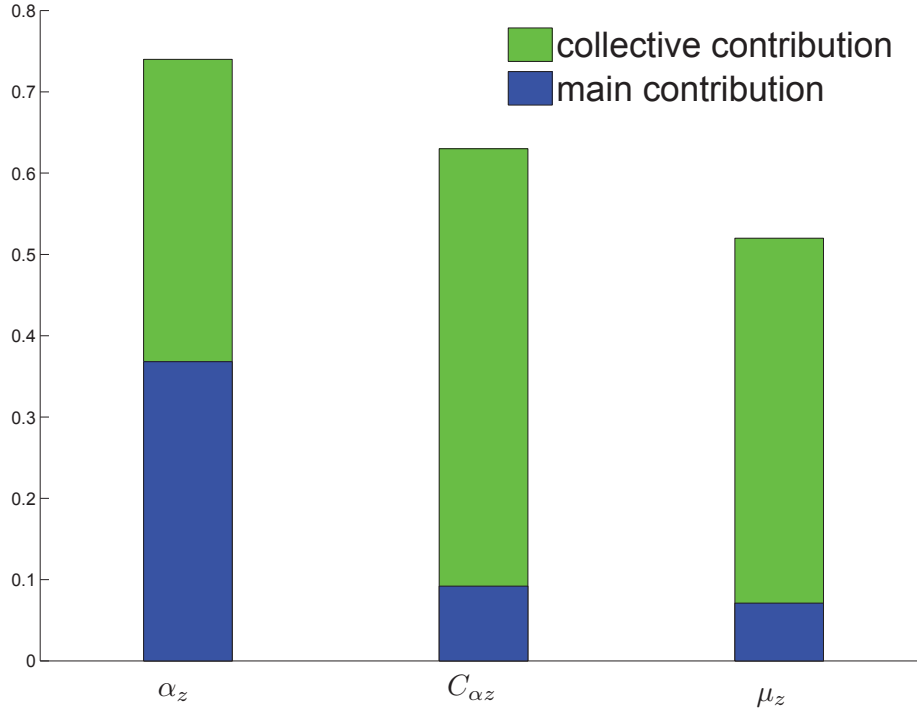


Figure 5.5: Sensitivity indices for the Fiala self-aligning moment model M_z

5.3.2 Magic Formula model

5.3.2.1 Lateral force model F_y

In pure cornering condition, an interpolation function, called Magic Formula, is proposed for the lateral force as presented in equation below:

$$F_y = D_y \sin \left[C_y \arctan B_y(\alpha_y + S_{hy}) - E_y(B_y(\alpha_y + S_{hy}) - \arctan(B_y(\alpha_y + S_{hy}))) \right] + S_{vy} \quad (5.25)$$

where $D_y = \mu_y F_z$ is the peak value of the lateral force F_y , $C_\alpha = B_y C_y D_y$ the cornering stiffness. Parameter C_y is called shape factor and B_y is given by $B_y = \frac{C_\alpha}{C_y D_y}$.

By using the above description of the parameters, equation (5.25) can be rewritten as

5.3. Application of sensitivity analysis on tyre models

follows.

$$F_y = \mu_y F_z \sin[C_y \arctan(\frac{C_\alpha}{\mu_y F_z C_y}(\alpha_y + S_{hy}) - E_y(\frac{C_\alpha}{\mu_y F_z C_y}(\alpha_y + S_{hy}) - \arctan(\frac{C_\alpha}{\mu_y F_z C_y}(\alpha_y + S_{hy})))))] + S_{vy} \quad (5.26)$$

The lateral force expression presented above corresponds to the basic (initial) version of the Magic Formula but the extended new versions [10] may be used. Next, a sensitivity analysis is carried out on the Magic Formula lateral force model using the proposed approach.

a) *Definition of the model*

The lateral force F_y presented in equation (5.26) is the model output. For the same reason as in the Fiala model, F_z is considered known and fixed at 90kN. Parameters μ_y , α_y , C_y , C_α , E_y , S_{hy} and S_{vy} are unknown and are under study.

b) *Assignment of the variation limits and probability density function*

Based on the tyre database, the variation limits of C_y , E_y , S_{hy} and S_{vy} are estimated by the following intervals: [1; 2], [-3; 0.5], [-0.0037rad; 0.0037rad] and [-3322N; 3322N] respectively. Similarly to the case of the Fiala model, the variation limits of parameters α_y , μ_y and C_α are [0; 20°], [0.4; 1] and [179.02kN/rad; 1165kN/rad], respectively. A uniform distribution law is assumed for parameters α_y , μ_y , C_y , C_α , E_y , S_{hy} and S_{vy} in their corresponding range of variation.

c) *Generation of input vectors*

The lateral force model as presented in equation (5.26) is not computationally demanding. So, random sampling has been adopted (function `rand` from Matlab software). A sample size of $N = 100000$ is considered for each parameter.

d) *Determination of the output distribution*

Output F_y is generated according to equation (5.26) using the samples for the parameters. Figure 5.6 presents the histogram of frequencies for the lateral force F_y , with respect to its classes. Figure 5.7 presents the cumulative frequencies for F_y which has been normalized.

The mean value of F_y is -75.07kN and its 95% confidence interval is [-180kN;-6.14kN], indicating an uncertainty of 173.85kN and equivalent to 231% of the mean value of F_y . The objective is to classify all the parameters according to their contribution to this uncertainty.

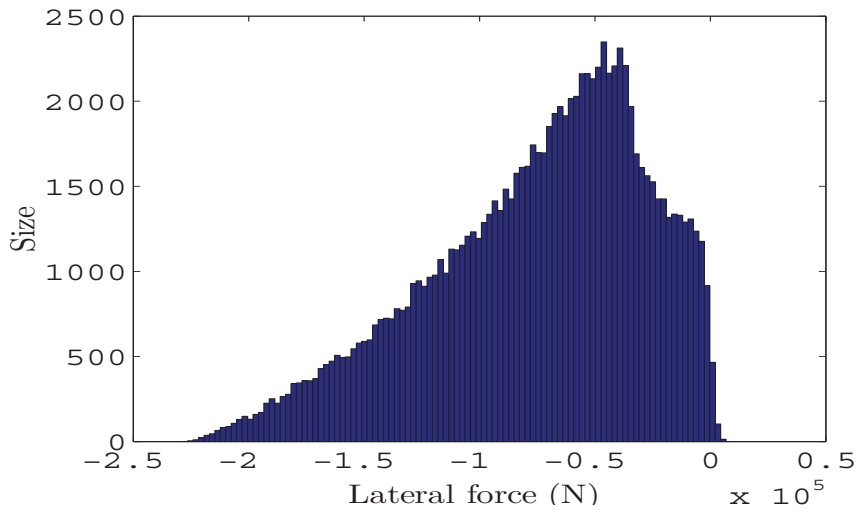


Figure 5.6: Magic Formula lateral force model F_y : Histogram of frequencies

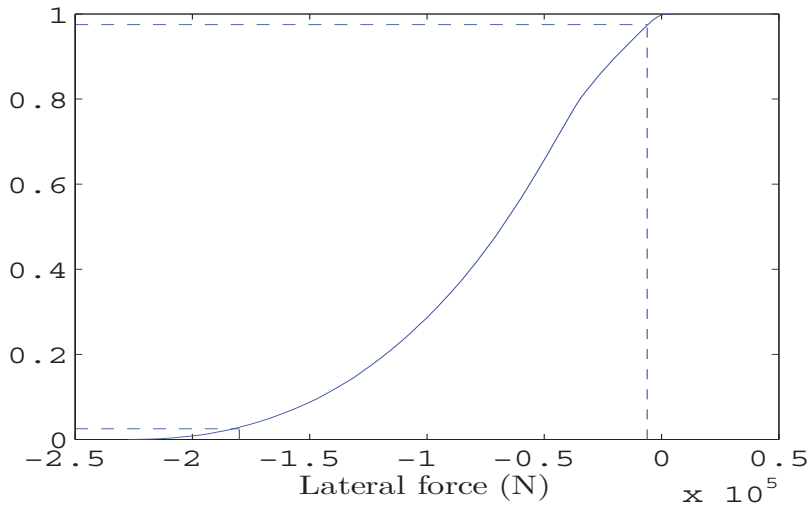


Figure 5.7: Magic Formula lateral force model F_y : Cumulative frequencies

e) *Calculation of the sensitivity indices*

Assume the expression of the lateral force F_y as described by equation (5.26). Two samples of the same size $N = 100000$ are considered for each parameter. The estimated mean value of F_y is $\hat{E}(F_y) = -75.07\text{kN}$ (equation (5.13)) and its estimated variance is $\hat{V}(F_y) = 2.23 \times 10^9$ (equation (5.14)). Equation (5.17) is used to estimate the first order indices S_{α_y} , S_{μ_y} , S_{C_α} , S_{C_y} , S_{E_y} , $S_{S_{h_y}}$ and $S_{S_{v_y}}$. The total sensitivity

5.3. Application of sensitivity analysis on tyre models

indices $S_{T\alpha_y}$, $S_{T\mu_y}$, S_{TC_α} , S_{TC_y} , S_{TE_y} , $S_{TS_{hy}}$ and $S_{TS_{vy}}$ are estimated using equation (5.21). The different indices are plotted in figure 5.8 and their corresponding values are given in table 5.3.

First order indices	Total indices
$S_{\alpha_y} = 0.4387$	$S_{T\alpha_y} = 0.5867$
$S_{\mu_y} = 0.1883$	$S_{T\mu_y} = 0.3661$
$S_{C_\alpha} = 0.1609$	$S_{TC_\alpha} = 0.2657$
$S_{E_y} \simeq 0$	$S_{TE_y} = 0.0072$
$S_{C_y} \simeq 0$	$S_{TC_y} = 0.0035$
$S_{S_{vy}} \simeq 0$	$S_{TS_{vy}} = 0.0017$
$S_{S_{hy}} \simeq 0$	$S_{TS_{hy}} \simeq 0$

Table 5.3: Sensitivity indices for the Magic Formula lateral force model F_y

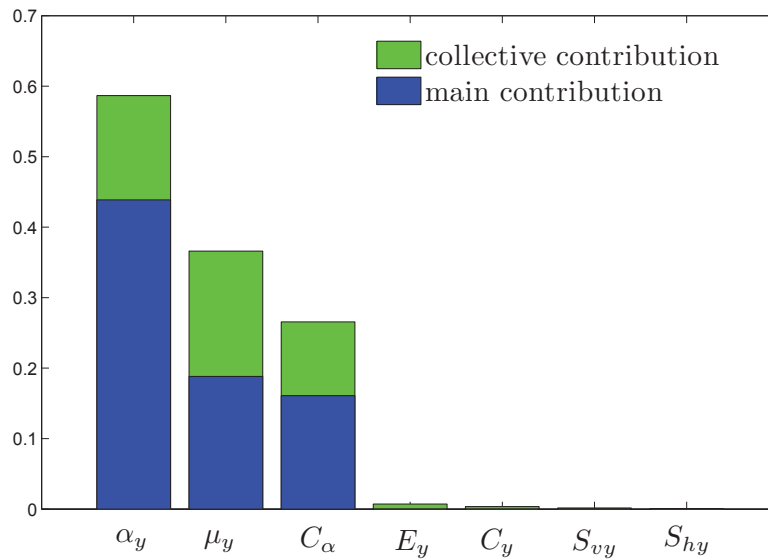


Figure 5.8: Sensitivity indices for the Magic Formula lateral force model (F_y)

Figure 5.8 allows the different parameters to be classified into a hierarchy accord-

ing to their influence on the total variance of the lateral force. It is shown that parameter α_y has the highest sensitivity index ($S_{\alpha_y} = 0.4387$). Therefore, this parameter is the most influential. Then, parameters μ_y and C_α follow ($S_{\mu_y} = 0.1883$ and $S_{C_\alpha} = 0.1609$). Finally, parameters C_y , E_y , S_{vy} and S_{hy} have their sensitivity indices close to 0. Therefore, their influence on the total variance of the model response can be considered negligible. Moreover, the sum of the first order sensitivity indices of the parameters is 0.7879. Thus, the interactions between the parameters have less influence on the lateral force when it is compared to the case of the Fiala model.

In the lateral force model of Magic Formula, parameters α_y , C_α (the same as C_{α_y} or C_{α_z}) and μ_y have the same physical meaning for the tyre as previously mentioned in the analysis of the Fiala model. Parameters C_y , E_y , S_{vy} and S_{hy} are empirical parameters used for adjusting the curve shape and for reducing the interpolation error. This might be the reason why their individual and total influence are negligible. To conclude, in the Magic Formula, only three parameters, the slip angle α_y , the friction coefficient μ_y and the cornering stiffness C_α , significantly influence the lateral force. Consequently, improving their accuracy would help to considerably improve the uncertainty in the lateral force F_y . Concerning parameters C_y , E_y , S_{vy} and S_{hy} , each one can be fixed at its nominal value in the corresponding interval of variation with no significant effect on the accuracy of the model response.

5.3.2.2 Self-aligning moment model M_z

The interpolation function (Magic Formula) proposed for the lateral force in equation (5.26) is a generic function that may be also used for representing the self-aligning moment.

$$M_z = D_z \sin \left[C_z \arctan B_z(\alpha_z + S_{hz}) - E_z(B_z(\alpha_z + S_{hz}) - \arctan(B_z(\alpha_z + S_{hz}))) \right] + S_{vz} \quad (5.27)$$

It can be noted that the function form of the self-aligning moment model M_z is the same as the one of the lateral force model F_y presented in equation (5.26). However, the definition of some parameters changes. Indeed, D_z is the peak value of the self-aligning moment, $C_{Mz} = B_z C_z D_z$, the self-aligning moment constant. Parameter C_z is termed shape factor and B_z is given by $B_z = \frac{C_{Mz}}{C_z D_z}$.

5.3. Application of sensitivity analysis on tyre models

By using the above definition of the parameters, equation (5.27) can be rewritten as follows:

$$M_z = D_z \sin[C_z \arctan\left(\frac{C_{Mz}}{D_z C_z}(\alpha_z + S_{hz}) - E_z\left(\frac{C_{Mz}}{D_z C_z}(\alpha_z + S_{hz}) - \arctan\left(\frac{C_{Mz}}{D_z C_z}(\alpha_z + S_{hz})\right)\right)\right)] + S_{vz} \quad (5.28)$$

Next, a sensitivity analysis is performed on the self-aligning moment model using the proposed approach.

a) *Definition of the model*

The self-aligning moment M_z presented in equation (5.28) is the model output. Similar to the case of the Magic Formula lateral force model F_y , equation (5.26), the parameters D_z , α_z , C_z , C_{Mz} , E_z , S_{hz} and S_{vz} are unknown and are then under study.

b) *Assignment of the variation limits and probability density function*

The variation limits of α_z , [0; 0.35rad], remain unchanged. Those of parameters C_{Mz} , C_z , D_z , E_z , S_{hz} and S_{vz} change and are estimated by the following intervals: [17.9kNm/rad; 51.2kNm/rad], [0.8; 1.6], [0.83kNm; 3.02kNm], [-13; -3], [-0.0011rad; 0.0011rad] and [-0.12kNm; 0.12kNm], respectively. The value of the vertical load F_z is fixed at 90kN (the same as in the case of the lateral force model). Moreover, a uniform distribution law is assumed for parameters α_z , C_{Mz} , C_z , D_z , E_z , S_{hz} and S_{vz} in their corresponding range of variation.

c) *Generation of input vectors*

The self-aligning moment model as presented here is not computationally demanding. So, random sampling has been adopted (function `rand` from Matlab software). A sample size of $N = 100000$ is considered for each parameter.

d) *Determination of the output distribution*

The output M_z is generated according to equation (5.28) using the samples for the parameters α_z , C_{Mz} , C_z , D_z , E_z , S_{hz} and S_{vz} . The mean value of M_z is 1.55kNm and its 95% confidence interval is [0.204kNm; 2.56kNm], this interval indicates an uncertainty of 2.356kNm, which is equivalent to 152% of the mean value of M_z .

e) *Calculation of the sensitivity indices*

Assume the expression of the self-aligning moment M_z as described by equation

(5.28). Two samples of the same size $N = 100000$ are considered for each parameter. The estimated mean value of M_z is $\hat{E}(M_z) = 1.55\text{kNm}$ (equation (5.13)) and its estimated variance is $\hat{V}(M_z) = 3.7284 \times 10^5$ (equation (5.14)). The first order and the total indices are plotted in figure 5.9 and their corresponding values are given in table 5.4.

First order indices	Total indices
$S_{\alpha_z} = 0.3$	$S_{T\alpha_z} = 0.42$
$S_{D_z} = 0.53$	$S_{TD_z} = 0.621$
$S_{C_{M_z}} = 0.005$	$S_{TC_{M_z}} = 0.0386$
$S_{E_z} \simeq 0.0033$	$S_{TE_z} = 0.0045$
$S_{C_z} \simeq 0.030$	$S_{TC_z} = 0.043$
$S_{S_{vz}} \simeq 0$	$S_{TS_{vz}} = 0$
$S_{S_{hz}} \simeq 0$	$S_{TS_{hz}} \simeq 0$

Table 5.4: Values of the sensitivity indices - Magic Formula self-aligning moment model M_z

The analysis shows that the parameter α_z is not the most influent, contrary to the case of the lateral force model. Indeed, the parameter D_z has the highest sensitivity index ($S_{D_z} = 0.53$). Then follows the parameter α_z ($S_{\alpha_z} = 0.3$). Parameter C_z has the third highest sensitivity index ($S_{C_z} = 0.03$), but this value is relatively low. The sum of the first order sensitivity indices is 0.8677. This value is relatively higher and close to 1. Similar to the case of the lateral force, the influence due to the interactions between the parameters may be considered negligible.

5.3. Application of sensitivity analysis on tyre models

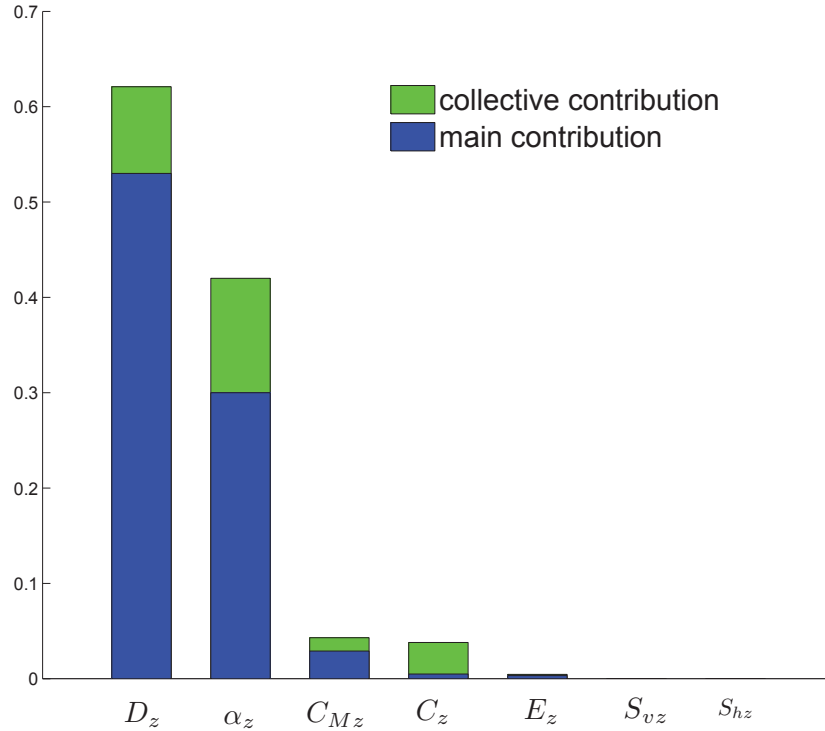


Figure 5.9: Sensitivity indices for the Magic Formula self-aligning moment model M_z

Remark

In this analysis, the same function form is used for representing both the lateral force and the self-aligning moment in the Magic Formula model. Indeed, the main difference between them is the variation limits of the parameters. The analysis has shown that the variation limits of the parameters are determinant for their influence on the model output. In fact, in the lateral force model, it is shown that three parameters have significant influence on the model output and the side slip angle α_y has the highest sensitivity index. However, in the case of the self-aligning moment, only two parameters have significant influence on the model output and the side slip angle α_z has the second highest sensitivity index. A good knowledge of the parameters variation limits is therefore necessary for performing a reliable sensitivity analysis.

5.4 Conclusion

A methodology for sensitivity analysis on a model has been presented. Then, variance-based global sensitivity analysis has been performed on two models, Fiala and Magic Formula models. This sensitivity analysis consists in quantifying the contribution of each parameter to the total variance of the model output.

In the Fiala model, the lateral force and the self-aligning moment depend on three parameters, the side slip angle, the friction coefficient and the cornering stiffness. It has been shown that, when considering each parameter alone, only the side slip angle and the cornering stiffness have significant influence on the lateral force. However, the interaction between the three parameters also have an important influence on the model response. Therefore, improving the accuracy of these three parameters would help to reduce the uncertainty of the lateral force and the self-aligning moment models.

In the case of Magic Formula model, the lateral force and the self-aligning moment expression depend on seven parameters. It has been shown that, only three of them, the side slip angle, the friction coefficient and the cornering stiffness, influence the lateral force model response significantly. Then, these parameters are to be estimated with more precision. In the self-aligning moment, only two parameters, the side slip angle and the peak value, have significant influence.

Moreover, it has been underlined that a good knowledge of the parameters variation limits of each model is necessary for performing a reliable sensitivity analysis.

Besides, the parameters of both models studied are assumed independent. However, tyre models often include correlated parameters. Thus, further investigations on methods of sensitivity analysis for models with correlated parameters may be necessary. It could also be interesting to compare the results of the proposed method with those obtained by other methods of sensitivity analysis (McKay, FAST, ...) in order to determine the best compromise between convergence of the sensitivity indices and computation time.

Dans les sciences, le chemin est plus important que le but. Les sciences n'ont pas de fin.

Erwin Chargaff

General conclusion

In the numerical simulation of ground vehicle, the tyre model plays a crucial role. For that reason, it is necessary to consider a representative tyre model. However, experience has shown that it is difficult to realistically represent the tyre dynamics from a physical point of view. In collaboration with Messier-Dowty company, this thesis has contributed to better understand the actual literature studies in the field of aircraft tyre-road interaction modelling and therefore, to help making an optimal choice of model for a specific application. To complete this study, a survey of the literature tyre models has been proposed first. The models are presented according to the main categories usually adopted for developing tyre models, physical, semi-physical and empirical.

Due to the tyre structure complexity, physical tyre models are more often developed under considerable simplification. The validity range as well as the representativeness of these models may present some limitations. The attempts of certain approaches to be more exhaustive in the tyre representation often lead to extensive and complex models, which involve an important number of the tyre physical and mechanical properties. The main drawback of these complex physical models is that several of the tyre mechanical parameters depend on the tyre dynamics and are not directly measurable. In the case of semi-empirical (or empirical) models, representative models not only are complex but also involve several empirical parameters without physical meaning. In each category of models, it can be underlined that choosing a suitable model for a particular application mainly depends on the possibility to obtain the required measurements data for estimating the model parameters.

Based on the objectives of the thesis, an a priori choice of physical models has been investigated and the validity range as well as the limitations of each model have been underlined. Indeed, the attempt to represent measurements data recorded at the particular case of pure lateral slip has shown significant dispersion. Some further improvement of these models is proposed but, because of the limited available measurements data in the context of this thesis, this improvement has not been exhaustive. The investigation of advanced physical models cannot be also considered because of the limited data. The

semi-empirical tyre model Magic Formula has shown better representation of the tyre characteristics at pure lateral slip. Despite the use of several empirical parameters in Magic Formula model, it allows the derivation and the interpretation of some physical tyre features such as the friction coefficient, the tyre slip stiffnesses. Nevertheless, some limitations are underlined:

- the assumption of zero longitudinal force at pure lateral slip was found to be non representative in the case of the measurements data used in this study
- the model proposes an interpolation function and therefore does not allow an exhaustive description of the tyre forces and moments generation.

To overcome these limitations, simple but comprehensive physical approach was adopted and a description of the longitudinal force generation at pure lateral slip is proposed. Then, by taking this force into consideration, an exhaustive description of the self-aligning moment generation is presented. It is shown that this longitudinal force at pure lateral slip significantly contributes to the generation of self-aligning moment at relative high lateral slip. Finally, an extension of Magic Formula is proposed in order to take into account the longitudinal force at pure lateral slip.

Besides, the different models involve parameters which have to be estimated from measurements data. However, all the parameters do not influence the model response in the same manner. It may be interesting to determine parameters with significant influence on the model response, and which should be estimated with more precision. For this sake, a methodology for carrying out sensitivity analysis on a model is presented and applied on the basic Magic Formula model and on the Fiala model.

In this thesis, it is shown that the Magic Formula model is applicable for representing the tyre response at pure lateral slip in steady-state condition. However, if measurements data are available, the next steps to investigate will be:

- *Influence of the forward velocity on the tyre response*

The majority of the tyre models are developed for rolling tyre and they are valid for rolling velocity beyond a certain limit. In fact, when the tyre is steered at very low or zero velocity, experiments have shown that the tyre response is significantly different and cannot be represented by the same approach as in relative high velocity. Such conditions, denoted parking manoeuvre, are commonly observed during taxiing and towing. Therefore, it is necessary to investigate the effect of the forward speed

on the pure lateral slip in order to complete the validation study of Magic Formula model.

- *Pure driving/braking condition*

Pure driving or braking is often denoted pure longitudinal slip. It allows to characterise the driving or braking capabilities of the tyre in a given operating condition (vertical load, inflation pressure, speed, etc). The driving or braking capabilities are also a part of the fundamental functions of an aircraft. Indeed, during acceleration to take off, the aircraft should reach a target speed within a short distance (for military aircraft, the acceleration may reach 9 times the gravitational acceleration G). The tyre is then submitted to important variation of longitudinal slip as well as forward speed. In the other hand, the aircraft should stop within a relative short distance after landing at considerable high speed. This implies an application of important braking torque on the wheels. Like in the case of pure lateral slip, reliable tyre longitudinal characteristics data at different forward speeds are necessary to exhaustively study the validity of the Magic Formula model. Moreover, in reality, the tyre vertical load may be considered to decrease progressively during acceleration to take-off. It might be an interest to investigate this aspect during longitudinal tyre experiments.

- *Combined cornering and driving/braking condition*

Magic Formula model proposes the combined slip tyre characteristics as function of the ones in pure longitudinal and pure lateral slip condition. Though, this approach has been successfully applicable on most ground vehicles tyres, the literature does not show such validation study for aircraft tyres.

Besides, if the knowledge of the tyre behaviour in steady-state conditions is necessary, the interest for its transient-dynamic behaviour should be at least the same. In fact, various studies have shown that the tyre dynamics plays an important role in the non-controlled oscillations of the landing gear, commonly called shimmy. Moreover, because the tyre transient-dynamic behaviour is more complex than the steady-state one, reliable tyre data as well as further development of advanced model are necessary in order to accurately model the shimmy phenomenon.

APPENDIX A

Coordinate systems

Figures A.1 and A.2 show the common coordinate systems used in the literature [61].

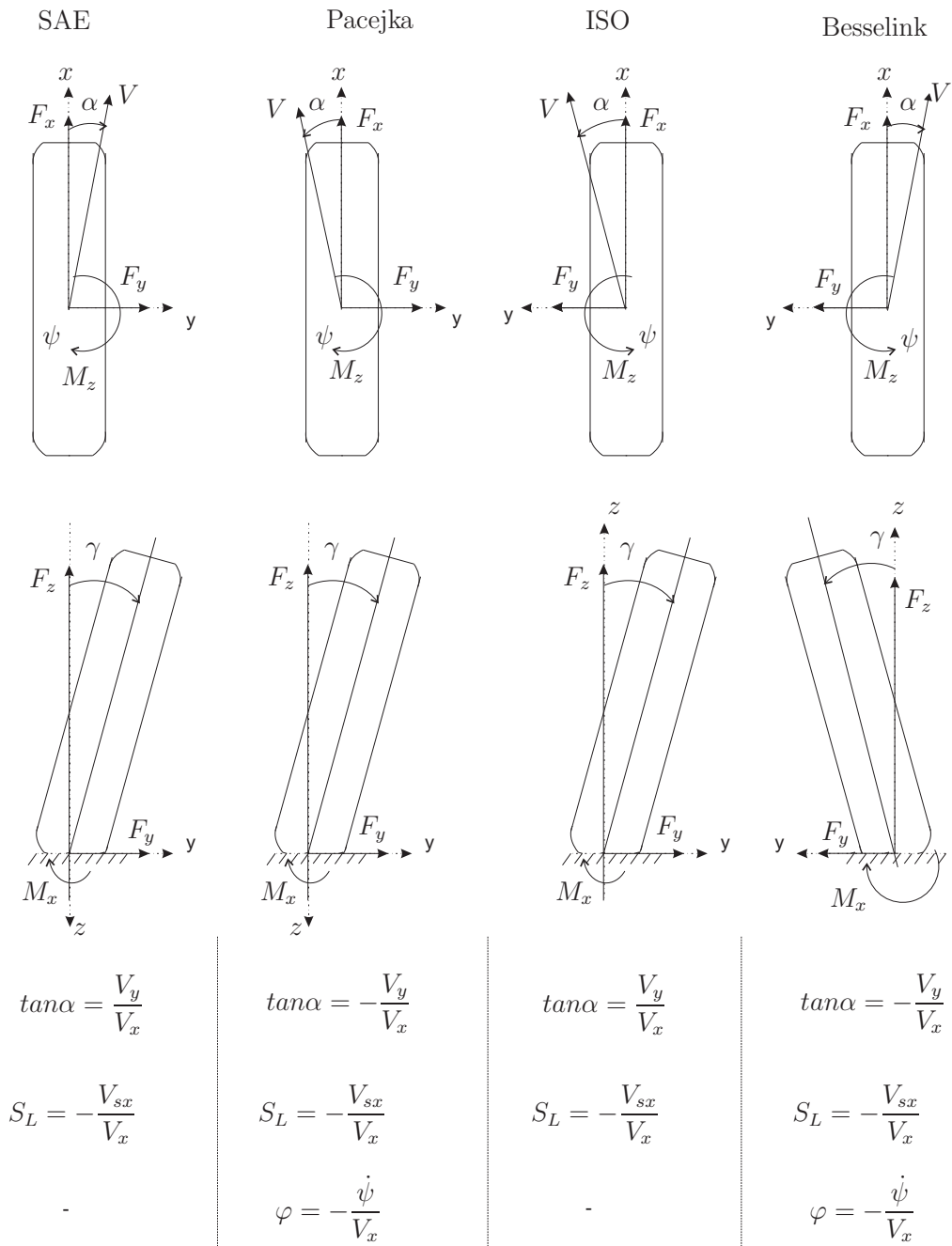


Figure A.1: Literature coordinate systems and sign conventions

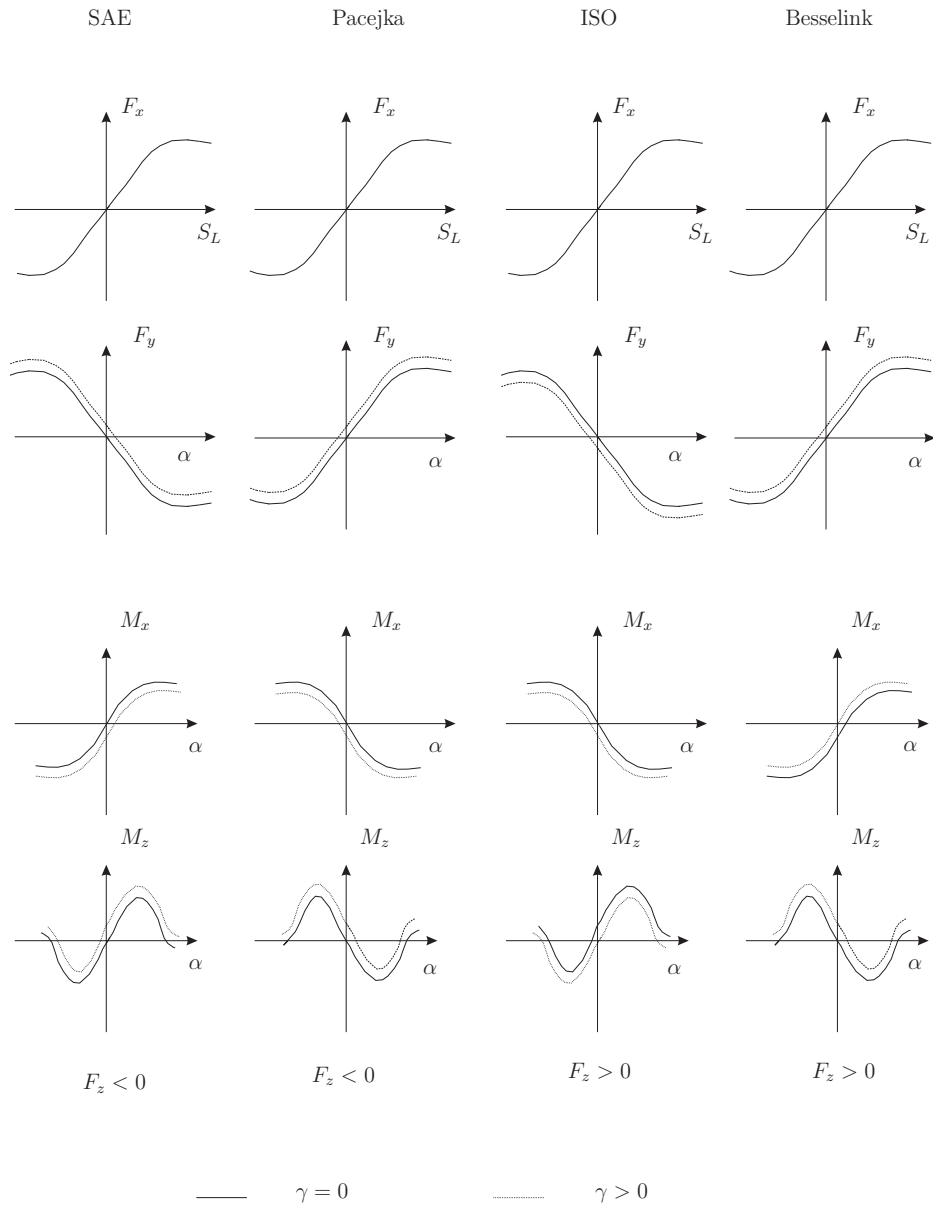


Figure A.2: Forces - moments sign conventions

APPENDIX B

Equations

In this section, the expressions for forces and moments, corresponding to some physical models described in chapter 1, are presented.

B.1 Physical Models

B.1.1 Brush Model (section 1.4.1)

The pure lateral slip force is derived as follows:

$$\begin{aligned} F_y &= -3\mu F_z \theta_y S_\alpha [1 - |\theta_y S_\alpha| + \frac{1}{3}(\theta_y S_\alpha)^2] & \text{if } |\alpha| \leq \alpha^* \\ F_y &= -\mu F_z \operatorname{sgn}(\alpha) & \text{if } |\alpha| > \alpha^* \text{ but } (< \frac{\pi}{2}) \end{aligned} \quad (\text{B.1})$$

The self-aligning moment is given by:

$$\begin{aligned} M_z &= \mu F_z a \theta_y S_\alpha [1 - 3|\theta_y S_\alpha| + 3(\theta_y S_\alpha)^2 - |\theta_y S_\alpha|^3] & \text{if } |\alpha| \leq \alpha^* \\ M_z &= 0 & \text{if } |\alpha| > \alpha^* \text{ but } (< \frac{\pi}{2}) \end{aligned}$$

where $\tan \alpha^* = \frac{1}{\theta_y}$ and $\theta_y = \frac{2k_y a^2}{3\mu F_z}$.

The pure longitudinal slip force is:

$$\begin{aligned} F_x &= C_S S_L & \text{if } |S_L| \leq S_L^* \\ F_x &= \operatorname{sgn}(S_L) \left\{ \mu F_z - \frac{(\mu F_z)^2}{4|S_L|C_S} \right\} & \text{if } |S_L| > S_L^* \end{aligned} \quad (\text{B.2})$$

where S_L^* is the longitudinal slip ratio at which full sliding occurs: $S_L^* = \frac{\mu F_z}{2C_S}$.

In combined slip condition, the resultant force F is developed under some simplifications such as:

- equal longitudinal and lateral tread stiffness: $k = k_y = k_x$
- isotropic friction coefficients: $\mu = \mu_x = \mu_y$
- isotropic model parameter $\theta = \theta_x = \theta_y = \frac{2ka^2}{3\mu F_z}$

$$\begin{aligned}
 |F| &= \mu F_z [3\theta S - 3(\theta S)^2 + (\theta S)^3] \quad \text{if } S \leq S^* \quad \text{with } S^* = \frac{1}{\theta} \\
 |F| &= \mu F_z \quad \text{if } S \geq S^* \\
 S &= \sqrt{S_L^2 + S_\alpha^2}
 \end{aligned} \tag{B.3}$$

B.1.2 Fiala model (section 1.4.2)

Fiala model expressions for forces and moments are developed for pure slip conditions.

- Expression of the pure longitudinal force F_x

$$\begin{aligned}
 F_x &= C_S S_L \quad \text{if } |S_L| \leq S_L^* \\
 F_x &= \text{sgn}(S_L) \left\{ \mu F_z - \frac{(\mu F_z)^2}{4|S_L|C_S} \right\} \quad \text{if } |S_L| > S_L^*
 \end{aligned} \tag{B.4}$$

- Expression of the pure lateral force F_y

$$\begin{aligned}
 F_y &= -\mu |F_z| (1 - H^3) \text{sgn}(\alpha) \quad \text{if } |\alpha| \leq \alpha^* \\
 F_y &= -\mu |F_z| \text{sgn}(\alpha) \quad \text{if } |\alpha| > \alpha^*
 \end{aligned} \tag{B.5}$$

- Expression of the self-aligning moment M_z

$$\begin{aligned}
 M_z &= 2\mu |F_z| R_2 (1 - H) H^3 \text{sgn}(\alpha) \quad \text{if } |\alpha| \leq \alpha^* \\
 M_z &= 0 \quad \text{if } |\alpha| > \alpha^*
 \end{aligned} \tag{B.6}$$

R_2 is the tyre carcass radius.

- Expression of the rolling resistance moment M_y

$$\begin{aligned} M_y &= -C_r F_z && \text{tyre in forward motion} \\ M_y &= C_r F_z && \text{tyre in backward motion} \end{aligned} \quad (\text{B.7})$$

The parameter H is given by:

$$H = 1 - \frac{C_\alpha |\tan \alpha|}{3\mu F_z} \quad (\text{B.8})$$

The critical limit of the longitudinal slip parameter is expressed as follows:

$$S_L^* = \frac{\mu F_z}{2C_s}$$

The critical limit of the slip angle is given by:

$$\alpha^* = \arctan|3\mu F_z / C_\alpha| \quad (\text{B.9})$$

B.1.3 HSRI-NBS-I model (section 1.4.4)

The longitudinal force in combined slip condition is expressed as follows:

$$F_x = \begin{cases} C_S \frac{S_L}{1 - S_L} & \xi_a = 2a \quad (\text{full adhesion}) \\ C_S \frac{S_L}{1 - S_L} \frac{\xi_a}{2a} \left(2 - \frac{\xi_a}{2a}\right) & \xi_a < 2a \\ C_S \mu F_z [C_S^2 + (S_\alpha C_\alpha)^2]^{-\frac{1}{2}} & \xi_a = 0 \quad (\text{full sliding}) \end{cases} \quad (\text{B.10})$$

The expression for the lateral force in combined slip condition is derived as shown below:

$$F_y = \begin{cases} -C_\alpha \frac{S_\alpha}{1 - S_L} & \xi_a = 2a \quad (\text{full adhesion}) \\ -C_\alpha \frac{S_\alpha}{1 - S_L} \frac{\xi_a}{2a} \left(2 - \frac{\xi_a}{2a}\right) & \xi_a < 2a \\ -C_\alpha S_\alpha \mu F_z [C_S^2 + (S_\alpha C_\alpha)^2]^{-\frac{1}{2}} & \xi_a = 0 \quad (\text{full sliding}) \end{cases} \quad (\text{B.11})$$

with $\frac{\xi_a}{2a} = \frac{1}{2} \mu F_z (1 - S_L) [(S_L C_S)^2 + (S_\alpha C_\alpha)^2]^{-0.5}$

B.1.4 HSRI-NBS-III Model (section 1.4.4)

The complete expressions for forces and moment are described below.

- Forces expressions in the adhesion zone

$$\begin{aligned}
 F_{xa} &= C_S \frac{S_L}{1 - S_L} \left(\frac{\xi_a}{2a} \right)^2 \\
 F_{ya} &= -C_\alpha \frac{S_\alpha}{1 - S_L} \left(\frac{\xi_a}{2a} \right)^2
 \end{aligned} \tag{B.12}$$

- Forces expressions in the transition zone

$$\begin{aligned}
 F_{xt} &= \left[\frac{1}{3} C_S \frac{S_L}{1 - S_L} \left(3 - \frac{\xi_a}{a} - \frac{\xi_s}{2a} \right) \frac{\xi_a}{2a} / \left(1 - \frac{\xi_a}{2a} \right) + \mu F_z \frac{S_L}{\sqrt{S_L^2 + S_\alpha^2}} \left(3 - \frac{\xi_s}{a} - \frac{\xi_a}{2a} \right) \frac{\xi_s}{2a} \right] \left(\frac{\xi_s}{2a} - \frac{\xi_a}{2a} \right) \\
 F_{yt} &= - \left[\frac{1}{3} C_\alpha \frac{S_\alpha}{1 - S_L} \left(3 - \frac{\xi_a}{a} - \frac{\xi_s}{2a} \right) \frac{\xi_a}{2a} / \left(1 - \frac{\xi_a}{2a} \right) + \mu F_z \frac{S_\alpha}{\sqrt{S_L^2 + S_\alpha^2}} \left(3 - \frac{\xi_s}{a} - \frac{\xi_a}{2a} \right) \frac{\xi_s}{2a} \right] \left(\frac{\xi_s}{2a} - \frac{\xi_a}{2a} \right)
 \end{aligned}$$

- Forces expressions in the sliding zone

$$\begin{aligned}
 F_{xs} &= \mu F_z \frac{S_L}{\sqrt{S_L^2 + S_\alpha^2}} \left[1 - 3 \left(\frac{\xi_s}{2a} \right)^2 + 2 \left(\frac{\xi_s}{2a} \right)^3 \right] \\
 F_{ys} &= -\mu F_z \frac{S_\alpha}{\sqrt{S_L^2 + S_\alpha^2}} \left[1 - 3 \left(\frac{\xi_s}{2a} \right)^2 + 2 \left(\frac{\xi_s}{2a} \right)^3 \right]
 \end{aligned} \tag{B.13}$$

- Self-aligning moment expression in the adhesion zone

$$M_{za} = \frac{2a}{3} \left[2(C_S - C_\alpha) \frac{S_L}{1 - S_L} \frac{\xi_a}{2a} - \frac{1}{2} C_\alpha \left(2 \frac{\xi_a}{a} - 3 \right) \right] \frac{S_\alpha}{1 - S_L} \left(\frac{\xi_a}{2a} \right)^2 \tag{B.14}$$

- Self-aligning moment expression in the transition zone

$$\begin{aligned}
M_{zt} = & 2aS_\alpha \left[(C_S - C_\alpha) \left\{ \frac{S_L}{(1 - S_L)^2} \left(\frac{\xi_a}{2a}\right)^2 \frac{1}{15} \left[6\left(\frac{\xi_a}{2a}\right)^2 + 3\frac{\xi_a\xi_s}{4a^2} \right. \right. \right. \\
& + \left. \left. \left(\frac{\xi_s}{2a}\right)^2 - 15\frac{\xi_s}{2a} - 5\frac{\xi_s}{2a} + 10 \right] / \left(1 - \frac{\xi_a}{2a}\right)^2 \right. \right. \\
& + \frac{S_L\mu F_z}{(1 - S_L)\sqrt{S_L^2 + S_\alpha^2}} \left(\frac{1}{C_S} + \frac{1}{C_\alpha} \right) \frac{\xi_a\xi_s}{40a^2} \left[3\left(\frac{\xi_s}{2a}\right)^2 \right. \\
& + \left. \left. 3\left(\frac{\xi_a}{2a}\right)^2 + \frac{\xi_a\xi_s}{a^2} - 5\left(\frac{\xi_a}{a} + \frac{\xi_s}{a}\right) + 10 \right] / \left(1 - \frac{\xi_a}{2a}\right) \right. \\
& + \frac{S_L\mu^2 F_z^2}{(S_L^2 + S_\alpha^2)C_S C_\alpha} \frac{3}{10} \left[6\left(\frac{\xi_s}{2a}\right)^2 + \frac{3\xi_a\xi_s}{4a^2} + \left(\frac{\xi_a}{2a}\right)^2 \right. \\
& \left. \left. - 15\frac{\xi_s}{2a} - 5\frac{\xi_a}{2a} + 10 \right] \right\} \\
& + \frac{C_\alpha}{1 - S_L} \frac{\xi_a}{12a} \left[3 - 3\frac{\xi_a}{2a} \left(2 - \frac{\xi_a}{2a}\right) - \frac{\xi_s}{2a} \left(3 - \frac{\xi_s}{2a}\right) + \frac{\xi_a\xi_s}{2a^2} \right] / \left(1 - \frac{\xi_a}{2a}\right) \\
& + \frac{\mu F_z}{\sqrt{S_L^2 + S_\alpha^2}} \frac{\xi_s}{4a} \left[3 - 3\frac{\xi_s}{2a} \left(2 - \frac{\xi_a}{2a}\right) - \frac{\xi_a}{2a} \left(3 - \frac{\xi_a}{2a}\right) \right. \\
& \left. + \frac{\xi_a\xi_s}{2a^2} \right] \left(\frac{\xi_s}{2a} - \frac{\xi_a}{2a} \right)
\end{aligned} \tag{B.15}$$

- Self-aligning moment expression in the sliding zone

$$\begin{aligned}
M_{zs} = & 2aS_\alpha \left\{ \left(\frac{1}{C_\alpha} - \frac{1}{C_S} \right) \frac{S_L\mu^2 F_z^2}{(S_L^2 + S_\alpha^2)} \frac{3}{5} \left[1 + 3\frac{\xi_s}{2a} + 6\left(\frac{\xi_s}{2a}\right)^2 \right] \left(1 - \frac{\xi_s}{2a}\right)^2 \right. \\
& \left. - \frac{\mu F_z}{\sqrt{S_L^2 + S_\alpha^2}} \left[1 + \frac{\xi_s}{2a} + \left(\frac{\xi_s}{2a}\right)^2 \right] \right\} \left(1 - \frac{\xi_s}{2a}\right)
\end{aligned} \tag{B.16}$$

- Final expressions for the longitudinal and lateral forces

$$\begin{aligned}
F_x &= F_{xa} + F_{xt} + F_{xs} \\
F_y &= F_{ya} + F_{yt} + F_{ys}
\end{aligned}$$

-
- Final expression for the self-aligning moment

$$M_z = M_{za} + M_{zt} + M_{zs}$$

Remark:

F_{xa}, F_{ya}, M_{za} are the contributions of the adhesion zone and exist only if $0 \leq \xi_a \leq 2a$.

F_{xt}, F_{yt}, M_{zt} are the contributions of the transition zone and exist only if $0 \leq \xi_a \leq \xi_s \leq 2a$.

F_{xs}, F_{ys}, M_{zs} are the contributions of the sliding zone and always exist if a parabolic normal pressure distribution is considered in the contact patch. For uniform normal pressure distribution for instance, the sliding zone occurs after a certain limit of the longitudinal slip parameter S_L or/and of the lateral slip parameter S_α .

The length of the adhesion zone ξ_a , figure 1.7 in section 1.4.4, is given by the following expression:

$$\frac{\xi_a}{2a} = 1 - \frac{\sqrt{(S_L C_S)^2 + (S_\alpha C_\alpha)^2}}{3\mu_0 F_z (1 - S_L)} \quad (\text{B.17})$$

The length of the transition zone ξ_s figure 1.7 in section 1.4.4, is given by:

$$\frac{\xi_s}{2a} = 1 - \left(\frac{C_S C_\alpha}{C_S + C_\alpha} \right) \frac{\sqrt{S_L^2 + S_\alpha^2}}{3\mu F_z (1 - S_L)} \quad (\text{B.18})$$

where $\mu = \mu_o(1 - A_s V_s)$ and $V_s = \sqrt{S_L^2 + S_\alpha^2} |V| \cos \alpha$.

B.1.5 Model of Sakai (section 1.4.5)

The expressions for the forces and moment in combined slip condition are derived as shown below.

- Tyre forces and moment before full sliding ($0 < \xi_a < 2a$)

$$F_x = C_S \frac{S_L}{1 - S_L} \left(\frac{\xi_a}{2a}\right)^2 - \mu_x F_z \frac{S_L}{\sqrt{S_L^2 + S_\alpha^2}} \left[1 - 3\left(\frac{\xi_a}{2a}\right)^2 + 2\left(\frac{\xi_a}{2a}\right)^3\right]$$

$$F_y = -(C_\alpha + C_S S_L) \frac{S_\alpha}{1 - S_L} \left(\frac{\xi_a}{2a}\right)^2 - \mu_y F_z \frac{S_\alpha}{\sqrt{S_L^2 + S_\alpha^2}} \left[1 - 3\left(\frac{\xi_a}{2a}\right)^2 + 2\left(\frac{\xi_a}{2a}\right)^3\right]$$

(B.19)

$$M_z = \frac{a}{3} \left[3(C_\alpha + C_S S_L) - 2C_\alpha \frac{\xi_a}{a}\right] \left(\frac{\xi_a}{2a}\right)^2 \frac{S_\alpha}{1 - S_L}$$

$$- a \left[\mu_x S_L \left(1 + 3\frac{\xi_a}{2a}\right) - 3\mu_y \frac{\xi_a}{2a}\right] F_z \frac{S_\alpha}{\sqrt{S_L^2 + S_\alpha^2}} \left(1 - \frac{\xi_a}{2a}\right)^2 \frac{\xi_a}{2a} - \frac{F_x F_y}{C_{cy}}$$

(B.20)

- Full sliding case ($\xi_a = 0$)

$$F_x = \mu_x F_z \frac{S_L}{\sqrt{S_L^2 + S_\alpha^2}}$$

(B.21)

$$F_y = -\mu_y F_z \frac{S_\alpha}{\sqrt{S_L^2 + S_\alpha^2}}$$

$$M_z = \frac{\mu_x \mu_y F_z^2 S_L S_\alpha}{C_{cy} (S_L^2 + S_\alpha^2)}$$

(B.22)

where the length of the adhesion zone ξ_a is expressed as follows:

$$\frac{\xi_a}{2a} = 1 - \frac{\sqrt{(S_L C_S)^2 + (S_\alpha C_\alpha)^2}}{3\mu_0 F_z (1 - S_L)}$$

(B.23)

B.1.6 Model of Ratti (section 1.4.6)

The contributions of the adhesion zone read:

$$F_{xa} = -C_S \frac{S_L}{1 - S_L} v_a^2$$

(B.24)

$$F_{ya} = -C_\alpha \frac{S_\alpha}{1 - S_\alpha} v_a^2$$

The contributions of the sliding zone read:

$$F_{xs} = -\frac{F_z S_L}{\sqrt{\left(\frac{S_L}{\mu_{xs}}\right)^2 + \left(\frac{S_\alpha}{\mu_{ys}}\right)^2}} \int_{v_a}^1 p(v) dv \quad (\text{B.25})$$

$$F_{ys} = -\frac{F_z S_\alpha}{\sqrt{\left(\frac{S_L}{\mu_{xs}}\right)^2 + \left(\frac{S_\alpha}{\mu_{ys}}\right)^2}} \int_{v_a}^1 p(v) dv$$

Total longitudinal and lateral forces:

$$\begin{aligned} F_x &= F_{xa} + F_{xs} \\ F_y &= F_{ya} + F_{ys} \end{aligned} \quad (\text{B.26})$$

where:

- $v = \frac{\xi}{2a}$ dimensionless variable ($0 \leq \xi \leq 2a \Rightarrow 0 \leq v \leq 1$), $v_a = \frac{\xi_a}{2a}$,
- ξ_a adhesion region length same as calculated in Sakai model, equation (2.5),
- $p(v)$ dimensionless normal pressure distribution ($\int_0^1 p(v) dv = 1$),
- μ_{xs}, μ_{ys} anisotropic friction coefficients in the sliding region.

B.1.7 Semi-Empirical models

Magic Formula (section 5.26)

The equations of the 2002 version of Magic Formula model [10] are presented below. For clarity reason it is chosen to only present the shear forces and moment equations of this version at both pure longitudinal and lateral slip conditions. The full set of equations are available in [10] for example. The presented version does not take the inflation pressure dependency into consideration.

At pure longitudinal slip condition, the longitudinal shear force F_x is given by:

$$F_x = D_x \sin[C_x \arctan B_x S_L - E_x (B_x S_L - \arctan B_x S_L)] + S_{Vx} \quad (\text{B.27})$$

where :

$$S_L = \alpha + S_{Hx} \quad (\text{B.28})$$

$$C_x = p_{Cx1} \cdot \lambda_{Cx} , \quad C_x > 0 \quad (\text{B.29})$$

$$D_x = \mu_x \cdot F_z \xi_1 , \quad D_x > 0 \quad (\text{B.30})$$

μ_x is the longitudinal friction coefficient

$$\mu_x = (p_{Dx1} + p_{Dx2} \cdot df_z)(1 - p_{Dx3} \cdot \gamma^2) \lambda_{\mu x} \quad (\text{B.31})$$

$$E_x = (p_{Ex1} + P_{Ex2} \cdot df_z^2)[1 - p_{Ex4} \cdot \text{sign}(S_L)] \lambda_{Ex} \quad \text{where } E_x \leq 1 \quad (\text{B.32})$$

The longitudinal slip stiffness is derived as follows:

$$K_x = \left. \frac{\partial F_x}{\partial S_L} \right|_{S_L=0} :$$

$$K_x = F_z (p_{Kx1} + p_{Kx2} \cdot df_z) \exp(p_{Kx3} \cdot df_z) \lambda_{Kx} \quad (\text{B.33})$$

$$B_x = \frac{K_x}{C_x D_x} \quad (\text{B.34})$$

where K_x is equivalent to the longitudinal slip stiffness C_S , see equation (1.6) in section 1.3.

$$S_{Hx} = (p_{Hx1} + p_{Hx2} \cdot df_z) \lambda_{Hx} \quad (\text{B.35})$$

$$S_{Vx} = (p_{Hx1} + p_{Hx2} \cdot df_z) \lambda_{Vx} \cdot \lambda_{H\mu x} \xi_1 \quad (\text{B.36})$$

At pure lateral slip condition, the lateral shear force F_y is given by:

$$F_y = D_y \sin \left[C_y \arctan B_y \alpha_y - E_y (B_y \alpha_y - \arctan(B_y \alpha_y)) \right] + S_{Vy} \quad (\text{B.37})$$

where :

$$\alpha_y = \alpha + S_H \quad (B.38)$$

$$\gamma_y = \gamma \cdot \lambda_{\gamma y} \quad (\text{corrected camber angle}) \quad (B.39)$$

$$C_y = p_{Cy1} \cdot \lambda_{Cy} \quad (B.40)$$

$$D_y = \mu_y F_z \xi_2 \quad (B.41)$$

μ_y is the lateral friction coefficient

$$\mu_y = (p_{Dy1} + p_{Dy2} \cdot df_z)(1 + p_{Dy3} \cdot \gamma_y^2) \lambda_{\mu y} \quad (B.42)$$

$$E_y = (p_{Ey1} + p_{Ey2} \cdot df_z)[1 - (p_{Ey3} + p_{Ey4} \cdot \gamma_y) \text{sgn}(\alpha_y)] \gamma_{Ey} \quad \text{where } E_y \leq 1 \quad (B.43)$$

The cornering stiffness is derived as shown below:

$$C_\alpha = K_y = \left. \frac{\partial F_y}{\partial s_\alpha} \right|_{s_\alpha=0}$$

$$C_{\alpha 0} = K_{y0} = p_{Ky1} \cdot F_{z0} \sin[2 \arctan(\frac{F_z}{p_{Ky2} F_{z0} \lambda_{Fz0}})] \lambda_{Fz0} \cdot \lambda_{Ky} \quad (B.44)$$

$$C_\alpha = K_y = K_{y0}(1 - p_{Ky3} |\gamma_y|) \xi_3 \quad (B.45)$$

$$B_y = \frac{C_\alpha}{C_y D_y} \quad (B.46)$$

$$S_{Hy} = (p_{Hy1} + p_{Hy2} \cdot df_z) \lambda_{Hy} + p_{Hy3} \cdot \gamma_y \cdot \xi_0 + \xi_4 - 1 \quad (B.47)$$

$$S_{Vy} = F_z \{ (p_{Vy1} + p_{Vy2} \cdot df_z) \lambda_{Vy} + (p_{Vy3} + p_{Vy4} \cdot df_z) \gamma_y \} \lambda_{\mu y} \cdot \xi_4 \quad (B.48)$$

The self-aligning moment M_z at pure lateral slip condition is proposed as follows :

$$M_z = -tF_y + M_{zr} \quad (\text{B.49})$$

where t represents the pneumatic trail and is expressed as shown below:

$$t = D_t \cos[C_t \arctan\{B_t \alpha_t - E_t(B_t \alpha_t - \arctan(B_t \alpha_t))\}] \cos(\alpha) \quad (\text{B.50})$$

$$\alpha_t = \alpha + S_{Ht}$$

The residual self-aligning moment M_{zr} is given by:

$$M_{zr} = D_r \cos[C_r \arctan(B_r \alpha_r)] \cos(\alpha) \quad (\text{B.51})$$

$$\alpha_r = \alpha + S_{Hf} \quad (\text{B.52})$$

$$S_{Hf} = S_{Hy} + S_{Vy}/K_y \quad (\text{B.53})$$

$$\gamma_z = \gamma \cdot \lambda_{\gamma z} \quad (\text{B.54})$$

$$B_t = (q_{Bz1} + q_{Bz2} \cdot df_z + q_{Bz3} \cdot df_z^2)(1 + q_{Bz4} \cdot \gamma_z + q_{Bz5} |\gamma_z|) \lambda_{Ky} / \lambda_{\mu y} \quad (\text{B.55})$$

$$C_t = q_{Cz1} \quad (\text{B.56})$$

$$D_t = F_z (q_{Dz1} + q_{Dz2} \cdot df_z)(1 + q_{Dz3} \cdot \gamma_z + q_{Dz4} \cdot \gamma_z^2) \frac{R_0}{F_{z0}} \lambda_t \xi_5 \quad (\text{B.57})$$

$$E_t = (q_{Ez1} + q_{Ez2} \cdot df_z + q_{Ez3} \cdot df_z^2) \left\{ 1 + (q_{Ez1} + q_{Ez2} \cdot \gamma_z) \left(\frac{2}{\pi} \arctan(B_t C_t \alpha_t) \right) \right\} \quad \text{with } E_t \leq 1 \quad (\text{B.58})$$

$$S_{Ht} = q_{Hz1} + q_{Hz2} \cdot df_z + (q_{Hz3} + q_{Hz4} \cdot df_z) \gamma_z \quad (\text{B.59})$$

$$D_r = F_z[q_{Dz6} + q_{Dz7} \cdot df_z] \gamma_r + (q_{Dz8} + q_{Dz9} \cdot df_z) \gamma_z] R_0 \lambda_{\mu\gamma} + \xi_8 - 1 \quad (\text{B.60})$$
$$df_z = \frac{F_z - F_{z0}}{F_{z0}}$$

APPENDIX C

How to enter data in MF-Tool? (TYDEX file format)

C.1 Introduction to the TYDEX file format

The tyre data exchange format (TYDEX) has been developed and unified by an international tyre working group to make the tyre measurement data exchange easier [35]. The data file may consist up to 12 keywords as shown below:

```
**HEADER  
**COMMENTS  
**CONSTANTS  
**MEASURCHANNELS  
**MEASURDATA  
**MODELDEFINITION  
**MODELPARAMETERS  
**MODELCOEFFICIENTS  
**MODELCHANNELS  
**MODELOUPUTS  
**MODELEND  
**END
```

- Each keyword starts in column 1 with 2 asterisks (**). They may be written in lower, upper or mixed case letters. They must not contain any blank,

-
- Each keyword (except ****MODELEND** and ****END**) is header of a block containing special information on the data,
 - The keyword ****HEADER** and ****END** must appear in every TYDEX file. The other keywords are optional and depends on the case of application.

This appendix focuses on TYDEX file format for use in the parameters identification software MF-Tool. MF-Tool is a parameters identification tool for tyre model Magic Formula and MF-Swift (see chapter 3). This type of TYDEX files contains only measurement data and do not define any model. In general, the required keywords are:

****HEADER**

****COMMENTS**

****CONSTANTS**

****MEASURCHANNELS**

****MEASURDATA**

****MODELPARAMETERS**

****MODELEND**

****END**

These keywords are described below through an example of lateral force and self-aligning moment data of an aircraft tyre. The data are recorded during steady state pure cornering. The example of TYDEX file format presented may be considered as a standard format for all steady state tyre forces and moments parameters identification in MF-Tool. However, for the tyre transient and dynamics data sets, the content of some keywords changes and it is recommended to see MF-tool manual for sample of examples for each case.

****HEADER**

This block contains information to identify the measurement. The content can be written in lower or upper case letters or mixed. Example of ****HEADER** block format:

```
**HEADER
RELEASE    1.3
MEASID     DT61-Ac0-200W-p17.tdx
SUPPLIER   TNO Automotive
DATE       27-Jun-2007
CLCKTIME   13:57
```

The content is not fix and one may include more information as needed.

****COMMENTS**

This block contains information that cannot be put into other blocks or which is additional user information. During post processing, these information can be read and printed. But if the line is preceded by '!' it will be ignored during post processing. Example of ****COMMENT** block format:

```
**COMMENTS
Copyright 2007 TNO
For more product information:
TNO Automotive, Integrated Safety
P.O.Box 756, 5700 AT Helmond, The Netherlands
Phone: +31 (0)40 265 2600
Fax: +31 (0)40 265 2601
E-mail: delft tyre@tno.nl
URL: http://www.delft-tyre.com
```

****CONSTANTS**

This block contains measured data, model data and characters information which are constant for whole measurement or model given in the file. In general, all information about tyre, rim and test conditions are mentioned in this block. The number of constant are unlimited. Their names are fixed and associated with definite meanings for use in the post processing. The unit of each constant is mentioned and can be easily changed by specifying it. Example of ****CONSTANTS** block format:

****CONSTANTS**

NOMWIDTH	Nominal section width of tyre	m	0.455
ASPRATIO	Nominal aspect ratio	%	71.6
RIMDIAME	Nominal rim diameter	m	0.5588
RIMWIDTH	Rim width	m	0.3493
MANUFACT	Manufacturer	Delft Tyre	
IDENTITY	Identity	1270x455R22	
INFLPRES	Infl. pres (tyre at amb.temp)	bar	14
TRCKSURF	Surface of track		Asphalt
TRCKCOND	Track condition		Dry
TRAJVELW	Trajectory velocity	m/s	8
FZW	Nominal wheel load	N	68280
LONGSLIP	Longitudinal slip	-	0.0000
INCLANGL	Nominal camber angle	rad	0.0000

****MEASURCHANNELS**

This block contains only measured data (e.g. time dependent data). This block gives the channel text, the unit and if necessary, the factors for conversion into physical units. Only parameters with numerical values are allowed. Parameters number is not limited and their names are fixed and associated with definite meanings for use in the post processing. Example of ****MEASURCHANNELS** block format:

****MEASURCHANNELS**

MEASNUMB	Measurement Point No.	-	1	0	0
SLIPANGL	Slip angle (Alpha)	rad	1	0	0
INCLANGL	Camber angle (Gamma)	rad	1	0	0
LONGSLIP	Longitudinal slip (Kappa)	-	1	0	0
FX	Longitudinal force (F_x)	N	1	0	0
FYW	Side force (F_y)	N	1	0	0
FZW	Wheel load (F_z)	N	1	0	0
MZW	Self aligning torque (M_z)	Nm	1	0	0

The fifth column contains factor to convert each corresponding parameters into physical unit. Let's call this factor a. The sixth column contains offset to shift measurement values. Let's call this factor b. The seventh column contains offset to shift physical values. Let's call this factor c. Finally, the following expression is used:

$$d_{physical} = a(d_{measured} + b) + c$$

$d_{measured}$ is the measured value,

$d_{physical}$ is the physical value.

****MEASURDATA n**

This block contains all measured data sample by sample. The measured data are given in the same order as mentioned in the ****MEASURCHANNELS**. The number of values per line, n, corresponds to the number of channels in ****MEASURCHANNELS**. Every new measurement sample starts in a new line. The number n can be omitted if all values of the same sample can be put into one line. The format of the values can be integer or real and all values have to be separated by at least one blank. Example of ****MEASURDATA** format:

```

**MEASURDATA
1.0000e+000      0      0 0 0 0      6.8280e+004  0
2.0000e+000      3.4907e-002  0 0 0 -5.1000e+002  6.8280e+004  0
3.0000e+000      1.0472e-001  0 0 0 -3.4700e+003  6.8280e+004  0
4.0000e+000      1.7453e-001  0 0 0 -6.9700e+003  6.8280e+004  0
5.0000e+000      2.6180e-001  0 0 0 -1.0880e+004  6.8280e+004  0
6.0000e+000      3.4907e-001  0 0 0 -1.4200e+004  6.8280e+004  0
7.0000e+000      5.2360e-001  0 0 0 -1.9410e+004  6.8280e+004  0
8.0000e+000      6.9813e-001  0 0 0 -2.3840e+004  6.8280e+004  0

```

****MODELPARAMETERS**

This block contains the list of parameters which describe the tyre characteristics. Each line is formatted and contains one single parameter. Example of ****MODELPARAMETERS** format:

```

**MODELPARAMETERS
RFREE           Unloaded radius           m    0.635
FZ_NOM         Nominal vertical load       N    243760
NOMPRES        Nominal inflation pressure  bar  16

```

C.2 Example of TYDEX file for use in MF-Tool

The example of TYDEX file provided in this section has been used in this work (see the modelling results of Magic Formula presented in chapter 3). It contains data recorded from pure cornering test on an aircraft tyre and concerns the lateral force and the self-aligning moment. This example can be used as a standard format for all tyre forces and moments parameters identification in MF-Tool.

Just copy the example below (from ****HEADER** block to ****END** block) into a text file, then modify each block by entering the right information concerning the new tyre characteristics and measured data. Finally, save the text file which is ready for Magic Formula (MF) or MF-Swift parameters identification in MF-Tool.

```
**HEADER
RELEASE      1.3
MEASID       DT61-Ac0-200W-p17.tdx
SUPPLIER     TNO Automotive
DATE         27-Jun-2007
CLCKTIME     13:57

**COMMENTS
Copyright 2007 TNO
For more product information:
TNO Automotive, Integrated Safety
P.O.Box 756, 5700 AT Helmond, The Netherlands
Phone: +31 (0)40 265 2600
Fax: +31 (0)40 265 2601
E-mail: delft tyre@tno.nl
URL: http://www.delft-tyre.com
```

**CONSTANTS

NOMWIDTH	Nominal section width of tyre	m	0.455
ASPRATIO	Nominal aspect ratio	%	71.6
RIMDIAME	Nominal rim diameter	m	0.5588
RIMWIDTH	Rim width	m	0.3493
MANUFACT	Manufacturer	Delft Tyre	
IDENTITY	Identity	1270x455R22	
INFLPRES	Infl. pres (tyre at amb.temp)	bar	14
TRCKSURF	Surface of track	Asphalt	
TRCKCOND	Track condition	Dry	
TRAJVELW	Trajectory velocity	m/s	8
FZW	Nominal wheel load	N	68280
LONGSLIP	Longitudinal slip	-	0.0000
INCLANGL	Nominal camber angle	rad	0.0000

**MEASURCHANNELS

MEASNUMB	Measurement Point No.	-	1	0	0
SLIPANGL	Slip angle (Alpha)	rad	1	0	0
INCLANGL	Camber angle (Gamma)	rad	1	0	0
LONGSLIP	Longitudinal slip (Kappa)	-	1	0	0
FX	Longitudinal force (F_x)	N	1	0	0
FYW	Side force (F_y)	N	1	0	0
FZW	Wheel load (F_z)	N	1	0	0
MZW	Self aligning torque (M_z)	Nm	1	0	0

**MEASURDATA

1.0000e+000	0	0	0	0	0	6.8280e+004	0
2.0000e+000	3.4907e-002	0	0	0	-5.1000e+002	6.8280e+004	0
3.0000e+000	1.0472e-001	0	0	0	-3.4700e+003	6.8280e+004	0
4.0000e+000	1.7453e-001	0	0	0	-6.9700e+003	6.8280e+004	0
5.0000e+000	2.6180e-001	0	0	0	-1.0880e+004	6.8280e+004	0
6.0000e+000	3.4907e-001	0	0	0	-1.4200e+004	6.8280e+004	0
7.0000e+000	5.2360e-001	0	0	0	-1.9410e+004	6.8280e+004	0
8.0000e+000	6.9813e-001	0	0	0	-2.3840e+004	6.8280e+004	0

****MODELPARAMETERS**

RFREE	Unloaded radius	m	0.635
FZ_NOM	Nominal vertical load	N	243760
NOMPRES	Nominal inflation pressure	bar	16

****MODELEND**

****END**

After completing the estimation of the model parameters, MF-Tool allows to export a file called 'tyre property file', which will be used in the simulation environment (software). An example of the tyre property file is presented in the next appendix.

APPENDIX D

Example of a tyre property file

This appendix shows an example of a tyre property file obtained after estimating the parameters of the Magic Formula model (version 2002) with MF-Tool. It corresponds to the tyre property file at inflation pressure 14 bars used for the application in chapter 3. It mainly contains the general information on the tyre (MDI_HEADER), then the USE_MODE which specifies the type of calculation performed, the tyre run type condition (pure or combined slip), the units of the different quantities used and the values of the Magic Formula parameters. Notice that only the values of the parameters that correspond to the pure lateral force are true. The others are default values associated to the parameters during the fitting process with MF-Tool.

```
[MDI_HEADER]
FILE_TYPE           ='tir'
FILE_VERSION        =3.0
FILE_FORMAT         ='ASCII'
! : FILE_NAME :      C: pneu1-03ms.tir
! : TIRE_VERSION :   MF-Tyre 5.2
! : MF-TOOL TEMPLATE : acar12_mftyre52
! : COMMENT :        Tire                1270x455R22
! : COMMENT :        Manufacturer         Delft Tyre
! : COMMENT :        Nom. section width (m) 0.455
! : COMMENT :        Nom. aspect ratio (-) 0.71
! : COMMENT :        Infl. pressure (Pa)   1400000
! : COMMENT :        Rim radius (m)        0.2794
! : COMMENT :        Measurement ID
! : COMMENT :        Test speed (m/s)      8
! : COMMENT :        Road surface         Asphalt
```

```

! : COMMENT :      Road condition      Dry
! : FILE_FORMAT :  ASCII
! : DATESTAMP :    15 octob. 2010, 07:11:15
! : USER :        MF-Tool 6.1
! : Generated by : Administrator1
! : Copyright TNO, 15 octob. 2010, 07:11:15
!
! USE_MODE specifies the type of calculation performed:
! 0:   Fz only, no Magic Formula evaluation
! 1:   Fx,My only
! 2:   Fy,Mx,Mz only
! 3:   Fx,Fy,Mx,My,Mz uncombined force/moment calculation
! 4:   Fx,Fy,Mx,My,Mz combined force/moment calculation
! +10: including relaxation behaviour
! *-1: mirroring of tyre characteristics
! example: USE_MODE = -12 implies:
! -calculation of Fy,Mx,Mz only
! -including relaxation effects
! -mirrored tyre characteristics

$-----units
[UNITS]
LENGTH  ='meter'
FORCE   ='newton'
ANGLE   ='radians'
MASS    ='kg'
TIME    ='second'

$-----model
[MODEL]
PROPERTY_FILE_FORMAT  ='MF-TYRE'
TYPE                  ='CAR'
FITTYP                = 6           $Magic Formula Version number
USE_MODE              = 2           $Tyre use switch (IUSED)
MFSAFE1               = 99
MFSAFE2               = 99
MFSAFE3               = 1

```

VXLOW = 1
 LONGVL = 1 \$Measurement speed

\$-----dimensions
 [DIMENSION]
 UNLOADED_RADIUS = 0.635 \$ Free tyre radius
 WIDTH = 0.455 \$ Nominal section width of the tyre
 ASPECT_RATIO = 0.71 \$ Nominal aspect ratio
 RIM_RADIUS = 0.2794 \$ Nominal rim radius
 RIM_WIDTH = 0.3493 \$ Rim width
 \$-----shape
 [SHAPE]
 radial width
 1.0 0.0
 1.0 0.4
 1.0 0.9
 0.9 1.0

\$-----parameter
 [VERTICAL]
 VERTICAL_STIFFNESS = 2000000 \$Tyre vertical stiffness
 VERTICAL_DAMPING = 500 \$Tyre vertical damping
 BREFF = 8.4 \$Low load stiffness e.r.r.
 DREFF = 0.27 \$Peak value of e.r.r.
 FREFF = 0.07 \$High load stiffness e.r.r.
 FNOMIN = 243760 \$Nominal wheel load
 \$-----long_slip_range
 [LONG_SLIP_RANGE]
 KPUMIN = -1.5 \$Minimum valid wheel slip
 KPUMAX = 1.5 \$Maximum valid wheel slip
 \$-----slip_angle_range
 [SLIP_ANGLE_RANGE]
 ALPMIN = -1.5708 \$Minimum valid slip angle
 ALPMAX = 1.5708 \$Maximum valid slip angle
 \$-----inclination_slip_range
 [INCLINATION_ANGLE_RANGE]
 CAMMIN = 0 \$Minimum valid camber angle
 CAMMAX = 0 \$Maximum valid camber angle
 \$-----vertical_force_range

[VERTICAL_FORCE_RANGE]		
FZMIN	= 2438	\$Minimum allowed wheel load
FZMAX	= 487520	\$Maximum allowed wheel load
\$		scaling
[SCALING_COEFFICIENTS]		
LFZO	= 1	\$Scale factor of nominal (rated) load
LCX	= 1	\$Scale factor of Fx shape factor
LMUX	= 1	\$Scale factor of Fx peak friction coefficient
LEX	= 1	\$Scale factor of Fx curvature factor
LKX	= 1	\$Scale factor of Fx slip stiffness
LHX	= 1	\$Scale factor of Fx horizontal shift
LVX	= 1	\$Scale factor of Fx vertical shift
LGAX	= 1	\$Scale factor of camber for Fx
LCY	= 1	\$Scale factor of Fy shape factor
LMUY	= 1	\$Scale factor of Fy peak friction coefficient
LEY	= 1	\$Scale factor of Fy curvature factor
LKY	= 1	\$Scale factor of Fy cornering stiffness
LHY	= 1	\$Scale factor of Fy horizontal shift
LVY	= 1	\$Scale factor of Fy vertical shift
LGAY	= 1	\$Scale factor of camber for Fy
LTR	= 1	\$Scale factor of Peak of pneumatic trail
LRES	= 1	\$Scale factor for offset of residual torque
LGAZ	= 1	\$Scale factor of camber for Mz
LXAL	= 1	\$Scale factor of alpha influence on Fx
LYKA	= 1	\$Scale factor of alpha influence on Fx
LVYKA	= 1	\$Scale factor of kappa induced Fy
LS	= 1	\$Scale factor of Moment arm of Fx
LSGKP	= 1	\$Scale factor of Relaxation length of Fx
LSGAL	= 1	\$Scale factor of Relaxation length of Fy
LGYR	= 1	\$Scale factor of gyroscopic torque
LMX	= 1	\$Scale factor of overturning couple
LVMX	= 1	\$Scale factor of Mx vertical shift
LMY	= 1	\$Scale factor of rolling resistance torque
\$		longitudinal

[LONGITUDINAL_COEFFICIENTS]		
PCX1	= 1.65	\$Shape factor Cfx for longitudinal force
PDX1	= 1	\$Longitudinal friction Mux at Fznom
PDX2	= 0	\$Variation of friction Mux with load
PDX3	= 0	\$Variation of friction Mux with camber
PEX1	= 0	\$Longitudinal curvature Efx at Fznom
PEX2	= 0	\$Variation of curvature Efx with load
PEX3	= 0	\$Variation of curvature Efx with load squared
PEX4	= 0	\$Factor in curvature Efx while driving
PKX1	= 20	\$Longitudinal slip stiffness Kfx/Fz at Fznom
PKX2	= 0	\$Variation of slip stiffness Kfx/Fz with load
PKX3	= 0	\$Exponent in slip stiffness Kfx/Fz with load
PHX1	= 0	\$Horizontal shift Shx at Fznom
PHX2	= 0	\$Variation of shift Shx with load
PVX1	= 0	\$Vertical shift Svz/Fz at Fznom
PVX2	= 0	\$Variation of shift Svz/Fz with load
RBX1	= 10	\$Slope factor for combined slip Fx reduction
RBX2	= 6	\$Variation of slope Fx reduction with kappa
RCX1	= 1	\$Shape factor for combined slip Fx reduction
REX1	= 0	\$Curvature factor of combined Fx
REX2	= 0	\$Curvature factor of combined Fx with load
RHX1	= 0	\$Shift factor for combined slip Fx reduction
PTX1	= 0	\$Relaxation length SigKap0/Fz at Fznom
PTX2	= 0	\$Variation of SigKap0/Fz with load
PTX3	= 0	\$Variation of SigKap0/Fz with exponent of load
\$	-----overturning	
[OVERTURNING_COEFFICIENTS]		
QSX1	= 0	\$Lateral force induced overturning moment
QSX2	= 0	\$Camber induced overturning couple
QSX3	= 0	\$Fy induced overturning couple
\$	-----lateral	

[LATERAL_COEFFICIENTS]

PCY1	= 2	\$Shape factor Cfy for lateral forces
PDY1	= 0.4072	\$Lateral friction Muy
PDY2	= -0.21897	\$Variation of friction Muy with load
PDY3	= 0	\$Variation of friction Muy with squared camber
PEY1	= 0.4536	\$Lateral curvature Efy at Fznom
PEY2	= 0.08415	\$Variation of curvature Efy with load
PEY3	= 0	\$Zero order camber dependency of curvature Efy
PEY4	= 0	\$Variation of curvature Efy with camber
PKY1	= -3.24	\$Maximum value of stiffness Kfy/Fznom
PKY2	= 1.1953	\$Load at which Kfy reaches maximum value
PKY3	= 0	\$Variation of Kfy/Fznom with camber
PHY1	= -0.002228	\$Horizontal shift Shy at Fznom
PHY2	= -0.00463	\$Variation of shift Shy with load
PHY3	= 0	\$Variation of shift Shy with camber
PVY1	= 0	\$Vertical shift in Svy/Fz at Fznom
PVY2	= 0	\$Variation of shift Svy/Fz with load
PVY3	= 0	\$Variation of shift Svy/Fz with camber
PVY4	= 0	\$Variation of shift Svy/Fz with camber and load
RBY1	= 16	\$Slope factor for combined Fy reduction
RBY2	= 0	\$Variation of slope Fy reduction with alpha
RBY3	= 0	\$Shift term for alpha in slope Fy reduction
RCY1	= 1	\$Shape factor for combined Fy reduction
REY1	= 0	\$Curvature factor of combined Fy
REY2	= 0	\$Curvature factor of combined Fy with load
RHY1	= 0	\$Shift factor for combined Fy reduction
RHY2	= 0	\$Shift factor for combined Fy reduction with load
RVY1	= 0	\$Kappa induced side force Svyk/Muy*Fz at Fznom
RVY2	= 0	\$Variation of Svyk/Muy*Fz with load
RVY3	= 0	\$Variation of Svyk/Muy*Fz with camber
RVY4	= 0	\$Variation of Svyk/Muy*Fz with alpha
RVY5	= 1.9	\$Variation of Svyk/Muy*Fz with kappa
RVY6	= 0	\$Variation of Svyk/Muy*Fz with atan(kappa)
PTY1	= 0	\$Peak value of relaxation length SigAlp0/R0
PTY2	= 0	\$Value of Fz/Fznom where SigAlp0 is extreme

\$-----rolling resistance

[ROLLING_COEFFICIENTS]

QSY1 = 0.01 \$Rolling resistance torque coefficient
QSY2 = 0 \$Rolling resistance torque depending on Fx
QSY3 = 0 \$Rolling resistance torque depending on speed
QSY4 = 0 \$Rolling resistance torque depending on *speed*⁴

\$-----aligning

[ALIGNING_COEFFICIENTS]

QBZ1 = 6.578 \$Trail slope factor for trail Bpt at Fznom
QBZ2 = 2.2864 \$Variation of slope Bpt with load
QBZ3 = 1.736 \$Variation of slope Bpt with load squared
QBZ4 = 0 \$Variation of slope Bpt with camber
QBZ5 = 0 \$Variation of slope Bpt with absolute camber
QBZ9 = 0.021653 \$Slope factor Br of residual torque Mzr
QBZ10 = 0 \$Slope factor Br of residual torque Mzr
QCZ1 = 1.2554 \$Shape factor Cpt for pneumatic trail
QDZ1 = 0.16092 \$Peak trail Dpt" = Dpt*(Fz/Fznom*R0)
QDZ2 = -0.13556 \$Variation of peak Dpt" with load
QDZ3 = 0 \$Variation of peak Dpt" with camber
QDZ4 = 0 \$Variation of peak Dpt" with camber squared
QDZ6 = 9.755E-4 \$Peak residual torque Dmr" = Dmr/(Fz*R0)
QDZ7 = 0.006212 \$Variation of peak factor Dmr" with load
QDZ8 = 0 \$Variation of peak factor Dmr" with camber
QDZ9 = 0 \$Variation of peak factor Dmr" with camber and load
QEZ1 = -1.5765 \$Trail curvature Ept at Fznom
QEZ2 = 1.27 \$Variation of curvature Ept with load
QEZ3 = 0 \$Variation of curvature Ept with load squared
QEZ4 = 0 \$Variation of curvature Ept with sign of Alpha-t
QEZ5 = 0 \$Variation of Ept with camber and sign Alpha-t
QHZ1 = -0.013036 \$Trail horizontal shift Sht at Fznom
QHZ2 = -0.026794 \$Variation of shift Sht with load
QHZ3 = 0 \$Variation of shift Sht with camber
QHZ4 = 0 \$Variation of shift Sht with camber and load
SSZ1 = 0 \$Nominal value of s/R0: effect of Fx on Mz
SSZ2 = 0 \$Variation of distance s/R0 with Fy/Fznom

SSZ3	= 0	\$Variation of distance s/R_0 with camber
SSZ4	= 0	\$Variation of distance s/R_0 with load and camber
QTZ1	= 0	\$Gyration torque constant
MBELT	= 50	\$Belt mass of the wheel

Bibliography

- [1] M. Blundell and D. Harty. *Multibody systems approach to vehicle dynamics*. Elsevier, 2004. 2
- [2] Y.P. Chang, M. El-Gindy, and D.A. Streit. Literature survey of transient dynamic response tyre models. *International Journal of Vehicle Design*, 34(4):369–376, 2004. 2
- [3] R. Rajamani. *Vehicle dynamics and control*. Springer Verlag, 2005. ISBN 0387263969. 2, 8, 22, 84, 92
- [4] J. Svendenius. *Tire modeling and friction estimation*. PhD thesis, Department of Automatic Control, Lund University, Sweden, 2007. 2, 18, 20, 23, 29
- [5] H. Sakai. Theoretical and experimental studies on the dynamic cornering properties of tires. *International Journal of Vehicle Design*, 2:1–4, 1981. 2, 8
- [6] H. Sakai. Study on cornering properties of tire and vehicle. *Tire Science and Technology, TSTCA*, 18(3):136–196, 1990. 2, 8
- [7] H.B. Pacejka and R.S. Sharp. Shear force development by pneumatic tyres in steady state conditions: a review of modelling aspects. *Vehicle System Dynamics*, 20:121–176, 1991. 2, 24, 26, 28, 58
- [8] H.T Szostak, R. Wade Allen, and T.J. Rosenthal. An interactive tire model for driver/vehicle simulation. *DOT HS 807271*, 1988. 2, 28, 29
- [9] R. Rimondi and P. Gavardi. A new interpolative model of the mechanical characteristics of the tire as an input to handling models. *FISITA Congress, Torino, Italy, SAE 905246*, 1990. 2, 24, 28
- [10] H. B. Pacejka. *Tyre and Vehicle Dynamics*. Elsevier, 2006. ISBN 0750669187. 2, 15, 25, 26, 27, 34, 54, 58, 59, 76, 77, 84, 92, 105, 107, 114, 121, 129, 152

-
- [11] H.B. Pacejka and E. Bakker. The Magic Formula tyre model. *Proc. of the 1rst International Colloquium on Tyre Models for Vehicle Dynamics Analysis*, pages 1–18, 1991. 2, 25, 58, 59
- [12] G. Gim. *Vehicle dynamics simulation with a comprehensive model for pneumatic tires*. PhD thesis, University of Arizona, 1988. 2
- [13] K. Guo and L. Ren. A unified semi-empirical tire model with higher accuracy and less parameters. *SAE paper N° 1999-01-0785*, pages 1513–1520, 1999. 2, 22
- [14] T. Sim, D. Margolis, and C.J. Belltawn. An analytical tire model for vehicle simulation in normal driving conditions. *SAE paper N° 2000-01-0356*, 2000. 2, 20
- [15] G. Somieski. Shimmy analysis of a simple aircraft nose landing gear model using different mathematical methods. *Aerospace Science and Technology*, 1997. ISSN 1270-9638. 2, 20
- [16] G. Dihua and S. Jin. Modeling of tire cornering properties with experimental modal parameters. *SAE N° 1999-01-0784*, 1999. 2, 26
- [17] H.B Pacejka. Spin: camber and turning. In P. Lugner, editor, *Proceedings of 3rd Colloquium on tyre models for vehicle analysis*, volume Suppl. Vehicle System Dynamics, Vienna, 2005. 7
- [18] J.E. Bernard, L. Segel, and R.E. Wild. Tire shear force generation during combined steering and braking manoeuvres. *SAE 770852*, 1977. 8
- [19] E. Fiala. Lateral forces on rolling pneumatic tires. In *Zeitschrift V.D.I. 96*, volume 29, October 1954. 10, 114
- [20] J. Lacombe. Tire model for simulations of vehicle motion on high and low friction road surfaces. *Proc. of the 2000 Winter Simulation Conference*, 2000. 11
- [21] J. T. Tielking and N. K. Mital. A comparative evaluation of five tire traction models. Technical Report UM-HSRI-PF-74-2, Highway Safety Research Institute, Ann Arbor, Michigan, 1974. Available at <http://deepblue.lib.umich.edu/handle/2027.42/330>. 12, 13, 14, 18, 34, 96
- [22] H. Sakai. Theoretical study of the effect of tractive and braking forces on cornering characteristics of tires. *Safety Research Tour Paper No 4, Stability and Control Committee, Society of Automotive Engineers of Japan*, October 1969. 14

-
- [23] P. Ratti. *Modélisation du pneumatique pour l'étude du comportement routier des véhicules automobiles*. PhD thesis, Ecole Nationale Supérieure des Arts et Métiers de Paris, 1986. 15
- [24] F. Mancuso, R. Sangalli, F. Cheli, and S. Bruni. A new mathematical-physical 2D tire model for handling optimization on a vehicle. *SAE paper No 1999-01-0789*, pages 1540–1547, 1999. 15, 19
- [25] R. F. Smiley and W. B. Horne. Mechanical properties of pneumatic tires with special reference to modern aircraft tires. Technical report, Langley Research Center Langley Field, Va., 1958. 20
- [26] W. F. Milliken and D. L. Milliken. Race car vehicle dynamics. *SAE*, 1995. 22
- [27] E. Bakker, N. Nyborg, and H.B. Pacejka. Tyre modelling for use in vehicle dynamics studies. *SAE 870421*, 1987. 25, 59
- [28] A.J.C. Schmeitz, I.J.M. Besselink, J. De Hoogh, and H. Nijmeijer. Extending the Magic Formula and SWIFT tyre models for inflation pressure changes. *available at: <http://yp.bmt.tue.nl/pdfs/5852.pdf>*, 2008. 25
- [29] H.B. Pacejka. Modelling of the pneumatic tire and its impact on vehicle dynamics behaviour. *CCG Course, Oberpfaffenhfen*, 1989. 26
- [30] W. Hirschberg, G. Rill, and H. Weinfurter. Tire model TMeasy. *Vehicle System Dynamics*, 45:101–119, 2007. 26, 105
- [31] P. Février and G. Fandard. A new thermal and mechanical tire model for handling simulation. *VDI Berichte*, 2014:261 – 276, 2007. 54
- [32] I.J.M. Besselink and A.J.C. Schmeitz. The MF-Swift tyre model: extending the Magic Formula with rigid ring dynamics and an enveloping model. *JSAE review*, 26(2):245–252, 2005. 58
- [33] A.J.C. Schmeitz, I.J.M. Besselink, J. de Hoogh, and H. Nijmeijer. Extending the Magic Formula and SWIFT tyre models for inflation pressure changes. Technical report, TU Eindhoven, Eindhoven, 2005. 59, 68, 71, 78, 107
- [34] K. Levenberg. A method for the solution of certain non-linear problems in least squares. *Quarterly of Applied Mathematics*, 2:164–168, 1944. 63

-
- [35] H.J. Unrau and J. Zamow. TYDEX FORMAT - standard tyre interface. Technical report, 2nd International Colloquium on Tire Models for Vehicle Dynamics Analysis Available in MF-Tool manual, 1997. 63, 157
- [36] P. Van der Jagt. *The road to virtual vehicle prototyping*. Dissertation. TU Eindhoven, 2000. 77
- [37] R. Kiébré, F. Anstett-Collin, and M. Basset. A physical model for induced longitudinal force on tyre during steady state pure cornering. *International Journal of Vehicle Systems Modelling and Testing*, 5, Nos. 2/3:161 – 175, 2010. 83, 84, 86, 92
- [38] R. Kiébré, F. Anstett-Collin, and M. Basset. Better understanding the self-aligning moment generation at pure lateral slip. *Vehicle System Dynamics*, Under review, 2010. 83, 84
- [39] R. Kiébré, F. Anstett-Collin, and M. Basset. Real shear forces and moment generated by tyre during pure lateral slip. In *Proceedings of the 2010 ASME International Mechanical Engineering Congress and Exposition*, November 12 - 18, 2010, Vancouver, Canada. 83, 84
- [40] P.H. Mott, J.R. Dorgan, and C.M. Roland. The bulk modulus and Poisson ratio of " incompressible " materials. *Journal of Sound and Vibration*, 312:572 – 575, 2008. 100
- [41] R. Kiébré, F. Anstett-Collin, and M. Basset. Using the magic formula model for induced longitudinal force at pure lateral slip. *International Journal of Vehicle Design*, Under review, 2010. 106
- [42] R. Kiébré, F. Anstett-Collin, and M. Basset. Analyse de sensibilité pour l'étude des paramètres influents dans les modèles d'interface pneu/sol. In *Proceedings of Sixième Conférence Internationale Francophone d'Automatique, CIFA 2010*, Nancy, France, 02-03 June, 2010. 113, 114, 122
- [43] R. Kiébré, F. Anstett-Collin, and M. Basset. Sensitivity analysis for tire/road interface model. In *Sixth International Conference on Sensitivity Analysis of Model Output*, volume 2, pages 7579 – 7782, Milan, Italy, 19-22 July 2010 2010. Procedia - Social and Behavioral Sciences. Available at <http://www.sciencedirect.com/science/journal/18770428>. 113, 114

-
- [44] R. Kiébré, F. Anstett-Collin, and M. Basset. Sensitivity analysis for studying influential parameters in tyre models. *Interational Journal of Vehicle Systems Modelling and Testing*, Accepted in September 2010. 113, 114
- [45] R.I. Cukier, R.I. Levine, and K.E. Shuler. Nonlinear sensitivity analysis of multi-parameter model systems. *Journal Computational Physics*, 26:1 – 42., 1978. 114, 119
- [46] I.M. Sobol. Sensitivity estimates for nonlinear mathematical models. *Mathematical Modelling and Computational Experiments*, 1:407 – 414, 1993. 114, 118, 119
- [47] A. Saltelli, S. Tarantola, and K. Chan. A quantitative model independent method for global sensitivity analysis of model output. *Technometrics*, 41:39–56, 1999. 114
- [48] A. Saltelli, K. Chan, and E.M. Scott. *Sensitivity Analysis*. John Wiley and Sons, 2000. 114
- [49] H. C. Frey and S. R. Patil. Identification and review of sensitivity analysis methods. *Risk analysis*, 3:553–578, 2002. 114
- [50] A. Saltelli. Sensitivity analysis for importance assessment. *Risk Analysis*, 22, n°3, 2002. 114
- [51] A. Saltelli, S. Tarantola, F. Campolongo, and M. Ratto. *Sensitivity analysis in practice*. John Wiley and Sons, 2004. 114
- [52] J. Jacques. *Contributions à l'analyse de sensibilité et à l'analyse discriminante généralisée*. PhD thesis, Université Joseph Fournier - Grenoble I, 05 décembre 2005. 114, 119
- [53] T. Turanyi and H. Rabitz. *Sensitivity analysis*. 2008. 114
- [54] J. C. Helton and F. J. Davis. Illustration of Sampling-Based methods for uncertainty and sensitivity analysis. *Risk Analysis*, 22(3), 2002. 116
- [55] J. C. Helton, F. J. Davis, and J. D. Johnson. A comparison of uncertainty and sensitivity analysis results obtained with random and Latin hypercube sampling. *Reliability Engineering and System Safety*, 89:305–330, 2005. 116
- [56] J. C. Heltona, J. D. Johnsonb, C. J. Sallaberryc, and C. B. Storlied. Survey of sampling-based methods for uncertainty and sensitivity analysis. *Reliability Engineering and System Safety*, 91:1175 –1209, 2006. 116

-
- [57] G. E. B. Archer, A. Saltelli, and I.M. Sobol. Sensitivity measures, Anova-like techniques and the use of bootstrap. *Journal of Statistical Computation and Simulation*, 58:99–120, 1997. 117, 118
- [58] A. Saltelli, M. Ratto, T. Andres, F. Campolongo, J. Cariboni, D. Gatelli, M. Saisana, and S. Tarantola. *Global sensitivity analysis*. John Wiley and Sons, 2008. 117, 118
- [59] V. Schwieger. Variance-based sensitivity analysis for model evaluation in engineering surveys. In *Proceedings of 3rd International Conference on Engineering Surveying, Bratislava, Slovaquie*, 11-13 novembre 2004. 119
- [60] T. A. Mara and S. Tarantola. Application of global sensitivity analysis of model output to building thermal simulations. *Journal of Building Simulation*, 1:290–302, 2008. 119
- [61] I. J. M. Besselink. *Shimmy of aircraft main landing gears*. PhD thesis, Technology University of Delft, 2000. 141

Summary

In the aeronautics transport domain, the improvement of the security, the reliability and the comfort requires also a reliable control of the aircraft on the ground. Since the tyre is the only contact point of the aircraft with the ground, the tyre properties would play a fundamental role when determining the aircraft dynamic behaviour. Thus advanced and representative tyre model is necessary. However, it may be difficult to realistically model the tyre due to the complexity of its structure (composite of polymers, fibres, steel, etc). Indeed, it is required to consider either extensive and complex models or models with considerable simplification for representing the tyre full behaviour on the road. In this context, getting a suitable model for a given application becomes a challenge for a simple model may not be realistic enough and a more complex one may be difficult to handle and perhaps, unnecessary for the given application.

In collaboration with Messier-Dowty company, this thesis has contributed to better understand the actual literature studies in the field of aircraft tyre-road interaction modelling and therefore, to help making an optimal choice of model for a specific application. The objectives have been to propose models for representing the tyre behaviour on the ground with respect to the aircraft run types. These run types include acceleration/braking (during landing) and cornering (during taxiing) at steady-state condition. Physical oriented models are preferred.

To complete this study, a literature survey of the previous researches in tyre modelling for steady-state responses is first carried out. The different models are then presented according to the three categories commonly used in the literature, physical, semi-empirical and empirical. The principle of development (assumptions or/and approximations) as well as the conditions of validity of each model are described. Then, based on the main factors playing an important role in tyre modelling, it is proposed a classification for the physical and the semi-empirical models, which are also investigated. It is underlined that choosing a tyre model for a given application requires a certain number of considerations, which mainly include the measurement data constraints, the expected level of accuracy, the needs in physical interpretation of the model parameters and results, and the time constraint.

Based on the classification of the models, the study requirements and the measurement data constraints, an a priori choice of suitable models is proposed. Then, the a priori chosen models are investigated and the advantages as well as the limitations of each model are discussed.

In the context of this study, a longitudinal force has been recorded at pure cornering performed on aircraft tyres. This force increases with side slip angle and also with relative significant magnitude when compared to the lateral force one. It is therefore underlined that in the particular case of aircraft tyres, the longitudinal component of the tyre-road interaction force may not be negligible as it has been widely assumed in the literature. Then, a further investigation of the tyre deformation in the contact patch at pure cornering is carried out. Based on a simple but comprehensive physical approach, it is demonstrated that, at pure cornering (pure lateral slip), the non uniform lateral tread stretching in the contact patch generates a longitudinal tread contraction (displacement) and as a result, a longitudinal force is developed. This force is referred as induced longitudinal force. Moreover, an exhaustive description of the self-aligning moment generation at pure cornering is carried out by decomposing it into contributions of the induced longitudinal force and the lateral force.

Besides, it should be underlined that tyre models are mainly nonlinear and depend on parameters obtained from measurement data. One of the problems of great importance related to this issue is to efficiently fix and plan the experiments. The sensitivity analysis is proposed as a means for determining the parameters that have most influence on the model output and thus, are responsible for the output uncertainty. It is then possible to significantly reduce the model response uncertainty by focusing on measurements data, which help to better estimate the most influential parameters.

Keywords: aircraft tyre model; steady-state behaviour; physical; sensitivity analysis; influential parameters; model uncertainty.
